DEVELOPMENT OF A ROBUST H-INFINITY LOOP SHAPING CONTROLLER FOR DFIG UNDER ABNORMAL CONDITIONS

Oscar Andrew Zongo

A Thesis Submitted in Partial Fulfillment of the Requirements for the Degree of Doctor of Philosophy of Engineering in Electrical Engineering

Suranaree University of Technology

Academic Year 2019

การพัฒนาตัวควบคุมการสร้างวงรอบ เอช-อินฟินิตี้ แบบคงทน สำหรับ DFIG ภายใต้สภาวะที่ไม่ปกติ

นายออสการ์ แอนดรู ซองกอ

วิทยานิพนธ์นี้เป็นส่วนหนึ่งของการศึกษาตามหลักสูตรปริญญาวิศวกรรมศาสตรดุษฎีบัณฑิต
สาขาวิชาวิศวกรรมไฟฟ้า
มหาวิทยาลัยเทคโนโลยีสุรนารี
ปีการศึกษา 2562

DEVELOPMENT OF A ROBUST H-INFINITY LOOP SHAPING CONTROLLER FOR DFIG UNDER ABNORMAL CONDITIONS

Suranaree University of Technology has approved this thesis submitted in partial fulfillment of the requirements for the Degree of Doctor of Philosophy.

Thesis Examining Committee

(Assoc. Prof. Dr. Kaan Kerdchuen)

Chairman

(Assoc. Prof. Dr. Anant Oonsivilai)

Member (Thesis Advisor)

(Asst. Prof. Dr. Boonruang Murungsri)

Member

(Assoc. Prof. Dr. Padej Pao-la-or)

Member

(Dr. Uthen Leeton)

Member

(Prof. Dr. Santi Maensiri)

Vice Rector for Academic Affairs and Internationalization

(Assoc. Prof. Flt. Lt. Dr. Kontorn Chamniprasart)

Dean of Institute of Engineering

ออสการ์ แอนดรู ซองกอ : การพัฒนาตัวควบคุมการสร้างวงรอบ เอช-อินฟินิตี้ แบบคงทน สำหรับ DFIG ภายใต้สภาวะที่ไม่ปกติ (DEVELOPMENT OF A ROBUST H-INFINITY LOOP SHAPING CONTROLLER FOR DFIG UNDER ABNORMAL CONDITIONS) อาจารย์ที่ปรึกษา : ผู้ช่วยศาสตราจารย์ ดร.อนันท์ อุ่นศิวิไลย์, 287 หน้า

วิทยานิพนธ์นี้นำเสนอตัวควบคุมการสร้างวงรอบ เอช-อินฟินิตี้ แบบคงทน ที่มีประสิทธิภาพสำหรับเครื่องกำเนิดไฟฟ้าแบบดับเบิ้ลเฟด โดยในรายละเอียดจะอธิบายข้อมูลพื้นฐานเกี่ยวกับการทำงานของระบบไฟฟ้าและการรวมพลังงานไฟฟ้าจากกังหันลมเข้าสู่ระบบไฟฟ้า โดยจะศึกษาทฤษฎีพื้นฐานและวรรณกรรมเกี่ยวข้องกับการเปลี่ยนพลังงานลม การควบคุมรหัสกริด ปัญหาที่เกี่ยวข้องกับการควบคุมกังหันลม และการควบคุม เครื่องกำเนิดไฟฟ้าเหนี่ยวนำป้อนสองเท่า ด้วยวิธีต่างๆ ในการวิเคราะห์ เครื่องกำเนิดไฟฟ้าเหนี่ยวนำป้อนสองเท่า จะอาศัยแรงดันไฟฟ้าที่ตกลงจากระดับปกติในการควบคุม ฟัซซี่ พีไอ แบบคู่ เพื่อแก้ปัญหาสภาวะที่ไม่สมดุล โดยเทคนิคนี้จะอาศัยตัวควบคุมฟัซซีลอจิก ในการความเร็วของกังหันลมและแรงดันไฟฟ้าที่บัสไฟฟ้ากระแสตรง การควบคุมเวกเตอร์จะอาศัยการตรวจสอบความคงทนของการควบคุมฟัซซี่ พีไอ แบบคู่ โดยจะพิจารณาจากผลการจำลองสถานการณ์ในสภาวะชั่วครู่ สภาวะความผิดพลาด และสภาวะหลังจากเกิดความผิดพลาด นอกจากนี้ในวิทยานิพนธ์ยังมีการใช้ตัวควบคุมที่เหมาะสมที่สุดของการวางตำแหน่งโพล และตัวควบคุมกำลังสองเชิงเส้น เพื่อรักษาความเร็วของ เครื่องกำเนิดไฟฟ้าเหนี่ยวนำป้อนสองเท่า ซึ่งตรวจสอบได้จากสัญญาณรบกวน ตัวควบคุมที่เหมาะสมจะจัดการเพื่อรักษาความเร็วให้คงที่ภายใต้เงื่อนไขนี้โดย ตัวควบคุมกำลังสองเชิงเส้น แสดงประสิทธิภาพที่ดีที่สุด

ในการดำเนินการจะสร้างแบบจำลองแบบไดนามิกและปริภูมิสเตต-สเปส ในรูปแบบ ดีคิว โมเดล ของ เครื่องกำเนิดไฟฟ้าเหนี่ยวนำป้อนสองเท่า และนำแบบจำลองนี้มาใช้ในการออกแบบคอนโทรลเลอร์ที่เหมาะสมของ เอช-อินฟินิตี้ แบบคงทน และตัวควบคุมการสร้างวงรอบ เอช-อินฟินิตี้ แบบคงทน ผลตอบสนองแบบชั้นบันได แสดงค่าเอกพจน์ และสเปกตรัมฮาร์มอนิกของ เครื่องกำเนิดไฟฟ้าเหนี่ยวนำป้อนสองเท่า ที่เหมาะสม และตัวควบคุมการสร้างวงรอบ การทดสอบวิธีการควบคุมนี้จะใช้แบบจำลองเครื่องกำเนิดไฟฟ้าเหนี่ยวนำแบบดับเบิ้ลเฟด ร่วมกับโปรแกรม MATLAB SIMULINK ในการจำลองผล ภายใต้ความผิดปกติระหว่างสายไฟกับสายไฟ ความผิดปกติแบบ 3 เฟส ความผิดปกติระหว่างสายไฟกับกราวด์ ความผิดปกติระหว่างสายไฟ 2 สาย กับกราวด์ และความผิดปกติระหว่างสายไฟ 3 สาย กับกราวด์

ผลการจำลองแสดงให้เห็นถึงแรงดันไฟฟ้าไม่สมมาตรที่มีสาเหตุจากความผิดปกติของการลัดวงจรแบบ ไลน์ ทู ไลน์ การควบคุมการสร้างวงรอบ แบบคงทนจะช่วยลดค่า ความผิดเพี้ยนของฮาร์มอนิกทั้งหมด ของแรงดันไฟฟ้าที่สเตเตอร์จาก 11.34% เป็น 1.36% ซึ่งต่ำกว่าการควบคุมที่เหมาะสม เอช-อินฟินิตี้ ที่ 4.05% การลดลงของค่า ความผิดเพี้ยนของฮาร์มอนิกทั้งหมด นี้ได้รับการตรวจสอบความเสถียรภาพและการคืนค่าของแรงดันไฟฟ้าที่สเตเตอร์เมื่อ เครื่องกำเนิดไฟฟ้าเหนี่ยวนำป้อนสองเท่า ถูกควบคุมโดยตัวควบคุมการสร้างวงรอบในระหว่างความผิดพลาดนี้ นอกจากนี้แรงบิดแม่เหล็กไฟฟ้าและค่ากระแสไฟฟ้าในแกน คิว ของ เครื่องกำเนิดไฟฟ้าเหนี่ยวนำป้อนสองเท่า ยังแสดงให้เห็นว่าตัวควบคุมแบบการสร้างวงรอบดีกว่าตัวควบคุมแบบที่เหมาะสมที่สุด ประสิทธิภาพของการควบคุมการสร้างวงรอบ เอช-อินฟินิตี้ แบบคงทน ที่มีประสิทธิภาพดีกว่าการควบคุมที่เหมาะสมของ เอช-อินฟินิตี้ เช่นกันสังเกตได้จากค่ากระแสไฟฟ้าในแกน ดี ที่มีค่าใกล้เคียงกับค่าอ้างอิง

สาขาวิชา วิศวกรรมไฟฟ้า ลายมือชื่อนักศึกษา _____

ปีการศึกษา 2562 ลายมือชื่ออาจารย์ที่ปรึกษา _____

OSCAR ANDREW ZONGO : DEVELOPMENT OF A ROBUST H-INFINITY LOOP SHAPING CONTROLLER FOR DFIG UNDER ABNORMAL CONDITIONS. THESIS ADVISOR: ASSOC. PROF. DR. ANANT OONSIVILAI, Ph.D., 287 PP.

LOOP SHAPING/ROBUST CONTROL/DOUBLY FED INDUCTION GENERATOR/WIND TURBINE

This thesis presents a robust h-infinity loop shaping control for a doubly-fed induction generator. In the thesis background information into the power system operation and integration of wind energy is thoroughly explained. The problems associated with the control of wind generators in the power system are discussed in detail. Fundamental theory and literature review regarding wind energy conversion system especially the doubly-fed induction generator is part of this work. A detailed study of the control theory, grid codes, and a review of different control strategies applied to the doubly-fed induction generator are given. Analysis of the doubly-fed induction generator under voltage dips is discussed and the methodology of fuzzy-PI dual control to tackle this unbalanced condition is developed and tested. In this technique speed and dc-link voltage are controlled using fuzzy logic controllers. The robustness of fuzzy-PI dual control over vector control is verified by simulations results for the transient state, faulty state, and post-fault state. Furthermore, in the thesis, optimal controllers of pole placement and linear quadratic regulator are employed to stabilize the speed of the doubly-fed induction generator affected by measurement noises. The optimal controllers manage to stabilize the speed under this condition with a linear quadratic regulator showing the best performance.

Finally, dynamic modeling and state-space representation of the *dq* - model of the doubly-fed induction generator is performed. The model is used to design a robust h-infinity optimal controller and a robust h-infinity loop shaping controller. The step response, singular values plots, and harmonic spectrum of the doubly-fed induction generator with optimal and loop shaping controllers are presented. The methods are tested with the doubly-fed induction generator under line to line fault, three-phase fault, single line to ground fault, double line to ground fault, and three-phase to ground fault. The system response plots are validated by SIMULINK simulations results.

Simulations results show that in the asymmetric voltage dip caused by line to line short circuit fault the robust loop shaping control reduces the total harmonic distortion of the stator voltage from 11.34% to 1.36% lower than the h-infinity optimal control at 4.05%. This reduction in total harmonic distortion is validated by the stability and restoration of the stator voltage when the doubly-fed induction generator is controlled by the loop shaping controller during this fault. Moreover, electromagnetic torque and quadrature axis current of the doubly-fed induction generator show better results with the loop shaping controller than with the optimal controller. The effectiveness of the robust h infinity loop shaping control over h-infinity optimal control is also proved by the results of the direct axis current which nearly tracks its reference value.

School of Electrical Engineering

Academic Year 2019

Student's Signature _____

Advisor's Signature _____

ACKNOWLEDGEMENT

I am taking this opportunity to thank my advisor Assoc. Prof. Dr. Anant Ooonsivilai for his support, guidance, and knowledge sharing during my study. I sincerely thank my other committee members, Assoc. Prof. Dr. Kaan Kerdchuen, Asst. Prof. Dr. Buruang Murungsri, Assoc. Prof. Dr. Padej Pao-la-or, and Dr. Uthen Leeton for their valuable suggestions and advice.

Additionally, I convey my thanks for the tuition fees scholarship I got from the Suranaree University of Technology.

Besides, thanks to all staff and students of the school of electrical engineering at the university, for their help and encouragement.

Finally, I sincerely thank my wife Sylvia, and my children Brian, Yvonne, and Adrian for their love and patience.

Oscar Andrew Zongo

TABLE OF CONTENTS

Page

TABLE OF CONTENTS (Continued)

Page

TABLE OF CONTENTS (Continued)

Page

TABLE OF CONTENTS (Continued)

Page

TABLE OF CONTENTS (Continued)

Page

TABLE OF CONTENTS (Continued)

Page

TABLE OF CONTENTS (Continued)

Page

TABLE OF CONTENTS (Continued)

Page

LIST OF FIGURES

Figure **Page**

LIST OF FIGURES (Continued)

Figure **Page**

LIST OF FIGURES (Continued)

Figure **Page**

LIST OF FIGURES (Continued)

Figure **Page**

LIST OF FIGURES (Continued)

Figure **Page**

LIST OF FIGURES (Continued)

Figure **Page**

LIST OF TABLES

Table **Page**

CHAPTER I

INTRODUCTION

1.1 Background

The control of an electric grid can be the most crucial portion of network operation. Doubly fed induction generator (DFIG) is one of the most widely used generators in the wind energy conversion system (Oonsivilai et al., 2019). DFIGs are capable of operating at variable speeds, so they are preferred over fixed-speed wind turbines. To manage DFIGs efficiently, proper control and protection schemes should be put in place for fulfilling the requirements of the international grid codes. The recent release of international grid codes puts it clear that large wind power plants (WPPs) are required to ride-through various fault conditions. Besides, wind power plants (WPPs) should inject active and reactive power to the grid in the event of a fault. This would enhance the stability of the power system. The grid codes mentioned that DFIG should continue to operate in case of a low or high voltage condition. In this thesis, a controller is designed to enable the DFIG to ride through various grid faults.

1.2 Problem statement

Nowadays, most grids have renewable energy generation, one of them being wind power plants, researches on the control of the generators making wind power stations have been of great importance. Most of the generators used in WPPs are of the DFIG type. This has led to the interests of many researchers on this induction

machine. Moreover, variable-speed DFIG technology is selected because it is the most dominated and well-recognized technology employed around. But, to operate DFIG optimally and efficiently proper control strategies should be part of the long-term plan. Any failure to the DFIG due to variation in the wind speed, unpredictable consumers′ load, and faults may endanger the life of the machine. A significant number of researches have been carried out to design control and protection schemes for optimal operation of the DFIG in standalone or grid-connected mode.

This thesis proposes a robust h-infinity loop shaping control for DFIG to ride through various grid faults in the power system. This thesis contributes to the study of robust control based on h-infinity loop shaping and extended Kalman filter.

1.3 Methodology

Through available literature and related control methods, the h-infinity loop shaping controller design is studied. DFIG used in the test of the developed controller is a 2 MW wind turbine. The power system is explained in general. The need for the integration of renewable energy is presented. The wind energy conversion system (WECS) is explained in detail. DFIG as one of the generators used in wind power generation is discussed. Different control methods developed and available in the literature are mentioned and reviewed. Vector control, which is the foundation of the controller designed is studied. Adaptive control based on Fuzzy Logic is presented. Besides, pole placement and linear quadratic regulator optimal controllers are part of this work. Then, a controller based on h-infinity loop shaping is developed and tested for various grid faults. Finally, the developed method is compared with the h-infinity optimal controller to verify its robustness.

1.4 Scope and limitations of the study

Conventional Vector control uses proportional-integral (PI) controllers, which have a slow response and not adaptive to changing system behavior. Moreover, Fuzzy dual control is adaptive but not robust enough to deal with some severe grid faults and it cannot optimally control a highly nonlinear system. In this research, a robust h-infinity loop shaping controller is introduced that can meet the design objectives of this study, which is to design a robust controller for a DFIG under abnormal conditions to ride through various grid faults. The proposed controller is developed based on the dynamic model of the DFIG using the robust control toolbox of MATLAB and implemented in SIMULINK. Simulations results are collected and presented.

1.5 Expected benefits

Results from this research can be used as a design guideline of the real-time system for the control of the DFIG in standalone or grid-connected mode. The approach applied is straight forward, and the implementation of the control strategy is easy. The results obtained have been used to write four papers that have been submitted to different journals.

1.6 Thesis organization

There are five chapters in this thesis which covers all the intended materials planned to be presented in this thesis.

- The background information to this thesis is given in the chapter which introduces the reader to this research work. Additionally, motivation, approach, and goals and expected benefits are also presented.
- Chapter II discusses in detail distributed generation, wind energy, wind turbines and wind generators, the WECS, grid codes governing the operation of wind turbines, the theory on DFIG, and the voltage dips.
- Chapter III introduces the control theory. Then, gives the theory behind conventional vector control and other control methods for the DFIG. The dual vector control technique, the extension of vector control is discussed in this chapter. A comparison is made between the two methods. It provides the application of fuzzy logic in the control of the DFIG. This adaptive control technique is introduced to the existing dual vector control. The chapter presents an optimal control design and implementation. This chapter also presents the main objective of this thesis, which is the design of the robust h-infinity loop shaping controller.
- Chapter IV shows the results obtained and gives a precise discussion of those results.
- Finally, chapter V presents conclusions and related remarks.

1.7 Thesis objectives

This thesis develops a robust control technique based on h-infinity loop shaping for the DFIG to ride through various grid faults. Besides, the objectives of this thesis can be summarized as follows:

- Improve conventional vector control of DFIG to design Fuzzy dual vector control and test the induction machine against asymmetric voltage dips.
- Apply optimal control theory to design pole placement and linear quadratic regulator for speed control of the DFIG subjected to measurement noises.
- Design a robust h-infinity loop shaping controller for the DFIG under various grid faults.
- Test the developed controller with the grid-connected DFIG and compare the results with a robust h-infinity optimal controller.

1.8 Chapter summary

This chapter has given the background of this study. The problem statement of the thesis has been explained in detail. The methodology used has been outlined. The scope and limitations of the study are part of this chapter. The benefits that the author and the university are expected to get are mentioned. Finally, the outline and objectives of the thesis are explained in short.

CHAPTER II

FUNDAMENTAL THEORY AND LITERATURE REVIEW

2.1 Introduction

A power system needs to be optimally planned and operated to minimize power cut off and disconnections that affect the economy of the customers, the utility, and the country (Zongo, et. al., 2019). To add to the present typical generations, utilities have opened doors for the incorporation of distributed generation (DG) from renewable energy sources into the distribution system (Zongo, et. al., 2019) with capability starting from 10 MW to 15 MW. Additionally, the fast growth of energy demand has paved the way for the utilization of this renewable power generation to decrease greenhouse gas emissions from fossil fuels (Ose-Zala, et. al., 2017). Wind turbine (WT) is among the technologies used as a distributed generation in power systems. In some rural regions not electrified from the utility grid, wind energy power provides an alternative in terms of reliability and cost.

2.2 Distributed generation

The parts involved in accomplishing the goal of supplying power to the customers are the generation, transmission, and distribution (Dugan, 2009). The generation is concerned with the production of power. Electricity is made at a

centralized generating station exploiting energy resources like coal, hydro, gas, nuclear, and fossil fuel. The power generating plants are typically placed in remote areas far away from the end-users. Typically, transmission refers to the transportation of bulk energy in an extended network of power lines. Transmission usually carries a huge amount of electricity as far as 150 kV of electricity or higher, however, in some cases, 30kV or higher is considered as transmission levels.

Due to increasing demand, the transmission network is in its major upgrades (Kersting, 2001). Upgrades to the power system tend to encounter economic, environmental, and political barriers. While these barriers bring several challenges, power utilities still have the responsibility to produce safe and reliable power to customers. Power corporations build large centralized power plants to accommodate a rise in energy consumption however, transporting the power across an aging and full-loaded network threatens safety and stability. Low transmission capability causes the investment of a lot of generation resources to fulfill the load demand (Poli et al, 2007). The presence of DGs reduces the prices of electricity and postpones the construction of new transmission lines and major enhancements of the power grid. If the total cost for power generation and the building of new lines weigh more than the installation of distributed generation, distributed generation tends to be a lot of economic benefits. The other alternatives can be synchronous condenser placement, conductor upgrades, and feeder reconfiguration. These are also effective in optimizing the performance of the power system however, distributed generating units are seen to be a lot economical and provide further edges in comparison to a number of these alternatives (Kersting, 2001).

Power distribution has faced a big amendment in recent years because of the introduction of good grid technology and a rise in distributed generation. Distributed generation may be delineated because of the decentralization of power plants by inserting smaller generating units having the capacity of not more than 10 MW (Kansa et al, 2011). Although distributed generation is not a brand new concept, it is gaining widespread interest because of a rise in power demand, advancements in technology, economics, deregulating, environmental, and national security considerations.

Distributed generation may be employed in industries, industrial activities, residential or utility (Zongo et al, 2019). Distributed generators may be sorted into either renewable or unrenewable energy sources. The unrenewable distributed generators are fuel cells, diesel, micro-turbines, or natural gas; whereas renewable distributed generators are biomass, and wind. The distributed generator may be used as a primary generator, standby generator, or supply for reactive power. Most of the operators of distributed generators are either non-utility or utility.

Distributed generation could also be mentioned as a small-scale electricity technology that's commonly linked to the distribution system. The electrical power analysis Institute (EPRI) defines a distributed generator as a generation from a couple of kilowatts up to 50MW (Kansal et al, 2011). Distributed generation can also be outlined as the generation smaller than 50-100MW that is neither centrally planned nor dispatched; it operates in standalone mode or connected to the distribution networks. A paper by (Ackermann et al, 2001) describes a distributed generator as the electrical power generation supply on the distribution network (DN) or the customer side of the power system.

Distributed generation resources also can be outlined as tiny, self-contained electrical generating plants that offer power to homes, businesses, or industrial facilities in DNs. Distributed generating units are usually accustomed to offer real and reactive power compensation in distribution systems (Ackermann et al, 2001).

2.2.1 Types of distributed generation

Distributed generations provide power support to the DN. The power supplied to the DN is based on the type of DG used (Acharya et al, 2006). Detailed below are the four classes of DGs categories:

1. DG1: Real power supply to the DN (power factor = at unity) - biogas photovoltaic cells, solar, etc.
2. DG2: Supply power to the DN (Power factor = 0.80 to 0.99 leading) - wind, tidal, wave, geothermal, etc.
3. DG3: Reactive power supply to the DN (Power factor = 0.00) - bank of inductors, synchronous condenser, and bank of capacitors.
4. DG4: Supply reactive power and absorb real power (Power factor = 0.80 to 0.99 lagging).

2.2.2 **Advantages of distributed generation** (Acharya et al, 2006)

1. Flexibility – this enables the generator to be placed at completely different locations of the power system thereby enabling the utility to match generation to the consumption.
2. Improved Reliability – This generation technology will improve voltage profile as a result of generations being placed to the load centers, thereby reducing disturbances caused by transmission and

distribution of electricity over long distances, and minimizing lines congestion on the utility grid throughout peak hours.

3. Improved Security – Some utility loads in remote areas may be supplied by local generations. This arrangement decreases power interruptions caused by electricity supply from generations far from the load centers which might be affected by natural disasters, power deficiency, interruptions, or coercion.
4. Reduced loading of transmission and distribution systems – the low-tension side of the existing distribution substations is selected as a suitable site for distributed generators because it facilitates the reduction of loadings on substations transformers in peak hours. This arrangement extends the lifetime of the instruments and avoids early station transmission and distribution upgrades.

2.2.3 Benefits of distributed generation

Basic advantages that will be derived from such a style of generation systems are (Mukhopadhyay, 2009).

1. Straightforward and fast installation
2. It lowers the cost of long-distance high voltage transmission.
3. Pollution reduction in areas supplied by renewable sources.
4. Overall power system running costs are reduced by the integration of renewable energy sources.
5. Simple and user-friendly system.
6. It has a simple construction, operation, and maintenance.
7. Reduces power losses in the power system.

8. Energy undelivered costs reduction.
9. Preventing or delaying network expansion.
10. Peak load operating costs reduction.
11. Improved voltage profile.
12. Improved load factor.

2.2.4 Drivers of distributed generation

The interest in distributed generation technology into the power distribution system is because of the following factors (Tautiva et al, 2008, Brown et al, 1997).

1. Power system efficiency improvement.
2. Power-sharing strategy.
3. Deregulation and competition of the power system operation.
4. Energy sources diversification.
5. Development of modular power units.
6. Placement for smaller generators is easy.
7. Easy commissioning of small plants.
8. Small capital cost.
9. Generation can be put near load centers.
10. Retail competition due to utility structuring.
11. The need for power is decided by customers.
12. Reduces the need for the construction of new transmission lines and possibly building of new large power generating stations.
13. The discovery of new methods that are environmentally friendly and conversion effective.

14. Advancement of computers that led to smart management of power flows, customer requirements, load demands.

Additionally, the following recent changes in the operation of utilities have increased interests in the integration of DG and installation of the energy storage devices at the DN level (Chiradeja, 2005):

1. Power companies restructuring causing retail competition.
2. The need for power supply is based on the customers' requirements.
3. The discovery of new technologies that are environmentally friendly and conversion effective.
4. Integration of robust and cheap power electronic interfaces for reliability and power quality improvement.

2.2.5 Features of DG systems

Distributed generation systems may be defined as tiny generation resources that are placed close to load centers. Increasing the size of distributed generators offers a significant solution to several synchronal installation issues because they are cost-efficient, friendly to the environment, have high power quality and sensible dependability (Nebrir et al, 2006). Distributed generation systems have the following features:

1. They can be run by independent power producers.
2. They are self-dispatched, but in some cases, they are operated together as one single unit comprising of many decentralized DG units.

3. Some utilities consider DGs to be smaller than 50 MW others rank as far as 300 MW.

2.2.6 Applications of DG systems (Gerwent, 2006)

1. Small generations for electricity and heat.
2. Businesses generations for electricity and heat.
3. Agricultural generations for power, thermal, and carbon dioxide.
4. Industrial generations for electricity and steam.
5. Integrated to the utility grid (for electricity supply).

These generation technologies are operating as an extra or different generation to the existing traditional installation. This is mainly to alleviate power interruption and the dependability of the power system. This is often supported by the type of fuel they use for their operation (Adefarati, 2016).

2.2.7 Non-renewable DG technologies

These DGs use gas, coal, and fossil fuel to generate electricity for various applications. Additionally, fossil fuel burning is a major factor in global warming, dangerous gas emissions, air, and organic compound pollution. These environmental damages have affected the world by degrading the quality of the ozone layer. Non-renewable resources are being used up more quickly than they can replace themselves. Its supply is finite. As a result of these reasons, they will eventually be finished due to the high rate of energy demand. These resources may be used for power generation, domestic heating, and industrial use in the co-generation arrangement. These generation technologies include mutual engines, micro-turbines, gasoline turbines, and steam turbines.

2.2.8 Renewable DG technologies

Electricity from renewable energy is traditionally fed to the customers connected to the DN. These consumers should be located at the medium voltage or low voltage (LV) part of the DN. Power generations that represent this class of generation include, biomass, wind power, photovoltaic (PV), small/mini/micro-hydropower apart from wind turbines. The electricity output of these generations may additionally be dispatched to the grid for improving the grid voltage profile or to work as a sole generation to serve a specific load in a neighborhood. Recent researches conducted by the globe energy council (GEC) show an increase in worldwide power output contributed by renewable energy assets from 23 MW in 2010 to nearly 24 MW in 2030.

2.2.9 Comparison between solar photovoltaic and wind energy as DG

In many power systems, an amount of power generation is provided by large-scale generators (Barker et al, 2000). This is often due to the economic benefits offered by these units over tiny ones. However, in the last decade, technological improvements and financial and regulative measures have motivated the interests of distributed generation. There are different technologies used as distributed generators like photovoltaic cells, wind power, combustion engines, fuel cells, and alternative forms of generation from the resources that are obtainable within the region.

The integration of wind and solar into the energy market has been beneficial to the DN because of being clean with no fuel costs (Shivarudraswamy et al, 2012). The most significant concern of these renewables is the intermittency nature of their sources, the sun, and the wind. Additionally, their start-up costs are the major

drawback of these pollution-free technologies. There is high hope that soon there would be a drop in the cost of building the power plants as the advancement in technology increases. Solar power is predictable and straightforward because it depends on solar irradiance, the surrounding temperature, and panel shading.

The behavior of the wind of being variable makes wind power generation more unpredictable caused by changing wind speed which makes the power output graph to have an exponential shape. Therefore there should be a trade-off between generation and consumption. Solar is more predictable than wind but suffers from proficiency as compared to wind generation although harder to anticipate but has higher generation proficiency. Since wind turbines offer higher productivity and low cost it attracts the interest of more investors than solar power generation.

One of the difficulties facing investors and energy market operators is the complexity of foreseeing wind power generation. After a long battle in advancing forecasting methods over the past decade, there has been an improvement in the prediction strategies increasing wind generator's capability to produce power, hence, classed as semi-scheduled or scheduled generators. The power system's expansion of the penetration level of renewable generations has caused some problems in the operation guidelines for the power system.

Wind farms being present all over the DN should not be the principal generators but they are there to support conventional generators for a portion of the load demand. Their capability to supply a bigger portion of the load requires the support of fast response generators such as hydroelectric generators and Combined Cycle Gas Turbine (CCGT). Solar generation is capable of serving a big portion of load daily. However, the support from wind, CCGT, and Hydro is inevitable in peak

hours. Hence it is essential to have large generating units in operation until the energy storage problems are sorted out.

The installation of big energy storage devices in the DN helps the renewables to support the power generation system at times of low generation from conventional generators because big storage is a solution to avoid the intermittent nature of the renewables. Additionally, renewables will also decrease the emissions from the power industry using fossil fuels thus extending the life span of the world's natural resources such as coal and gas.

2.2.10 Distributed generation impact on the distribution network

Transmission lines, loads, and generation capability play an enormous role within the initial stages of coming up with and type of the new distributed generation. If the DGs are integrated into the power system while not correctly arranged it may downgrade the operation of the system as a result their presence may affect system power flow and voltage profile (Lopes et al, 2006).

Distributed generation position and its sizing affect the direction and magnitude of the power (El-Ela et al, 2010, author et al, 2006). Due to uncoordinated operations for regulation, a lot of challenges could arise like power loss increment and uncoordinated switch of protective devices.

2.2.11 Technical challenges facing DG

Distributed Generation encounters several integration challenges, however, the most important overall issue is that the DN and transmission system is designed in a layout whereby few big power stations push power to the various smaller customers located very far (Pujhari, 2017).

Additionally, DG has negative impacts like frequency deviation, voltage deviation, and harmonics on the network (Kumpulainen et al, 2004). The rise of power losses is another drawback that would occur (Tautiva et al, 2008, Reddy et al, 2012). Therefore, engineers should take into account all vital factors which will affect the operation of the distributed generation before making any decision of sizing and placement of the DGs within the distribution system.

The following are technical challenges created by distributed generation in the DN (Pujhari, 2017):

1. Difficulties in voltage regulation and reducing losses.
2. The system faces a voltage flickering condition.
3. The shaft of the generator is affected by over-torque in faults.
4. Harmonic filtering, control, and injection.
5. The surge in the level of short circuits.
6. Problems with the grounding and interface of the transformers.
7. Stabilizing of the system in case of transient conditions.
8. Protection schemes' sensitivity increment.
9. Synchronization of generators operating together.
10. Lack of knowledge of the impacts of penetration level.
11. Islanding detection of the system.

2.2.12 Protection challenges to distribution networks caused by DG

Several challenges are facing the distribution system because of the integration of the distributed generation in the DN (Conley, 2010).

1. Unintentional islanding with considerations regarding dependability.
2. The distributed generator will cause failure within the operation of protection of the distribution of the power system. Fault current caused by a distributed generator could cause unintentional functioning of the feeder relay. This is often known as protection under-reach.
3. Distributed generators could be the source of failure or unplanned operation of the protection system. Distributed generators will cause the loss of healthy feeders in adjacent feeder lines.
4. Distributed generators could need improvement of the primary station bus-bar protection system to avoid bus-bar fault, caused by tripping of the HV/MV electrical device. As a result of these faults, currents may add each other within the feeders themselves. The presence of distributed generation within the distribution system could represent changes within the protection inter-locking and nuisance tripping of the generating units.
5. Change in the fault magnitude of the DN. The level of the fault will either intensify or drop because of distributed generation. The DN is also expected to experience variations in fault magnitude at a definite area of the DN, considering the number and type of the generating units' operation. A rise of fault intensity will need changes in the protection equipment like switchgear. Furthermore, a decrease in fault magnitude could cause issues like over-currents.

2.2.13 Voltage Control

When the DG produces power which is less than or equal to the consumption and the main generator supplies power to the loads, the transmission lines will have the duty to feed the loads with only reactive power. Besides, if power from the DG exceeds the load requirement there would be active power flow from the DG to the transmission network making the load need only reactive power from the network causing a reverse power flow.

Apart from increasing levels of generation, the line impedance and power flow constitute a lot to the voltage rise in the DN (Francis, 2014). Since distribution lines have high resistance as compared to transmission lines, the active power flow on these networks affects the voltage profile of the DN.

For DN with a small number of distributed generators, these machines are not involved in voltage improvement activities at the grid connection point (Senanayaka, 2014)). Instead, they can operate to improve power factor, wherever the power factor keeps nearer to unity.

2.2.14 Power and frequency control

To realize frequency control through renewable sources, many methods should be involved. The subsequent list shows some vital ways of achieving power flow management and frequency management (Senanayaka, 2014).

1. If the renewable energy supply may be a dispatchable supply like Solid compound electric cell (SOFC), bio-energy based mostly micro-turbine, Hydro will participate in power and frequency management activities.

2. Energy storage systems are the simplest to be accustomed to as they can convert non-dispatchable renewable sources (PV, Wind) to dispatchable ones. Batteries, supercapacitors or pump hydro turbines may be used as energy data-storage mediums.
3. Change the power delivery purpose of intermittent renewables from its most operative purpose and run them with some reserve power margin. During this methodology, renewables (PV, wind) will not capture the most obtainable power from sources and that ends up in economic challenges of the operations. With these ways, renewables also can participate in frequency control of the power system to support synchronous generators.
4. Demand-side control with non-critical load schedules may be shifted to a period when the grid has excess power.

2.2.15 Effects of DG Penetration

Adding a distributed generator into a heavily loaded distribution network (DN) abruptly changes the DN setting and variables (Ilse et al, 2014). One of the benefits of distributed generation technology is the alleviation of the strain facing the nearest feeder and associated tie lines caused by load growth. This could lead to the delay or postponement of system upgrades. Furthermore, distributed generation is capable of supporting the DN by improving the voltage stability of a DN from poor voltage condition before the installation of the distributed generator during peak loading periods. In (Richardson et al, 2009) the authors prove that under regular operations, it is likely100 % of distributed generation integration ended in voltages fluctuations. However, there are some crucial negative consequences on the planning,

voltage control, and protection of the DN. The number of DGs present in the network will determine the impacts brought by these consequences.

The distributed generation has the behavior of rising voltages and at a small level destabilizes the protection instrumentation due to variation in the demand. The losses within the DN also are reduced, thereby reducing the cost of the distribution network operation (Quezada et al, 2006). Once the distributed generator is integrated into the power system is of the induction generator, condenser banks are needed at the PCC to boost the power factor of the DN.

2.2.16 DG opportunities and challenges

The introduction of DG (standby generators) onto the power system has numerous positive impacts on the power companies and their consumers (Zobaa et al, 2006). The DG gives customer utilization choices that can diminish their energy consumption costs by consolidating DGs that are fueled by cheaper fuel sources such as those generators fueled by methane gas. This gas can be kept in an adjacent landfill and the heat required can be created from the burning of waste in incinerators or created using electricity. The use of huge sums of metropolitan waste which are cheap sources of fuel requires tremendous landfill sites that can increase the power generation capacity of the city. Distribute generations may cause undesirable re-distribution of load, presence of faulty current, over-voltage, and unintentional islanding operation (Nigim et al, 2003).

The radial feeders' circuitry practice in the DN usually is the main reason for the cut-off of the supply for all the downstream clients if one feeder is faulty. Subsequently, this does not affect the reliability of the system before and after DG integration with the system (Barker, 2000, Dugan et al, 2002, Kojovic et al,

2001). Additionally, another problem emerges of some loads being unsupplied and unutilized DG capacity. If in the event of power outages some DGs which are interconnected are permitted to supply loads, the system unwavering quality will be highly improved and the customers will not enter any irregularity of their power supply. This objective can be fulfilled by basically arranging the intentional islanding of DG units (Friedman, 2002).

2.3 Wind energy

The wind is the power radiated to the planet Earth from the Sun. Nuclear reactions within the sun's core turn out temperatures as high as one x 107 K. They turn out 4 x 1026 J of non-particulate radiation in a second. All this energy has been radiated to our planet for over four billion years. Sun's radiation or daylight strikes the Earth's equator right away and diffuses on the Northern hemisphere making the poles receive a low quantity of daylight for the whole year (Kelley, 2016).

Earth's surface heating ends up in temperature variations between the land, water, and air, because of their specific physical properties, like density, thus poignant their heat absorption (Kelley, 2016). The power generation by renewable energy sources has increased considerably in recent years (Zongo et al., 2019).

The wind energy conversion system (WECS) is the most widely used technology since it has a lower cost apart from being environmentally friendly. This renewable energy technology is environmentally friendly because it is carbon and pollution-free. The advantages that governments enjoy from wind generation inspire them to extend their investment in this renewable energy supply.

2.3.1 Wind energy assessment

Before a place is chosen for wind turbine installation assessment, the distance from the load center, and the speed of the wind in the area have to be checked first (Elmabruk et al, 2014). An entire wind assessment involves a dense community of anemometers (wind chase stations) recording non-stop wind records for a minimum of twelve months. Given this wind, tracking records are time-consuming and expensive. Wind researchers unremarkably acquire information that is antecedently recorded. Varied sources are also useful in getting current meteorologic databases. As an example, climatologically stations, and airports are the areas expected to have good records. If attainable, existing facts units should be supplemented with spot measurements. Nowadays some internet sites possess good wind data for use in wind energy assessment. Many researchers ought to concentrate on areas most likely thought to possess accurate wind speeds information.

The following are prominent wind resource assessment (WRA) challenges (ADB, 2014):

1. Since wind is an intermittent climate phenomenon, this makes it very difficult to determine the long-term wind resource of a place and the yearly power generation capability of a wind power plant (WPP). Wind speed data obtained by yearly measurements give only a preview of the wind data of the particular area. The year-to-year variation in wind speed may be affected by El Niño, La Niña, and the other long-term phenomena. Extrapolation of some measurements of wind to the lifetime of a WPP is needed before a

decision is made for the suitability of the area for wind turbine installation.

2. Wind measurement requires robust instruments placed at a precise location, and a group of instruments should be used in rotation to avoid the efficiency deterioration of sensors due to age. The big amount of data obtained should be audited annually. All of these procedures require a competent, dedicated, qualified, and experienced team to operate and maintain the measurement campaign.
3. In a traditional wind farm, usually 10–15 wind turbines are allocated in each measurement. Depending on the terrain a tolerance of ±10% in speed is acceptable. Additionally, the height and the turbine hub height may not be equal. Normally extrapolation of wind speed from the measurement location to turbine locations and from measurement height to hub height is performed using wind flow modeling. Wind flow models are one of the most complex computational models in physics. Due to their complexity simplifying assumptions like linearity, thermal stability and simple terrain are used for solving these models. These factors contribute to the uncertainty in the estimation of the average wind speed and average annual power production.

2.3.2 Wind energy harnessing limitations

There is a limitation on the amount of wind that a wind turbine can convert to mechanical energy. This means that the wind converted to mechanical

energy for power generation is of a certain limit (Kelley, 2017). The turbine can be stalled if it forces to pull more wind than what is capable to utilize for conversion to mechanical energy. An attempt by a turbine to extract excessive wind energy than its capacity would make the air move away with the zero speed inflicting the air to fail to drive the turbine, thereby prohibiting energy extraction. Betz Law states that an ideal turbine is capable of extracting 2/3 of wind speed.

2.3.3 Characteristics of the wind

The height above the earth's surface and geographical locations are among the major factors affecting the wind speed of the area. Others being the season, time of the day, weather, and landforms (Tong, 2010). The turbine design optimization is ensured by knowing the wind characteristics, develop wind measurement techniques, and decide sites for wind farms.

2.3.3.1 Wind speed

This parameter is among the most vital characteristics of wind energy. The speed of the wind varies based on location and time, because of factors like weather. This parameter is random and its information can be obtained using statistical methods.

2.3.3.2 Weibull distribution

This method is usually employed in analyzing the statistical wind information of a site for a certain duration in preparation for (WPP) installation. The wind speed distribution of a site represents the amount of wind available in the area. This is done by the Weibull function which is expressed as shown below (Kumaraswamy et al, 2015):

$$f(v)=\frac{k}{c}\left(\frac{v}{c}\right)^{k-1}\exp\left(-\left(\frac{v}{c}\right)^{k}\right) \quad (2.1)$$

Where:

C = Weibull scale parameter in m/s

k = Weibull shape parameter.

v = wind velocity in m/s.

2.3.3.3 Wind turbulence

This is the variation of the wind speed in brief time durations, particularly for the wind velocity (horizontal component). There are two components of the wind speed at any instant of time known as the mean wind speed and the instantaneous speed fluctuation, i.e.

$$v(t)=\bar{v}+v'(t) \quad (2.2)$$

2.3.3.4 Wind gust

This occurs when there is a sudden change in the wind speed within a very short time. Within this time of abrupt wind turbulence, wind speed, and wind shear changes drastically. Reducing turbine rotor imbalance and maintaining the power output of the turbine may be a huge challenge to control engineers. To keep the generator speed constant throughout such abrupt turbulent gusts needs speedy changes within the pitch angle of the blades.

2.3.3.5 Wind shear

This is also a meteorologic condition which shows that there is a direct proportionality between the rise in wind speed and the height. The height's impact on the wind velocity is directly related to the roughness available on the earth's surface. This is estimated by the Hellmann equation. This equation relates to the wind speeds between two completely exceptional heights:

$$v(z) = v(z_0)\left(\frac{z}{z_0}\right)^a \tag{2.3}$$

Where:

z = height above the earth's surface.

z_0 = reference height for which wind speed $v(z_0)$ is known.

a = wind shear coefficient.

2.3.4 Factors affecting wind power production

The three factors affecting the power generation of the WT are the density and speed of the wind, and space swept by the blades of the WT (Marimuthu et al, 2014). These factors are explained as follows:

- Wind speed

This parameter is divided into four categories depending on the wind turbine operation.

1. Start-up speed - Rotor and blade system begins to rotate.
2. Cut-in speed - 7 and 10 mph, a wind turbine generates electricity.

3. Operating speed - 25 to 35 mph for rated power output.
4. Cut-out Speed - 45 to 80 mph, wind turbine stops producing electricity and comes to a standstill to avoid damage.

- Air density

When the air has a high density more energy is received by the wind turbine. This parameter varies with elevation and temperature. When the altitude increases, the air decreases in opposite to the decreasing altitudes. Additionally, heated air is less-denser than cold air. If all these parameters are equal the turbine can generate more power.

- The swept area of the turbine

As the area sweptback by the blades increases (the size of the area through which the rotor spins), the wind turbine will capture more wind hence the higher the rotational energy. Since the sweptback space is given by *GD2/4*, any increase in blade length will cause a bigger power produced by the turbine given that *D* is the diameter of the rotor.

2.3.5 Utilization of wind energy

Wind power utilization started around 5000 B.C. At this time sailors used boats to cross the river Nile (Cao, 2012). From the year 200 B.C. wind energy was the source of power for water pumping, grinding grains, and drive cars and ships in historical China and the Mideast. Information about the existence of windmill used in the world can be found in the book (Pneumatics - Hero of Alexandria). These windmills were used to generate mechanical energy from wind.

Wind power generation started in the late nineteenth century (Cao, 2012). Its presence was not recognized because of the dominance of steam power plants. Countries started to consider wind for power generation in the mid-1970s due to an abrupt increase in oil prices. This led utilities to consider conserving energy resources. In its early application, this energy gained its important quality in power generation mainly for charging batteries in remote areas, residential buildings, isolated areas or islands, and DNs. The wind turbines used were tiny generations of about 100 kW. In some cases, they can reach a size of 5 MW. It was until the 1990s when the wind started to conquer the world, owned by the governmental and industrial suppliers. Also, the globe has shifted from onshore to offshore wind turbines.

Most wind turbines available in the market are capable of producing 1.5-5 MW. Big machines of 7.5 MW to 10 MW will be in use shortly after being manufactured. In recent years wind power has become more reliable, quieter, cost-efficient, and commercially competitive. This is good proof that wind turbine technology is maturing. The challenges associated with the technical part of the wind turbine are related to an increase in turbine size, energy storage, power transmission, energy demand, fault tolerance, and system stability. Nowadays, this type of generation is used in a large amount referred to as the main source of power supply in large quantity and operated economically. One of the simplest examples is the UK generation capacity from offshore wind turbines to be big enough to supply thrice the desired electricity consumption inside the country if the farms are given enough support from the funding agencies. Unfortunately, the biggest drawback of wind power is its intermittency nature.

2.3.6 Contribution of wind power

Standalone wind generation plants are a brand new concept in renewable energy power generation technology (Maegaard, 2009). Standalone wind generation systems combined with power from alternative sources form a hybrid generation system. The replacement of the existing conventional generation by new energy sources has resulted in energy-saving and emission reductions.

Standalone wind generation plants can still prove their importance as another power source around the world (Maegaard, 2009). The analysis and development of standalone wind generation have paved the way for large-scale wind power plants. The contribution of wind power offers a lot of opportunities for developing countries' poor people.

2.3.7 Key growth drivers for wind energy

- Climate change and global warming

This energy generation technology is a zero-carbon source of power. Some of the global targets suggested are (Kane, 2009):

1. The Kyoto Protocol to reduce CO_2 emissions by 5.2% by the year 2012;
2. EU declared 20% of power will be from renewable energy by the year 2020;
3. US target is to use renewable energy to generate 10% to 20% of its power for 21 states.
4. China's renewable energy power generation is expected to be 20% by the year 2020.

5. India planned to power 10 states with 2% to 10% of power from renewables.

- Energy security

There is no hedge against geopolitical dangers and no risk of fuel price instability for wind energy (Kane, 2009). It has a socially, environmentally, and financially feasible development.

- Increased electricity demand

Reliable power plays a key role in economic growth in developing countries (Kane, 2009). Highly populated developing nations like India and China require all sources of energy to quickly meet their fast-growing energy demand. The world's wind power generation significantly increased from 0.82% in 2006 to 4.04% in 2016.

2.3.8 Wind energy harvesting characterization

The tests were performed in the office and a fan was used as a wind stream generator (Jushi, 2016). An anemometer was additionally included for wind speed measurement in (m/s).

The devices used to accomplish this were:

1. Fan
2. Anemometer
3. Computer interface
4. Connection to the wind turbine

2.3.9 Wind Siting

The factors which have to be thought of in selecting a suitable site for a turbine installation are (Kuhn et al, 2010):

- Land size

There should be a sufficient amount of land for the turbine (Kuhn, 2010). Generally, there are specific laws on how much surface area should be unoccupied close to the turbine tower. The height should be higher by 1.5 times the blade and 100 feet from the closest boundary line and personal way.

- Distance from the turbine to DN

The distance between the turbine site and the local power distribution or station is additionally an element to be considered (Kuhn, 2010). If the distance is simply too huge, the positioning is assumed to be much unsuitable for the installation of a turbine. The reason is that electricity would have to be transmitted long distances before reaching customers which is not economically beneficial.

- Surrounding landscape and structures

If there is a necessity for electricity "behind the grid," however, this is often a choice for the turbine (Kuhn, 2010). This suggests that if the local demand is high at the area the turbine was installed, the power would directly be transmitted to those locations rather than being shipped to areas distant from the electrical distribution center.

- Social constraints

The use of electricity should be analyzed and therefore the most economically helpful choice ought to be chosen. If there are not any helpful choices, a distinct site ought to be chosen (Kuhn, 2010).

- Air zone constraints

There are some limitations to the air zones when choosing the position for wind turbine installation (Kuhn, 2010). Some aviation laws do not permit the development of the tower of heights over 200 feet, which embraces most utility-scale turbines.

2.3.10 Issues with Wind Energy

Scientists and engineers need to do more to make wind energy be an important energy source. Although this renewable energy is clean because apart from being intermittent, it is difficult to harness (Grogg, 2005). Any effective turbine is highly affected by its location. The area chosen for wind turbine installation must have the wind at reasonable speeds at most times for turbine operation. Things like wind turbine height, edge number, generator type, rated speed, total power must be related to the location environment. Some sitting prerequisites are exceptionally specific for each turbine type and cause several negative effects if not handled carefully. Conflicting factors like location and visual sites or wildlife should be taken into account when choosing the site. The site might be good for turbines but the presence of turbines affects people with visual problems or the noise disturb animals. In the past, there was a problem of electromagnetic interference between the T.V. reception because the blades were made of metal. That problem does not exist nowadays because the blades are made of composites. Lightning still poses a threat to the technology, even with the utilization of composites as a raw material for making the blades. There are also some complaints of noise from the blades, although newer designs minimize noises to a higher amount, and most turbines are now installed very far from human residences. Noise from the wind turbines has been difficult because

the level of the foundation and the turbine are the same. In recent years there has been some effort from design engineers to investigate changes to improve the proficiency of the wind turbines.

2.3.11 Wind resource estimation

The mean wind speed is demonstrative of the wind climate but distant from adequate when assessing the potential wind asset (Hasager, 2007). A wind turbine can deliver power within a specified working limit. Away from this constrain, the turbine is set to halt producing electricity possibly stop if the speed is dangerously very high. Since the output power is proportional to the cube of the wind speed, this parameter has a high effect on the operation of the wind turbine. There are working speed ranges for the wind turbine. The initial working speeds are between 4 m/s to 13 m/s; if it passed 13 m/s to 24 m/s, a consistent (full) rated power is delivered. When this speed limit is exceeded, the wind turbine is ceased to operate. This action protects wind turbine mechanical parts from serious damage.

The intermittent nature of wind causing its speed to vary for most of the time is a major drawback of this renewable energy generation technology which extends from seconds to decades at all time scales (Hasager, 2007). The wind direction is very important in doing the layout of a wind farm because one wind turbine upwind of another turbine will provide a shadowing (wake) effect downstream. This will consequently affect the power delivered by a turbine located in the wake. The output of this turbine will be less as the mean wind speed is lower and the turbulence intensity is bigger (Hasager, 2007). Hence measures have to be taken to avoid wake impacts as much as possible in offshore wind farms. This should be done in the planning stage.

2.3.12 Future of WECS

Renewable energy technologies have become more advanced. This has made them have low operation costs hence economically viable. This increases the number of installed turbines around the world (El Chaar et al, 2011). This maturity begins to confirm that wind energy is becoming more comparable to conventional generations forcing a rise in the need from utilities for more wind turbine installations. Unfortunately, these fast demands for turbine installations have created serious drawbacks like have more poor products on the market due to shorter tests and development phases.

Modern turbine technology is considering an increased wind capturing capability whereas reducing stresses and losses, thus raising the potential of the system (El Chaar et al, 2011). In recent years, the analysis is aimed at generating lighter turbines. The other improvements considered are for them to be more versatile, noise-free, advanced material, and simplify the production process. Additionally, many control techniques for extracting the utmost power from variable wind, making a certain quick response to wind fluctuations are the interests of many researchers. The most important consideration of wind power is to become the most promising power generation technology. Besides wind characteristic parameters, the study also involves measurements of wind speed, geographical location, distribution, and local wind flow. All these should be assessed to confirm implementation success.

2.3.13 Wind turbines

The turbine is made in such a way blade airfoil is curved at the top half and flat at the bottom (Shen, 2012). When wind flow over the thicker, curved section of the blade is of a massive quantity, the wind initially slows down and then quickens

to cope with the speed of the relative wind. The increase in wind speed above the airfoil causes the air on top of the airfoil to have low pressure while the air beneath the airfoil remains at the high pressure. The lift created on the turbine is perpendicular to the wind flow, facing the low-pressure area. Besides lift, the blades of the turbine also experience drag (D) due to friction on the blades. The presence of drag causes the variation of the direction of the lift. The two phenomena cause the turbine blades to rotate hence rotating the rotor the generator.

The nacelle is responsible for power generation within the turbine system. This part is the housing of the mechanical components of the turbine which are essential for power generation (Shen, 2012). The turbine converts the moving kinetic energy (K.E.) of the wind to electricity. Being mounted on the same shaft the hub and the rotor blades spin at the same speed. There is a connection between the shaft and a large gear which is mechanically engaged with a small gear making the smaller gear to turn 100 times quicker. The rotating windings of the rotor are between two sets of stationary magnets and they are connected to the faster-moving shaft. The coils rotate cutting the magnetic field produced by the magnets. From Faraday's law, the electricity generated mainly depends on the rate of change of magnetic flux and the number of turns.

Most of the modern WTs operating around the world have rotors with three blades of diameters 70-80 m. They are usually installed at 60-m to 80-m above the ground (Lyons et al, 2008). The total number of generators is between 30 to 150 machines. This cluster of machines is anticipated to produce 1.5 MW. The blade pitch adjustment can be used to control the power output of a wind turbine. The angle of

attack of the WT can be varied by rotating the blades about their axis relative to the wind because of the blades spin relative to the rotor hub.

The yaw control mechanism rotates the nacelle about the tower, thus pointing the turbine in the direction of the wind (Lyons et al, 2008). A WT is fitted with wind sensors accountable to send a signal to the nacelle required by the yaw controller that changes the direction of the turbine.

The turbine is set to start generating electricity when the speed is approximately 5 m/s (Lyons et al, 2008). The utmost power output is reached at 12–13 m/s. Adjusting blade pitch is known as “pitching” is used to move the wind turbine from higher wind speeds to lower speeds. This is often done when the turbine reaches a speed of 22-25 m/s. Up-wind machines are more preferred in grid-connected WTs and they function with the blades upwind of the tower to avoid tower shadow. Nowadays, the performance of cost-efficient wind turbines is higher.

2.3.14 Wind turbine characteristics

The guidelines for WT operation depend on two important and well-known forms (Camm et al, 2016). The primary objective is the conversion of wind energy into mechanical energy. This is accomplished by utilizing streamlined turbine blades and several other techniques to control the mechanical power of the moving rotor. Then, the conversion from mechanical to electrical energy takes effect by a generator where electricity is produced and fed to the network.

Turbine classes are distinguished based on their mechanical power and speed control (Camm et al, 2016). Turbine blades are designed to convert the wind moving over the airfoils to torque and after that control that torque to capture the greatest sum of wind energy whereas avoiding harm to the mechanical parts of the

turbine system. There are two classes of turbines that are either stall directed (with dynamic stall as an enhancement) or pitch controlled.

Shaping the turbine blades can be used for stall control such that the airfoil produces less streamlined constrain when the wind speed is high, hence slowing down, or lessening the turbine's torque. This can be a straightforward, cheap, and vigorous mechanical system (Camm et al, 2016). Pitch control is achieved through the utilization of a pitching mechanism within the turbine hub, turning the blades around their axes. The change in the wind speed causes the blades to pitch rapidly controlling the torque making the turbine capture the most extreme energy or protect itself as much as possible. Some turbines are designed with an independent blade pitching mechanism. This enables them to easily adjust rotor shaft torques regardless of the wind speed contrasts at both ends of the blade curves.

In addition to mechanical power control, WTs are technically found as fixed speed -Type 1, limited variable speed-Type 2, or variable speed (partial - type 3/ full - type 4) (Camm et al, 2016).

2.3.15 Turbine types

The horizontal axis wind turbine (HAWT) includes a tubular tower (smaller towers may have a lattice frame) and three rotor blades connected to the nacelle of the gear-box, drive-chain, generator, and other items (Lebsir et al, 2015). When the wind strikes the rotor blades will cause them to turn. The turning of the blades from the wind converts the wind's kinetic energy to useful mechanical energy. The mechanical part of the turbine is attached to the generator enabling the conversion of the mechanical energy to electricity.

The difference between the HAWT and the vertical-axis wind turbine (VAWT) is at the positioning of the shaft (Lebsir et al, 2015). The mounting of the shaft determines the heading and the shape of the propeller blades. This easily visible feature separates the horizontal axis and vertical axis WTs.

Both designs have their advantages and drawbacks (Lebsir et al, 2015). Generally, horizontal axis WTs are more preferred than their counterpart and broadly used showing that their designs and technologies are more broadly understood and created. Vertical axis wind turbines are still uncommon to numerous wind power clients and professionals because they are unfamiliar to many.

2.3.16 Wind turbine generators

They can work at unsteady power levels to ride through possible voltage deviations (Lebsir et al, 2015). Wind turbine generators suitable for this technology can either be induction generators, direct-current generators, synchronous generators, or other newly developed machines.

2.3.16.1 DC generator technology

The main equipment is a WT, a DC generator, an inverter. Additionally, there are controllers and transformers. The whole system can be connected to the grid. For shunt-wound DC generators, the field current (and thus magnetic field) is directly proportional to the operating speed while the actual speed of the wind turbine is decided by balancing drive torque and the load torque (Cao et al, 2012). The presence of commutators and brushes makes it expensive. They are not sometimes employed in wind power supply unless if the demand from the consumer side is low.

2.3.16.2 AC synchronous generator technologies

AC synchronous generators used in wind rely on DC field excitations. This can be obtained from either permanent magnets or electromagnets. This is the reason why they are named permanent magnet synchronous generators (PMSGs). The other choice is electrically excited synchronous generators (EESGs) (Cao et al, 2012).

2.3.16.3 AC asynchronous generators

Most of the power plants generate electricity using synchronous machines. On the other hand, modern wind power turbines use induction machines as their generating machine (Cao et al, 2012). In wind energy, the use of squirrel-cage induction machines is for fixed speed operation which is not common for many utilities preferring variable speed ones (Lebsir et al, 2015). Bulky construction causes the SCIG to have very low efficiency and reliability with high maintenance costs. Moreover, the slip ring, brushes, and three-stage gearbox are to blame for the huge mass of the wind turbine. Additionally, the machines have high electric and mechanical losses. Drive train links the rotor of the generator to the WT. This system usually contains high and low-speed shafts, bearings, and a gearbox (Lebsir et al, 2015). The rotor receives power from the bi-directional voltage-source converters. This allows the rotor side converter (RSC) to control the speed and torque of the generator using a gate signal from pulse width modulation (PWM). The other choice in this group is the doubly-fed induction generator (DFIG) which is explained in detail later in this chapter. This generator can operate at variable speeds.

Table 2.2 (Goudarzi et al, 2013) below, shows generators available for wind power generation around the world. The meaning of the letters used in the table is P(Poor), E(Excellent), G(Good), and F(Fair).

Table 2.1 Performance comparison of different generator concepts

Factor	SCIG	DFIG	EESG	PMSG
Torque density	P	F	P	E
Speed range	P	G	E	E
Cost	G	G	P	P
Size	G	F	P	E
Footprint	G	G	P	G
Gearbox requirement	F	F	E	E
Converter size	G	E	G	G
Efficiency	F	G	G	E
Reliability	G	G	G	G
Maintenance	F	F	G	G
Noise level	F	G	G	G
Fault detection	F	F	G	E
Power factor	F	G	G	E
Power quality	F	G	G	E
Power range	G	F	E	G
Simple structure	G	F	F	G
Reduced head-mass	F	F	P	E

2.3.17 Generator characteristics

The majority of generators in wind power generation have the following characteristics:

1. Torque and power density are very high.
2. The minimum number of machine parts.
3. High power output efficiency.
4. Their maintenance cost is very low.
5. They are highly reliable and robust and can be used in many wind operating conditions.
6. Cheap in terms of cost.

2.3.18 Design considerations and challenges

Generally speaking, minor modifications are enough for some commercially available electrical machines to use them as wind turbine generators (Cao et al, 2012). The key issues that should be taken into account after the selection of the site for wind turbine installation are:

1. Machine choice
2. Drive train used
3. Structure of the brush used
4. Rated speed of the machine
5. Rated torque of the machine
6. Tip speed ratio
7. Power and current
8. Voltage regulation (synchronous generators)
9. Methods of starting
10. Starting current (induction generators)
11. Synchronizing (synchronous generators)
12. Cooling arrangement
13. Power factor and reactive power compensation (induction generators)
14. Power converter topology
15. Weight and size
16. Protection (offshore environment)
17. Capital cost and maintenance.

2.3.19 Wind power density

This parameter is normally estimated before the establishment of any wind power plant (Sharma et al, 2017). The wind energy available in a particular area can be determined by using wind power density (WPD). This parameter is very important because it shows how capable a site is for power generation from available wind energy. Wind power density can be estimated using two methods, the first being calculating it using the available wind speed data. Another method is the Weibull distribution.

- WPD estimation based on measured wind speed

Wind power density is the function of the cube of the wind speed. Therefore WPD is given by the following equation (Sharma et al, 2015):

$$WPD = \frac{1}{2n}\rho\sum_{i=1}^{n} v^3 = \frac{1}{2}\rho\bar{v}^{-3}\left(W/m^2\right) \tag{2.4}$$

Where:

ρ = air density in kg/m3,

v = mean wind speed in m/s, and

n = number of observations in the specific period.

- wind power density estimation by Weibull distribution function

Wind power density can also be calculated by using (2.5) (Kumaraswamy et al, 2015):

$$WPD = \frac{p(v)}{A} = \int_0^{\infty} \frac{1}{2}\rho A v^3 f(v)\,dv = \frac{1}{2}\rho c^3 \Gamma\left(1+\frac{3}{k}\right) \quad (2.5)$$

Where A is rotor swept area is m^2 given by,

$$A = \pi r^2 \quad (2.6)$$

Thus, the average wind speed v is,

$$v = \int_0^{\infty} v f(v) dv = \frac{c}{k}\tau\left(\frac{1}{k}\right) \quad (2.7)$$

The Euler's gamma function τ given by,

$$\tau(z) = \int_0^{\infty} t^{z-1} e^{-t} dt \quad (2.8)$$

The scale factor (Rayleigh distribution), *c* is given by,

$$c = \frac{2}{\sqrt{\pi}} \quad (2.9)$$

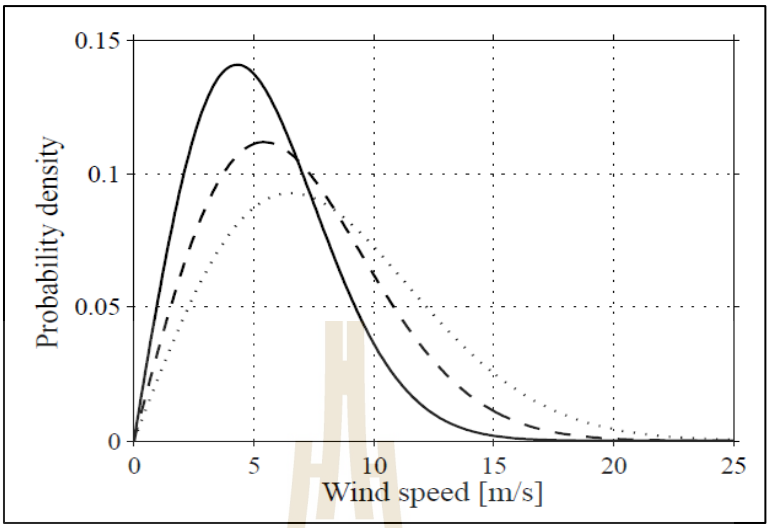

Figure 2.1 Probability density of the Rayleigh distribution.

2.3.20 Aerodynamic conversion

The work W done for moving an object from rest to a distance s is equal to the energy used,

$$E = W = Fs \tag{2.10}$$

The force F is given by,

$$F = ma \tag{2.11}$$

Where:

m = mass of air

a = acceleration

Hence,

$$E = mas \tag{2.12}$$

In the linear motion:

$$v^2 = u^2 + 2as \tag{2.13}$$

Where:

v = final velocity

u = initial velocity

s = distance

Hence:

$$a = \frac{v^2 - u^2}{2s} \tag{2.14}$$

Assuming that u is zero,

$$a = \frac{v^2}{2s} \tag{2.15}$$

Substituting (2.15) into (2.12), the K.E:

$$E = \frac{1}{2}mv^2 \tag{2.16}$$

Wind power is given by:

$$P = \frac{dE}{dt} = \frac{1}{2}v^2\frac{dm}{dt} \tag{2.17}$$

As the mass flow rate is given by:

$$\frac{dm}{dt} = \rho A \frac{dx}{dt} \tag{2.18}$$

Where:

A_r = Area swept by the rotor given by:

$$A = \pi r^2 \tag{2.19}$$

Differentiating the distance *x*, velocity is obtained:

$$\frac{dx}{dt} = v \tag{2.20}$$

This gives:

$$\frac{dm}{dt} = \rho A v \tag{2.21}$$

Hence, from (2.17), power can be defined as (Ghosh, 2015):

$$P = \frac{1}{2} \rho A v^3 \tag{2.22}$$

In 1919, Albert Betz proved that wind turbines cannot convert wind energy of more than 16/27 (59.3%) into mechanical energy (Wagner, 2017). This law is called Betz Limit or Betz' law. In other words, the theoretical maximum power efficiency of any wind turbine is 0.59. The constant is called the “power coefficient” $C_{p\max} = 0.59$

It has been proved that it is possible to convert only 0.35-0.45 of wind to mechanical energy for power generation even if the turbine is optimally designed.

Furthermore, taking into consideration other factors such as gearbox, bearings, mechanical losses, and others the system can convert only about 10-30% of the wind to electricity. By taking the power coefficient into account, the mechanical energy from the wind turbine is determined by the following (Yanning et al, 2009),

$$P = \frac{1}{2}\rho A_r C_p(\lambda, \beta) v^3 \tag{2.23}$$

$$\lambda = \frac{\Omega_r r_r}{\omega} \tag{2.24}$$

Where:

C_p = Power coefficient

β = Pitch angle

λ = Tip speed ratio

ω = Wind speed

Ω_r = Rotor speed

r_r = Rotor-plane radius

The $C_{p\max}$ obtained from the Betz limit is 0.593. The power coefficient C_p is obtained using a lookup table. The torque of the turbine is given by the ratio of the turbine output power to the low shaft speed, and is given by,

$$T_t = \frac{P_t}{\omega_t} \tag{2.25}$$

Where:

$C_{p\max}$ = turbine output power.

ω_t = shaft speed

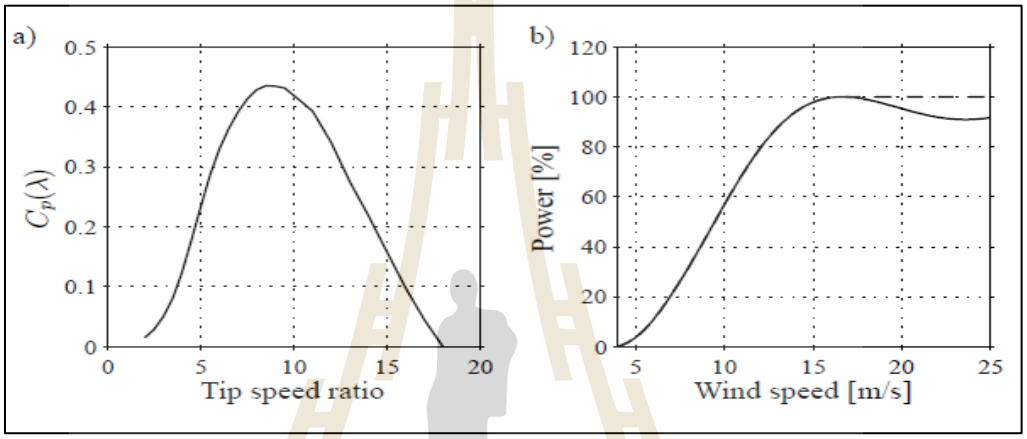

Figure 2.2 Power coefficient against tip speed ratio (LHS) and Mechanical power versus wind speed (RHS).

The mechanical torque and speed of the wind turbine drive train shaft are related to turbine torque, turbine speed, and gearbox ratio by using the equations below:

$$T_m = \frac{T_t}{G} \tag{2.26}$$

$$\omega_m = \omega_t G \tag{2.27}$$

Where:

T_t = The turbine torque

ω_t = The turbine speed

G = The gearbox ratio

2.3.21 Factors affecting power output

The amount of energy drawn from the wind is dependent on the following factors (Kelley, 2016):

1. The area swept out from the rotating blades.
2. The speed of the wind.
3. The efficiency of the gear-box generator devices.

Table 2.2 shows the power output of the WT for a given rotor diameter.

Table 2.2 Power output vs rotor diameter

Rotor diameter (m)	Kilowatt output (kW)
80	2500
72	2000
64	1500
54	1000
48	750
44	600
40	500
33	300
27	225

Wind speed usually increases with a rise in height (Kelley, 2016). This phenomenon is known as “wind shear”. This is because air friction is low at higher altitudes. Therefore, wind travels slower near the bottom. There are specific “roughness” values for various ground surfaces.

The parameters can be expressed in a block diagram shown in Figure 2.3 (Badran, 2009).

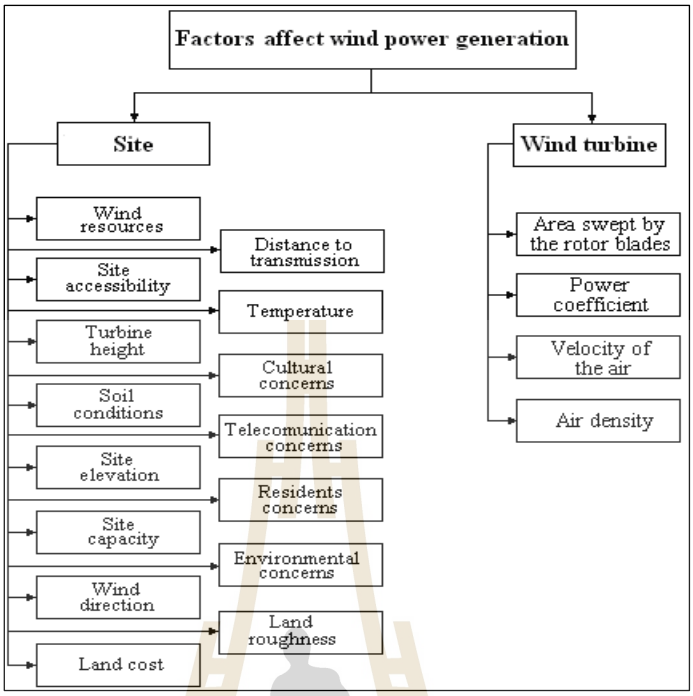

Figure 2.3 Block diagram of factors affecting wind power generation.

2.4 Grid codes requirements for a WT

This section presents and discusses the latest grid codes governing power production from the WT integrated into the utility grid to enhance the grid's generation capability. The analysis and comparison of the different requirements are performed and highlighted. The low voltage ride through (LVRT) capability, among the most vital prerequisites for the smooth day to day operation of the WT amid network disturbances, is discussed in detail.

Under normal working conditions, wind farms are required to be able to work persistently around the voltage and frequency variation limits. On the other hand, they should remain in operation and supply a specific active power output during a set period of frequency deviations from its rated value. The ability of the WT to continue operating despite wider frequency variation, bolster the network amid irregular

working conditions, and permit for a quick restoration of the overall system frequency. Wind turbine's designs take into consideration that, an unusual frequency may have some negative effects like generator windings overheating, insulation weakening, and damage to the power electronic devices. In many cases, there is a direct relationship between active power reduction and the frequency deviation from the nominal value.

Most grid codes allow the network operators to perform active power curtailment at a specified set-point. There are two options to achieve this action which are WTs disconnection or blades' pitch angle control. The latter limits the capability of the blades to extract power from the wind. There also grid codes concerning derivative of active power limitations known as maximum and minimum ramp-up and ramp-down rates which aim to protect the network from large frequency fluctuations mainly due to extreme wind conditions. These conditions may cause voltage steps of high magnitude and in-rush currents when the WT is started or stopped.

Wind turbines should be operating to support the grid in times of faults. This means that WTs should keep injecting power to the grid during a certain percentage of voltage deviation from the nominal value for the specified time durations. Disconnection is prohibited out of that limit. If the grid voltage is below the limit circuit breakers are programmed to disconnect WTs from the network.

Some codes introduced require a supply of reactive currents from the WTs to the network during grid faults to improve the performance of the network hence stabilizing the residual terminal voltages (Okedu et al, 2014). The optimal reactive power balance between the load and the grid ensures robust voltage control due to the direct proportionality between the voltage and the reactive power. Therefore, without

proper reactive power management, the system will always be in trouble with facing voltage instability conditions. The active power output control should work out to avoid a reduction in active power output during rated power operations of the generating plant. Many suppliers permit a tolerance ±0.5 Hz for the frequency to deviate from its rated value in the event of a sudden change in generation or load.

Some grid codes require wind power plants (WPP) to operate within a specific voltage and frequency range at the point of common coupling (PCC) to avoid instabilities caused by the grid disturbances (Altın et al, 2010). This requirement can be executed in the following three steps:

1. Stay connected within the nominal point limit.
2. Timely operation with possible output reduction is out of set limits.
3. Disconnect immediately if operating out of range.

Involvement in voltage recovery operations by continuing operation during voltage dips as low as 0 pu. to support the grid. This is done in the form of injecting reactive current and active power in faulty conditions.

Wind generation plants should remain in operation if a two-phase fault causes the voltage measured at the high voltage (HV) point of the generator at the PCC is higher than the grid voltage. The time of 0.07s is acceptable for wind generation plants to ride through a voltage swell of 1.3 p.u.

The codes governing the operation of the grids require grid-connected wind turbines to remain in operation even in the event of various faulty conditions to support the grid with power throughout the faulty duration to reinforce the stability of the DN (Chandrasekaran, 2014). They must additionally be in operation even during various voltage failures and attain power restoration once the system is in good

condition. In this thesis, a controller is designed to enable the DFIG to ride through various grid faults.

A few codes demand wind farms bigger than 50 MW be equipped with a frequency control device able to provide essential and auxiliary frequency control mechanism which will protect the DFIG against over-frequency. Moreover, some codes need tests to be conducted to check the capability of wind farms for the above frequency response requirement. Other codes need wind power plants (WPPs) to grant active power increment or diminish active power supply corresponding to the changes in frequency at the PCC. The frequency control mechanism must work as a droop controller in varying between 0.02 and 0.06 p.u. based on WPP ratings. The response speed is 10% of the rated value in 250 ms.

2.5 Doubly fed induction generator

Power utilities prefer doubly-fed induction generator (DFIG) as the best generator for wind energy power production. This is due to its benefits as compared to alternative forms of generators. A number of these benefits are the ability to contribute to the grid's power needs, the smaller size of its converters, approximately half of the machine rating, and its ability to work at variable speeds. This has motivated many researchers to have the interest to try and do researches on this induction machine.

The generator connected to the grid is as shown in Figure 2.4. The stator of this generator is attached to the grid. The rotor is fed by the bidirectional converter referred to as the RSC. Another converter is called a grid side converter. Both converters have controls.

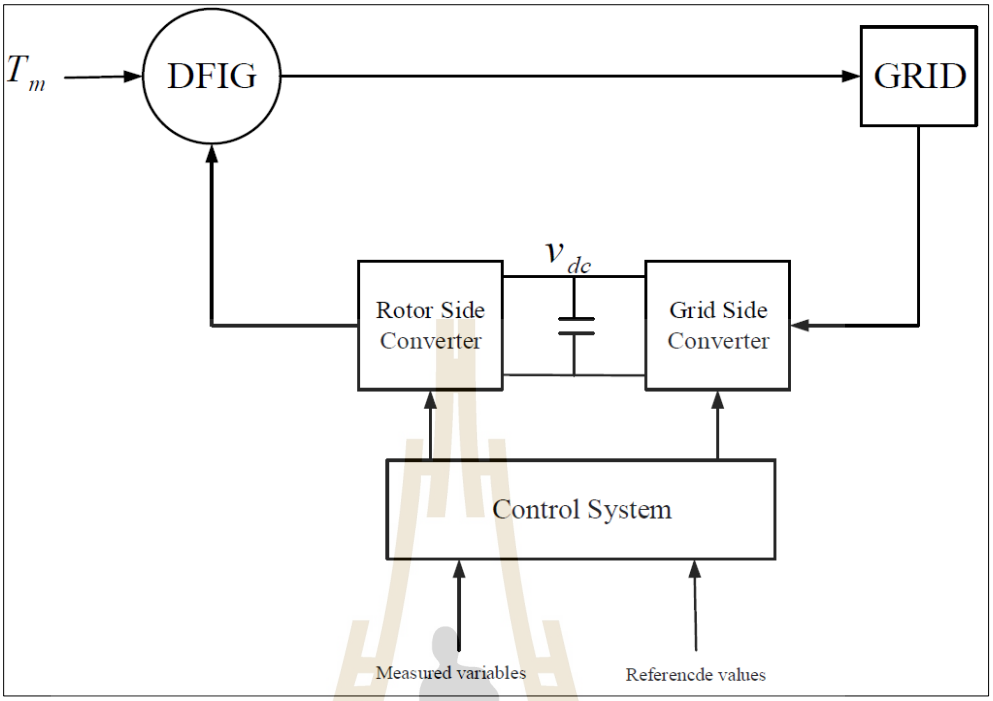

Figure 2.4 Doubly fed induction machine-based wind turbine with a controller.

The stator is powered by the grid's three-phase voltages. The amplitude and frequency of this voltage are always constant. This arrangement causes the flux in the stator windings. The rotor also receives three-phase voltages from the RSC. This voltage is different in terms of amplitude and frequency and this allows different operating conditions of the generator. All this is possible due to the application of back-to-back three-phase converters. These converters, at different sides of the DC bus, are responsible for supplying the specified rotor voltages for controlling the general DFIG operation. Additionally, the converters support the power exchange between the machine and the grid. Therefore, the stator consists of three windings that are shifted 120 degrees and some pairs of poles. A balanced three-phase voltage of constant frequency supply power to the three stator windings to

generate stator flux. This stator flux rotates at synchronous speed given by the following expression:

$$\omega_s = \frac{60 f_s}{p} \left(rev/\min \right) \tag{2.28}$$

The stator frequency ω_s , rotor frequency ω_r , and rotor electrical speed ω_m are related as follows:

$$\omega_s = \omega_r + \omega_m \tag{2.29}$$

Pole pairs determine the relationship between the mechanical speed of the shaft and the synchronous speed of the machine:

$$\omega_m = p\Omega_m \tag{2.30}$$

The slip s of the machine is the ratio of the rotor speed to the synchronous speed as shown below:

$$s = \frac{\omega_s - \omega_m}{\omega_s} = \frac{\omega_r}{\omega_s} \tag{2.31}$$

Equation (2.31) can be written as,

$$\omega_r = s\omega_s \tag{2.32}$$

The relation between the rotor and stator frequencies is,

$$f_r = sf_s \tag{2.33}$$

Slip sign can be used to distinguish three operating modes for the machine:

$$\omega_m < \omega_s \Rightarrow \omega_r > 0 \Rightarrow s > 0 \Rightarrow Subsynchronous \tag{2.34}$$

This happens throughout the slow wind speeds. The rotor is fed by a DC bus condenser via the RSC. A GSC is employed to manage the DC bus voltage. This scheme makes the DFIG absorb power from the grid. The GSC works as a rectifier and RSC as an electrical converter. The grid receives power from the stator.

$$\omega_m > \omega_s \Rightarrow \omega_r > 0 \Rightarrow s < 0 \Rightarrow Hypersysnchronous \tag{2.35}$$

This condition occurs at higher wind speeds. The power produced is sent to the grid by the rotor via the voltage source inverters. Using the power supplied by the rotor, the DC capacitor of the DFIG raises the DC link voltage to the desired level. The GSC is liable to maintain the DC-link voltage constant. Power is extracted from the rotor RSC and delivered to the grid. The RSC works as a rectifier and therefore the GSC as an electrical converter. The output power is delivered to the grid by the stator and via the VSCs by the rotor. The rotor power is inductive.

$$\omega_m = \omega_s \Rightarrow \omega_r = 0 \Rightarrow s = 0 \Rightarrow Synchronous \tag{2.36}$$

The RSC provides DC excitation for the rotor. The induction machine runs as a synchronous generator. The RSC will not offer any reasonably AC power to the

rotor winding causing the rotor power to be zero. Despite this condition, the reactive power of a considerable amount will still be injected into the grid by the RSC.

2.6 Voltage dips

Voltage dips also called “voltage sags” are short-duration (less than 1 minute) reductions in voltage magnitude. Regarding the number of changes in RMS voltage, voltage dips fall into general types: single-stage (normal) voltage dips and multi-stage voltage dips. The normal voltage dip corresponds to the events that present just one level change in RMS voltage while multi-stage voltage dips show the sudden changes in RMS voltage.

2.6.1 Voltage dip characteristics

Voltage dips are qualified and quantified by several characteristics (Bagheri, 2016). The characteristics can be calculated as a single value, for instance, voltage dip magnitude and duration, or calculated as continuous values versus time. Single-event characteristics are calculated from the characteristics as a function of time. Some of the single-event characteristics are listed below:

- Residual Voltage

The lowest voltage magnitude during the event is considered as residual voltage.

- Dip duration

Is the total time from when the voltage magnitude of one or more phases falls below the threshold value (90% of nominal value) until all phases recover above the threshold.

- Point-on-wave of voltage recovery.

The point-on-wave of voltage recovery is the phase angle of the fundamental voltage wave at which the main recovery takes place.

- Missing voltage.

The maximum missing voltage is a single-event characteristic that describes the change in momentary voltage experienced by the equipment.

2.6.2 Voltage dips causes

Temporary or short-duration increases in current magnitudes lead to short duration reductions in voltage magnitude and consequently voltage dips (Bagheri, 2016). There are several causes for such increases in current, some of the most important origins are:

1. Power system faults.
2. Load switching.
3. Switching of transformers.
4. Network Switching.
5. Power Swing.

Short-circuit and earth fault are presented as the major cause of severe voltage dips in the DN (Bagheri, 2016). Electrical faults may be divided into balanced faults (three-phase faults) and unbalanced faults including all types of single-phase and two-phase faults. The voltage dips caused by the three-phase fault can be more severe than the others. However, the number of three-phase (balanced) faults is less than the number of unbalanced faults. The typical types of unbalanced faults are single-phase faults and phase-to-phase faults.

Switching loads onto the supply can result in voltage dips (Bagheri, 2016). Both types of switching, inside or outside of the plant, can affect the voltage. The direct online induction motors are the main type of loads resulting in voltage dips. The voltage dip caused by the starting of the induction motor is a balanced dip type which is featured by prompt voltage drop in all phases at the start and slow recovery after that.

The voltage dip caused by transformer energizing is similar to the voltage dip caused by motor starting in terms of sudden voltage drops and slow recovery (Bagheri, 2016). But this type of voltage dip shows different voltage drops in the different phases. Additionally, heavy even-harmonic distortion is present in the voltages during transformer energizing.

Switching on either the supply system or the internal distribution network of the plant can lead to different types of voltage dips (Bagheri, 2016). Paralleling two supplies or running at different phase-angles, results in voltage transients before setting at the new steady-state magnitude and phase-angle. The resulting events are not typically classified as voltage dip because they are either too short (as with capacitor energizing) or too shallow (as with load connection). However, their impacts on equipment are similar to the impact of short or shallow voltage dips.

Either because of the loss of transmission lines or after several faults on the supply network, power swings occur between generating stations and lasting several seconds on the network (Bagheri, 2016).

2.6.3 DFIG under voltage dips

Voltage dip phenomenon causes over current and over-voltages within the rotor windings. This condition can harm the converter connected to the terminals of the DFIG in case no countermeasures are introduced (Abu-Rub, et. al., 2014).

2.6.3.1 Electromagnetic force induced in the rotor

Rotor voltage expression can be written as (Abu-Rub, et. al., 2014),

$$\vec{v}_r^{\,r} = R_r \vec{i}_r^{\,r} + \frac{d}{dt}\vec{\psi}_r^{\,r} \tag{2.37}$$

The relation between rotor flux and the stator flux can be calculated as,

$$\vec{\psi}_r^{\,r} = \frac{L_m}{L_s}\vec{\psi}_s^{\,r} + \sigma L_r \vec{i}_r^{\,r} \tag{2.38}$$

Combining (2.37) and (2.38), the following expression is obtained:

$$\vec{v}_r^{\,r} = \frac{L_m}{L_s}\frac{d}{dt}\vec{\psi}_s^{\,r} + \left(R_r + \sigma L_r \frac{d}{dt}\right)\vec{i}_r^{\,r} \tag{2.39}$$

Thus, the rotor voltage induced in the rotor by the stator flux is the voltage in the rotor open-circuit terminals (where $i_r = 0$) given by the following expression,

$$\vec{e}_r^{\,r} = \frac{L_m}{L_s}\frac{d}{dt}\vec{\psi}_s^{\,r} \tag{2.40}$$

In the stator reference frame,

$$\vec{e}_r^{\,s} = \frac{L_m}{L_s}\left(\frac{d}{dt}\vec{\psi}_s^{\,s} - j\omega_m\vec{\psi}_s^{\,s}\right) \tag{2.41}$$

In the presence of current in the rotor, the second term in (2.39) emerges. This is caused by the voltage drop in both the rotor resistance R_r and the rotor transient inductance σL_r.

2.6.3.2 The normal operation of the machine

Under normal operation, the grid is balanced and the three-phase voltages are shifted by an angle of 120^o (Abu-Rub, et. al., 2014).

$$\begin{aligned} v_a &= \hat{V}_g \cos(\omega_s t + \varphi) \\ v_b &= \hat{V}_g \cos(\omega_s t + \varphi - 2\pi/3) \\ v_c &= \hat{V}_g \cos(\omega_s t + \varphi - 4\pi/3) \end{aligned} \tag{2.42}$$

The space vector of the stator voltage $\hat{V}_g$ rotates at synchronous speed ω_s and is given by,

$$\vec{v}_s^{\,s} = \hat{V}_g e^{j\varphi} e^{j\omega_s t} = \sqrt{2}\underline{V}_g e^{j\omega_s t} \tag{2.43}$$

Where:

$\hat{V}_g$ = grid voltage phasor.

The stator resistance R_s is very small in such a way that its voltage drop (about 1% in a multi-megawatt machine) can be neglected. Neglecting it, the stator flux is found to be,

$$\underline{\psi}_s = \frac{\underline{V}_g}{j\omega_s} \tag{2.44}$$

So, under steady-state conditions, the stator flux space vector is given by this expression:

$$\vec{\psi}_s^{\,s} = \sqrt{2}\underline{\psi}_s e^{j\omega_s \cdot t} = \frac{\widehat{V}_g e^{j\varphi}}{j\omega_s} e^{j\omega_s t} \tag{2.45}$$

Expressing the variable flux across the rotor in the rotor reference frame:

$$\vec{\psi}_s^{\,r} = \vec{\psi}_s^{\,s} e^{-j\omega_m \cdot t} = \sqrt{2}\underline{\psi}_s e^{j(\omega_s - \omega_m)t} = \sqrt{2}\underline{\psi}_s e^{j\omega_r t} \tag{2.46}$$

The emf induced in the rotor due to this flux is given by the following expression:

$$\vec{e}_r^{\,r} = \frac{L_m}{L_s}\frac{d}{dt}\vec{\psi}_s^{\,r} = j\omega_r \frac{L_m}{L_s}\vec{\psi}_s^{\,r} \tag{2.47}$$

Expressing the amplitude of this emf as a function of the stator voltage:

$$\left|\hat{E}_r\right| = \omega_r \frac{L_m}{L_s} \frac{\hat{V}_g}{\omega_s} = \hat{V}_g \frac{L_m}{L_s} s \tag{2.48}$$

2.6.3.3 Voltage dips analysis

This phenomenon can be described as a sudden drop in grid voltage, caused by contingencies, disturbances, or faults occurring in the power system (Abu-Rub, et. al., 2014). There are two types of voltage dips known as symmetric voltage dip and asymmetric dip.

In a grid-connected DFIG, the behavior of stator flux during voltage dip is given by:

$$\frac{d\vec{\psi}_s^s}{dt} = \vec{v}_s^s - \frac{R_s}{L_s}\vec{\psi}_s^s + R_s \frac{L_m}{L_s}\vec{i}_s^s \tag{2.49}$$

$$\frac{d\vec{\psi}_s^s}{dt} = \vec{v}_s^s - \frac{R_s}{L_s}\vec{\psi}_s^s + R_s \frac{L_m}{L_s}\vec{i}_s^s \tag{2.50}$$

It may be noticed that during an abrupt voltage dip, the speed of the stator flux to reach its final steady-state is slow as opposed to the stator voltage. An equivalent circuit (modified) of the DFIG for voltage dip analysis is shown in Figure 2.5.

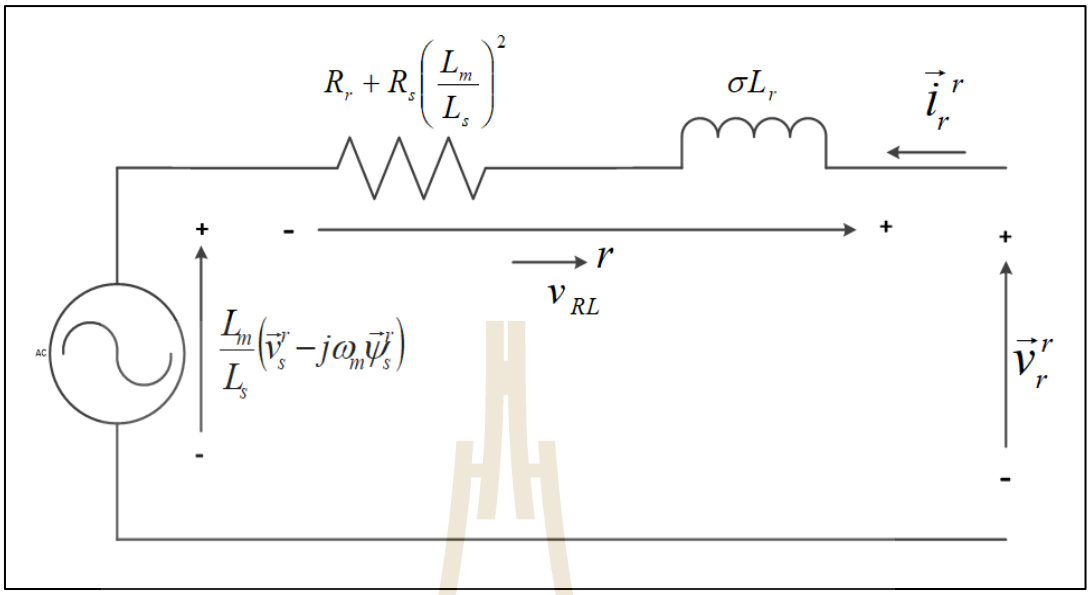

Figure 2.5 Modified equivalent circuit of the DFIG for the analysis of voltage dips.

From the equivalent circuit, the rotor voltage vector is given by the following expression,

$$\vec{v}_r^{\,r} = \frac{L_m}{L_s}\left(\vec{v}_s^{\,r} - j\omega_m\vec{\psi}_s^{\,r}\right) + \left[R_r + \left(\frac{L_m}{L_s}\right)^2 R_s\right]\vec{i}_r^{\,r} + \sigma L_r \frac{d}{dt}\vec{i}_r^{\,r} \qquad (2.51)$$

The space vector plot at sub synchronous speed is shown in Figure 2.6.

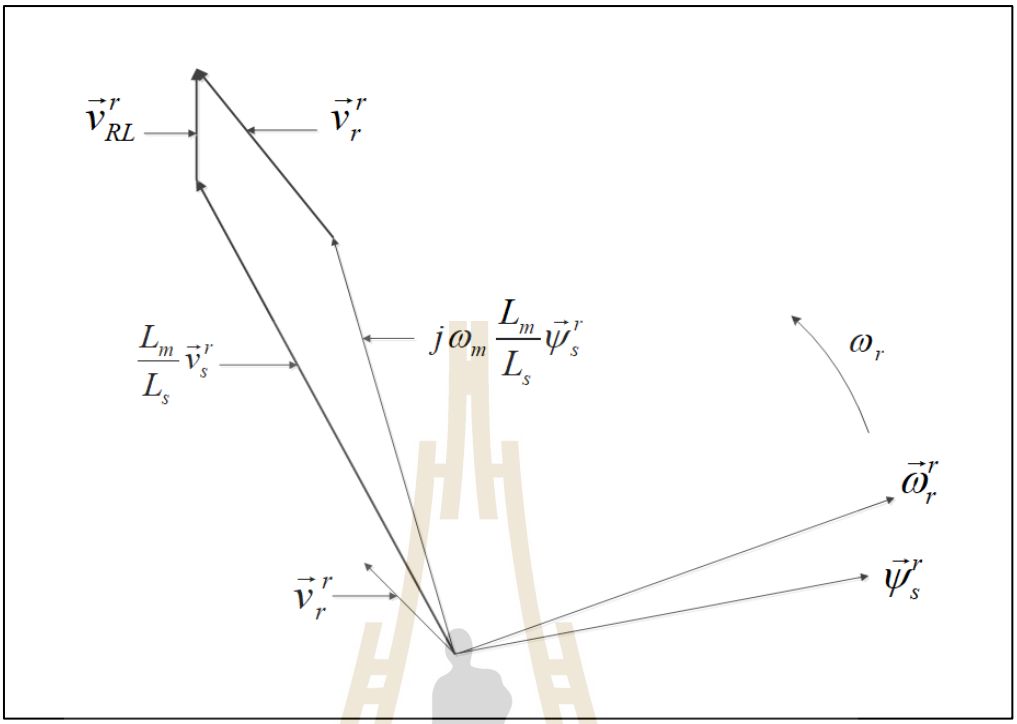

Figure 2.6 Space vector diagram at sub synchronism in a generator mode.

Hence, when the machine works close to steady-state and a sudden stator voltage dip happens, the variation in the stator voltage causes a sudden rotor voltage change happens to prevent a high increase in the rotor current. Note that, since the stator flux diminishes gradually (a few cycles depending on the machine), as shown in Figure 2.7, the desired rotor voltage gets to be higher than at a steady-state, owing to the change caused by the voltage dip.

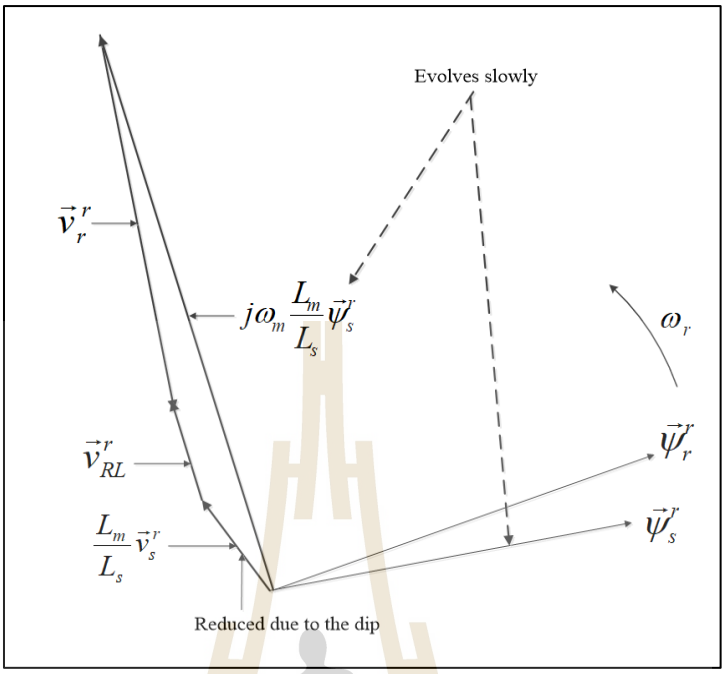

Figure 2.7 Evolution of the space vector magnitudes at the transient period.

In Figure 2.8 the new steady-state of the stator flux and voltage is reached, which is comparative to the one obtained just before the dip. The contrast seen is the amount of lower amplitude due to the stator voltage being diminished. This causes a lower electromagnetic torque and reactive power.

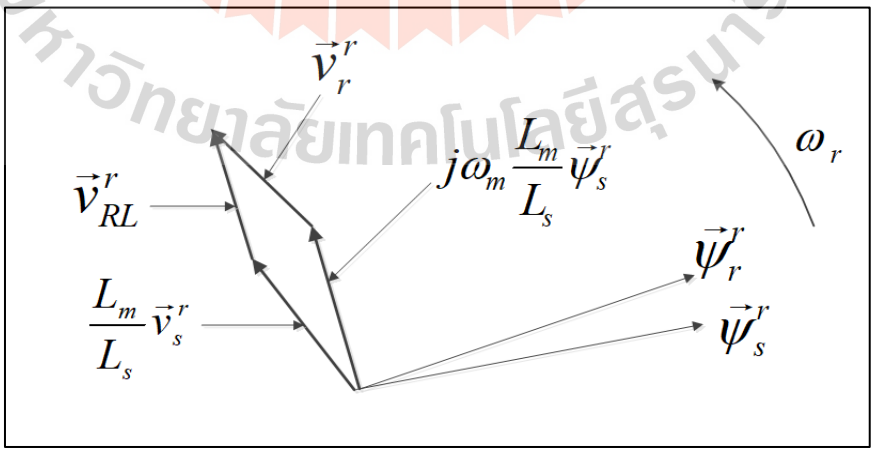

Figure 2.8 Evolution of the space vector magnitudes at a new steady state.

To get rid of the loss of control by keeping up the rotor currents inside their secure limits (no high increase), it is vital to extend rotor voltage levels, as soon as the voltage dip begins. The worst-case situation happens when the stator voltage dip is 100%. At this point, the rotor voltage should overhaul the stator voltage that has vanished. Unfortunately, the standard capability of the converter controlling the rotor can only inject a maximum of around 1/3 of the stator voltage. Subsequently, due to this restriction (converter restriction), these sorts of generators cannot keep up the rotor current inside its secure limits, without losing control amid serious voltage plunges.

2.6.3.4 Asymmetric voltage dips phenomenon

In most cases, the faults that cause voltage dips don't affect the three phases in the same way. The most common fault in electrical networks is a single line to ground short-circuit but the, short-circuit between two lines might also be frequent in the power system (Abu-Rub, et. al., 2014).

In such a situation, the remaining voltage is not the same in all three phases, and/or the system voltages are no longer shifted by 120^{o}. In a condition like this, the system becomes unbalanced or asymmetrical. The problem of asymmetrical fault in the power systems has been studied using the symmetrical component method, developed by Charles Legeyt Fortescue.

2.6.3.5 Fundamentals of the symmetrical component method

In a balanced system, the voltages of the three phases have the same amplitude, and their waveforms are 120^{o} (or $2\pi/3$ radians) offset in time. Using the phasor notation, the voltages can be represented by (Abu-Rub, et. al., 2014).

$$\begin{bmatrix} \underline{V_a} \\ \underline{V_b} \\ \underline{V_c} \end{bmatrix} = \begin{bmatrix} \hat{V}_g e^{j\varphi} \\ \hat{V}_g e^{j\varphi - 2\pi/3} \\ \hat{V}_g e^{j\varphi - 4\pi/3} \end{bmatrix} = \hat{V} e^{j\varphi} \begin{bmatrix} 1 \\ a \\ a^2 \end{bmatrix} \tag{2.52}$$

Where "a" is a vector of 120^o. It is easy to see that $a^2 = a^* = 1\angle 240^o$, $a^3 = 1$, and $1 + a + a^2 = 0$. Thus, any phasor can be decomposed as the addition of three phasors of a balanced system. These three balanced systems are called:

The positive sequence "abc", represented by subscript 1.

1. The negative sequence "abc", represented by subscript 2.
2. The zero sequence, represented by subscript 0.

A balanced system has only a positive sequence. When building an inverse system by switching two of the phases, the system will have a negative sequence only. In situations other than these, the system can have three sequences. When these three sequences of voltage are added will give the voltage in one phase.

This means that a line-to-ground short-circuit in phase "a" originates a single-phase voltage dip. In this condition phases "b" and "c" remain almost unchanged while phase "a" drops. With the symmetrical component method, this unbalanced system can be decomposed into the named three sequences. The three sequences can be summed to the original voltages.

For the most part, due to this condition, wind turbines of DFIG type apply additional crowbar security to handle excessive voltage dips conditions. It

has to be recognized that related conditions may occur at hypersynchronous speeds additionally while the machine is subjected to deviated voltage dips. In this manner, it is recommended that once a serious voltage dip happens, when the stator flux is evolving, there may be a brief period a generator loses control. The loss of control causes over-currents in the stator windings and the rotor of the generator until the flux is sufficient such that the converter voltage can guarantee the generator control. Therefore, DFIG needs to be protected because the loss of control causes over-currents within the rotor of the induction machine. Besides high rotor currents, the DFIG also experiences negative sequence currents and over-voltages at its DC bus. Under these circumstances, the DFIG needs enhancement in its control strategy. This study proposes a Fuzzy-PI dual control strategy to deal with the negative sequence and harmonics arising after faults due to the imbalance in the system.

2.7 Chapter summary

Introduction to wind energy is discussed. An extensive review of distributed generation technology is part of this study. A brief review of renewable and nonrenewable DG technologies can be found in this chapter. Wind energy, in general, is explained in detail. Some of the topics discussed are wind energy conversion systems, aerodynamic power control, and aerodynamic conversion. The wind turbine model and modeling of the drive train system are presented. Wind turbine generators are described in short. Grid connection requirements and the international grid codes for LVRT and HVRT requirements are presented and compared. The DFIG is introduced and explained in detail. Voltage dips analysis is part of this chapter.

CHAPTER III

METHODOLOGY

3.1 Control theory

Control theory deals with the analysis and design of the controllers for dynamical systems in engineered processes and machines. The theory learned enables the designer to develop a control model for optimally controlling the system avoiding delay or overshoot and ensuring system stability. The required system characteristics are specified, designed, or synthesized.

3.1.1 Control systems types

The two types mostly known are:

i. Regulator – maintaining a designated characteristic regardless of the perturbations.

ii. Servo mechanism– negative feedback is used to correct the action of the mechanism.

3.1.2 State-space model of a system

Consider a continuous-time state-space model

$$\dot{x}(t) = Ax(t) + Bu(t)$$ - Is the state equation (3.1)

$$y(t) = Cx(t) + Du(t)$$ - Is the measurement equation (3.2)

3.1.3 Open-loop transfer function

The transfer function of the system describes the input/output relation of the system.

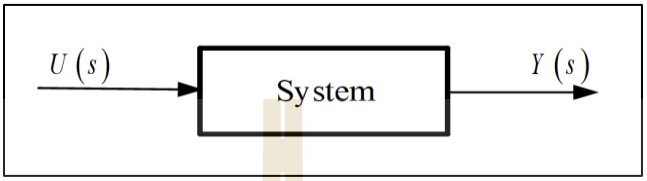

Figure 3.1 An open loop system with input/output signals.

The transfer function of the system shown in Figure 3.1 is given by (3.3) and represented by Figure 3.2.

$$G(s)=\frac{Y(s)}{U(s)} \tag{3.3}$$

Figure 3.2 Transfer functions in the open-loop control system.

3.1.4 Closed-loop transfer function

The system is shown in Figure 3.6. Equation (3.4) shows the transfer function representation of the system.

$$G(s)=\frac{G(s)}{1+G(s)H(s)} \tag{3.4}$$

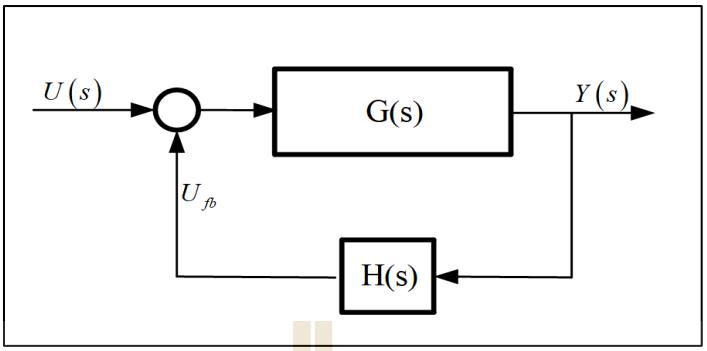

Figure 3.3 Transfer functions in the closed-loop control system.

3.1.5 Closed-loop control system

Some of the parts of a control system are:

i. Sensor – measures a variable or signal

ii. Plant –A controlled system.

iii. Controller – Uses the error signal to control the system

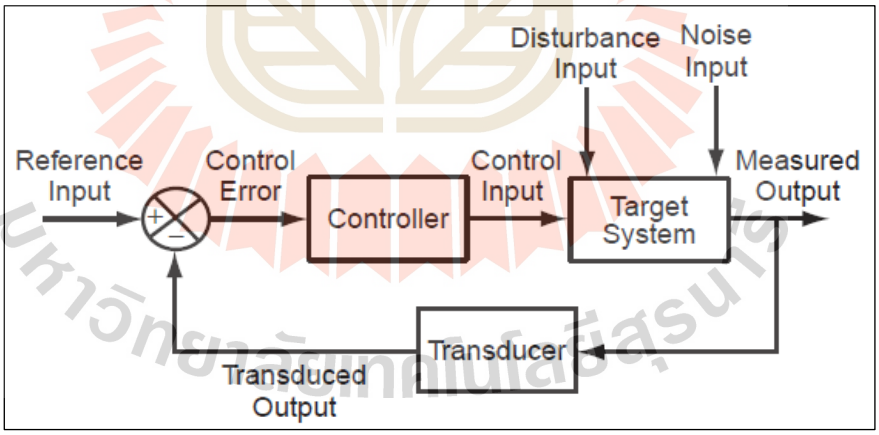

Figure 3.4 Closed-loop control.

The closed-loop system developed may be a system in which the inputs are determined, by the output of the system.

3.1.6 Feedback control loop

Feedback is a return path created in the system to feedback the output to the input for controlling the system itself. This loop created is termed as the feedback path. The feedback maintains stability during a system despite external changes.

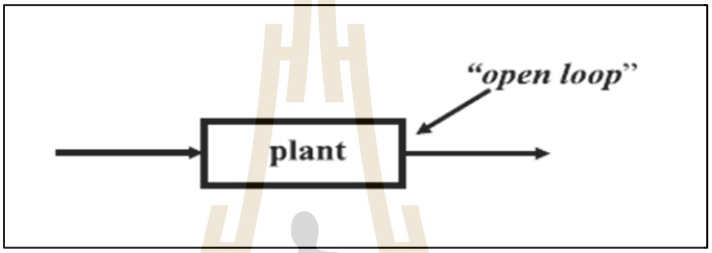

Figure 3.5 Open-loop control system.

To improve the plant performance, the output of the system is observed and appropriate correction is applied by adding feedback signal to the system (Simrock, 2008).

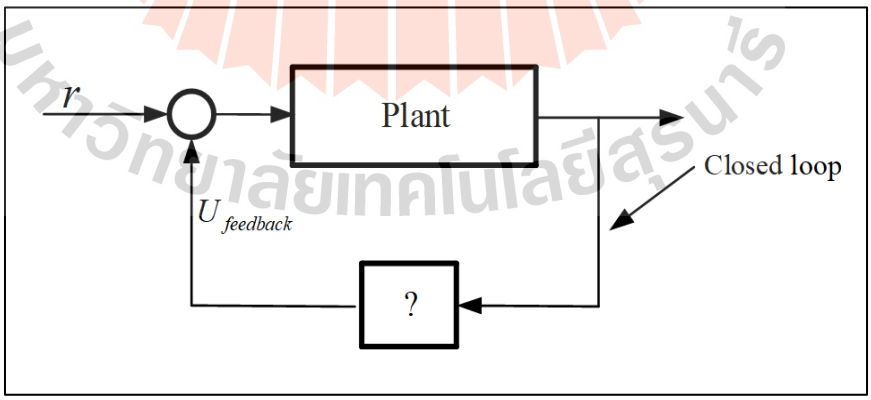

Figure 3.6 Closed-loop control system with feedback.

3.1.7 Full state feedback

From a system depicted by (3.1) and (3.2). The input control for the controlled system is given by,

$$u = -K_1 x_1, -\cdots, -K_n x_n = -Kx \tag{3.5}$$

Where:

$$k = \begin{bmatrix} k_1 \cdots k_n \end{bmatrix}$$

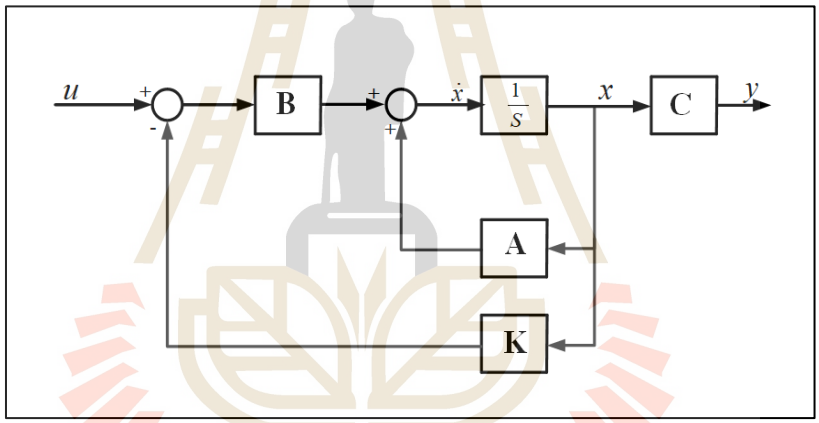

Figure 3.7 State-space representation of the full state feedback control system.

The state-space equation with feedback is given by,

$$\dot{x} = Ax + B\left(u + u_{fb}\right) \tag{3.6}$$

Expanding, the equation becomes,

$$\dot{x} = Ax + Bu + Bu_{fb} \tag{3.7}$$

The feedback control law is given by,

$$u_{fb} = -Kx \tag{3.8}$$

Substituting (3.8) into (3.7) gives,

$$\dot{x} = Ax + Bu - BKx \tag{3.9}$$

Finally, (3.9) state feedback is,

$$\dot{x} = \left(A - BK\right)x + Bu \tag{3.10}$$

$$y = Cx \tag{3.11}$$

Therefore, a new closed-loop matrix is given by,

$$A_{cl} = \left(A_{ol} - BK\right) \tag{3.12}$$

Eigenvalues of the new matrix offer information regarding the controllability of the system. The linear time-invariant system (3.1), (3.2) is controllable if some inputs may transfer the initial state of the system to the origin.

3.1.8 Classical control theory

This strategy is based on a proportional integral derivative (PID) controller. This control methodology is the conventional control strategy that has been used for decades to control several systems. The function of the PID controller is to make the measured output to track the reference input of the controlled system by

minimizing the error between them. This error is used to calculate an accurate signal value to produce the corrective action that may modify the system in step with the requirement of the controller designer.

This controller is the combination of three control actions; the proportional, the integral, and the derivative. The proportional term decides the response to this error, the integral term decides the response depending on the present error, and therefore the derivative term decides the response based on the speed at which the error has been evolving. The weighted total of the three terms is used to change the system behavior.

This control mechanism name is depicted from its three rectifying terms, whose entirety comprises the controlled variable (MV) as,

$$MV(t) = P_{out} + I_{out} + D_{out} \tag{3.13}$$

Where P_{out}, I_{out}, and D_{out} contribute to the output from the PID controller.

3.1.8.1 Proportional term

This term is responsible for the improvement of the output. This output is directly related to the present error obtained. Then, the response is adjusted by multiplying the error by a proportional gain K_P.

The output of this term is,

$$P_{out} = K_p e(t) \tag{3.14}$$

Where:

P_{out} : Proportional term output

e : Error = $SP - PV$

t : Instantaneous time

3.1.8.2 Integral term

There is a proportionality between the contribution of the integral term and the magnitude and the lasting of the error.

$$I_{out} = K_i \int_0^t e(\tau) d\tau \tag{3.15}$$

Where:

I_{out} : Output integral term

K_i : Integral gain

τ : Previous time

This term speeds up the execution of the procedure in the direction of the desired output by removing the steady-state error present than when applying a proportional controller alone.

3.1.8.3 Derivative term

The pace of progress of the state error is decided by deciding the slant of the error once a while (for example its first derivative w.r.t. time) and multiplying the results by K_d .

The derivative term is given by:

$$D_{out} = K_d \frac{de}{dt} \tag{3.16}$$

Where:

D_{out} = Output derivative term.

K_d = Derivative gain.

Then, the output from proportional, integral, and derivative terms is added together. In terms of the PID gains and the error, the controller output *u(t)* can be written as,

$$u(t) = MV(t) = K_p e(t) + K_i \int_0^t e(\tau) d\tau + K_d \frac{de}{dt} \quad (3.17)$$

Several methods are available for PID loop tuning. These methods normally contain the improvement of the system model, selecting the P, I, and D to support the dynamic modal parameters. It has been seen that most of the standardization approaches are comparatively inefficient.

3.1.8.4 PD Controller

The controller transfer function is,

$$G_c(s) = K_p(1 + T_d s) \quad (3.18)$$

Where:

K_p = proportional gain

T_d = derivative time

Constants K_p and T_d are the controller parameters. Equation (3.18) can also be written as,

$$G_c(s) = K_p + K_d s \quad (3.19)$$

Where:

K_d = derivative gain, note that $K_d = K_p T_d$

In this case K_p and K_d are the controller parameters to be determined. PD introduces zero at,

$$s = -\frac{1}{T_d} = -\frac{K_p}{K_d} \tag{3.20}$$

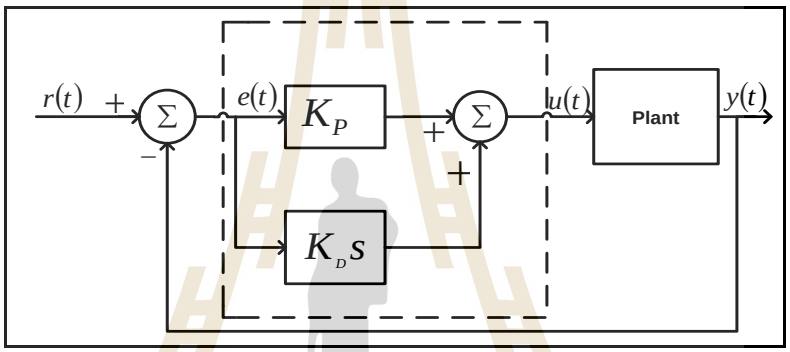

Figure 3.8 A system with proportional and derivative gains.

Given the input to the PD controller as the error $e(t)$, then the output is given by:

$$u(t) = K_p \left[e(t) + T_d \frac{de(t)}{dt} \right] \tag{3.21}$$

3.1.8.5 PI Controller

The controller transfer function is,

$$G_c(s) = K_p \left(1 + \frac{1}{T_i s} \right) \tag{3.22}$$

Where:

T_i = integral time

Constants K_p and T_i are the controller parameters. Equation (3.22) can also be written as,

$$G_c(s) = K_p + \frac{K_i}{s} \tag{3.23}$$

Where:

K_i is the integral gain.

Note that $K_i = \frac{K_p}{T_i}$.

In this case, K_p and K_i are the controller parameters to be determined. PI introduces zero at $s = -\frac{1}{T_i} = -\frac{K_i}{K_p}$ and a pole at $s = 0$. Hence PI increases the type of the system by 1.

If the error signal $e(t)$ is the PI controller input, then the controller output (actuating signal) is given by:

$$u(t) = K_p\left[e(t) + \frac{1}{T_i}\int_0^t e(t)dt\right] \tag{3.24}$$

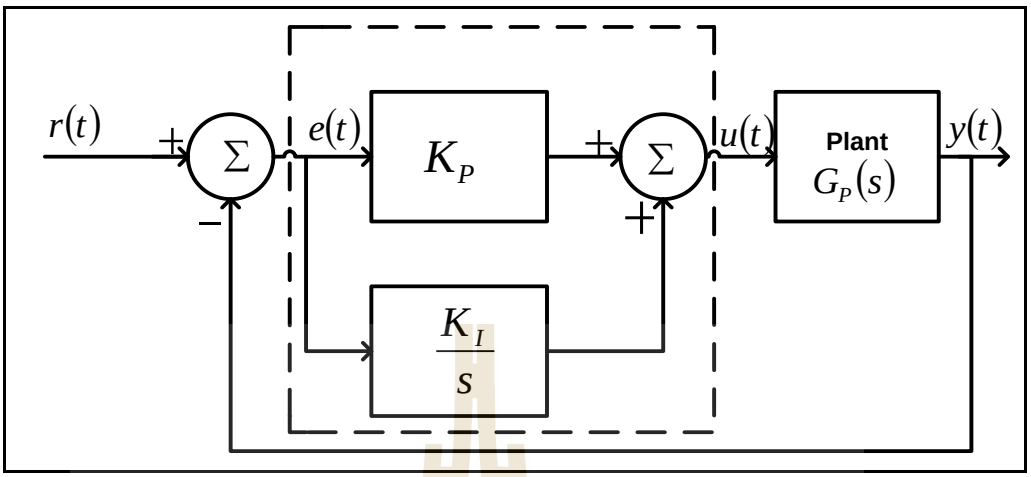

Figure 3.9 Proportional and integral gains in a closed-loop system.

3.1.8.6 PID Controller

The controller transfer function is,

$$G_c(s) = K_p\left(1 + \frac{1}{T_i s} + T_d s\right) \tag{3.25}$$

Constants K_p, T_i and T_d are the controller parameters. Equation (3.25) can also be written as,

$$G_c(s) = K_p + \frac{K_i}{s} + K_d s \tag{3.26}$$

In this case K_p, K_i and K_d are the controller parameters to be determined. If the error $e(t)$ is the PID controller input, then the controller output (actuating signal) is given by:

$$u(t) = K_p\left[e(t) + \frac{1}{T_i}\int_0^t e(t)dt + T_d\frac{de(t)}{dt}\right] \tag{3.27}$$

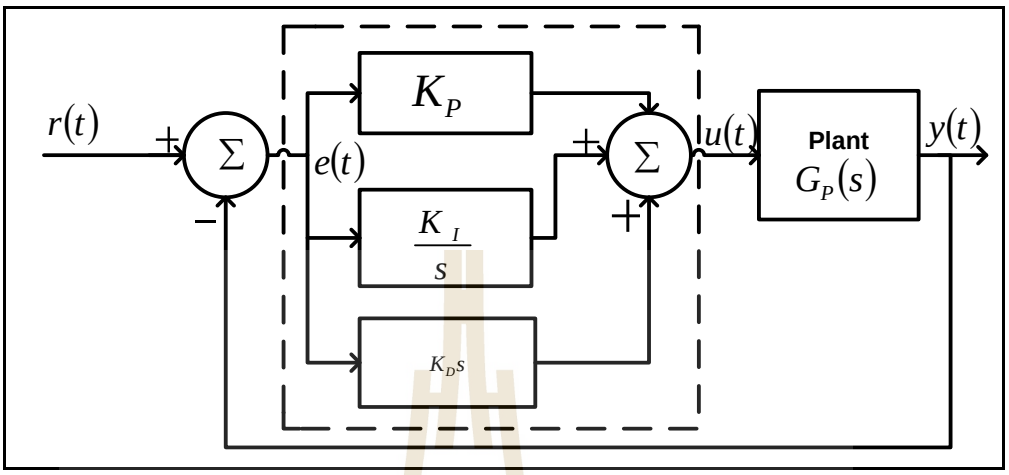

Figure 3.10 Proportional, integral, and derivative gains in a closed-loop system.

PID controller will have both properties of PI + PD and where their properties contradict each other PID will compensate the properties to somewhere in between.

3.1.9 Transformations theory

The voltage and current determine the behavior of the three-phase machines. These parameters can be transformed into different rotating frames to meet the needs of the controller designer. The frames are:

i. Clarke Transformation

ii. Park Transformation

These transformations can be used to transform voltages or currents from one reference frame to the other. The reference frames involved are a three-phase stationary reference frame, two-phase stationary reference frame, and two-phase rotating reference frame. The methods are highly applied in vector control techniques for electrical machines.

3.1.9.1 Clarke Transformation

In this methodology, the three-phase parameters are transformed from the three-phase frame of reference to the two-axis orthogonal stationary frame of reference. The transformation may be given by the subsequent equations:

$$I_\alpha = \frac{2}{3} I_a - \frac{1}{3}\left(I_b - I_c\right) \tag{3.28}$$

$$I_\beta = \frac{2}{\sqrt{3}}\left(I_b - I_c\right) \tag{3.29}$$

Where:

I_a, I_b, and I_c are three-phase quantities

I_α and I_β are stationary orthogonal reference frame quantities

When I_α is superimposed with I_a and $I_b + I_b + I_c = 0$, I_a, I_b and I_c can be transformed to I_α and I_β as:

$$I_\alpha = I_a$$

$$I_\beta = \frac{1}{\sqrt{3}}\left(I_a + 2I_b\right) \tag{3.30}$$

Where:

$$I_b + I_b + I_c = 0$$

3.1.9.2 Inverse Clarke Transformation

The parameters are transformed from a two-axis stationary reference frame to another stationary reference frame in a three-phase configuration derived by the following equations:

$$V_a = V_\alpha$$

$$V_b = \frac{-V_\alpha + \sqrt{3} * V_\beta}{2} \tag{3.31}$$

$$V_c = \frac{-V_\alpha - \sqrt{3} * V_\beta}{2} \tag{3.32}$$

Where:

$V_a V_b V_c$ = The voltages in a three-phase stationary reference frame.

$V_\alpha V_\beta$ = The voltages in a two-phase stationary reference frame.

3.1.9.3 Park Transformation

In this approach, the two-axis stationary reference frame parameters are transformed into a two-axis rotating reference frame.

3.1.10 Optimal control theory

The method searches for a control law for a given system in iteration mode considering the stopping criterion. The problem to be controlled consists of an objective function comprising of state and control variables. The control law $u_{fb}(k)$ is found which is used to move the state vector $x(k)$ to zero quickly subject to the initial condition.

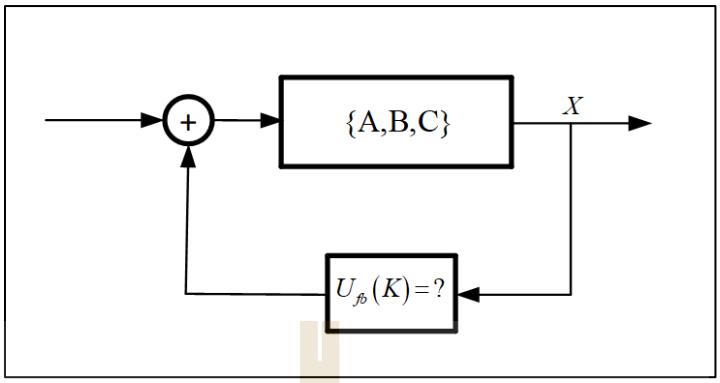

Figure 3.11 Schematic diagram of the optimal control problem formulation.

A vector of state variables in a quadratic form is given by:

$$x=\begin{bmatrix} x_1 \\ x_2 \end{bmatrix} \tag{3.33}$$

$$f(x)=f(x_1,x_2)=ax_1^2+bx_1x_2+cx_1+dx_2^2 \tag{3.34}$$

$$[x_1,x_2]\begin{bmatrix} a & \frac{1}{2}b \\ \frac{1}{2}b & d \end{bmatrix}\begin{bmatrix} x_1 \\ x_2 \end{bmatrix}+\begin{bmatrix} c & 0 \end{bmatrix}\begin{bmatrix} x_1 \\ x_2 \end{bmatrix} \tag{3.35}$$

$f(x)=x^TQx$, quadratic part, $+P^Tx$, linear part, $+e$ constant.

Consider:

$$J=\sum_{i=0}^{\infty}x_i^TQx_i+u_i^TRu_i \tag{3.36}$$

In (3.36), the conditions for the matrices Q and R is $R \geq 0, Q > 0$

Variation of matrices Q and R brings a trade-off between state excursions and control. This is decided by the programmer.

3.2 Kalman Filter

By exploiting recursive calculations, the Kalman filter is capable of estimating the state of a system from a series of noisy measurements to improve system performance (Shah, et al., 2019). A distinct state-space illustration of a linear dynamic system with noises is written within the following type.

$$x_n = Ax_{n-1} + Bu_{n-1} + w \tag{3.37}$$

$$y_n = Cx_n + v \tag{3.38}$$

The discrete model may be constructed as a block diagram as shown Figure 3.12:

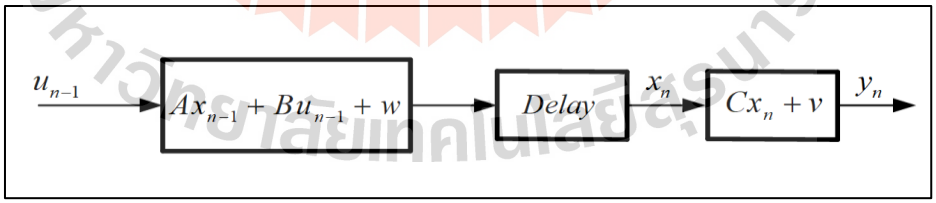

Figure 3.12 Discrete model of a linear dynamic system.

Figure 3.13 shows the connection of the basic Kalman filter with the system. The input is u and the output is y . The system also has an estimated state x and

estimated output variable y . The state estimation of the basic discrete Kalman filter may be expressed as follows:

i. Prediction of state:

$$\dot{x}_n = A\hat{x}_{n-1} + Bu_{n-1} \tag{3.39}$$

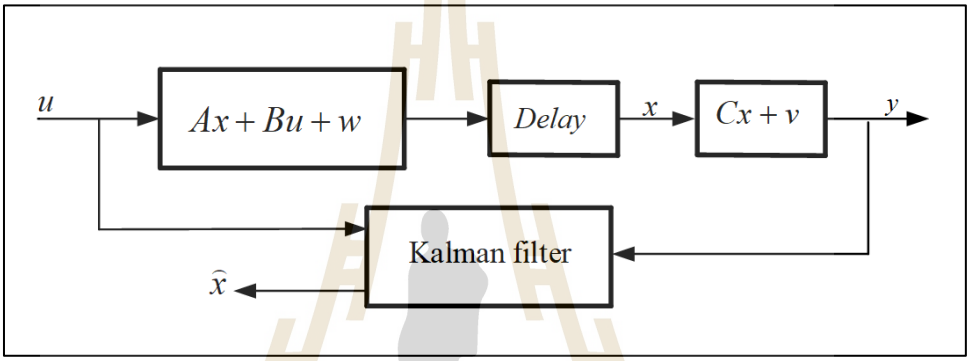

Figure 3.13 A system model and a basic Kalman Filter.

ii. Prediction of the error covariance matrix:

$$\bar{P}_n = A\hat{P}_{n-1}A^T + Q \tag{3.40}$$

iii. Calculation of Kalman filter gain:

$$K_n = \bar{P}_n C^T \left(C\bar{P}_n C^T + R\right)^{-1} \tag{3.41}$$

iv. State estimation:

$$\hat{x}_n + K_n\left(y_n - C\bar{x}_n\right) \tag{3.42}$$

v. Update of the error covariance matrix:

$$\hat{P}_n - K_n C \bar{P}_n \tag{3.43}$$

3.2.1 Extended Kalman filter

This filter applies the Kalman Filter to linearize the non-linear dynamics of the system at each iteration around the last consecutive loop and filtered estimates of the state (Ribeiro, 2004). In each iteration, the extended Kalman filter (EKF) consists of the subsequent consecutive steps:

i. $\hat{x}(k|k)$ - filter state estimate.

ii. $x_{k+1} = f(x_k) + w_k$ around $\hat{x}(k|k)$ - linearize system dynamics.

iii. $\hat{x}(k+1|k)$ and $P(k+1|k)$ - output from dynamics prediction.

iv. $y_k = h(x_k) + v_k$ around $\hat{x}(k+1|k)$ - linearize observed dynamics.

v. $\hat{x}(k+1|k+1)$ and $P(k+1|k+1)$ - output of filtering or update cycle of the observed dynamics.

The extended Kalman filter technique may be derived as follows:

i. Prediction of state

$$x_{n+1n} = \Phi(n+1, n, x_{n+1}, u_n) \tag{3.44}$$

$$\Phi(n+1, n, x_{nn-1}, u_n) = A_n(x_{nn})x_{nn} + B_n(x_{nn})u_n \tag{3.45}$$

ii. Estimation of Error Covariance Matrix

$$P_{n+1n} = \left.\frac{\partial \Phi}{\partial x}\right|_{x=x_{nn}} P_{nn} \left.\frac{\partial \Phi^T}{\partial x}\right|_{x=x_{nn}} + \Gamma_n Q \Gamma_n^T \tag{3.46}$$

$$\Gamma = \int_n^{n+1} \Phi(t_{n+1}, t) G(\tau) d\tau \tag{3.47}$$

The initial value P_{nn} is a constant matrix.

iii. Computation of Kalman Filter Gain

$$K_n = P_{nn-1} \left.\frac{\partial H^T}{\partial x}\right|_{x=x_{nn-1}} \left(\left.\frac{\partial H}{\partial x}\right|_{x=x_{nn-1}} P_{nn-1} \left.\frac{\partial H^T}{\partial x}\right|_{x=x_{nn-1}} + R \right)^{-1} \tag{3.48}$$

Where;

$$H(x_{nn-1}, n) = C_n(x_{nn-1}) x_{nn-1} \tag{3.49}$$

iv. State Estimation

$$x_{nn} = x_{nn-1} + K_n(y_n - H(x_{nn-1}, k)) \tag{3.50}$$

v. Error Covariance Matrix Update

$$P_{nn} = P_{nn-1} - K_n \left.\frac{\partial H}{\partial x}\right|_{x=x_{nn-1}} P_{nn-1} \tag{3.51}$$

3.3 Control strategies applied to DFIGs

Many techniques are developed to control DFIG in standalone or grid-connected mode. In this study, several publications discussing the control of DFIG are reviewed. The techniques are described as follows:

3.3.1 Electromagnetic torque control

This controller varies the torque of the DFIG in steps corresponding to wind speed fluctuations and vary the generator speed for the sake of reaching the desired operating reference (Gogineni, 2012). The active power and the rotor speed measurements, given as inputs to the electromagnetic torque block shown in Figure 3.14, generate a reference torque signal exploiting the utmost wind generation extraction control.

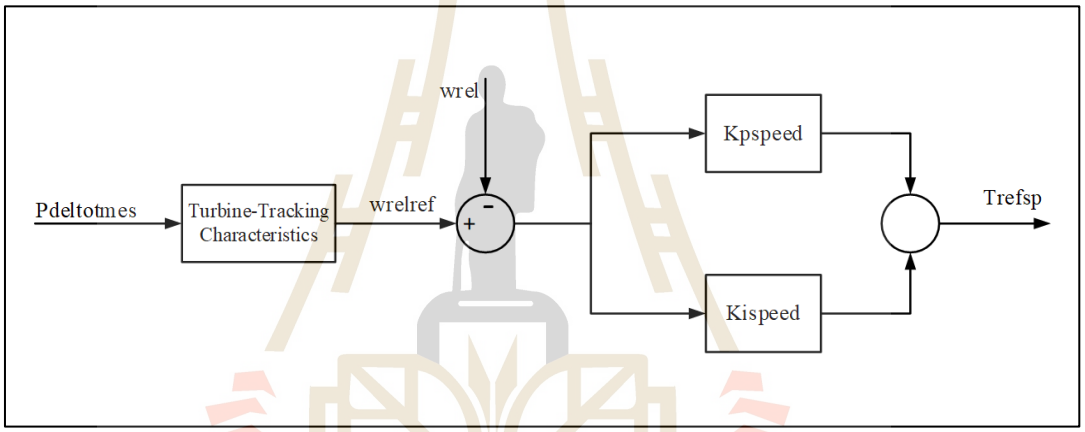

Figure 3.14 DFIG torque control.

The torque signal T_{refsp} and the input from the stator flux estimator block are processed in the calculation block and generate the d-axis rotor current reference i_{rdref} by using the stator flux estimator block as shown in Figure 3.15:

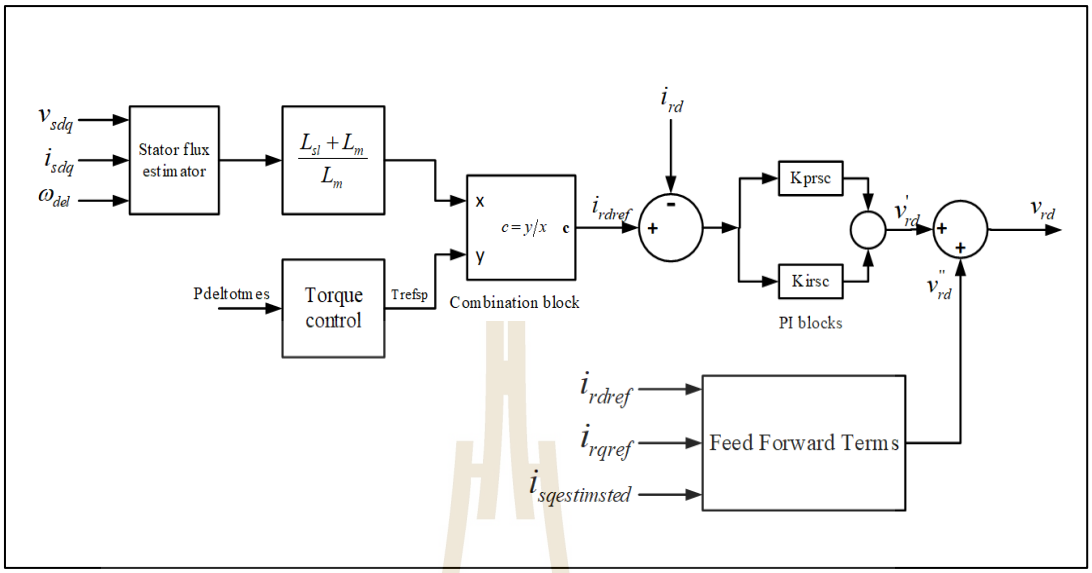

Figure 3.15 Torque control strategy with feedforward terms.

The PI controllers are used to create the d-axis component of the rotor voltage responsible for the generation of the reference torque. This conventional controller is assisted by the feed-forward terms that compute the resulting direct axis component of the rotor voltage that needs to be applied to the rotor input of the DFIG.

Bakouri et al. (2014) present three control strategies for the DFIG. These are direct torque control (DTC), pitch control, and maximum power point tracking (MPPT) method. The DTC regulates the flux and the torque, MPPT enables the generator to acquire maximum power from wind, and pitch control limits the output power of the WT. This control mechanism was tested on a 1.5 MW DFIG WT.

In (Tamalouzt, et al., 2017) a control strategy is proposed, which makes DFIG operate in all three modes of subsynchronous, synchronous, and super synchronous speed. This scheme control torque and reactive power of the generator using fuzzy logic. The proposed method takes care of the influence of the physical

system state. The interest of using DFIG in the synchronized asynchronous mode is that it can work as a synchronous generator, unlike the induction generator.

In (Mahmoodzadeh, et al., 2016) a control technique to control overshoot of electromagnetic torque in the event of a fault is developed. This controller is in short known as SPAACE. The method changes the voltage control loop of the STATCOM placed at the terminals of the squirrel cage induction generator (SCIG). In this method, the desired voltage is, in brief, switched to a lower value using real-time and expected torque values. The developed method has two advantages, one is not sensitive to the variation of parameters, and the other is that it uses simple torque measurement to reduce the overshoot, and eliminate the need for a fault detection circuit. Results show that the technique is successful in eliminating the torque overshoot throughout the recovery period.

Li et al. (2016) present an improved DTC technique for DFIG. Modeling of DFIG is presented. Block diagram of an improved DTC method and its switching table is part of this work. The application of this method ensures precise measurement of the rotor position and the basic voltage vectors. The results obtained from simulations show that the developed DTC method reduces the ripples in the rotor flux, torque, and the dc voltage.

Authors (Pura, et al., 2016) propose a technique that reduces electromagnetic torque oscillations. The controller is developed in a stationary reference frame and avoids signal decomposition for the first target. The second target requires the determination of the positive sequence of symmetrical stator current vector components. Besides a reference signal limitation method is proposed which

allows overcurrent protection under unbalanced grid voltages. Results show that torque oscillations have been reduced to a significant amount.

In (Kashkooli, et al., 2016) an improved DTC for DFIG is presented. This method is more robust than conventional DTC. The technique offers constant switching frequency, reduced torque, and flux ripples for a DFIG. A hysteretic controller enables the rotor voltage vector selection from its outputs. The method applies the SVM technique to control a two-level VSI. This inverter injects voltage vector to the rotor windings of the DFIG. This controller eliminates the use of the transformation of quantities, speed sensors, and PI regulators. Results show that the method achieves an excellent steady-state and dynamic performance and allows variable speed operation of the generator making it suitable for WECS.

Dias, et al., (2016) propose a generalized predictive control (GPC) for a DFIG. DFIG-Based Topology, mathematical model, and proposed control system are shown. The GPC method is mathematically formulated and the transfer function blocks shown. Simulations show that the controller minimizes oscillations in the generator electromagnetic torque.

The authors (Nian, et al., 2017) present a control technique in which a resonant regulator is added in the torque compensator for the DFIG. System configuration and mathematical modeling are presented. The torque ripple mitigation method is explained in detail. Results obtained show that this method has an excellent dynamic performance. Second, the method is independent of the DFIG parameters. Third, the torque ripple minimization is successfully achieved.

In (Gundavarapu, et al., 2017) a DC link voltage of a standalone DFIG is regulated using DTC strategy. This generator feeds a DC load, and its connection

diagram is shown. The scheme is described and analyzed. The behavior of the torque and power in the DC section of DFIG, power-sharing to isolated load, are explained in detail. This controller is capable of reducing stator current harmonics, and it is sensorless thus reducing the cost to maintain the sensor. The scheme is tested on a 4 kW DFIG.

Authors (Al-Quteimat, et al., 2016) show the robustness of a twelve sector DTC method through simulations when applied to a DFIG. The performance of this method is compared to a traditional DTC scheme. The developed scheme reduces torque ripples better than conventional DTC.

Table 3.1 Researches on direct torque control.

Ref	Techniques	Controlled parameter	Important findings
Bakouri et al	DTC, MPPT	Torque, flux, power	NA
Tamalouzt et al	DTRPC, FL	Torque, reactive power	Investigation of generator physical state disturbances, DFIG work as a synchronous generator unlike the induction generator
Mahmoodzadeh et al	SPAACE	Torque	No need for faulty detection, not sensitive to the model parameters uncertainties
Li et al	DTC	Torque, flux, DC-link voltage	Increases division accuracy of rotor flux position and the number of basic voltage vectors
Pura et al	DPC	Torque, stator current	reference signal limitation method which allows overcurrent protection under unbalanced grid voltage
Kashkooli et al	SVM	Torque, flux	Use of synchronous reference frame transformation, speed sensor, and *PI* regulators is avoided
Dias et al	GPC	Torque, power	Noise attenuation and disturbance rejection by tuning of σ
Nian et al		Torque	Resonant regulator introduced into rotor current control loop
Gundavarapu et al	DTC	Torque, DC-link voltage, stator frequency	Stator and rotor functionality are interchanged, with no position sensor. Possible to be applied to the DFIG-dc system connected to the dc grid.
Al-Quteimat et al	DTC	Torque	Comparison of six sectors and twelve sector DTC methods in torque ripple reduction

3.3.2 Direct power control

This method was tested with the DFIG in 1998 (Liu, et al., 2011). The DPC initially controls the inverter states, using hysteresis comparators of the error between the reference and the predicted output of active and reactive power. This method applies the instantaneous space vector theory. Direct Power Control is adopted due to its simplicity, independence of machine parameters, and its robust performance. Its drawbacks are that it is difficult to manipulate it at low speeds causing torque ripples, and a shortage of online control. Fast energy response can be obtained without the complex field-orientation block. The technique can work without the knowledge of the system parameters thus suggests exceptional robustness. The approach selects suitable voltage vectors from the switching table, using the stator flux function and active and reactive power errors. There is not any necessity to estimate the rotor flux. Figure 3.16 shows the block diagram for the DPC method.

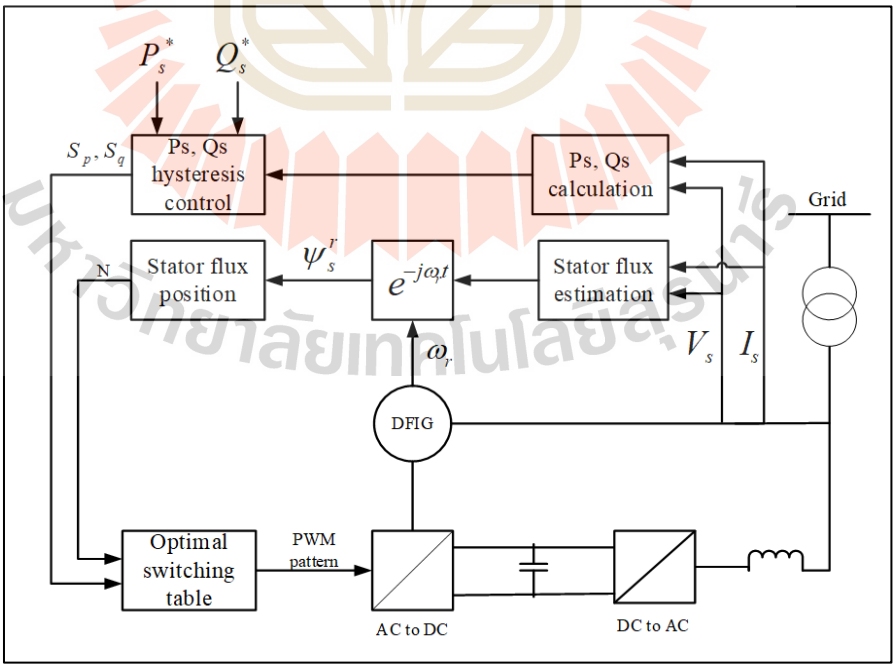

Figure 3.16 Direct Power Control block diagram.

The theory and schematic diagram show that DPC is simpler than FOC. In each sampling period, the ultimate switching table is chosen using three inputs: the power hysteresis comparators output and the stator flux position sector. By referring the machine equations to the rotor reference frame, the d-axis aligned with the stator flux, and neglecting the stator resistance, the equations for the power are:

$$P_s = \frac{3}{2}\frac{L_m}{\sigma L_s L_r}\omega_s \left|\overrightarrow{\lambda_s}\right|\left|\overrightarrow{\lambda_r}\right| \sin\theta \tag{3.52}$$

$$Q_s = \frac{3}{2}\frac{\omega_s}{\sigma L_s}\left|\overrightarrow{\lambda_s}\right|\left(\frac{L_m}{L_r}|\lambda_r|\cos\theta - \left|\overrightarrow{\lambda_r}\right|\right) \tag{3.53}$$

Where:

$\overrightarrow{\lambda_s}, \overrightarrow{\lambda_r}$ = Stator and rotor flux linkage vectors.

θ = Angle between linkage vectors of rotor and stator flux.

Leakage factor

$$\sigma = 1 - \frac{L_m^2}{L_s L_r} \tag{3.54}$$

It can be seen from (3.52) and (3.53) that the stator powers can be controlled by varying the angle θ. This angle is between the rotor and stator flux linkage vectors.

In (Errouissi, et al., 2017), a comparison is made between the performance of a robust continuous-time model predictive control (RCTMPC) and

vector control (VC) for a DFIG. The robust controller is capable of reducing the deviation of the stator current. The disturbance observer enables the elimination of the steady-state error of the stator current. Moreover, the proposed controller shows good performances than VC when the machine is under transient and steady-state periods.

The authors (Mehdi, et al., 2016) present a sensorless DPC applied to a DFIG. This controller is more robust than classical LUT DPC as it overcomes the disadvantages of large power ripple and variable switching frequency occurring in the c1assical LUT DPC. With this controller no synchronous coordinate transformations involved in matching references and measured values. The effectiveness and robustness of the developed controller are shown by simulation performed on a 2 MW DFIG. Results show that the output power ripples are reduced and better harmonic distortion for stator and rotor currents.

Authors in (Zarei et al., 2017) presents an improved predictive direct power control (PDPC) tested on a 2MW DFIG. Minimum numbers of controllers are involved in this control strategy. Simulation is done using MATLAB/Simulink. Results show that the DFIG manages to reduce THD.

Authors in (Tao, et al., 2016) propose a Direct Virtual Power Control (DVPC). The controller doesn't need a PI regulator. Apart from grid voltages, the inputs to this controller are the measured rotor currents and position. This controller alone is enough for controlling the DFIG connected to the grid. The method is tested on a 7.5KW experimental prototype of a digital signal processer (DSP) and a complex programmable logic device. Results show the method improves the dynamic response and eases the connection to the grid.

Authors in (Hashemnia, et al., 2016) present a DPC of active and reactive powers for a DFIG. In this control strategy, two reference frames are used to estimate the stator flux space vector: the stationary reference frame and the rotor reference frame. The proposed controller avoids the drawbacks of the traditional DPC, which suffers from the variable switching frequency. The proposed method optimally minimizes power errors. Simulations show the robustness of the proposed technique over the conventional one by lowering power ripple and Total Harmonic Distortion (THD).

Jang et al., 2006 proposes a method to control the output power of the DFIG. The topology of the grid-connected WECS used by DFIG is shown. Results show that the developed method makes the DFIG to have stable toque and speed during wind speed variation. This reduces fatigue to the rotating parts of the system. Besides, the control strategy smooths the stator active or reactive power ripple components, eliminates the negative sequence component of the rotor current, speed, and torque ripples.

Authors in (da Costa, et al., 2011) present a controller design for an 850 kW DFIG to work as a STATCOM without wind to control output power at PCC. The controller can protect the DFIG from thermal breakdown under large load variations. The controller has three operation modes. Simulation results show that mode 1 is the best operating mode.

The reactive power control and low voltage ride through (LVRT) capability of the DFIG during voltage sag are studied in (Lima, et al., 2012). The DFIG is connected to the grid with a crowbar protection circuit protecting the RSC during voltage sag is presented. The study shows that there is an increase in the

current after the fault clearance. This problem can be overcome by control of the reactive power offered by the capacitor that controls the DFIG's currents to improve voltages at the PCC to avoid voltage dip which may be caused by the increase in the WT currents. (Zhai, et Al., 2016) presents a controller that controls some DFIGs in a wind farm to inject reactive power thus minimizing the number of devices installed for reactive power compensation. The problem of reactive power during voltage sag in the presence of wind farms is explained. The paper details the possibility of controlling the DFIGs in the wind farm for reactive power injection to improve the voltage stability of the distribution system (DS). Simulation is done on the PSCAD/EMTDC platform.

In (Zhu, et al., 2016) a controller is developed to control the output power of the DFIG. This controller is capable of eliminating stator transient flux occurring during voltage disturbances. This enables the DFIG to have stable output power and torque. The technique is tested on a 2-MW and 7.5-kW DFIG. Simulation is performed in MATLAB/SIMULINK. Results show that there is an improved dynamic performance of the DFIG. In (Heng Nian et al., 2016) a controller is designed which coordinates the control actions of the DPC technique for the RSC and the GSC of the DFIG during grid faults. This controller eliminates the need for a phase-locked loop (PLL). This is performed by the use of a virtual phase angle in place of the actual one.

Authors (Kim, et al., 2016) propose a control strategy where a WPP with high reactive power capability is tasked to inject more reactive power to the system to improve voltage at POI, hence achieve fast voltage recovery and reduce the additional reactive power. This is an adaptive method working based on (Q–V)

characteristic of the DFIG which enables a generator that produces a huge amount of reactive power to supply to the grid to improve the voltage profile. Simulations show that the developed method can restore the voltage very fast.

Authors (Ding, et al., 2015) propose a controller to coordinate SVC, GSC, and RSC to control voltage and reactive power for a DFIG to tackle the problem of over-voltage several seconds after LVRT on the wind farm in China. Simulation is done in MATLAB/Simulink for symmetrical short-circuit faults.

Authors (Xiong, et al., 2016) compare the performances of three control strategies, the back-stepping method which is based on direct power control (BS-DPC), vector control look-up table DPC (LUT-DPC). These controllers are tested on a 2-MW DFIG under normal and abnormal grid voltages. Simulations show that BS-DPC has higher dynamic performance and steady performance than VC and LUT-DPC. Additionally, the developed strategy includes a higher capability in suppressing the harmonic stator current than VC.

Authors (Kim, et al., 2016) present a voltage control strategy that relies on (Q−V) characteristics. This method increases the reactive power reserve of the WPP better than the fixed method. Besides, the method enables the DFIG to supply reactive power to the maximum limit, assisting voltage improvement at the PCC. To avoid overvoltage in the system after the disturbance, washout filters are added to the DFIG controllers. These filters are capable of preventing an additional reactive power to appear after the fault clearance. The accumulated values are eliminated from the PI controllers when the machine is operating under abnormal conditions.

In (Moghadasi, et. al., 2016) fuzzy logic control is applied to control the reactive power coordination between the DFIG and the STATCOM during grid

faults. An optimization is solved by the NSA for a fuzzy logic controller. The problem is also solved by NSGA-II and a comparison is made. Results show that the NSA is 3.7 times faster than NSGA-II.

Authors (Yang, et. al., 2016) present control of GSC during asymmetrical voltage swell. This control strategy eliminates variations of DC voltage and an abrupt increase in energy at the GSC.

Authors (Junli, et al., 2016) present a control strategy where an ESD is added to the DFIG circuit to enhance its LVRT during unsymmetrical voltage dips. This technique is based on reconfiguring the circuit of DFIG to include ESD and DC-DC converter. When the system is in fault state a series connection is established between the GSC, the stator, and the grid. This reconfiguration makes ESD and GSC act as a dynamic voltage restorer (DVR). The distorted stator voltage is improved by the addition of the controllers for the positive and negative sequences. Besides, ESD maintains the dc voltage through the DC-DC converter. This reconfiguration protects the DFIG from grid faults thereby continue its regular operation. The method is tested on a 1.5 MW DFIG and shows better performance than the traditional control strategy.

Authors (Mengxi, et al., 2016) present a PSO-based reactive power control strategy. This method can improve the voltage profile and operate the system economically. In this method, PSO is responsible for solving a minimization problem of reactive compensation. Simulation results show the robustness of the developed technique by compensating the reactive power demand of each wind farm and meet the real-time requirement of the power system.

Authors (Saeidi, et al., 2016) present a nonlinear model predictive control to tackle the problems of rotor speed variation, changes in active power, and voltage for a DFIG. Simulations show that this controller is fast and accurate. The controller is capable of providing reactive power at a voltage dip of 80%.

In (Shen, et al., 2017) an ESD is incorporated in a DFIG circuit to enhance its transient voltage support capacity and improve the rotor current dynamics under fault conditions. The ESD is responsible for regulating the dc voltage. Moreover, there is another control for the rotor speed and the pitch angle. These controls are for increasing the rotor speed and the pitch angle to decrease the captured wind power.

Table 3.2 Researches on direct power control.

Ref	Method	Controlled parameters	Important findings
Nian et al	DPC	Torque, Power, Current	Frequency discrimination capability
Errouissi et al	RCTMPC, MPC	Stator current	No extra power control loop is required in the control structure
Mehdi et al	DPC	Output power	Hysteresis comparator is used instead of a PI controller
Zarei et al	PDPC	Power, Torque, Current	NA
Saravanan et al	DPC	Output power	Use Vienna rectifier as an RSC and three-stage MOSFET inverter as a GSC
Tao et al	DVPC	Grid voltage, Rotor current, Rotor position	No need for PI controllers
Rodriguez-Ayerbe et al	MPDPC	Flux, Rotor current, and DC-link voltages	NA
Hashemnia et al	DPC	Power, THD	The controller doesn't suffer from the variable switching frequency
Jang et al	NA	Rotor current, Speed, Torque	Reduces the fatigue of the rotating parts of the system
da Costa et al	Intelligent control	Grid voltage	The grid-side converter works as STATCOM
Lima et al	FRT	Reactive power	NA
Zhai et al	Power control	Reactive power	Selected DFIGs generate reactive power only, hence less reactive power compensation devices
Zhu et al	Dual-loop control	Torque, Active power	Increase of lifetime of the drive train
Nian et al	DPC	Torque, Power,	Use of virtual phase angle instead

		Current	of the actual one, no PLL employed
Kim et al	(Q–V) characteristic	Reactive power	DFIG reactive power injection in proportion to its reactive power capability
Ding et al	Coordinated control	Voltage and Reactive power	NA
Xiong et al	Back-stepping Algorithm, DPC	Harmonic stator current	The founding of a unified mathematic model of a DFIG under normal and harmonic grid voltage
Kim et al	(Q−V) characteristic	Reactive power	Implementation of washout filters in the WPP and DFIG controllers
Moghadasi et al	NSA, NSGA-II, FL	Reactive power	NSA is 3.7 times faster than NSGA-II
Yang et al	GSC control	DC-link voltage, Energy of GSC	NA
Junli et al	DVR	Voltage	DFIG continue operation under voltage dips
Tian et al	PSO	Reactive power	Improvement of the lifetime of upstream WT's power converters
Zarei et al	PDPC	Power, Torque	Injection of sinusoidal and balanced currents into the grid during voltage dips
Mengxi et al	PSO	Reactive power	NA
Saeidi et al	MPC	Reactive power	NA
Shen et al	NA	Stator voltage, Rotor current	NA

3.3.3 The DC-link voltage control strategy

This control strategy is implemented in the control level I. This controller is applied to the GSC of the DFIG. The controller is employed to maintain the dc-link capacitor voltage constant at the specified reference value V_{dcref}. The implementation of the dc-link voltage control is shown in Figure 3.17. As shown, the control strategy consists of a V_{dc} regulator block, grid current measurement block, and a current regulator block.

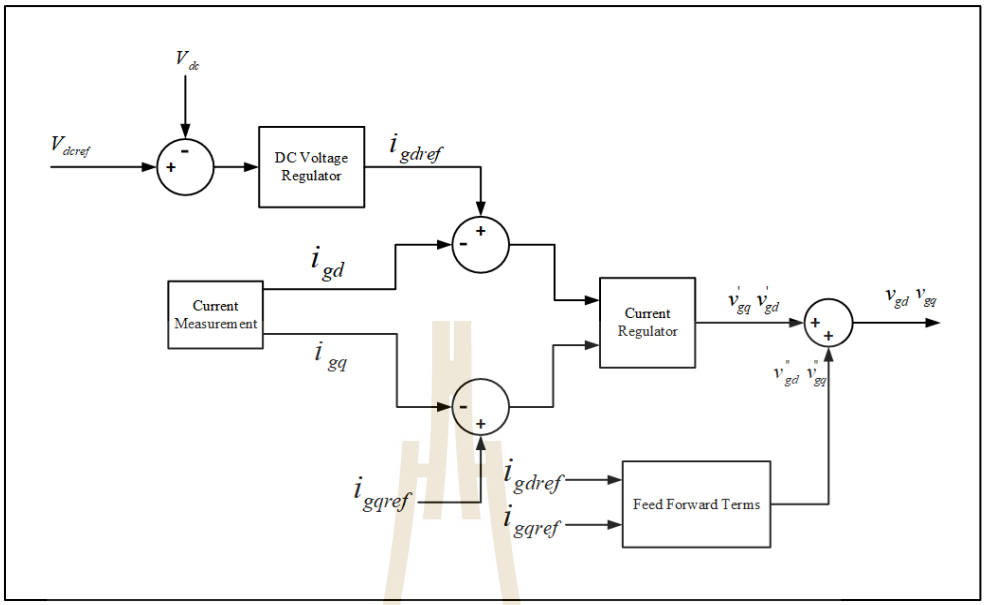

Figure 3.17 DC-link voltage control.

Authors (Huchel, et al., 2015) propose a parallel capacitor protection scheme for the dc-link of the DFIG. This technique is compared with the traditional dc chopper, crowbar, and series braking resistors protection schemes and found to be having superior performance in stabilizing the dc voltage, varying rotor voltages, and currents within the set limit during faults. The other faults that were used to test the proposed schemes are asymmetrical grid faults. Besides, this scheme eliminates the need for blocking GSC and RSC during grid faults.

Authors (Li, et al., 2017) present a controller to control stator frequency and the output power of the DFIG. This sensorless flux-oriented control scheme uses a three-phase diode bridge to connect the stator of DFIG to the dc-link. Two parameters are used as control variables which are the stator frequency and the d-q axis voltage of the diode bridge. Simulation is done in MATLAB/Simulink. This

scheme is cost-effective as the diode rectifier is much less expensive than the power converter. The scheme is capable of eliminating low-order stator current harmonics.

Authors (Marques, et al., 2016) present the optimization of the field-weakening operation of a DFIG dc-link. In this method, the stator supplies a constant voltage to dc-link through a bridge rectifier. The rotor current of the generator is controlled by a voltage-source inverter connected to the same dc link. The method uses torque instead of rotor speed to control field weakening to improve the efficiency of the DFIG.

Authors (Din, et al., 2016) present a hybrid control technique involving the Adaptive Sliding Mode Controller (ASMC) and Adaptive Fuzzy controller (AFC). These controllers apply the Levenberg-Marquardt method and a crowbar protection circuit. The crowbar protects DFIG against faulty currents during voltage dips while the hybrid control is introduced to control DC link voltage during normal and abnormal conditions. The method is tested on the IEEE 5 bus test system with a 9MW DFIG interfaced with a 120 kV grid and found to have robust performance as compared to the PI controller. Furthermore, the proposed controller has the capability of DC-link voltage tracking, fast and high dynamic response, reduced transient oscillations, low undershoot, overshoot, rise-time, settling time.

Authors (Wang, et al., 2013) present the control of DC-link voltage for a DFIG-wind farm. The reduced analytical model is developed considering operating points of the WT, the strength of the grid, and the dc voltage dynamics. Eigenvalue analysis is employed to assess the model performance to determine system stability. The plot of the eigenvalue locus proves that tuning of a phase-locked loop (PLL) has

a significant effect on this operation under a weak AC grid, and larger PLL gain can efficiently improve the damping of the entire system.

Authors (Misra, et al., 2017) develop a scheme that does not need stator side sensing for a DFIG-DC system having distorted stator voltages and currents. The proposed method is developed utilizing rotor circuit currents, and the output dc-link voltage. This avoids the requirement to sense the intermediate stator side variables. Results obtained from simulations show that the controller maintains the stator frequency at its rated value by appropriate variation of flux reference, against load variations. This method is a pretty solution for variable speed dc power generation. The developed controller is tested on a 5.5 kW slip-ring induction machine.

Authors (Misra, et al., 2017) develop a double crowbar protection scheme for the RSC and GSC of a DFIG. The parallel rotor side crowbar (PRSC) is applied to shield the RSC and DC link capacitor. The protection is achieved by dissipating the rotor energy throughout grid disturbances. The DC-link capacitor crowbar (DCCC) functions as long as the DC capacitor voltage is above a set value. To reach this goal the series rotor side crowbar (SRSC) coordinates with the DCCC. This improves the fault ride-through (FRT) capability of the DFIG. SRSC allows the RSC to continue its operation even throughout grid faults to inject reactive power to the grid to support the voltage at the PCC. SRSC not only dissipates the rotor thermal energy in fault conditions but also limits the RSC current value and thereby protecting the RSC and reduces the harmful DC link voltage.

Table 3.3 Researches on dc-link voltage control strategy.

Ref	Method	Controlled parameters	Important findings
Huchel et al	Parallel capacitor	DC-link voltage	Eliminates the need for blocking GSC and RSC
Li et al	Sensorless FOC	Frequency, Power output	Use diode rectifier which is much less expensive than a power converter
Marques et al	Field-weakening control	Rotor field	Uses torque instead of rotor speed to control field weakening to improve the efficiency
Ud Din et al	ASMC, AFC, Crowbar protection	DC-link voltage	The controller is fast and has a high dynamic response, reduced transient oscillations, low undershoot, overshoot, rise-time, settling time
Wang et al	Reduced analytical model	DC-link voltage	Larger PLL gain can improve system damping.
Misra et al	NA	The load current, DC voltage, stator frequency, and stator voltages.	NA
Tang et al	NA	DC-link voltage	Optimizing control parameters of the DC voltage control loop
Misra et al	NA	DC-link voltage	NA
Haidar et al	PRSC, DCCC	DC-link voltage	RSC continues its operation to control the DFIG during a fault condition

3.3.4 Pitch control strategy

In the pitch control, an angle of attack of the blades of a wind turbine rotor is turned in such a way that the wind turbine can control the generation of electricity by monitoring the speed of the turbine (Reyala, et al., 2014). The mechanism of pitch control in the wind turbine has an electronic controller that checks in real-time the output power of the turbine. This control strategy enables the wind turbine to control the power output by using the blade pitch mechanism that can turn the rotor blades slightly out of the wind when the power output is very high and vice versa. Figure 3.18 shows the rotation of the rotor blades around their longitudinal axis (pitching).

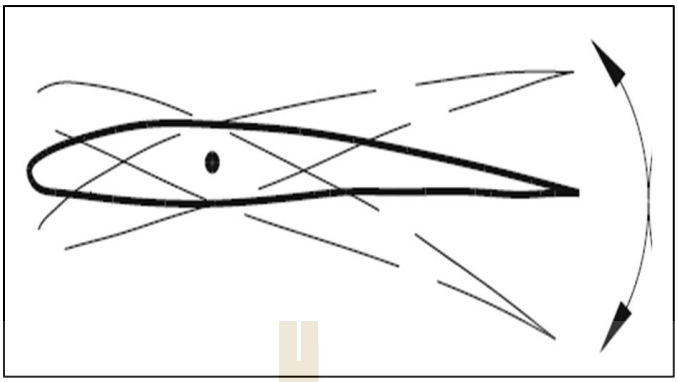

Figure 3.18 Variable pitch blades.

The total power of the wind is given by (2.22).

The received power is:

$$P_R = c_p \cdot P \tag{3.55}$$

The performance coefficient c_p is a function of λ and φ. Therefore received power becomes

$$P_R = c_p(\lambda, \varphi) \cdot P \tag{3.56}$$

But, tip speed ratio is given by,

$$\lambda_r = \frac{\omega \cdot r}{v} = \lambda(v) \tag{3.57}$$

Thus;

$$\begin{aligned} P_R &= C_p(\lambda(v),\varphi)\cdot P \\ &= C_p(\lambda(v),\varphi)\cdot \frac{1}{2} A\rho v^3 \\ &= P_R(v,\varphi) \end{aligned} \tag{3.58}$$

Equation (3.58) shows that the received power is a function of the wind speed and the pitch angle. Therefore, a wind turbine should be equipped with a suitable technique to obtain the best pitch angle corresponding to the input wind data.

In (Chatterjee, et al., 2016) a control algorithm is created for improving the active power of the system. The working guideline of this controller is based on the frequency response curve of the system. This curve utilizes a lookup table. Maximum power point technique (MPPT) method is utilized to track the speed of the generator. To adjust the blades pitch angle PI controllers are employed. The strategy is tested on a 1.5 MW DFIG. The pitch controller is subjected to gain constraints which are optimized by the Hooke-Jeeves design search method.

Islam, et. al., 2016) apply LQR to control the pitch angle of the DFIG WT. This machine employs a seven-order model. The results obtained are compared with the conventional method. The strength of the proposed controller can be verified by the results obtained which show that the proposed strategy improves LVRT capability and improves system damping under huge disturbances.

Table 3.4 Researches on Pitch control.

Ref	Method	Controlled parameters	Important findings
Chatterjee et al	MPPT, Hooke-Jeeves	Real power, Pitch angle	NA
Islam	LQR	Pitch angle	NA
Li et al	de-loading	Pitch angle	NA
Mohammad et al	MRC, PIP	Pitch angle	NA
Eisa et al	Eigenvalue Analysis	Pitch angle	Analyzing bifurcation in parameter space

3.3.5 Vector control

The RSC controller of the DFIG controls the stator active and reactive power of the machine. The strategy controls the direct and quadrature axis rotor current components *idr* and *iqr* (Masaud, 2013). The RSC control strategy comprises of two control loops. The internal current control loop and the external current control loop. The internal loop controls the d-axis rotor current and the external loop controls the q-axis rotor current component. They work depending on the synchronously rotating reference frame. In the case of vector control oriented with the stator-flux, the d-axis and stator flux linkage vector are aligned together, i.e. $\psi_{ds} = \psi_s$ and $\psi_{qs} = 0$ as shown in Figure 3.19. In the stationary reference frame, $d^s - q^s$ usually, the stator flux of the DFIG is estimated by the stator machine equation shown below.

$$\psi_{ds}^{s} = \int v_{ds}^{s} - R_s i_{ds}^{s} \tag{3.59}$$

$$\psi_{qs}^{s} = \int v_{qs}^{s} - R_s i_{qs}^{s} \tag{3.60}$$

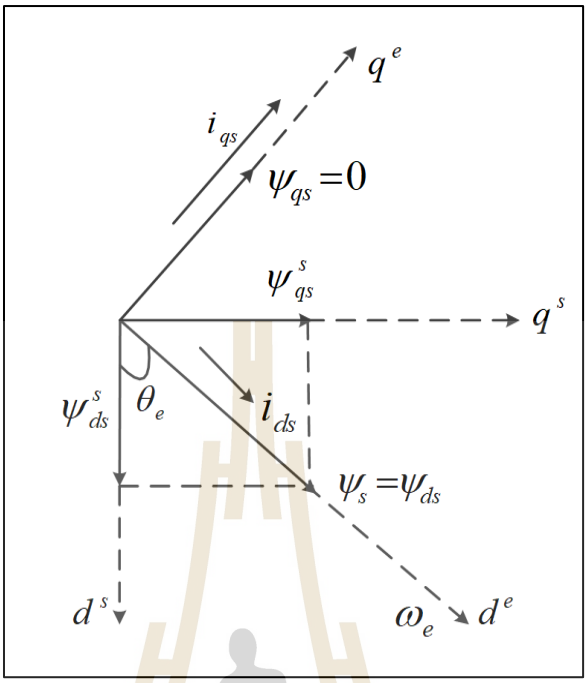

Figure 3.19 Phasor representation of the vector control (stator-flux oriented).

The direct and quadrature axes stator voltages can be written as,

$$v_{ds} = R_s i_{ds} - \omega_s \psi_{qs} + \frac{d\psi_{ds}}{dt} \tag{3.61}$$

$$v_{qs} = R_s i_{qs} - \omega_e \psi_{ds} + \frac{d\psi_{qs}}{dt} \tag{3.62}$$

Where:

ω_s = Stator flux angular speed

R_s = Stator resistance

i_{ds} = Direct axis stator current

i_{qs} = Quadrature axis stator current

ψ_{ds} = Direct axis stator flux

ψ_{qs} = Quadrature axis stator flux

At steady state conditions and in the stator flux reference frame the generator's rotor voltages are:

$$v_{dr} = R_r i_{dr} - (\omega_s - \omega_r)\psi_{qr} + \frac{d\psi_{dr}}{dt} \tag{3.63}$$

$$v_{dr} = R_r i_{dr} - (\omega_s - \omega_r)\psi_{qr} + \frac{d\psi_{dr}}{dt} \tag{3.64}$$

Where:

R_r = Rotor resistance

i_{dr} = Direct axis rotor current

i_{qr} = Quadrature axis rotor current

ψ_{dr} = Direct axis rotor flux

ψ_{qr} = Quadrature axis rotor flux

The direct and quadrature axes machine fluxes can be written as,

$$\psi_{ds} = L_s i_{ds} + L_m i_{dr} \tag{3.65}$$

$$\psi_{qs} = L_s i_{qs} + L_m i_{qr} \tag{3.66}$$

$$\psi_{dr} = L_r i_{dr} + L_m i_{ds} \tag{3.67}$$

$$\psi_{qr} = L_r i_{qr} + L_m i_{qs} \tag{3.68}$$

The other machine equations obtained at this condition are:

$$\psi_{ds} = \psi_s \text{ and } \psi_{qs} = 0 \tag{3.69}$$

$$v_{ds} = 0 \tag{3.70}$$

$$v_{qs} \cong |V_s| \cong \omega\psi_{ds} \tag{3.71}$$

$$i_{ds} = \frac{L_m}{L_s}\left(i_{dms} - i_{dr}\right) \tag{3.72}$$

$$i_{qs} = \frac{-L_m}{L_s} i_{qr} \tag{3.73}$$

$$i_{dms} = \frac{v_{qs} - R_s i_{qs}}{\omega_e L_m} \tag{3.74}$$

Where:

V_s = Stator voltage

i_{dms} = Direct axis stator mutual current.

L_s = Stator inductance

L_r = Rotor inductance

L_m = Mutual inductance

The stator powers written using stator voltages and currents are:

$$P_s = 1.5\left(v_{ds}i_{ds} + v_{qs}i_{qs}\right) \tag{3.75}$$

$$Q_s = 1.5\left(v_{qs}i_{ds} - v_{ds}i_{qs}\right) \tag{3.76}$$

Equations (3.75) and (3.76) can also be expressed as,

$$P_s = -1.5|V_s| \cdot \frac{L_m}{L_s} i_{qr} \tag{3.77}$$

$$Q_s \cong 1.5|V_s| \cdot \frac{L_m}{L_s} \cdot \left(\frac{|V_s|}{2\pi f L_m} - i_{dr} \right) \tag{3.78}$$

The electromagnetic torque of DFIG is given by,

$$T_e = 1.5 \frac{L_m}{L_s} \left(\psi_{ds} i_{qs} - \psi_{qs} i_{ds} \right) \tag{3.79}$$

By substituting (3.65) and (3.66) in (3.61) and (3.62) and rearranging a set of simplified equations is obtained:

$$v_{ds} = R_s i_{ds} \tag{3.80}$$

$$v_{qs} = R_s i_{qs} + \omega_s \psi_{ds} \tag{3.81}$$

Where:

$$i_{ds} = \frac{L_m}{L_s}\left(i_{dms} - i_{dr}\right) \tag{3.82}$$

$$i_{qs} = \frac{-L_m}{L_s} i_{qr} \tag{3.83}$$

$$i_{dms} = \frac{v_{qs} - R_s i_{qs}}{\omega_s L_m} \tag{3.84}$$

Where:

V_s = Stator voltage

i_{dms} = Direct axis stator mutual current.

Substituting (3.82) to (3.84) in the stator active and reactive power equations (3.75) and (3.76), the stator powers as functions of the rotor currents are:

$$P_s = \frac{-3}{2}\frac{L_m^2}{L_s}\omega_s i_{ms} i_{qr} \tag{3.85}$$

$$Q_s = \frac{3}{2}\frac{L_m^2}{L_s}\omega_s i_{ms}\left(i_{ms} - i_{dr}\right) \tag{3.86}$$

By substituting (3.67) and (3.68) in (3.63) and (3.64):

$$v_{dr} = R_r i_{dr} + \sigma L_r \frac{di_{dr}}{dt} - \left(\omega_s - \omega_r\right)\sigma L_r i_{qr} \tag{3.87}$$

$$v_{qr} = R_r i_{qr} + \sigma L_r \frac{di_{qr}}{dt} - \left(\omega_s - \omega_r\right)\left(\frac{\sigma L_r i_{dr} + L_m^2 i_{ms}}{L_s}\right) \tag{3.88}$$

Where:

$\sigma = 1 - \frac{L_m^2}{L_s L_r}$ = Leakage coefficient.

Ignoring R_s, which is an acceptable practice to simplify the analysis for large generators, the final expression for stator real and reactive power is given below.

$$P_s = \frac{-3}{2}\frac{L_m}{L_s} i_{qr} \tag{3.89}$$

$$Q_s = \frac{3}{2}\frac{L_m}{L_s}\left(\frac{v_{qs}}{\omega_e L_m} - i_{dr}\right) \tag{3.90}$$

With the PI-controllers the rotor voltages in dq reference frame are,

$$v_{dr} = \left(k_p + \frac{k_i}{s}\right)\left(i_{dr}^* - i_{dr}\right) - s\omega_e \sigma L_r i_{qr} \tag{3.91}$$

$$v_{qr} = \left(k_p + \frac{k_i}{s}\right)\left(i_{qr}^* - i_{qr}\right) + s\omega_e\left(\sigma L_r i_{dr} + \frac{L_m^2}{L_s} i_{ms}\right) \tag{3.92}$$

Where:

k_p = proportional gain.

k_i = integral gain.

Figure 3.20 shows the full vector control technique for the RSC. The two current controllers produce the rotor voltages v_{dr} and v_{qr}. These voltages control the converter through pulse width modulator *PWM*.

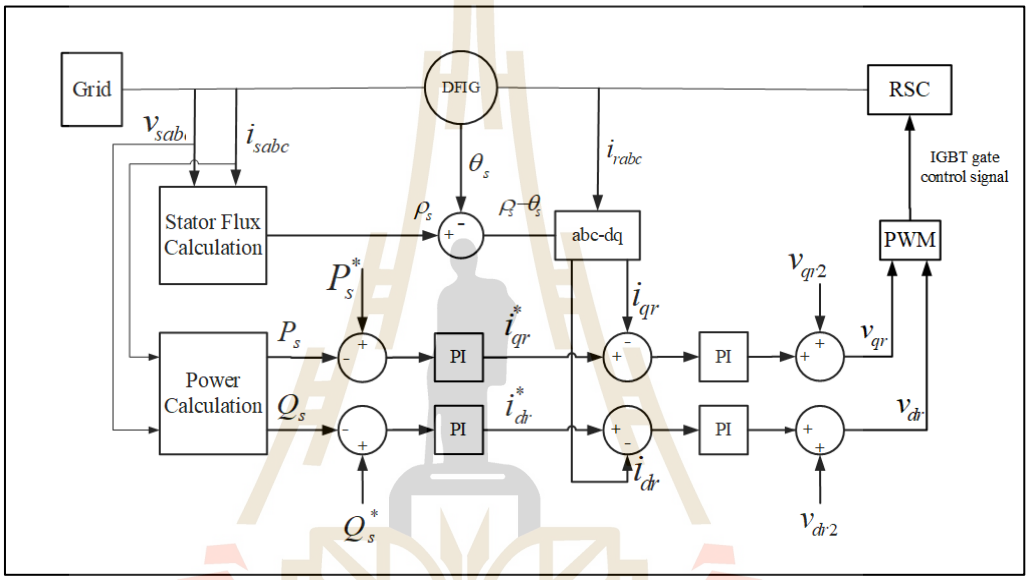

Figure 3.20 Vector control scheme of RSC.

The terms v_{dr2} and v_{qr2} in Figure 3.20 are the third terms in equations (3.91) and (3.92) as shown below.

$$v_{dr2} = -s\omega_m \sigma L_r i_{qr} \tag{3.93}$$

$$v_{qr2} = s\omega_m \left(\sigma L_r i_{dr} + \frac{L_m^2 i_{ms}}{L_s} \right) \tag{3.94}$$

Where:

$$s\omega_s = \left(\omega_m - \omega_r\right) \tag{3.95}$$

Authors (Cheng, et al., 2017) present the direct stator current vector technique, which uses a virtual phase angle generated by the nominal frequency. This eliminates the need for a *PLL*. Instantaneous power theory is employed to calculate stator currents hence a reduction in parameter dependency by the controller. Since the DFIG should be synchronized with the grid an improved synchronization procedure is used which generates a smooth stator voltage. To test the robustness of the proposed controller the small-scaled laboratory setup of 1.0 kW DFIG is used.

Authors (Hu, et al., 2016) propose a vector controller for a grid-connected brushless doubly-fed induction generator (BDFIG). This controller does not evaluate rotor flux, rotor current, or control windings' flux and has a smaller dependency on the BDFIG model and parameters. To show its robustness, the controller is tested on a 64 kW BDFIG and results show that the developed controller can optimally operate the machine in variable-speed-constant-frequency conditions. Besides, the controller can control active and reactive power independently and has good dynamic and stable performance.

Authors (Peresada, et al., 2016) present a vector control that regulates the voltage of the DFIG. Apart from stator voltages, and currents, the speed or position is also among the inputs to the controller. The proposed controller has good dynamic performance as the DFIG can operate with the speed safe limits around the synchronous speed of the DFIG.

Authors (Li, et al., 2016) present a fuzzy-enabled vector control for a DFIG. This controller operates on stator flux orientation. The controller ensures good stability of the system, robustness, small overshoot, and fluctuation.

Authors (Srirattanawichaikul, et al., 2016) develop two vector control strategies for a DFIG-WT. These controllers are stator-flux oriented and voltage oriented. Stator-flux oriented uses a rotating reference frame oriented along the stator flux vector, which calculates the stator flux position while the voltage orientated one is controlled by the usage of a reference oriented with the stator voltage vector. Moreover, the two techniques are compared in terms of their performances. The controllers are tested on a 1-kW DFIG-WT. Both controllers give a good performance.

Authors (Mannah, et. al., 2016) present an analysis of DFIG-WT. Block diagram of WECS and DFIG based WECS is presented. Real-time simulator and hybrid in the loop (HIL) concepts block diagram and a short description is given. Modeling of WECS involving Park's transformation, DFIG, and unidirectional power converters is part of this work. The concept of HIL is verified. The virtual power system simulated shows similar behavior as the one simulated according to real-time requirements. New researches show that PWM inverters are about to be replaced by pure sine wave inverters.

Authors (Abdallah, et al., 2016) present a model reference adaptive control (MRAC) for a DFIG based on vector-oriented control. MRAC-based totally VOC layout of the DFIG is, in brief, explained including system modeling in the synchronously rotating frame, modeling of DFIG in synchronously rotating frame, and controller design. Then, the outer control loops, the speed, and the DC-link

voltage loops are designed using PI controllers. Simulation is executed in MATLAB/Simulink under different conditions to check the validity of the designed controller. Results show that the GSC maintains the DC-link voltage constant with an overshoot of less than 7%.

Authors (Dyanamina, et al., 2016) present a vector control method for controlling the active and reactive power of a DFIG. This control strategy applies diode clamped multilevel inverter (DCMLI) in place of a two-level inverter to improve the performance of the vector controller proposed. Besides, ANFIS controllers take the position of the commonly used PI controllers. The latter is done to improve steady-state and transient performance. Simulation is done in MATLAB/SIMULINK and results show that the developed controller reduces torque ripples, improves voltage total harmonic distortion (THD) and its current waveform is more sinusoidal thus improves the integration to the grid as compared to TLI.

Authors (Aydn, et al., 2016) propose a field oriented control (FOC) for a variable speed DFIG to increase its efficiency in delivering power to the grid. Simulation is done in MATLAB/Simulink. Results show that the controller optimally controls the power output and DC capacitor voltage of the DFIG.

Authors (Sahoo, et al., 2016) present a vector control strategy for a DFIG. The controller works without a speed sensor to enable the generator to remain connected to the grid even if there is a grid fault, hence fulfilling the grid code requirement of continuous operation. The controller has an LVRT capability to maintain a stable and safe operation of the power system. The technique is tested on a 22 kW DFIG.

Authors (Verma, et al., 2016) present a control strategy to remove THD in a grid-connected DFIG using a vector control approach. Reference and measured values of stator current are the inputs to the controller, which supply a control signal to the IGBT controlled inverter. The output from this VSC is fed to the rotor.

Authors (Naamane, et al., 2011) present the technique which can keep the rotor flux constant even during changes in load torque. This controller is based on a matrix converter and a unified power flow controller (UPFC) instead of conventional PI controllers used with a squirrel cage induction generator (SCIG) and a DFIG respectively.

Authors (Marques, et al., 2012) present an analysis of the performance of different control techniques in damping flux oscillations. The first controller decreases the bandwidth of the current control loop, thereby improving the stability of the DFIG but the response to disturbances becomes slower, causing bigger disturbance currents. The two-axis damping method allows the use of higher bandwidths but its damping system is superior to the back-method.

Electromagnetic torque is controlled by regulating the stator frequency in (Esmaeeli, et al., 2012). This can be achieved by adjusting the *dq* components of the reference rotor currents. Results show that the controller is capable of controlling the torque and regulating the frequency.

Authors (Marques, et al., 2012) present a scheme for power oscillations damping. A battery energy storage system (BESS) is added to the system to boost power to reduce power oscillations every time there is imbalance.

Table 3.5 Researches on Vector control.

Ref	Method	Controlled parameters	Important findings
Cheng et al	VC	Stator voltage	No need for PLL, Minimum parameter
Hu et al	VC	Output power	NA
Peresada et al	VC	Stator voltage and flux	NA
Li et al	FL-based VC	Stator voltage	NA
Srirattanawichaikul et al	VC	NA	NA
Mannah et al	HIL	NA	Pure sine wave inverters will be used instead of basic PWM inverters
Abdallah et al	MRAC	Power, DC-link voltage	Feeding reactive power to the grid in just only one cycle
Dyanamina et al	DCMLI, ANFIS	Power, Torque, DC-link voltage	Integration of DFIG to the grid is improved
Aydn et al	FOC	Power, DC-link voltage	NA
Sahoo et al	Sensorless VC	Power, DC-link voltage	NA
Aydin et al	FOC-VC	Power, DC-link voltage	Fast response and makes sure that reactive power consumption/generation is limited
Verma et al	VC	THD	THD of GSC improved up to 16.50%.
Naamane et al	FOC	Rotor flux	Use of matrix converter and UPFC
Marques et al	I_{ms}, back-I_{ms}	Flux oscillations	NA
Marques et al	FOC, MRAS	Stator voltage, current, Rotor current	NA
Esmaeeli et al	FOC	Torque, Frequency	Uses of a simplified model of FOC
Marques et al	FOC	Power	Use of BESS in control

3.4 Fuzzy – PI dual control

In this controller, a conventional vector control discussed above is improved by the addition of another current control loop for the negative sequence currents (Abu-Rub et. al., 2014). Moreover, speed and DC bus voltage control are enhanced by the Fuzzy logic controller instead of conventional PI controllers for the RSC and GSC. This method has a control loop for the negative sequence currents caused by asymmetric voltage dips ensuring the elimination of negative sequence components. The method is applied to both RSC and GSC, enumerating the control method of each

converter, consequently controlling the torque and improving the dc voltage. The input to the FLC is the error obtained by subtracting reference input speed from the speed of the generator measured at the shaft. A similar approach is equipped with the GSC to control the DC bus voltage.

3.4.1 The fuzzy logic origin

This method was developed by Professor Lotfi Zadeh. In his initial presentation, Professor Zadeh showed it as a method for processing data instead of a control method. Professor Zadeh preferred a set membership (partial) instead of set membership (crisp) or a non-membership set. It took up to the late 1970s for fuzzy logic (FL) to be recognized as a control method for many systems. This was caused by a lack of computational capability before that time. Professor Zadeh argued that FL was adaptive and does not need precise knowledge of the controlled plant as its input. Additionally, Professor Zadeh explained that if feedback controllers are superior to the extent that they accept imprecise and noisy inputs, this would make them efficient and simplify its implementation.

3.4.2 Fuzzy logic method

The primary step in executing FL is to choose precisely the parameter to be controlled and find a way to control it among possible methods. For example, assume there is a need to design a controller for controlling the temperature with an electric warming system and equipped with a cooling fan with options to vary the speed. A positive and negative signal output range is 0-100 % for warm and cooling respectively. The accomplishment of the control objective is through legitimate adjustment and control of the two dynamic devices.

Fuzzy logic offers a distinctive and suitable means to tackle a control problem. This technique focuses on system actions instead of attempting to understand the system's working behavior. This method does not concentrate on problem tackling instead it attempts to demonstrate the system numerically. This nearly perpetually leads to speedier and cheaper arrangements. Once understood, this innovation is simple to implement and the procedure is very astounding and pleasing.

3.4.3 The rule of fuzzy logic

This technique involves a basic If X AND Y Then Z which is a rule-based method to understand a problem to be controlled instead of endeavoring to demonstrate a system scientifically. The FLC is user-friendly, depending on the knowledge of the operator instead of the technical know-how of the model of the system controlled. In FLC, temperature control is not implemented by numbers like "SP =500F", "T <1000F", or "210C <TEMP <220C", instead terms like "IF (cold) AND (cooling continue) THEN (apply heat)" or "IF (too hot) AND (heating continue) THEN (apply cooling)" are used. These terms are flawed, however extraordinarily expressive of what happens. Someone taking a shower would like to increase the temperature rapidly when the water is too cold, to make the water comfortable for bathing. FLC is competent in mirroring this sort of behavior but very fast. Fuzzy logic controls the nonlinearity of the system. Fuzzy logic is independent of the plant's numerical model. Its rules are subjectively relying on logic language variety.

3.4.4 The working principle of fuzzy logic

This method requires parameters like error and the rate-of-change-of-the error to function efficiently, but the precise values of these numbers are usually

not necessary unless under exceptionally responsive execution. In that case, experimental tuning is required to obtain good results. For illustration, a simple temperature controller utilizes a one temperature input sensor whose information is subtracted from the command signal to compute "error" and then time-differentiated to obtain the rate-of-change-of-error shortened as “error-dot”. An error might have units of degrees Fahrenheit (F) and a small error is denoted as 2F whereas a large error is 5F. The "error-dot" might then have units of degrees/min with a small error-dot being 5F/min and a huge one being 15F/min. These values should not be necessarily symmetrical and can be "changed" once the system is working to optimize execution. For the biggest part, the method is simple to implement and is expected to work smoothly. Initially, this method was considered a much better procedure for data sorting and management but has outlined as an exceptional choice to deal with different control system problems. The method mirrors human control logic. The technique can control little, hand-held things to wide computerized systems. It employs simple but extraordinarily expressive language to process input data like humans. It is particularly overpowering and acquitting of operator and data input since mostly it works soon after being executed with small or without tuning.

3.4.5 Advantages of fuzzy logic

This control method has special features making it an especially great choice for numerous control issues.

1. No requirement for noise-free inputs making it intrinsically vigorous. In any case of the input varieties, the output, as a rule, remains smooth.

2. The rules of the FL for the target control system are user-defined thus it can be adjusted and changed effectively to make strides or modify the execution of the controlled system. The design engineer can present unused sensors effectively into the system by essentially creating fitting administering rules.
3. Fuzzy logic is independent of the inputs from the available feedback path or the outputs of the plant and the estimation or computation of the rate-of-change parameters for its usage. This permits the fuzzy logic controller to be actualized with cheap sensors making the overall system simple and cheap.
4. To minimize the problem's complexity the control problem can be broke-up into littler chunks allowing littler fuzzy logic controllers located on the system, to deal with separate constrained duties.
5. FL is capable of controlling nonlinear systems that are troublesome or outlandish to model scientifically. This has opened entryways to control complex systems that were considered unautomated.

3.4.6 The structure of the FLC

The fundamental setup of an FLC includes a fuzzification stage, the knowledge base, the rule base and then does the decision before the de-fuzzification step (Lee, 2015).

1. Fuzzification: input variables measurement, followed by scale mapping, and then convert data (input) into appropriate linguistic variables.
2. The knowledge base: deals with the know-how of the problem and objective of the controller. It too comprises a database and linguistic rules.
3. The database: it has the essential definitions for fuzzy logic. These definitions are utilized to characterize linguistic rules in the control structure and data control.
4. The rule base: is capable of achieving the targets of the controller and control approach of the design specialists by using a set of linguistic rules.
5. The decision-making step: is a small portion of an FLC; it mimicks human decision-making behavior by applying fuzzy ideas and concepts, gathering fuzzy control activities, utilizing the implication step, and finally the inference step in fuzzy logic.

3.4.7 The main idea of fuzzy logic

1. Characterize the control objectives and criteria: how the system is controlled and its reaction when controlled.
2. Decide the input and output connections and select the least number of factors for input to the FL engine (ordinarily error and rate-of-change-of-error).
3. From the rule-based structure of fuzzy logic, the problem is broken down into a set of If X AND Y Then Z rules. These rules

characterize the required system output reaction for given system input conditions. The number and complexity of rules are decided based on the number of input parameters that are to be prepared and the number of fuzzy factors related to each parameter. For simplicity, utilize at slightest one variable and its time derivative.

4. Make FL membership functions that characterize the meaning (values) of Input / Output terms utilized within the rules.
5. Make the crucial pre- and post-processing FL plans in case of executing the program in the FL engine.
6. Test the program, survey the results, tune the rules and participation functions, and retest until satisfactory results are obtained.

3.4.8 Linguistic variables

Think of them as items or words, as opposed to numbers (Jantzen, 1999). The sensor input can be temperature, flow, displacement, velocity, pressure, etc. To simplify matters, positive, zero, and negative can be applied as variables for all the parameters. Moreover, factors like "very big" and "very small" might be included to amplify the responsiveness of the system.

3.4.9 Fuzzy reasoning or logic operations

Fuzzy operators can be characterized using fuzzy sets. The application of fuzzy logic faces a few challenges in knowing the fitting of the fuzzy operator (Singh et al, 2015). This makes this method utilize IF-THEN rules or develops rules that can be compared, one case being fuzzy affiliated matrices.

When conclusions are exchanged from the nine rules to the matrix, the matrix gets to be symmetric. There are a few complexities but this strategy increases the quality of the control. These rules are always communicated in the form: IF variable IS quantity THEN action. The rules of a simple temperature control could be written as follows:

IF speed IS very high THEN stop pressing the accelerator

IF pressure IS very high THEN turn down the pump

IF the distance IS very small THEN apply the brakes

It can be noticed that it does not have "ELSE". All of these rules ought to be assessed since the temperature may be felt "cold" and "ordinary" at a time to distinctive degrees.

The basic Boolean algebra operators AND, OR, and NOT are an important part of fuzzy logic. They are named as Zadeh operators characterized as the minimum, maximum, and complement. If the fuzzy variables are x and y, then:

NOT x means 1 – true x

x AND y means minimum (truth x , true y)

x OR y means maximum (truth x , true y)

The other group of operators in the form of linguistic variables, are called hedges. They are for the most part adverbs such as "*very*" or "*somewhat*", which adjust the meaning of a set employing a scientific formula.

3.4.10 Membership functions

These are used to show a degree of the size of the support of the inputs of FLC. Weights are utilized to modify the inputs to the FL. A output reaction is

obtained with the assistance of weights which are utilized to characterize the useful overlap between inputs. Weighting components can be represented by input participation factors utilized by the fuzzy rules. These weights affect the fuzzy output sets of the final output. After the steps of inferencing, scaling, and a combination of functions, the rules are de-fuzzified into a fresh output that controls the system. Triangular is the most common one, but other shapes like trapezoidal, bell, exponential, and haversine. There some complex functions but they are rarely used because they are expensive. Fuzzy membership degree can be obtained by putting the chosen input variables (error or its rate of change) into the horizontal axis and then anticipating vertically to the upper boundary of the membership function(s). Within the strategy, the rule-base is assessed as inputs received by the system.

3.4.11 Fuzzy Inferencing step

The logical items in each rule are combined or deduced before the beginning of the de-fuzzification process for the crisp output. There are a few inference strategies within the literature. After testing all the magnitudes of each rule the *MAX-MIN* control strategy selects the one with the highest magnitude. The output is taken as the horizontal coordinate of the region's "fuzzy centroid" in the specific function. In this technique, only the effects of some rules are combined, but still, the method is simple to implement and produces a nonstop output function.

The MAX-DOT or MAX-PRODUCT procedure matches each member function with its individual best value. Then, it recognizes the function composite area's horizontal coordinate of the "fuzzy" centroid as the output. The member functions are contracted to make sure their best output equals the size of their function

which is negative, zero, and positive. In this strategy, the impact of all dynamic rules is combined to produce a smooth output.

The “averaging” strategy functions properly but cannot provide an expanded weighting to more than one rule per output. An extraordinary outline is when three "negative" rules are called, but because it was one "zero" rule does, the averaging methodology will not reflect this contrast since both midpoints will rise to 0.5. Since each function is clipped at the “average”, the "fuzzy" centroid of the composite zone is calculated.

The root-sum-square (RSS) is the combination of the impacts of all appropriate rules, scales, and the capacities of each magnitude, and calculates the "fuzzy" centroid of the region. The disadvantage of this strategy is its complexity numerically compared to other strategies but can be chosen for a few cases since it gives the best-weighted impact to all terminating rules.

3.4.12 A fuzzy centroid algorithm

The crisp output is obtained from the de-fuzzification process. The results of the inference process are combined and then the area’s "fuzzy centroid" is calculated. The multiplication and summation of the weighted qualities of each output member function and their particular output participation function center focuses are performed. Finally, the region obtained is divided by the entirety of the weighted member function qualities and then the result is treated as the crisp output. Since the center of zero is situated at zero, any zero quality will be denoted as zero. In case the center of the zero function cannot be found at zero (which is normal in an honest to goodness system where warming and cooling impacts are not eminently equal), at that point the effect, at last, the entirety of the weighted member function qualities

partitions the area obtained to get the result which is the crisp output. Since the center of zero, is at zero, therefore zero value will consequently end up being zero. In case the center of the zero function happened to be away from zero (which is likely in an honest to a good system in which warming and cooling impacts are not eminently equal), at that point, this factor should not be ignored.

3.4.13 Speed and DC-Link voltage control using fuzzy logic controllers

In this thesis, an application of fuzzy logic control is considered to regulate the DFIG for speed and dc voltage control. The controllers replace the *PI* controllers in the rotor speed and dc bus voltage for the RSC and GSC, respectively.

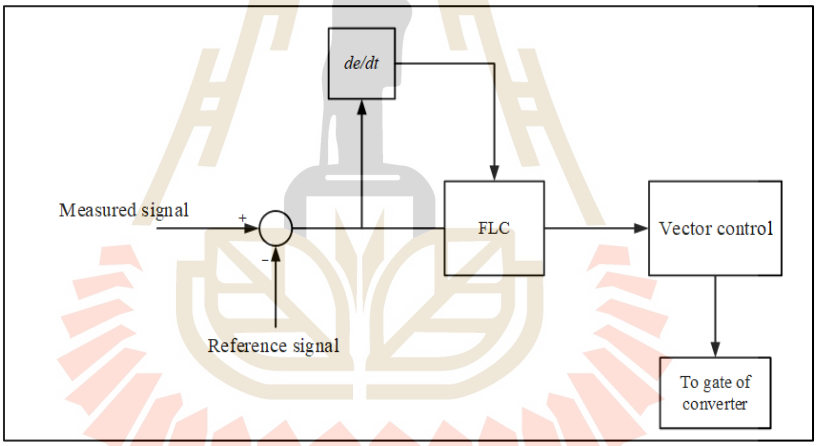

Figure 3.21 A simple Fuzzy logic controller.

The RSC controls the desired variables in three steps. The remaining two stages are handled by *PI* controllers. The proposed controller takes advantage of the beauty of both controllers. The fuzzy controller is applied to control the speed producing reference electromagnetic torque T_{em}^{*} on the difference between ω_{m}^{*} and ω_{r}.

Since the difference in speed is in the range of few percentages occurring within hundreds of microseconds, the best way is to implement an FLC instead of a conventional controller for better sensitivity of the error signal. Fuzzy logic language is used to describe all the variables used.

In the fuzzification stage, linguistic variables are used to express in fuzzy set notation all input/output variables used in the controller design. The notations of error Negative Very Big (NVB), Negative Big (NB), Negative Medium (NM), Negative Small (NS), Negative (N), Zero (ZO), Positive (P), Positive Small (PS), Positive Medium (PM), Positive Big (PB) and Positive Very Big (PVB), are characterized by the triangular and trapezoidal membership functions. For output torque reference, nine membership functions as in the error signal are also chosen. The error and the torque reference are passed through all fuzzy logic stages before being expressed as fuzzy sets.

The control strategy defines the fuzzy sets obtained into the IF-THEN rules. As the behavior of the DFIG is known to the FLC designer the fuzzy rules are easily expressed in the fuzzy domain like “If the error is NB then electromagnetic torque is NVB”.

In the defuzzification step, the linguistic variables are transformed into crisp values for speed and torque control. The center of gravity (COG) method is used as the defuzzification technique,

$$y(x)=\frac{\sum_j^N \omega_j \mu_j(x)}{\sum_j^N \mu_j(x)} \tag{3.96}$$

Where:

$y(x)$ = output reference torque

ω_j = weight for a given output fuzzy set

$\mu_j(x)$ = fuzzy rule degree.

x = input vector.

3.4.14 Current loops dual control for the unbalanced system

The original control loop is separated into two: the primary which deals with the positive rotating reference frame, and the other for the negative sequence component (Abu-Rub et. al., 2014). Control reasoning is the dual-vector control method.

The power transferred between the converter and the grid is given by the following equation:

$$P_g = \frac{3}{2} R_e \left\{ \vec{v}_g \cdot \vec{i}_g^{\,*} \right\}$$
$$Q_g = \frac{3}{2} I_m \left\{ \vec{v}_g \cdot \vec{i}_g^{\,*} \right\} \quad (3.97)$$

Where:

P_g = Grid active power from the converter

Q_g = Grid reactive power from the converter

v_g = Grid voltage.

i_g = Grid current.

Decomposing the voltages and currents in the positive and negative sequences give,

$$\begin{aligned}\vec{v}_g &= V_1 e^{j\omega gt} + V_2 e^{-j\omega gt} = \left(v_{d1} + jv_{q1}\right)e^{j\omega gt} + \left(v_{d2} + jv_{q2}\right)e^{-j\omega gt} \\ \vec{i}_g &= I_1 e^{j\omega gt} + I_2 e^{-j\omega gt} = \left(i_{d1} + ji_{q1}\right)e^{j\omega gt} + \left(i_{d2} + ji_{q2}\right)e^{-j\omega gt}\end{aligned} \tag{3.98}$$

Where:

ω_g = grid frequency

The subscripts 1 refer to the positive sequence and 2 for the negative sequence, and the subscript g has been omitted.

Decomposition the grid powers leads to,

$$\begin{cases} P = P_0 + P_{\cos}\cos\left(2\omega_g t\right) + P_{\sin}\sin\left(2\omega_g t\right) \\ Q = Q_0 + Q_{\cos}\cos\left(2\omega_g t\right) + Q_{\sin}\sin\left(2\omega_g t\right) \end{cases} \tag{3.99}$$

Where the coefficients $P_0, P_{\cos}, P_{\sin}, Q_0, Q_{\cos}, Q_{\sin}$ are given by the following matrix:

$$\begin{bmatrix} P_0 \\ Q_0 \\ P_{\cos} \\ P_{\sin} \\ Q_{\cos} \\ Q_{\sin} \end{bmatrix} = \frac{3}{2}\begin{bmatrix} v_{dp} & v_{qp} & v_{dn} & v_{qn} \\ v_{qp} & -v_{dp} & v_{qn} & -v_{dn} \\ v_{dn} & v_{qn} & v_{dp} & v_{qp} \\ v_{qn} & -v_{dn} & -v_{qp} & v_{dp} \\ v_{qn} & -v_{qn} & v_{qp} & -v_{dp} \\ -v_{dn} & -v_{qn} & v_{dp} & v_{qp} \end{bmatrix} \cdot \begin{bmatrix} i_{dp} \\ i_{qp} \\ i_{dn} \\ i_{qn} \end{bmatrix} \tag{3.100}$$

With a balanced grid, there will be no negative sequence; that is v_{dn}, v_{qn}, i_{dn}, and i_{qn} are zero. Therefore, the coefficients $P_{\cos}$, $P_{\sin}$, $Q_{\cos}$, $Q_{\sin}$ are zero. With unbalanced input voltages, however, these coefficients are nonzero and the powers are dynamically varying. The dc voltage level is decided by the amount of active power from the DC link to the grid. Hence, if there is a variation of P_g, then the DC-link voltage faces instability, and a ripple appears at twice the grid frequency. The coefficients $Q_{\cos}$, $Q_{\sin}$ express the variation of reactive power and do not affect the voltage and they are removed from the matrix (Abu-Rub et. al., 2014).

$$\begin{bmatrix} P_0 \\ Q_0 \\ P_{\cos} \\ P_{\sin} \end{bmatrix} = \frac{3}{2}\begin{bmatrix} v_{dp} & v_{qp} & v_{dn} & v_{qn} \\ v_{qp} & -v_{dp} & v_{qn} & -v_{dn} \\ v_{dn} & v_{qn} & v_{dp} & v_{qp} \\ v_{qn} & -v_{dn} & -v_{qp} & v_{dp} \end{bmatrix} \cdot \begin{bmatrix} i_{dp} \\ i_{qp} \\ i_{dn} \\ i_{qn} \end{bmatrix} \tag{3.101}$$

For obtaining a constant DC level, the coefficients $P_{\cos}$, $P_{\sin}$ are nullified. By inverting the matrix (3.101) the currents necessary to achieve that goal can be calculated:

$$\begin{bmatrix} i_{dp} \\ i_{qp} \\ i_{dn} \\ i_{qn} \end{bmatrix} = \frac{P_0}{D} \cdot \frac{2}{3}\begin{bmatrix} v_{dp} \\ v_{qp} \\ -v_{dn} \\ -v_{qn} \end{bmatrix} + \frac{Q_0}{R} \cdot \frac{2}{3}\begin{bmatrix} v_{qp} \\ -v_{dp} \\ v_{qn} \\ -v_{dn} \end{bmatrix} \tag{3.102}$$

Where:

$$D = \left(v_{dp}^2 + v_{qp}^2\right) - \left(v_{dn}^2 + v_{qn}^2\right)$$
$$R = \left(v_{dp}^2 + v_{qp}^2\right) + \left(v_{dn}^2 + v_{qn}^2\right) \quad (3.103)$$

In a GSC, the current references are computed to avoid oscillations in the generator's DC link voltage between back to back converters while obtaining the desired average powers. In a DFIG, different strategies may be adopted to minimize:

1. Stator power oscillations
2. RMS Stator current
3. Torque ripple
4. RMS Rotor current
5. Rotor voltage

It is simpler to get adjusted rotor currents within the DFIG by presenting a negative sequence null for the reference values of the rotor current. The strategy is additionally included in the ordinary vector control. The distinction between double control and vector control is that in double control the negative sequence is expressly driven to zero employing the negative current controller. The references for this methodology are calculated as follows:

$$\begin{bmatrix} i_{dp} \\ i_{qp} \\ i_{dn} \\ i_{qn} \end{bmatrix} = \frac{2}{3}\frac{L_s}{L_m}\frac{1}{v_{dp}^2 + v_{qp}^2}\begin{bmatrix} v_{qp} & v_{qp} \\ -v_{dp} & -v_{dp} \\ 0 & 0 \\ 0 & 0 \end{bmatrix}\begin{bmatrix} P_{s0} \\ Q_{s0} \end{bmatrix} + \frac{1}{\omega_s L_m}\begin{bmatrix} v_{qp} \\ -v_{dp} \\ 0 \\ 0 \end{bmatrix} \quad (3.104)$$

The sequence decomposition of current loops and voltage references generation is graphically represented in Figure 3.22.

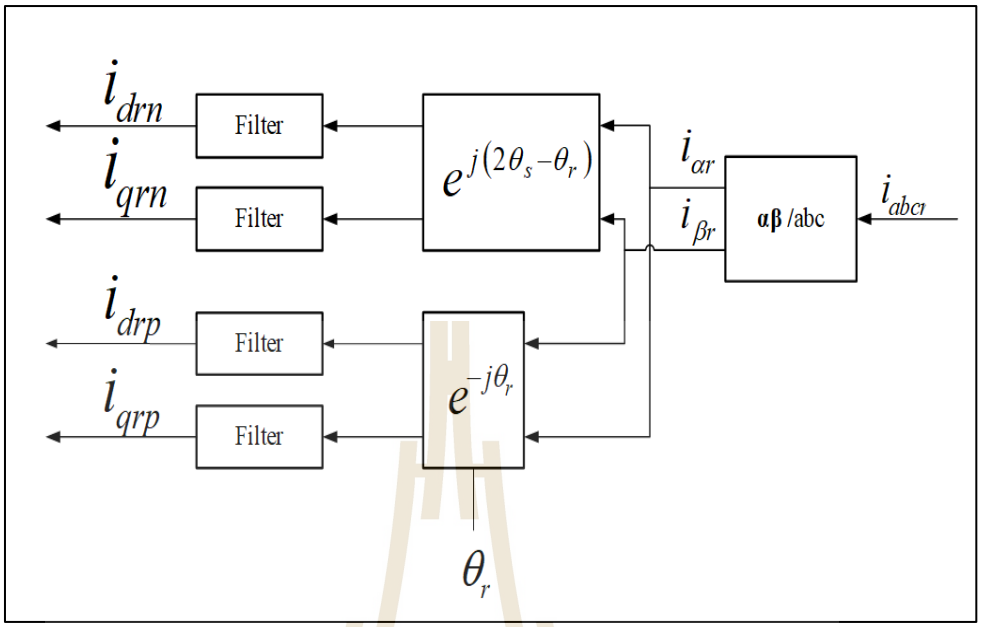

Figure 3.22 Rotor current sequence decomposition.

The same procedure is done with the GSC as shown in Figure 3.3.

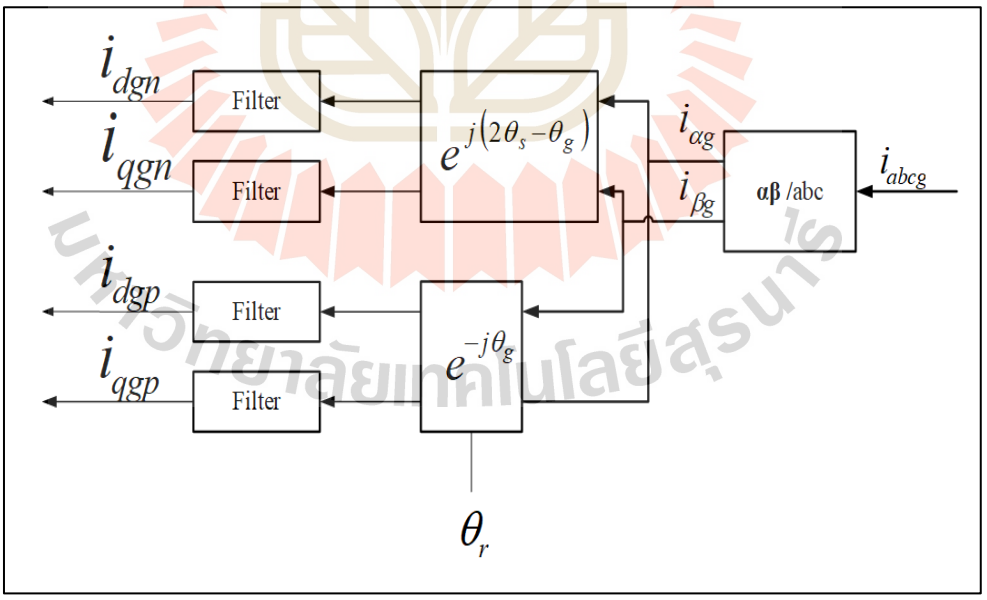

Figure 3.23 Grid current sequence decomposition.

A complete circuit of the proposed controller is shown in Figure 3.24.

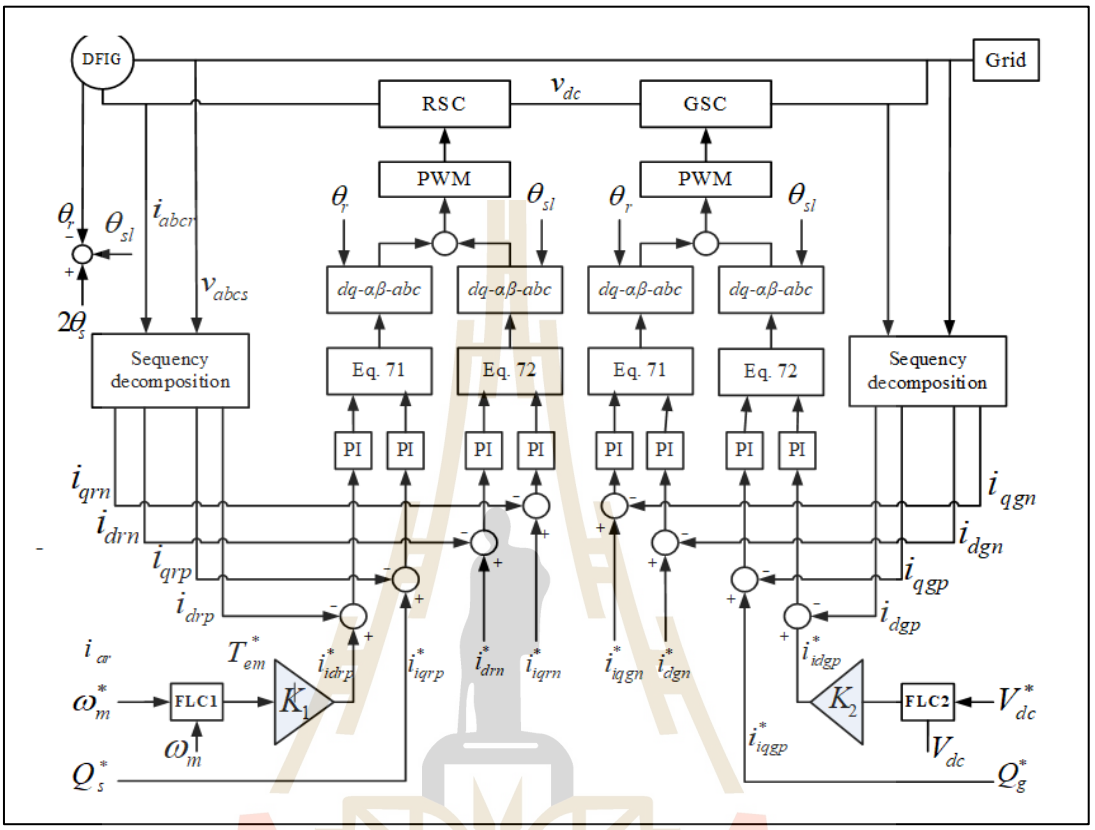

Figure 3.24 Fuzzy-PI dual controller for a DFIG.

3.5 Optimal control and Kalman filter for a DFIG

In the past, conventional methods used proportional-integral (PI) controllers to control the DFIG. One of these classical controllers is a well-known Vector control. Nowadays, modern optimal control techniques are applied to control the DFIG (Oonsivilai, et. al., 2019). Linear quadratic regulator (LQR) is one of those optimal controllers.

There is a lot of researches on the control of DFIG using LQR. In a recent publication, Prajapat, et al., 2018 compared LQR and power system stabilizer

performances and costs in damping oscillations in the grid-connected DFIG. The authors apply the Uncedented Kalman filter (UKF) to estimate unobservable states (Prajapat, et. al., 2018).

Particle swarm optimization is used to tune LQRI weighting matrices Q and R in (Murari, et. al., 2019). The authors in (Taveiros, et. al., 2019) present a new method known as heightened state feedback control (HSFC). In the paper rotor, currents are regulated by model predictive control.

A hybrid technique of linear quadratic regulator-optimal preview control (LQR-OPC) is applied to damp power oscillations in a grid-connected DFIG (Subudhi, et. al., 2018). After comparison authors found that LQR-OPC has the best performance compared to SM-FOC. The trajectory sensitivity analysis (TSA) method is applied to find a suitable state weighting matrix for the LQR. The optimal controller obtained through the method developed by Abdelsalam, et al., 2017 significantly damps oscillations. Moreover, this method enables the DFIG to support the grid. LQR is applied to damp subsynchronous interaction in a farm of DFIGs (Ghafouri, et. al., 2017). The contributions of this work are oscillations damping of the DFIG using LQR and Pole Placement and comparing the two optimal control methods.

Electromagnetic torque is given by,

$$T_{em} = -\frac{3}{2} p \frac{L_m}{L_s} |\vec{\psi}_s| i_{qr} \tag{3.105}$$

The rotor mechanical speed is,

$$\frac{d\omega_m}{dt} = \frac{p}{2J}\left(T_{em} - T_m\right) \tag{3.106}$$

Where:

J = Inertia of the rotor

T_m = Turbine aerodynamic torque

Reference torque and rotor current can be generated from a given reference speed (Chen, et. al., 2011). The error obtained is $\omega_m^{ref} - \omega_m$ processed by the proportional and integral controllers to give reference torque T_{em}^{ref}. This is multiplied with the gain G_1 to generate a reference rotor current i_{qr}^{ref}. Then the transfer function TF_1 is used to obtain measured quadrature axis rotor current i_{qr}. This current is multiplied with the gain G_2 to obtain the required electromagnetic torque T_{em}. The error between electromagnetic torque T_{em} and the load torque T_m is multiplied by TF_2 to produce rotational mechanical speed Ω_m. Mechanical speed Ω_m is multiplied by the pole pairs p to obtaining the required rotor speed ω_m.

The equivalent speed control scheme with feedback loop is shown in Figure 3.25 (Oonsivilai, et. al., 2019).

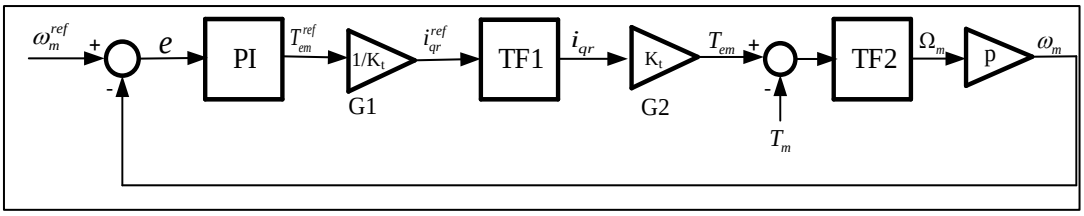

Figure 3.25 Speed loop control of the DFIG.

The torque constant is given by,

$$K_t = -\frac{3}{2} p \frac{L_m}{L_s} |\vec{\psi}_s| \tag{3.107}$$

From Figure 3.25, the transfer function between the reference rotor current i_{qr}^{ref} and its measured value i_{qr} is,

$$TF_1 = \frac{sk_p + k_i}{\sigma L_r s^2 + \left(k_p + R_r\right)s + k_i} \tag{3.108}$$

The transfer function between measured electromagnetic torque T_{em} and rotational mechanical speed Ω_m is given by,

$$TF_2 = \frac{1}{Js} \tag{3.109}$$

The closed-loop speed loop in Figure 3.25 can be represented by this transfer function (Chen, et. al., 2011),

$$G(s) = \frac{sk_{pn} + k_{in}}{(J/p)s^2 + k_{pn}s + k_{in}} \tag{3.110}$$

The proportional and integral gains are given by,

$$k_{pn} = \frac{2 \cdot \omega_n \cdot J}{p} \,\&\, k_{in} = \frac{\omega_n^2 \cdot J}{p} \tag{3.111}$$

Where:

τ = Torque constant

ω_m^* = Reference speed.

ω_m = Measured speed.

J = Inertia.

p = Pole pairs.

k_{pn} = Proportional controller for speed.

k_{in} = Integral controller for speed.

S = Laplace operator.

The transfer function (3.111) is used to design a pole placement based optimal controller to improve the stability of the system.

3.5.1 Pole placement

In this method, the state variables obtained are fed back to the system through a feedback loop having a regulator with constant gains to fulfill the control objective (Saadat, 2011). The system (3.1-3.2) can be represented in Figure 3.26. In

the figure, *A*, *B*, and *C* are state, input, and output matrices respectively and *K* is the controller. The matrix *D* is assumed to be equal to zero.

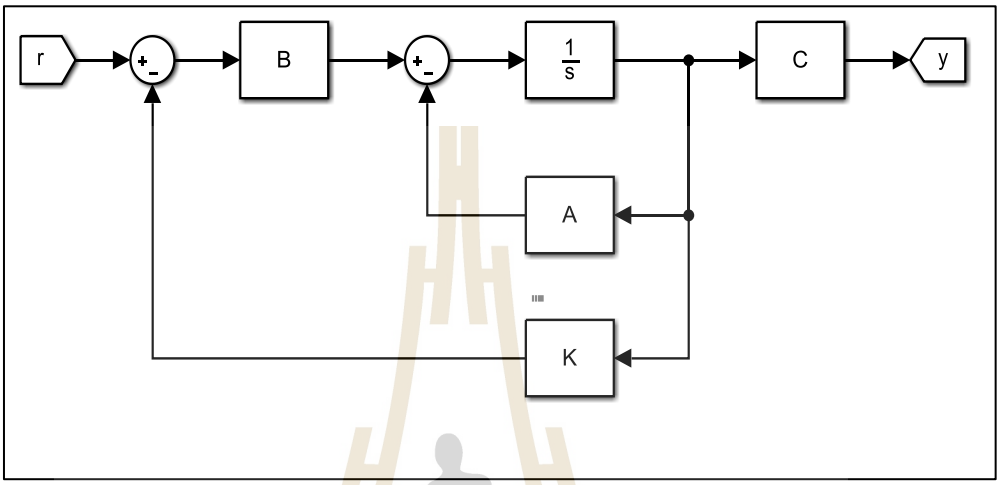

Figure 3.26 Block diagram system representation.

The system representation in the form of the block diagram is in Figure 3.26. Adding (3.5) to the state vector gives,

$$\dot{x}(t) = \left(A - BK\right)x(t) = A_f x\left(t\right) \tag{3.112}$$

The compensated system characteristic equation is

$$\left|sI - A + BK\right| = 0 \tag{3.113}$$

The gain *K* is calculated using (3.113). The transfer function (3.110) is converted to state-space matrices A, B, C and D as shown below:

$$A = \begin{bmatrix} -160 & -100 \\ 64 & 0 \end{bmatrix}$$

$$B = \begin{bmatrix} 16 \\ 0 \end{bmatrix}$$

$$C = \begin{bmatrix} 10.0000 & 6.2500 \end{bmatrix}$$

$$D = 0$$

Using the pole placement method, the gain vector obtained is K_1 = [-2.3843 -2.6251].

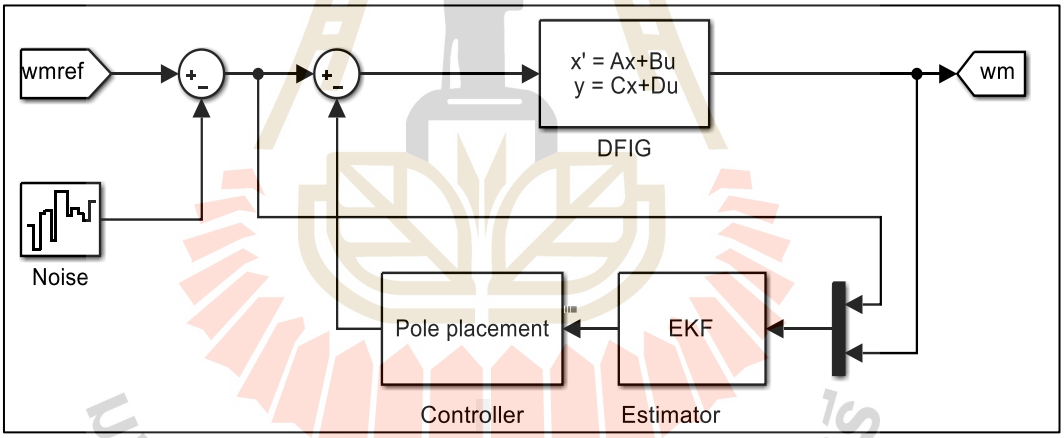

Figure 3.27 DFIG with pole placement controller and EKF.

3.5.2 Linear quadratic regulator

This study aims to design an optimal controller for linear systems. It has the name linear quadratic regulator (LQR) controller because it works by minimizing the index which is in the form of a quadratic function (Oonsivilai, et. al.,

2019). Consider the plant described by (3.1). The process seeks the vector $K(t)$ of the control law (3.5) to minimize the quadratic performance index,

$$J = \int_{t=0}^{t=f} \left(x'Qx + u'Ru\right)dt \tag{3.114}$$

Where:

Q = positive semidefinite matrix.

R = real symmetric matrix.

Lagrange multipliers are applied to solve the constraint problem by augmenting (3.1) into (3.114) utilizing the Lagrange multipliers vector λ. This problem diminishes to the minimization of the unconstrained function.

$$\mathscr{L}\left(x,\lambda,u,t\right) = \left[x'Qx + u'Ru\right] + \lambda'\left[Ax + Bu - \dot{x}\right] \tag{3.115}$$

The optimal values (indicated by the subscript (*) are computed by comparing the fractional derivatives of (3.115) to zero,

$$\frac{\partial L}{\partial \lambda} = AX^* + Bu^* - \dot{x}^* = 0 \;\Rightarrow\; \dot{x}^* = AX^* + Bu^* \tag{3.116}$$

$$\frac{\partial L}{\partial u} = 2Ru^* + \lambda'B = 0 \;\Rightarrow\; u^* = -\frac{1}{2}R^{-1}\lambda'B \tag{3.117}$$

$$\frac{\partial L}{\partial x} = 2x'^*Q + \dot{\lambda}' + \lambda'A = 0 \;\Rightarrow\; \dot{\lambda} = -2Qx^* - A'\lambda \tag{3.118}$$

The assumption is made that there exists a symmetric, time-varying positive definite matrix $p(t)$ satisfying,

$$\lambda = 2p(t)x^* \tag{3.119}$$

Substituting (3.119) into (3.117) gives the optimal closed-loop control law,

$$u^*(t) = -R^{-1}B'p(t)x^* \tag{3.120}$$

Obtaining the derivative of (3.119) gives,

$$\dot{\lambda} = 2\left(px^* + p\dot{x}^* \right) \tag{3.121}$$

Finally, equating (3.118) with (3.121), this is obtained,

$$\dot{p}(t) = -p(t)A - A'p(t) - Q + p(t)BR^{-1}B'p(t) \tag{3.122}$$

The matrix Riccati equation is shown in (3.122). The boundary condition imposed for (p) is $p(t_f) = 0$. The solution to (3.122) is a gateway to the state equation (3.122) and the optimum control equation (3.120). The developed control system with noise in the input signal is as shown in Figure 3.28.

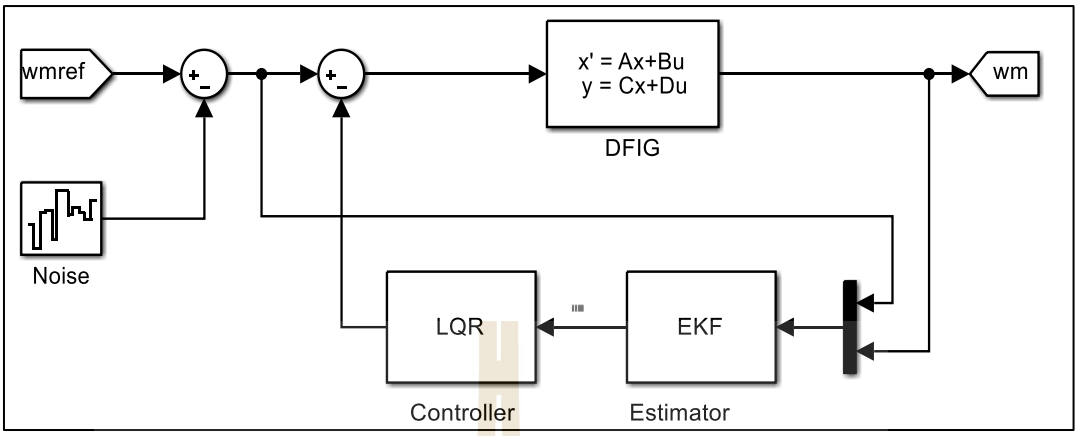

Figure 3.28 DFIG with linear quadratic regulator and EKF.

3.6 Dynamic modeling of DFIG

The important parameters of the machine can be depicted by the following equations starting with the three-phase stator voltages:

$$v_{as} = R_s i_{as} + \frac{d\psi_{as}}{dt} \tag{3.123}$$

$$v_{bs} = R_s i_{bs} + \frac{d\psi_{bs}}{dt} \tag{3.124}$$

$$v_{cs} = R_s i_{cs} + \frac{d\psi_{cs}}{dt} \tag{3.125}$$

Similarly, the rotor magnitudes are described by,

$$v_{ar} = R_r i_{ar} + \frac{d\psi_{ar}}{dt} \tag{3.126}$$

$$v_{br} = R_r i_{br} + \frac{d\psi_{br}}{dt} \tag{3.127}$$

$$v_{cr} = R_r i_{cr} + \frac{d\psi_{cr}}{dt} \tag{3.128}$$

The voltage equations of the DFIG, in space vector form:

$$\vec{v}_s = R_s \vec{i}_s + \frac{d\vec{\psi}_s}{dt} \tag{3.129}$$

$$\vec{v}_r = R_r \vec{i}_r + \frac{d\vec{\psi}_r}{dt} \tag{3.130}$$

Where

$\vec{v}_s$ = Space vector of the stator voltage.

$\vec{i}_s$ = Space vector of the stator current.

$\vec{\psi}_s$ = Space vector of the stator flux.

$\vec{v}_r$ = Space vector of the rotor voltage.

$\vec{i}_r$ = Space vector of the rotor current.

$\vec{\psi}_r$ = Space vector of the rotor flux.

Space vector quantities for fluxes in terms of inductances and the currents are:

$$\vec{\psi}_s = L_s\vec{i}_s + L_m\vec{i}_r \tag{3.131}$$

$$\vec{\psi}_r = L_m\vec{i}_s + L_r\vec{i}_r \tag{3.132}$$

Where:

L_s = stator inductance

L_r = rotor inductance

L_m = magnetizing inductance.

The leakage inductances $L_{\sigma s}$ and $L_{\sigma r}$ of the stator and the rotor respectively are given by,

$$L_s = L_{\sigma s} + L_m \tag{3.133}$$

$$L_r = L_{\sigma r} + L_m \tag{3.134}$$

Multiplying (3.129) and (3.130) with $e^{-j\theta_s}$ and $e^{-j\theta_r}$, respectively, the stator and rotor voltage is:

$$v_{as} = R_s\vec{i}_{as} + \frac{d\vec{\psi}_{as}}{dt} + j\omega_s\vec{\psi}_{as} \tag{3.135}$$

$$v_{ar} = R_r\vec{i}_{ar} + \frac{d\vec{\psi}_{ar}}{dt} + j\omega_r\vec{\psi}_{ar} \tag{3.136}$$

Fluxes are given by,

$$\vec{\psi}_{as} = L_s \vec{i}_{as} + L_m \vec{i}_{ar} \tag{3.137}$$

$$\vec{\psi}_{ar} = L_m \vec{i}_{as} + L_r \vec{i}_{ar} \tag{3.138}$$

The torque and power in dq reference frame:

$$P_s = \frac{3}{2}\left(v_{ds} i_{ds} + v_{qs} i_{qs}\right) \tag{3.139}$$

$$P_r = \frac{3}{2}\left(v_{dr} i_{dr} + v_{qr} i_{qr}\right) \tag{3.140}$$

$$Q_s = \frac{3}{2}\left(v_{qs} i_{ds} + v_{ds} i_{qs}\right) \tag{3.141}$$

$$Q_r = \frac{3}{2}\left(v_{qr} i_{dr} + v_{dr} i_{qr}\right) \tag{3.142}$$

Therefore, the torque expression also yields,

$$T_{em} = \frac{3}{2} p \frac{L_m}{L_s}\left(\psi_{qs} i_{dr} - \psi_{ds} i_{qr}\right) \tag{3.143}$$

Taking the fluxes as state variables, the model of the DFIG is given by,

$$\frac{d}{dt}\begin{bmatrix}\vec{\psi}_s^a \\ \vec{\psi}_r^a\end{bmatrix} = \begin{bmatrix}\frac{-R_s}{\sigma L_s} - j\omega & \frac{R_s L_m}{\sigma L_s L_r} \\ \frac{R_r L_m}{\sigma L_s L_r} & \frac{-R_r}{\sigma L_r} + j\omega_r\end{bmatrix}\begin{bmatrix}\vec{\psi}_s^a \\ \vec{\psi}_r^a\end{bmatrix} + \begin{bmatrix}\vec{v}_s^a \\ \vec{v}_r^a\end{bmatrix} \tag{3.144}$$

Expanding this last expression in the dq components,

$$\frac{d}{dt}\begin{bmatrix}\psi_{ds}\\ \psi_{qs}\\ \psi_{dr}\\ \psi_{qr}\end{bmatrix}=\begin{bmatrix}\frac{-R_s}{\sigma L_s} & \omega_s & \frac{R_s L_m}{\sigma L_s L_r} & 0\\ -\omega_s & \frac{-R_s}{\sigma L_s} & 0 & \frac{R_s L_m}{\sigma L_s L_r}\\ \frac{R_r L_m}{\sigma L_s L_r} & 0 & \frac{-R_r}{\sigma L_r} & \omega_r\\ 0 & \frac{R_r L_m}{\sigma L_s L_r} & -\omega_r & \frac{-R_r}{\sigma L_r}\end{bmatrix}\begin{bmatrix}\psi_{ds}\\ \psi_{qs}\\ \psi_{dr}\\ \psi_{qr}\end{bmatrix}+\begin{bmatrix}v_{ds}\\ v_{qs}\\ v_{dr}\\ v_{qr}\end{bmatrix} \quad (3.145)$$

3.7 Robust H-infinity control

In the H∞ configuration shown in Figure 3.29, the method seeks for the controller K which to minimize the error z . This reduces the H∞-norm of the transfer function from w to z (Makouf, et al., 2002).

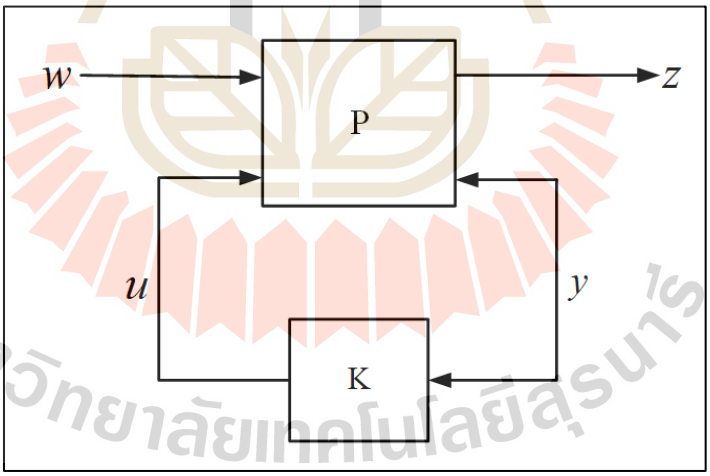

Figure 3.29 The standard H∞ configuration.

Where:

w = disturbance inputs

u = control inputs

z = error outputs to be minimized.

y = outputs of the plant fed back to the controller.

The method seeks K to stabilize the plant P. The performance level γ is achieved, which is the H∞ norm of the closed system.

3.7.1 H-infinity method

H∞ strategies are applied in control theory to design controllers accomplishing vigorous execution or stabilization (Wang, et al., 2013). To utilize H ∞ strategies, an architect in control engineering expresses it as an optimization problem and finds the method that exactly tackles this problem. One of the preferences of H∞ methods over classical control strategies is their applications to problems including multivariable systems. The drawbacks of H∞ procedures are that they are numerically complex and the system to be controlled needs to be optimally modeled. Problem detailing is critical since any controller developed will only be 'optimal' within the defined range because sometimes optimizing the wrong thing may make things worse instead of being superior. This optimization approach is a productively strong design strategy for straight, time-invariant systems.

3.7.2 H-infinity optimal control

This controller calculates the optimal controller K used to regulate the plant . The partitioned form of the plant is shown in Figure 3.29. Consider the dynamic system equation written as (Khargonekar et al, 1988).

$$\frac{dx}{dt}(t) = A(x)(t) + Bu(t) + Dw(t) \tag{3.146}$$

$$z(t) = Ex(t) \tag{3.147}$$

Where:

$x(t) \in \Re^n$ = state

$u(t) \in \Re^m$ = control input.

$w(t) \in \Re^p$ = disturbance, or more the exogenous signal

$z(t) \in \Re^q$ = controlled output.

A, B, D, E = matrices of appropriate sizes.

The assumption is that the measured output is the state $x(t)$ sent back to the input through feedback. The controllers applied are expressed as follows:

$$u(t) = Kx(t)$$

Where $K \in \Re^{m \times n}$, in the static case, and

$$(\Sigma_d) \qquad \frac{dv}{dt}(t) = Fv(t) + Gx(t) \tag{3.148}$$

$$u(t) = Hv(t) + Jx(t) \tag{3.149}$$

Where:

$(F, G, H, J) \in \Re^{r \times r} \times \Re^{r \times n} \times \Re^{m \times r} \times \Re^{m \times n}$ for the dynamic state feedback.

Let $T_s(s) := E\left[sI-(A-BK)\right]^{-1}D$ represent the closed-loop transfer function z . On the other hand, let $T_d(s)$ be the closed-loop transfer function from the w to z ,

$$\gamma_s := \inf\left\{\|T_s\|_\infty : K \in \aleph\right\} \tag{3.150}$$

$\aleph := \left\{K \in \Re^{m\times n} : A+BK\right\}$, $A+BK$ is a stability matrix.

$$\gamma_d := \inf\left\{\|T_d\|_\infty : (F,G,H,J) \in \Im\right\} \tag{3.151}$$

$\Im := \left\{(F,G,H,J) \in \Re^{r\times r}\Re^{r\times n}\Re^{m\times r} \times \Re^{m\times n} : \begin{bmatrix} A+BJ & BH \\ G & F \end{bmatrix}\right\}$ is a stability matrix.

$\|X\|_\infty = \sup\left\{\|X(j\omega)\| : \omega \in \Re\right\}$ and $\|X\|$ denotes the maximum singular value of the matrix X .

Finding γ_d and a controller making $\|T_d\|_\infty$ as close to γ_d as thought is a standard problem in H_∞ optimal control theory. Undoubtedly, optimal control theory goes further than that by dealing with more difficult problems of output feedback. Note that the problem detailing in this work is equivalent to the general problem with two extra assumptions:

- The measured output is the state $x(t)$,
- No direct transmission from $u(t)$ to $z(t)$ (the transfer functions from u and w to the controlled output z are strictly proper)

3.7.3 Robust h-infinity loop shaping control

This may be a new design strategy in modern control techniques (Gilev, 2017). This method combines the conventional classical control strategies and h infinity optimization procedures to get controllers whose steadiness and execution properties are great despite the slight contrasts between the first plant assumed in the plan and the genuine plant. At that point, the controller architect has the task of describing the required responsiveness and noise suppression properties. The open-loop system is improved by pre and post compensators to provide the specified open-loop frequency response. The method is usually done by weighing the plant transfer function within the frequency domain and the resulting loop shape is then robustly characterized by optimization robustification. The pre-compensator or weighting function is first chosen as the original PI controller transfer function. The obtained system was robustly stabilized concerning the general class of coprime factor uncertainty using H∞ optimization. This has a small impact at high and low frequencies but the response around unity gain crossover is balanced to maximize the system's stability margins. H infinity loop shaping can be applied to multiple input multiple output systems. The loop shaping method allows the control architect to apply classical loop-shaping concepts to the multivariable frequency response to induce a distant better vigorous execution and after that optimizes the response close the system bandwidth to realize great robust stabilization.

The goals of a robust feedback control system like the one shown in Figure 3.30 can be as follows:

i. Stability improvement

ii. Uncertainty compensation

iii. Disturbance rejection

iv. Noise attenuation

Consider the system shown below:

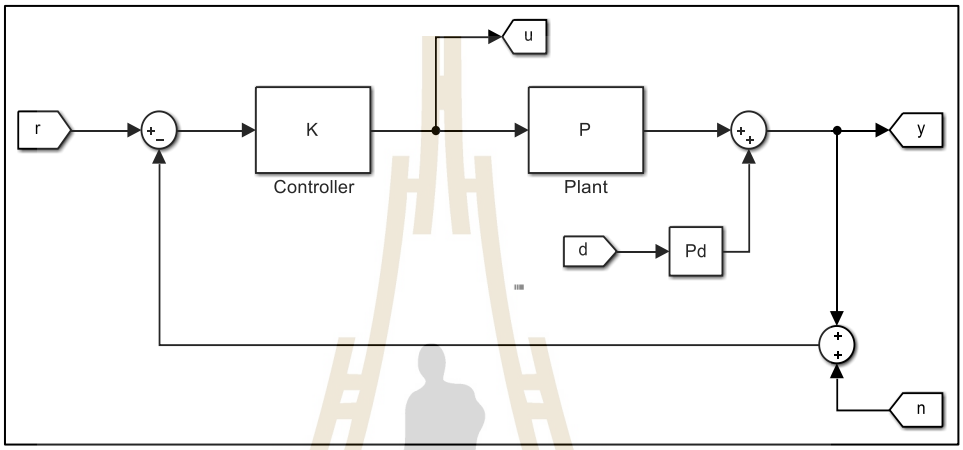

Figure 3.30 Closed-loop system with controller, disturbance, and noise.

The open-loop transfer function of the system in Figure 3.30 is given by,

$$L = PK \tag{3.152}$$

Where:

P = Plant

K = Controller

The output y can be given by,

$$y = P_d d + PK(r - y - n) \tag{3.153}$$

The error is,

$$\varepsilon = r - y - n \tag{3.154}$$

Multiplying the LHS of (3.153) by identity matrix I gives,

$$Iy = P_d d + PK(r - y - n) \tag{3.155}$$

$$Iy = P_d d + PKr - PKy - PKn \tag{3.156}$$

Collecting terms in y

$$(I + PK)y = PKr + P_d d - PKn \tag{3.157}$$

Making y the subject

$$y = (I + PK)^{-1} PKr + (I + PK)^{-1} P_d d - (I + PK)^{-1} PKn \tag{3.158}$$

The sensitivity of the system can be given by (Astr¨om and Murray, 2006),

$$S = (I + PK)^{-1} \tag{3.159}$$

Substituting (3.152) into (3.159), Sensitivity can be written as,

$$S = (I + L)^{-1} \tag{3.160}$$

Therefore, complementary sensitivity can be given by (Astr¨om and Murray, 2006),

$$T = \left(I + PK\right)^{-1} PK \tag{3.161}$$

Substituting (3.152) into (3.161) gives,

$$T = \left(I + L\right)^{-1} L \tag{3.162}$$

Let the addition of sensitivity and complementary sensitivity equal the identity,

$$S + T = I \tag{3.163}$$

Therefore, the error can be written as,

$$\varepsilon = Sr - SP_d d + Tn \tag{3.164}$$

The study designs a controller that would make the error equal to zero. That would have the following advantages:

1. Good reference tracking for a slow change in reference. Therefore, sensitivity S should be very small at low frequencies
2. Good disturbance rejection at low frequencies
3. Good noise attenuation at high frequencies. Therefore, complementary sensitivity should be very small at higher frequencies.

The requirements above show that reference tracking and disturbance rejection are low-frequency phenomena while noise attenuation is a high-frequency phenomenon.

This behavior of the controller can be shown by the bode plot in Figure 3.31.

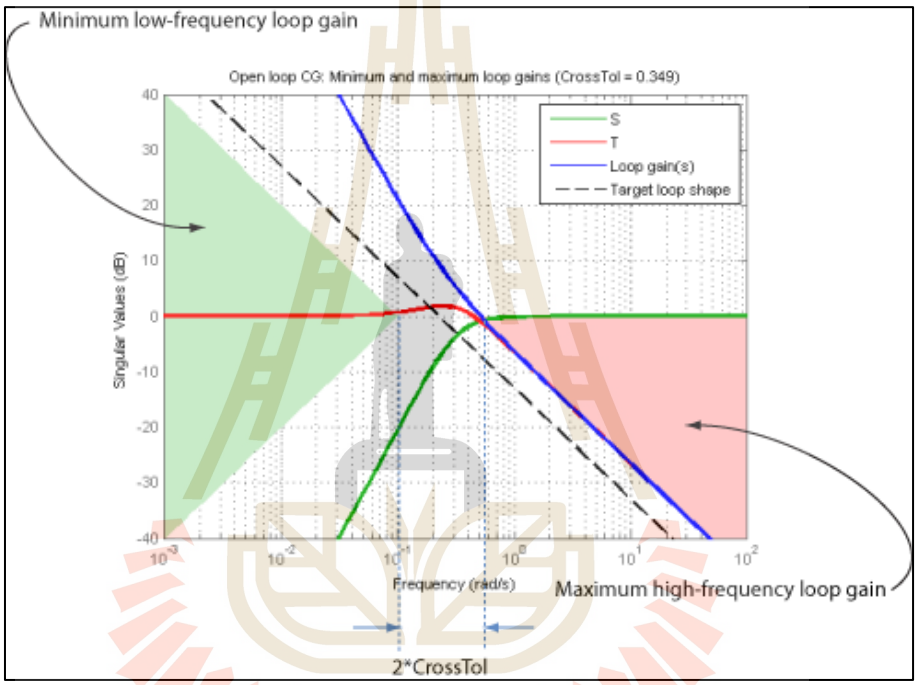

Figure 3.31 Sensitivity, Complementary sensitivity, and Target loop shapes of a closed-loop system (Mathworks).

The crossover frequency ω_c is the point where sensitivity S crosses complementary sensitivity T. The task is to design a controller which would make the loop transfer function L to be very big at low frequencies because sensitivity is low at low frequencies and to make L to be very small at high frequencies because complementary sensitivity is low at high frequencies. The two actions would bring

good reference tracking, disturbance rejection, and noise attenuation. Therefore, a controller is designed to make the loop transfer function to look like an integrator as,

$$L = \frac{W_b}{s} \tag{3.165}$$

Where:

W_b = bandwidth

If W_b is big the loop will move to the right and have higher frequency performance. If W_b is small, the loop will move to the left for low-frequency performance. The zero dB line is where there is a tradeoff between sensitivity and complementary sensitivity.

If the bandwidth, $W_b = 8$ the desired loop transfer function becomes,

$$L = \frac{8}{s} \tag{3.166}$$

Since $L = PK$ and if the system is controllable,

$$T.F. = \frac{1}{s+1} \tag{3.167}$$

Therefore, $\frac{1}{s+1}K = \frac{8}{s}$

This gives the controller gain

$$K = \frac{8(s+1)}{s} \tag{3.168}$$

The design goals may be summarized as follows.

- The working of this technique requires *S to be* small and *T* close to 1 at low frequencies.

$$S = \frac{1}{1+L} \tag{3.169}$$

$$T = \frac{L}{1+L} \tag{3.170}$$

- Equations (3.169) and (3.170), show that these targets may be reached simultaneously when the loop gain *L* is large ($|L(j\omega)| >> 1$) in the low-frequency region.
- At high frequencies, *T* should be small and *S* close to 1. This can happen when the loop gain *L* is small ($|L(j\omega)| << 1$) in the high-frequency region.

The specifications on *S* in the low-frequency region, and *T* in the high-frequency region shows how to result in bounds on the loop gain *L* in Figure 3.32.

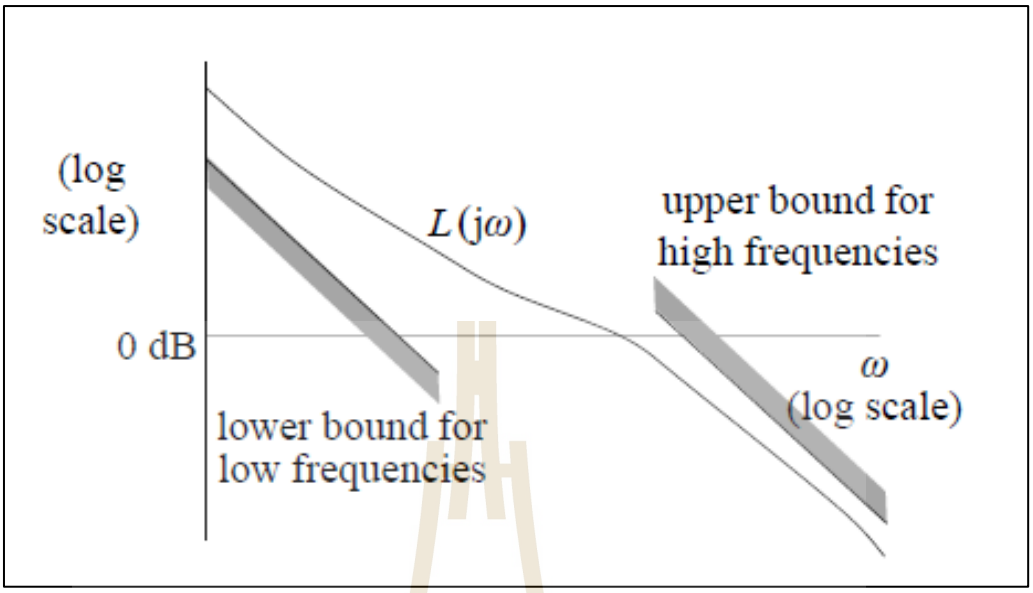

Figure 3.32 Robustness bounds on L in the Bode magnitude plot.

- In the crossover region $L(j\omega) \leq 1$ and the behavior L (magnitude and direction) is considered to decide how closely the Nyquist plot approaches the basic point −1. As the Nyquist plot of L approaches point −1 the system's stability increases.

3.7.4 Singular values

The singular values of a transfer matrix $H(s)$ of dimensions $p \times m$ are defined as the square roots of the eigenvalues of the product of its frequency response $H(j\omega)$ by its conjugate:

$$\sigma_i(H(j\omega)) = \sqrt{\lambda_i\left(H(j\omega)H(-j\omega)^T\right)} \tag{3.171}$$

$$\sigma_i(H(j\omega)) = \sqrt{\lambda_i\left(H(-j\omega)^T H(j\omega)\right)} \qquad i = [1,\ldots,\min(m,p)] \tag{3.172}$$

The singular values are positive or null real numbers and can be classified. The largest singular value, also called the maximum singular value, is denoted as $\bar{\sigma}(H)$, and the smallest also called the minimum singular value, is denoted as $\underline{\sigma}(H)$.

$$\bar{\sigma}(H(j\omega)) = \sigma_1(H(j\omega)) \geq \sigma_2(H(j\omega)) \geq \ldots \geq \underline{\sigma}(H(j\omega)) \tag{3.173}$$

In the case of a non-over readable system (i.e. *m*=*p*=1), the unique singular value is equal to the gain of the frequency response:

$$\bar{\sigma}(H(j\omega)) = \underline{\sigma}(H(j\omega)) = |H(j\omega)| \tag{3.174}$$

Hence, the singular values extend the notion of gain established with non-overridable systems to multivariable systems. It can be concluded that H is high-gain if $\underline{\sigma}(H)$ is large and is low-gain if $\bar{\sigma}(H)$ is small.

3.7.5 H∞ norm

Consider a transfer function, $G(s)$ the H∞ norm is the peak value of the largest singular value $\bar{\sigma}$ of the plant model $G(j\omega)$ as a function of frequency (Shivalingappa, 2013), that is,

$$\|G(s)\|_\infty \equiv \max_\omega \bar{\sigma}(G)(j\omega) \tag{3.175}$$

In the case of a Single Input Single Output (SISO) system, the H∞ norm is simply the peak value $|G(j\omega)|$.

The H∞ control method minimizes the H∞ norm of some selected closed-loop transfer functions like Sensitivity (*S*) or Complementary Sensitivity Function (*T*) by including weighting functions in the H∞ control problem, closed-loop transfer functions can be shaped according to the needs of the designer for his specific needs about a particular application.

3.7.6 MIMO Loop shaping

Singular value plots are used to analyses the frequency responses of MIMO systems. For any MIMO system (Feyel, 2013),

$$\sigma_{\max}(AB) \le \sigma_{\max}(A)\sigma_{\max}(B) \tag{3.176}$$

If $\sigma_{\max}(CD) \le 1$, and $|D| \neq 0$ then,

$$\sigma_{\max}(C) < \frac{1}{\sigma_{\min}(D)} \tag{3.177}$$

Almost identical with the SISO, except

$$\sigma_{\max}\left[(I + P(j\omega)K(j\omega))^{-1}\right] \le \frac{\gamma}{\sigma_{\max}[W(j\omega)]} \tag{3.178}$$

Loop performance constraints are:

- The disturbance *d* is within the low-frequency region.
- The conditions are $\sigma_{\max}(T_s(j\omega))$ small within $0 \le \omega \le \omega_{\max}$
- The noise n is within the high-frequency region.

- The conditions are $\sigma_{\max}\left(T_c\left(j\omega\right)\right)$ small within $\omega \geq \omega_{\max}$
- The reference *r* is within the low-frequency region.
- The conditions are $T_c\left(j\omega\right) \approx I$ within the range (3.179).

$$0 \leq \omega \leq \omega_r \tag{3.179}$$

$$\Rightarrow \quad \begin{aligned} \sigma_{\max}\left(T_c\left(j\omega\right)\right) &\approx 1 \\ \sigma_{\min}\left(T_c\left(j\omega\right)\right) &\approx 1 \end{aligned}$$

The control signal must be kept small for d and n

$$u = \left(I + KP\right)^{-1} Kr - \left(I + KP\right)^{-1} K\left(d + n\right) \tag{3.180}$$

Must keep $\sigma_{\max}\left[\left(I + KP\right)^{-1} K\right]$ small where n and d are active, i.e.

$$\omega \in \left(0, \omega_{ry}\right) \cup \left(\omega_{ty}, \infty\right)$$

3.7.7 H-infinity loop shaping and EKF for DFIG under abnormal conditions

Consider the system shown in Figure 3.29. The plant P is controlled by a controller K to be designed using a loop shaping method. The input to the plant is a vector w that includes reference signals and disturbances. The output of the plant is a vector of an error signal z considered for minimization, and the measured variable y that is the input to K (Feyel, 2013).

The method seeks a controller K for plant P such that the system transfer characteristics are similar to the desired system. Therefore, a stabilizing feedback control law $u = K \cdot y$ is sought such that the $H\infty$ norm of the closed-loop transfer function is minimized. The method synthesizes a controller which optimally satisfies singular value loop shaping specifications.

Shivalingappa (2013) presented a thesis on robust h∞ control and analysis: Application to electrical drives. In this thesis, a Genetic Algorithm-based technique and a graphically based acceleration stabilization in PMSM with fixed and multiple rotor mass are proposed to accomplish effective stability in controlling operations.

Rodríguez and Marcela (2012) applied sliding mode control to the RSC and the GSC. The method is tested on DFIG operating in grid-connected mode. Mohsen Ghafouri design a controller to solve the stability problem and the poor execution caused by the sub-synchronous control interaction (SSCI) problem for the DFIG-based wind farm connected to a series compensated transmission line.

Howlader, et al. (2013) displayed a digital H1 controller to control a permanent magnet synchronous generator (PMSG) used in a WECS. The robust control is to discover a controller, for a given system, such that the closed-loop system becomes strong that assures high-integrity and fault-tolerant control systems.

Yun, et al. (2016) displayed a strong current control strategy for a DFIG-WT subject to grid voltage distortions, which incorporate asymmetric voltage dips and grid current harmonics. The flux saturation, the skin effect, and other variables cause the generator parameters to be perturbed. Weighting functions

empower an effective track of the unbalanced current components and the 5th and 7th current harmonics.

In this thesis, the objective of the robust $H\infty$ loop shaping controller is to efficiently track the machine rotor currents and maintain the torque stability of the system hence improving the voltage stability during different grid faults.

Rearranging equations (3.145), and taking the currents as state variables, the model of the DFIG can be written as,

$$\frac{d}{dt}\begin{bmatrix} i_{ds} \\ i_{qs} \\ i_{dr} \\ i_{qr} \end{bmatrix} = \begin{bmatrix} -\frac{R_s}{L_s} & \omega_s & -\frac{sL_m}{L_s} & \frac{\omega_s L_m}{L_s} \\ \omega_s & -\frac{R_s}{L_s} & -\frac{\omega_s L_m}{L_s} & -\frac{sL_m}{L_s} \\ -\frac{sL_m}{L_s} & \frac{(\omega_s-\omega_r)L_m}{L_r} & -\frac{R_r}{L_r} & (\omega_s-\omega_r) \\ -\frac{(\omega_s-\omega_r)L_m}{L_r} & -\frac{sL_m}{L_s} & (\omega_s-\omega_r) & -\frac{R_r}{L_r} \end{bmatrix} \begin{bmatrix} i_{ds} \\ i_{qs} \\ i_{dr} \\ i_{qr} \end{bmatrix} + \begin{bmatrix} \frac{1}{L_s} & 0 & 0 & 0 \\ 0 & \frac{1}{L_s} & 0 & 0 \\ 0 & 0 & \frac{1}{L_r} & 0 \\ 0 & 0 & 0 & \frac{1}{L_r} \end{bmatrix} \begin{bmatrix} v_{ds} \\ v_{qs} \\ v_{dr} \\ v_{qr} \end{bmatrix} \tag{3.181}$$

The uncertain state-space model for the $H\infty$ loop shaping controller is developed as follows:

$$\dot{x} = Ax + B_1 w + B_2 u \tag{3.182}$$

The state matrix A and the input matrix B are:

$$A=\begin{bmatrix} -\frac{R_s}{L_s} & \omega_s & -\frac{sL_m}{L_s} & \frac{\omega_s L_m}{L_s} \\ \omega_s & -\frac{R_s}{L_s} & -\frac{\omega_s L_m}{L_s} & -\frac{sL_m}{L_s} \\ -\frac{sL_m}{L_s} & \frac{(\omega_s-\omega_r)L_m}{L_r} & -\frac{R_r}{L_r} & (\omega_s-\omega_r) \\ -\frac{(\omega_s-\omega_r)L_m}{L_r} & -\frac{sL_m}{L_s} & (\omega_s-\omega_r) & -\frac{R_r}{L_r} \end{bmatrix}$$

$$B=\begin{bmatrix} \frac{1}{L_s} & 0 & 0 & 0 \\ 0 & \frac{1}{L_s} & 0 & 0 \\ 0 & 0 & \frac{1}{L_r} & 0 \\ 0 & 0 & 0 & \frac{1}{L_r} \end{bmatrix}$$

The states, the disturbance vector, and input vector are:

$$x=\begin{bmatrix} i_{ds} \\ i_{qs} \\ i_{dr} \\ i_{qr} \end{bmatrix}, w=\begin{bmatrix} v_{ds} \\ v_{qs} \end{bmatrix}, u=\begin{bmatrix} v_{dr} \\ v_{qr} \end{bmatrix}$$

The controlled outputs and measured outputs are:

$$z = \begin{bmatrix} e_{idr} \\ e_{iqr} \end{bmatrix}, \quad y = \begin{bmatrix} i_{ds} \\ i_{qs} \\ i_{dr} \\ i_{qr} \end{bmatrix}$$

Where $e_{idr} = i_{idr}^{ref} - i_{dr}$ and $e_{iqr} = i_{iqr}^{ref} - i_{qr}$ are tracking errors. The state variable x consists of the stator and rotor currents in the dq reference frame. The exogenous input variables w (disturbances) are stator voltages, and the reference rotor currents (external inputs). The controller input is the state variables $\hat{i}_{dr}$ and $\hat{i}_{qr}$ estimated by extended Kalman filter. The output of the controller is a vector u of direct and quadrature axis rotor voltages as shown below (Nguyen, et. al., 2007):

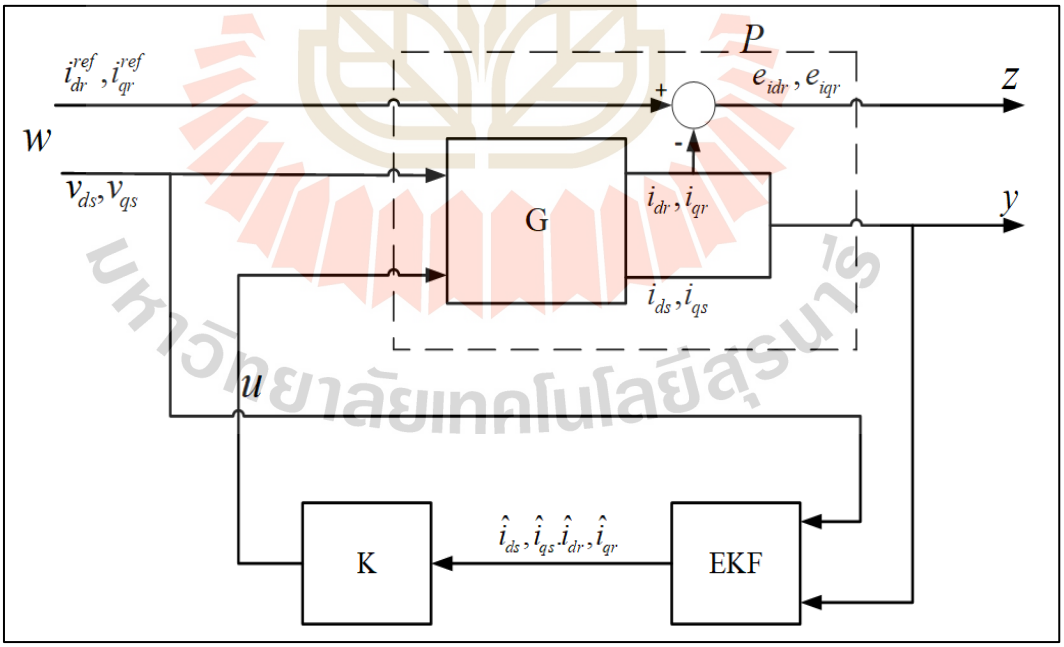

Figure 3.33 Loop shaping controller and extended Kalman filter controlling the DFIG.

3.7.8 Controller synthesis

The commands "*hinfsyn*" for the robust h-infinity optimal controller and "*loopsyn*" for robust h-infinity loop shaping control from the robust control toolbox of MATLAB are used to find the controller K. The open-loop step response and singular value plot of the system (3.181) with a loop shaping controller are shown in Figure 3.34 and Figure 3.35, respectively.

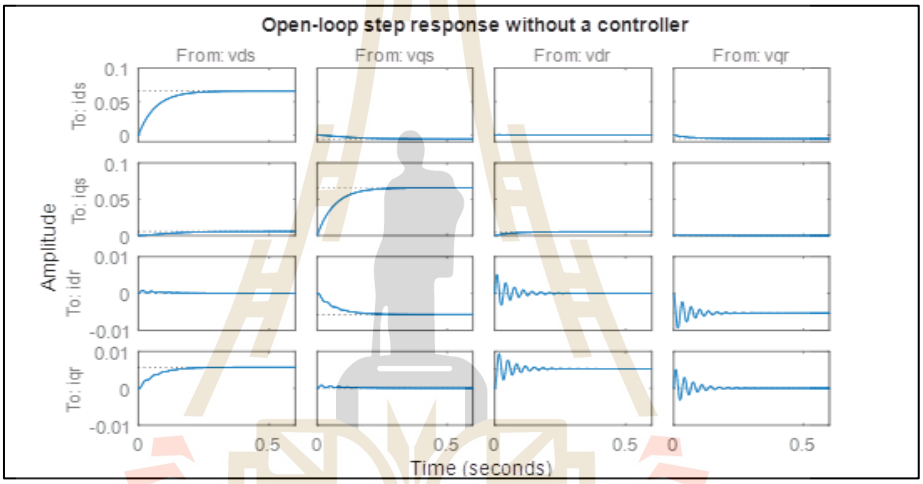

Figure 3.34 DFIG step response without a robust controller.

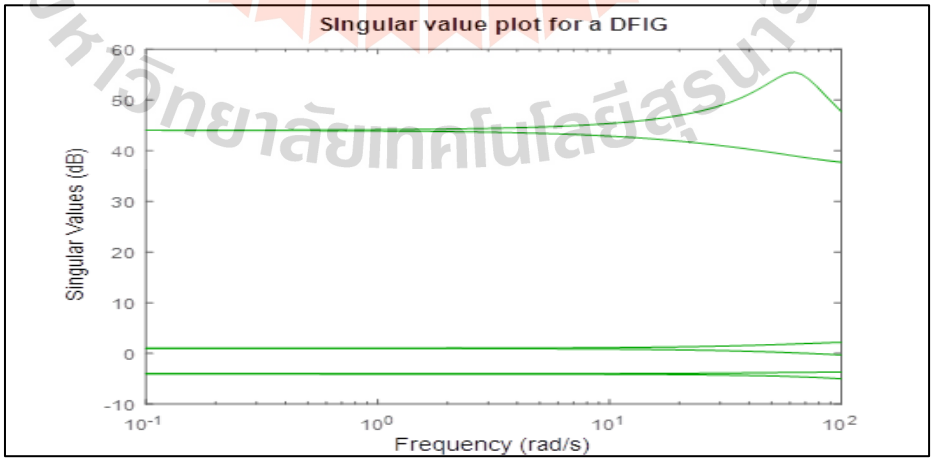

Figure 3.35 Singular value plot of a DFIG without a controller.

The desired frequency response is chosen as,

$$G_d(s) = \frac{8}{s} \tag{3.183}$$

The desired loop shape with its crossover frequency is shown below:

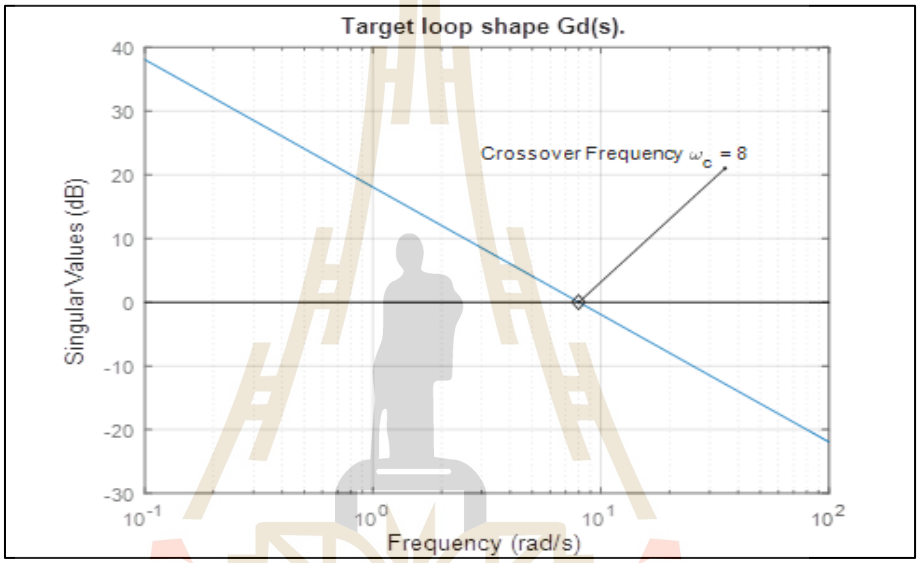

Figure 3.36 Desired loop shape of the system showing crossover frequency.

The value of GAM obtained is 1.4163 (Gilev, 2017). This indicates that the target-loop shape was met. To prove that the target loop shape has been reached singular values plot of the open-loop $L = G(s)K(s)$ optimally tracks the target-loop shape $G_d(s)$ as shown Figure 3.37.

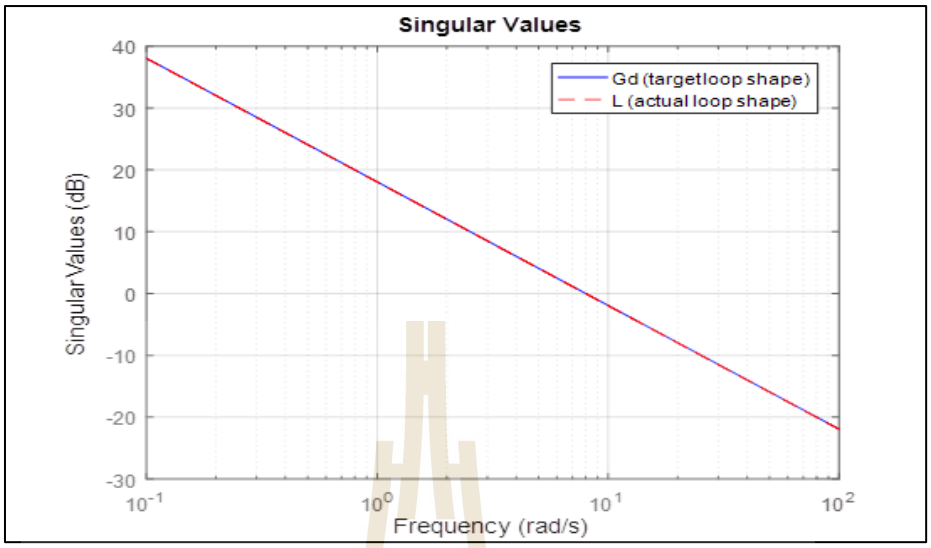

Figure 3.37 Singular value plot of the DFIG and target loop shape.

Comparison of the gains of the open-loop transfer function L, target loop shape K, and sensitivity function S is shown in Figure 3.38.

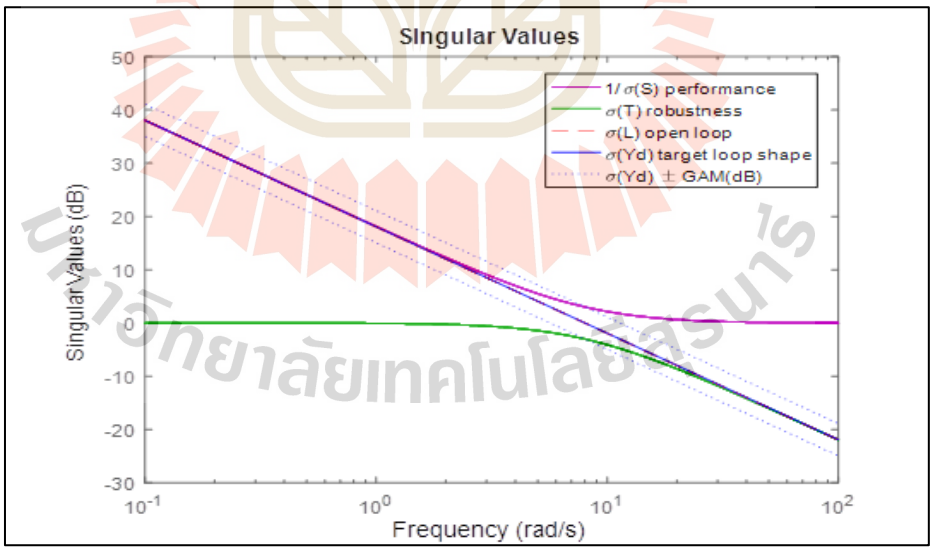

Figure 3.38 Singular value plot of the DFIG is showing performance and robustness.

The closed-loop response is tested if it meets specifications. The step response is shown in Figure 3.39.

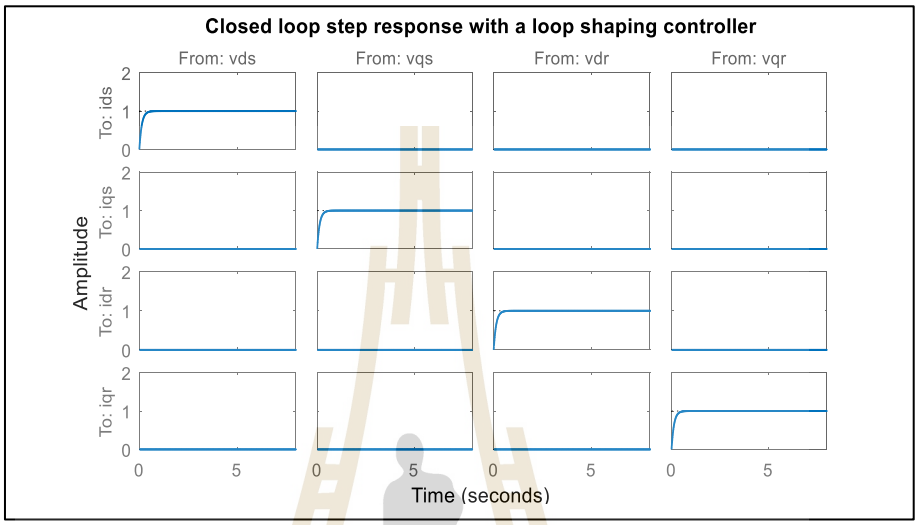

Figure 3.39 DFIG step response with a loop shaping control.

The h-infinity optimal controller and robust h-infinity loop shaping controller obtained were implemented in SIMULINK with the state-space model of the DFIG and extended Kalman filter as shown in Figure 3.41.

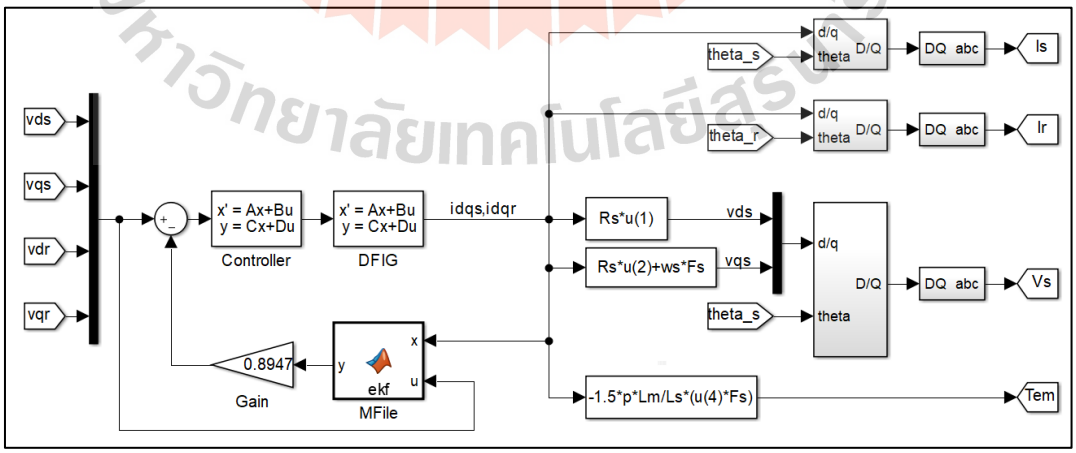

Figure 3.40 DFIG with a loop shaping controller.

3.8 Chapter Summary

Introduction to control theory is presented. Parts of a closed-loop control system and types of the control system are shown and discussed. Kalman filter and extended Kalman filter overview is part of this chapter. Introduction to voltage dips phenomenon is presented. A review of control methods for a DFIG is discussed in detail. The fuzzy logic method is presented in this chapter. The technique is discussed in detail from its origin to its implementation to control a system. Dual control strategy which is an improvement of the conventional vector control is explained in detail. The fuzzy dual controller is developed to control the DFIG. Then, an optimal controller based on pole placement controller and the linear quadratic regulator is designed. Finally, the dq dynamic modeling of the DFIG is presented. The state-space representation of dq model is given. The model is used to design the h-infinity optimal controller and the robust h-infinity loop shaping controller. Then, the controllers are implemented in SIMULINK to control the DFIG for different grid faults.

CHAPTER IV

RESULTS AND DISCUSSION

4.1 Fuzzy PI dual controller testing

The system tested is a 2 MW DFIG. The grid-connected generator faces asymmetric voltage dips. Generator data are shown in Table 4.1.

Table 4.1 Ratings and parameters of the DFIG.

Parameter	Value
Rated power: P	2 MW
The number of poles: p	2
Stator voltage: V_s	690 V/50 Hz.
DC bus voltage: V_{dc}	1150 V.
Rotor resistance: R_r	0.56 Ω.
Stator resistance: R_s	2.14 Ω.
Rotor inductance: L_r	0.052953 H.
Stator inductance: L_s	0.052953 H.
Mutual inductance: L_m	0.04847 H.

To assess the capability of the presented technique to ride-through voltage failures, the system has been mimicked with some severe voltage dips, subjecting the controller to maximum disturbances. To prove the robustness of the machine against disturbances simulation of the system is conducted. It is incredibly crucial to maintain

the steady-state value of both the dc voltage and the electromagnetic torque while the converter is operating at its secure working mode.

The system considered is shown in Figure 3.24. The wind turbine injects power into the grid to support loads connected to the DN. The RSC and GCS are controlled with the Fuzzy-PI dual control technique. This control strategy enhances the stability of the system during grid faults because it has better dynamic performance features than a traditional vector control. The role of RSC is to inject constant three-phase voltages to the rotor circuit of the WT, making the generator rotate at an optimal speed. The GSC maintains the stability of the DC link capacitor voltage hence improving the stator output voltage profile. Furthermore, the GSC supplies or absorbs rapidly the required reactive power. The GSC also protects the windings of the machine by bypassing the surge current and stores it in the capacitor bank. It then re-injects the excess power after fault clearance. To compare the proposed control mechanism and conventional vector control, the DFIG has been tested for three cases to prove the robustness of the developed controller:

- Transient state
- Faulty state
- After fault state

4.1.1 Transient state

In this case, all three voltages are balanced. There is no fault in the system. The conventional method and proposed control strategy were tested. The results are shown below. Figure 4.1 (a) and (b) depict the system at the initial stages of the simulation. In (a) the speed rises to 188.3 rad/s and then drops to its steady-state value within 2s. It can be observed that speed is slow in reaching the steady-state

value when using the proposed controller than with vector control but after a transient period, they both settle to a steady-state value.

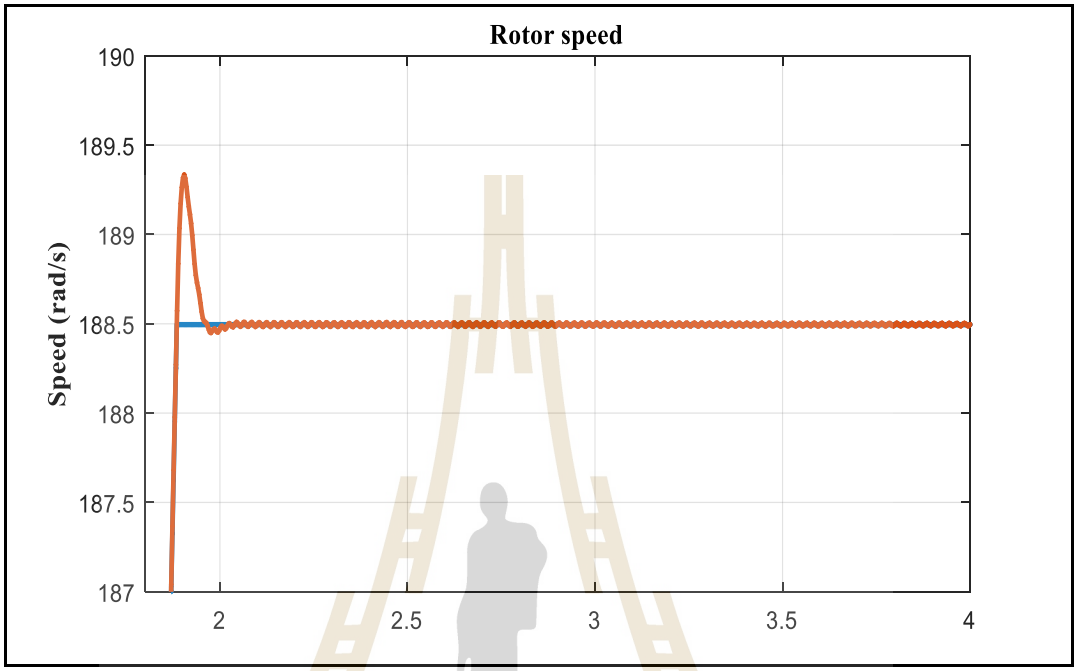

(a)

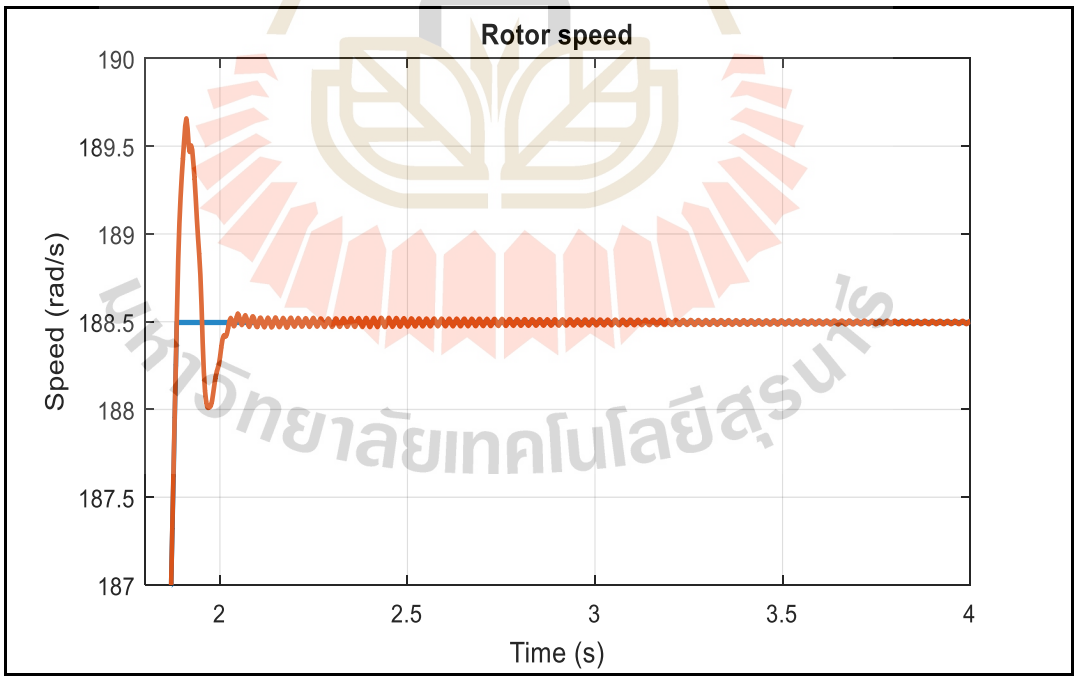

(b)

Figure 4.1 Rotor speed in transient state (a) Vector control (b) Fuzzy dual control.

The behavior of electromagnetic torque is very similar in both techniques as shown in Figure 4.2. They both start at 10000 N/m and T = 1.91 s reaches a steady-state value of 5000 N/m.

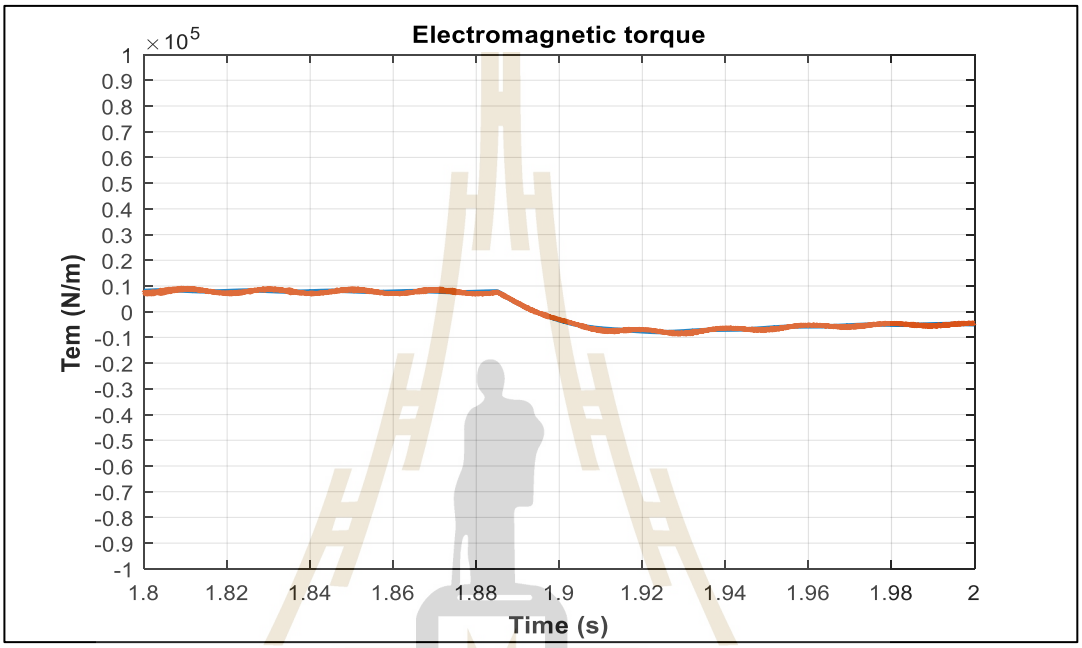

(a)

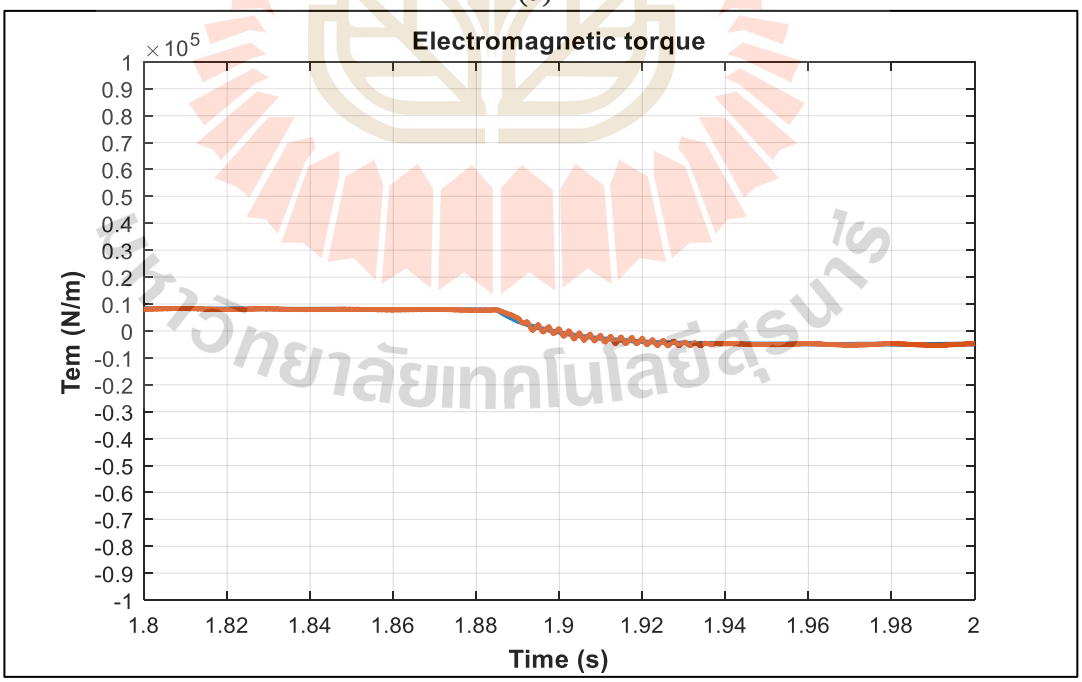

(b)

Figure 4.2 Torque in transient state (a) Vector control (b) Fuzzy dual control.

The voltages in both cases shown in Figure 4.3 start directly with a steady-state value of around 550 V because the system has a fast response.

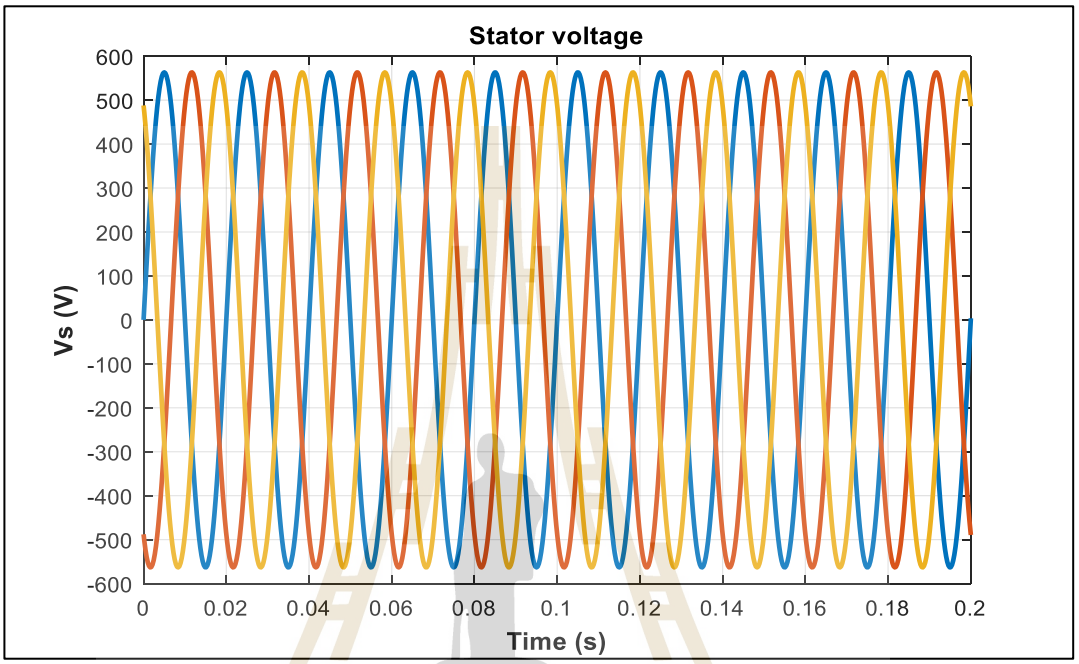

(a)

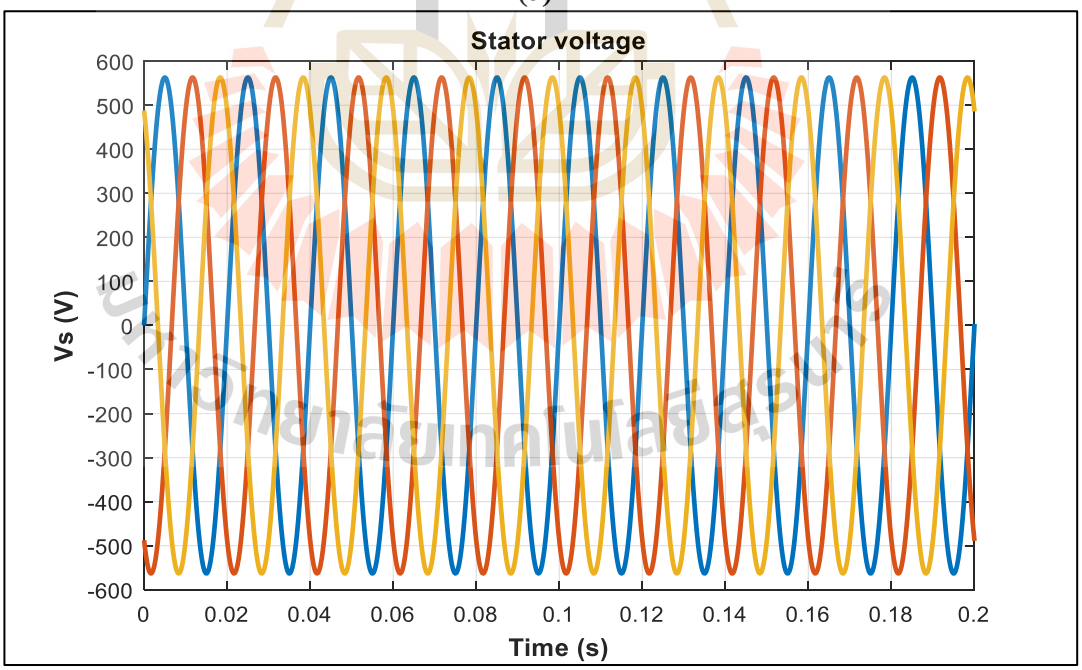

(b)

Figure 4.3 Stator voltage transient state (a) Vector control (b) Fuzzy dual control.

In Figure 4.4 (a) and (b) stator current reaches a steady-state value at almost the same time although there more oscillations with the Vector control than the proposed technique.

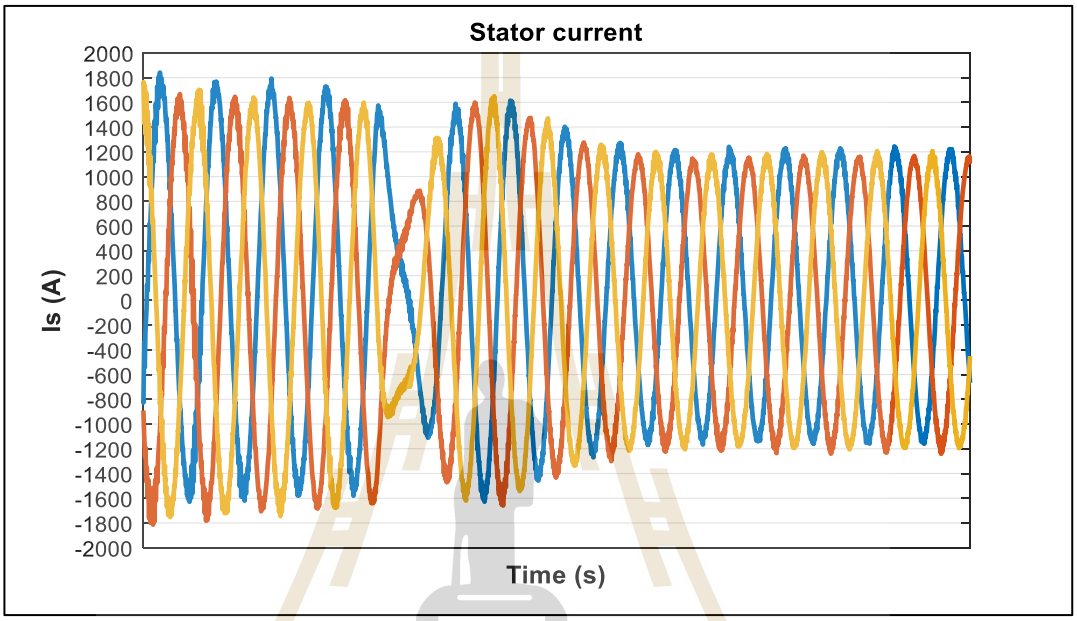

(a)

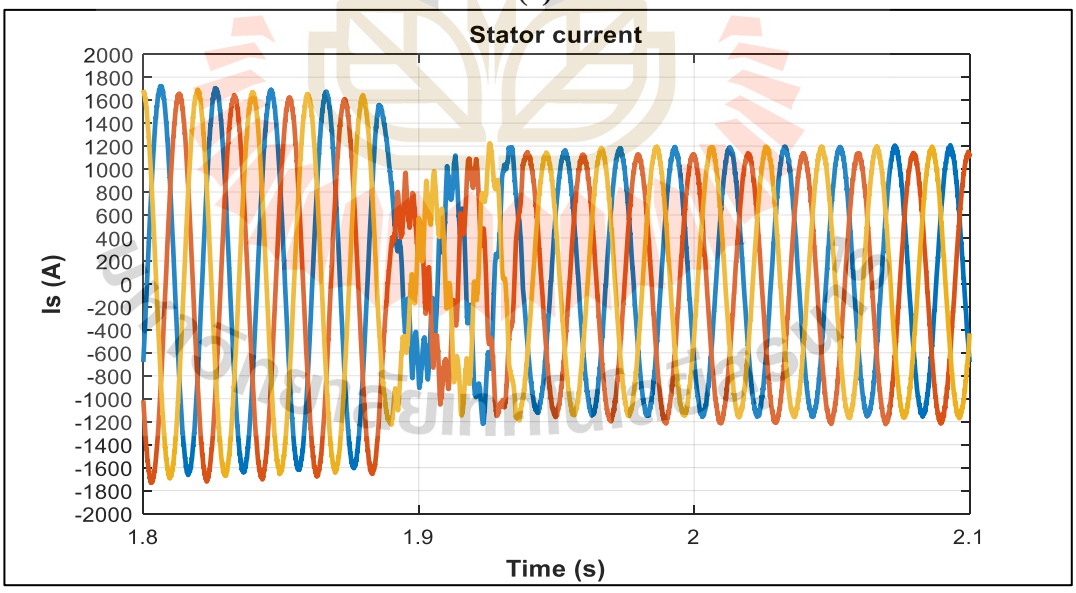

(b)

Figure 4.4 Stator current transient state (a) Vector control (b) Fuzzy dual control.

In Figure 4.5 (a) and (b) rotor current reaches a steady-state value at almost the same time although there more oscillations with the Vector control than the proposed technique.

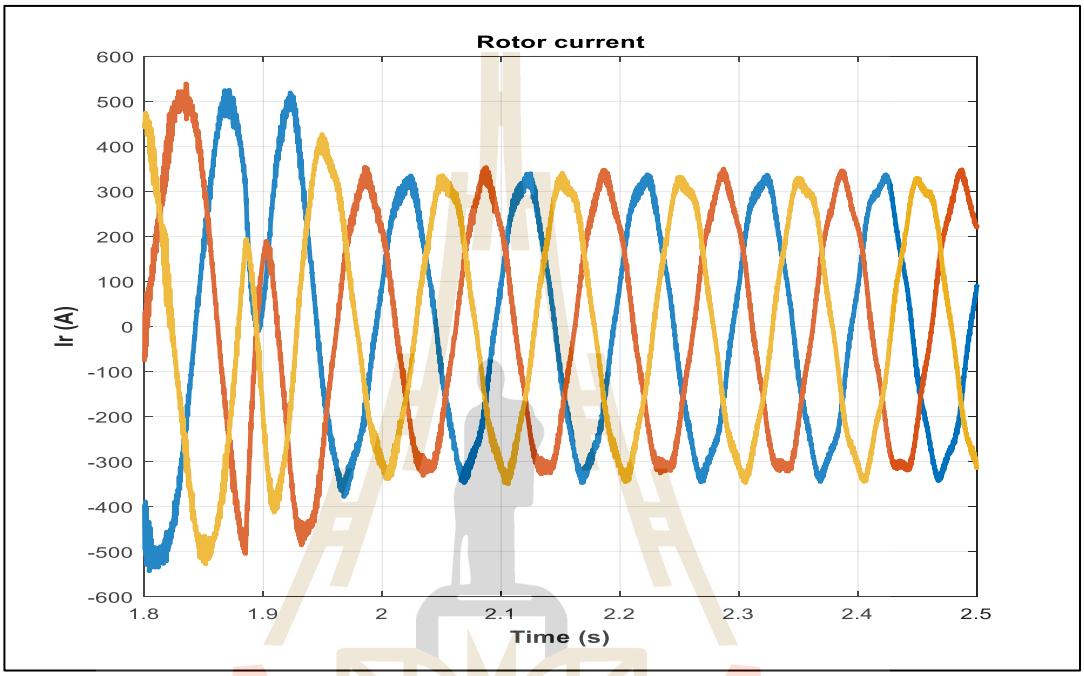

(a)

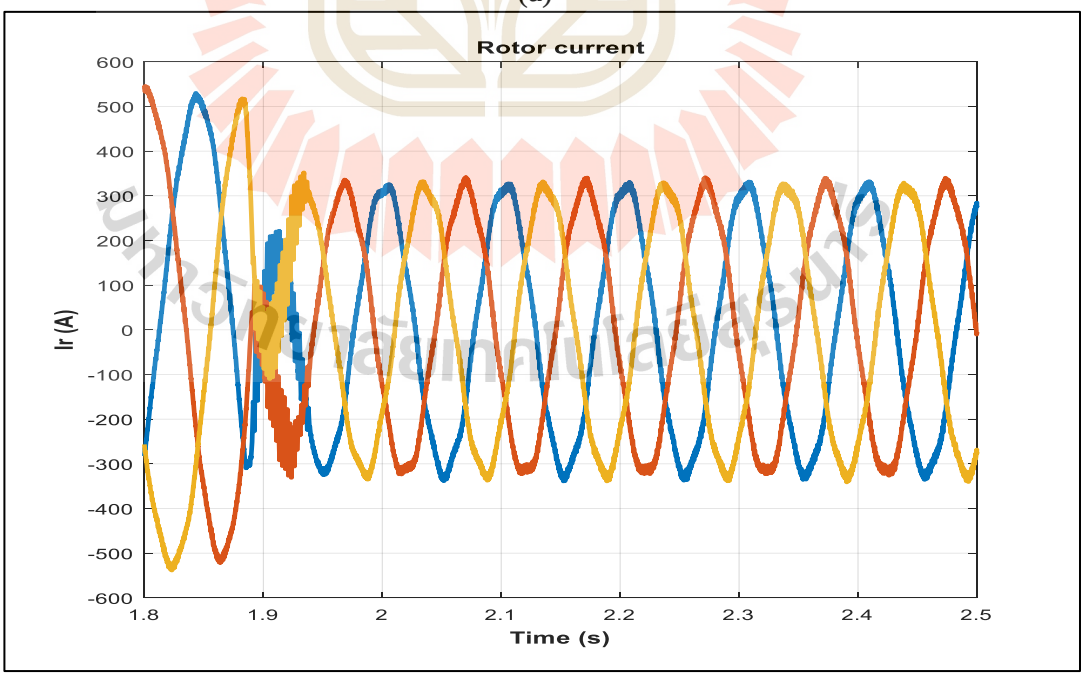

(b)

Figure 4.5 Rotor current transient state (a) Vector control (b) Fuzzy dual control.

In Figure 4.6 (b) of the proposed controller, the DC link voltage reaches a steady-state value at 2.2 s while in Figure 4.6 (a) of the conventional Vector control the voltage reaches a steady-state value when T=2.8.

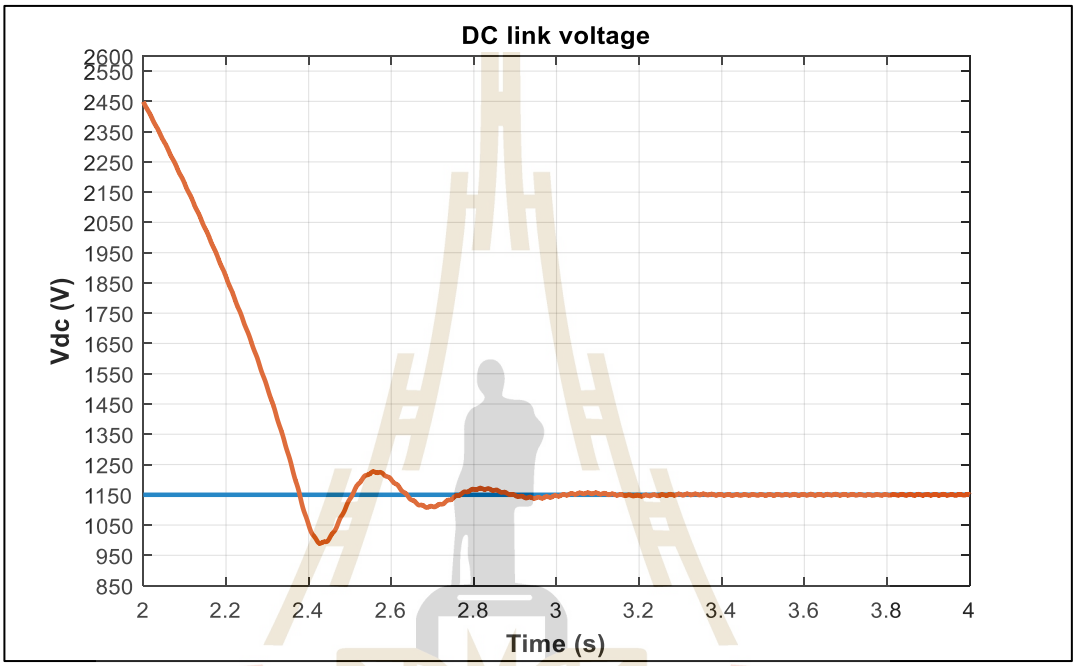

(a)

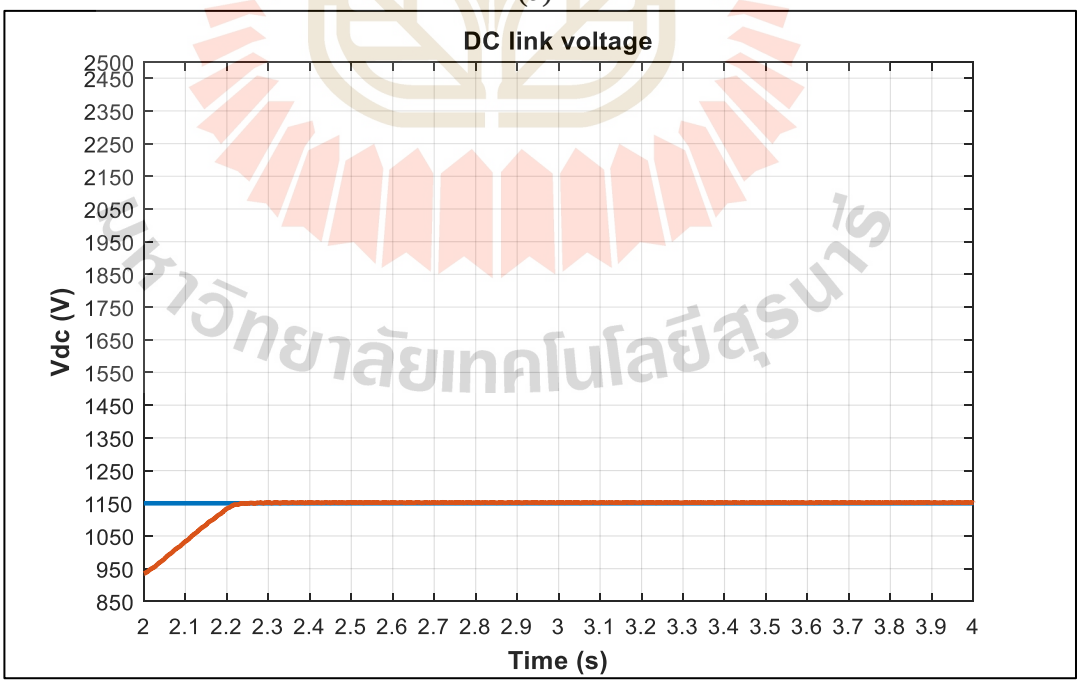

(b)

Figure 4.6 DC link voltage transient state (a) Vector control (b) Fuzzy dual control.

Figure 4.7 (b) shows that the proposed control strategy shows better performance than Vector control as the grid current reaches steady-state value faster than the conventional method.

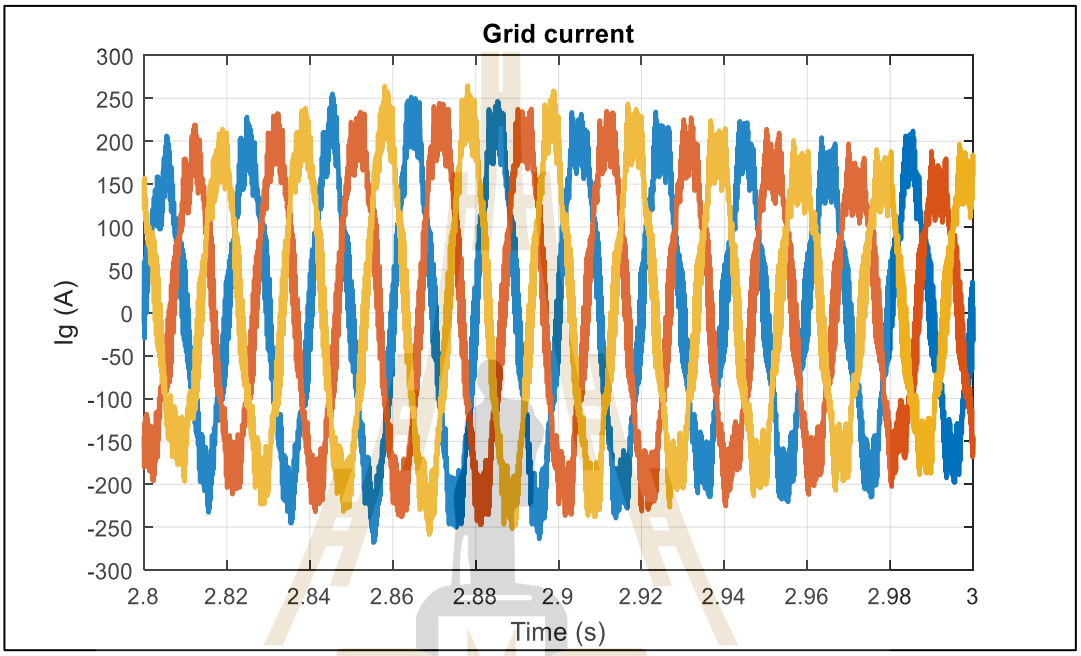

(a)

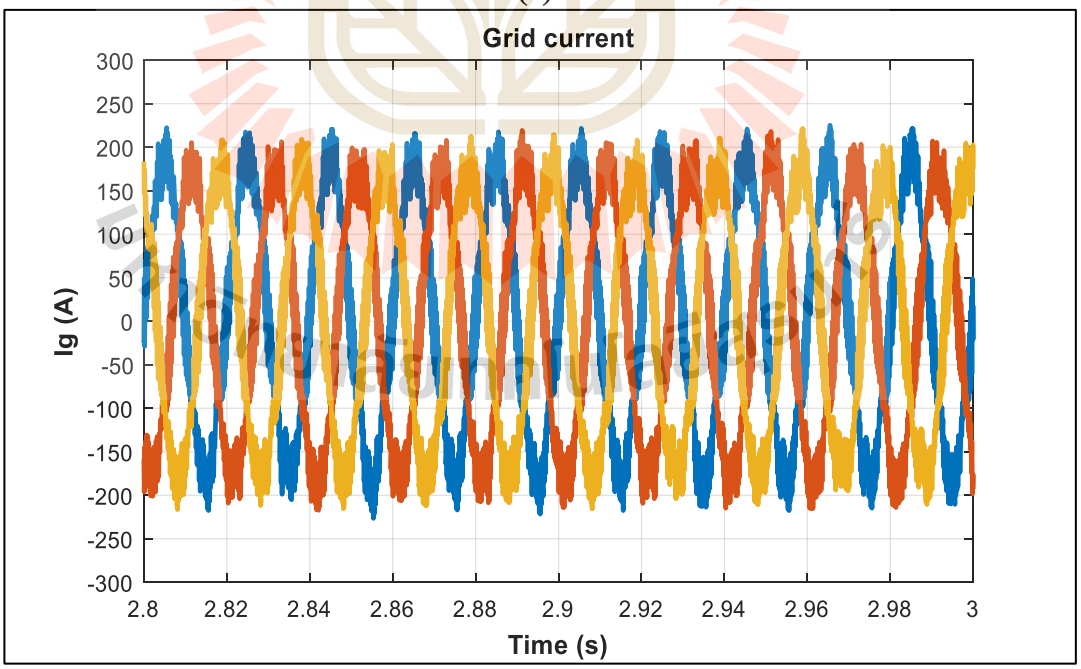

(b)

Figure 4.7 Grid current transient state (a) Vector control (b) Fuzzy dual control.

4.1.2 Fault state

In this control approach, there are unbalanced voltage disturbances in the power system. Voltages are unbalanced due to the occurrence of the voltage dip. The system is in a fault state. The conventional method and proposed control strategy were tested. The results are shown below.

Oscillations experienced with vector control are higher than those experienced when the proposed method is tested. Figure 4.8 shows that with vector control rotor speed shoots to 189.6 rad/s. Then oscillations decrease to small values but the speed continues to be unstable. With the proposed control although there are oscillations, they end up being around 188.8 rad/s up and 188.2 rad/s down.

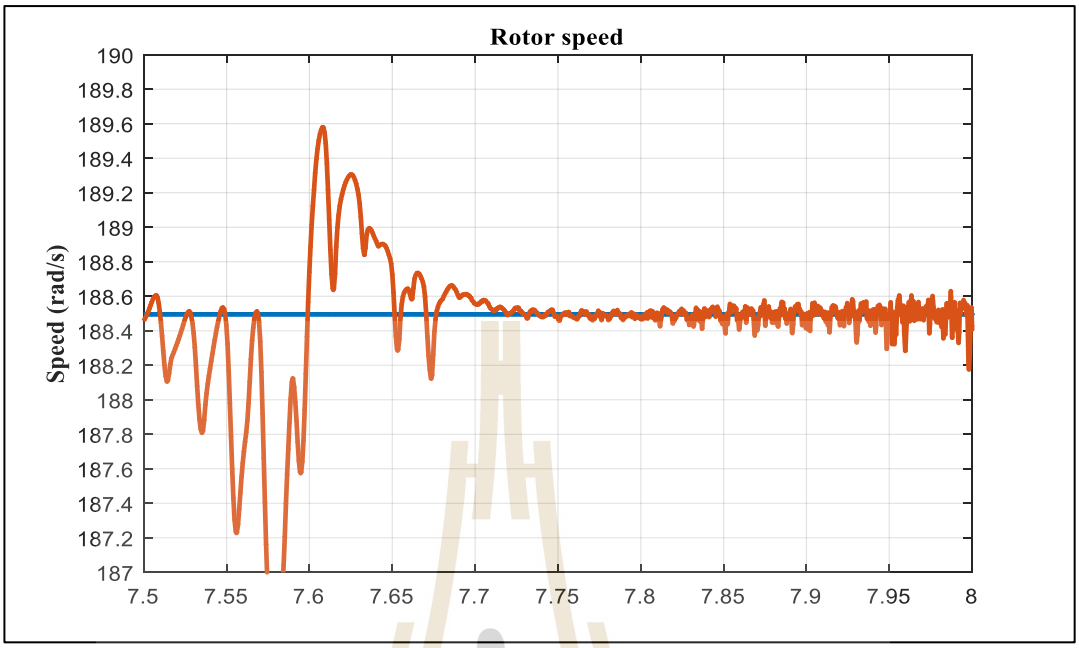

(a)

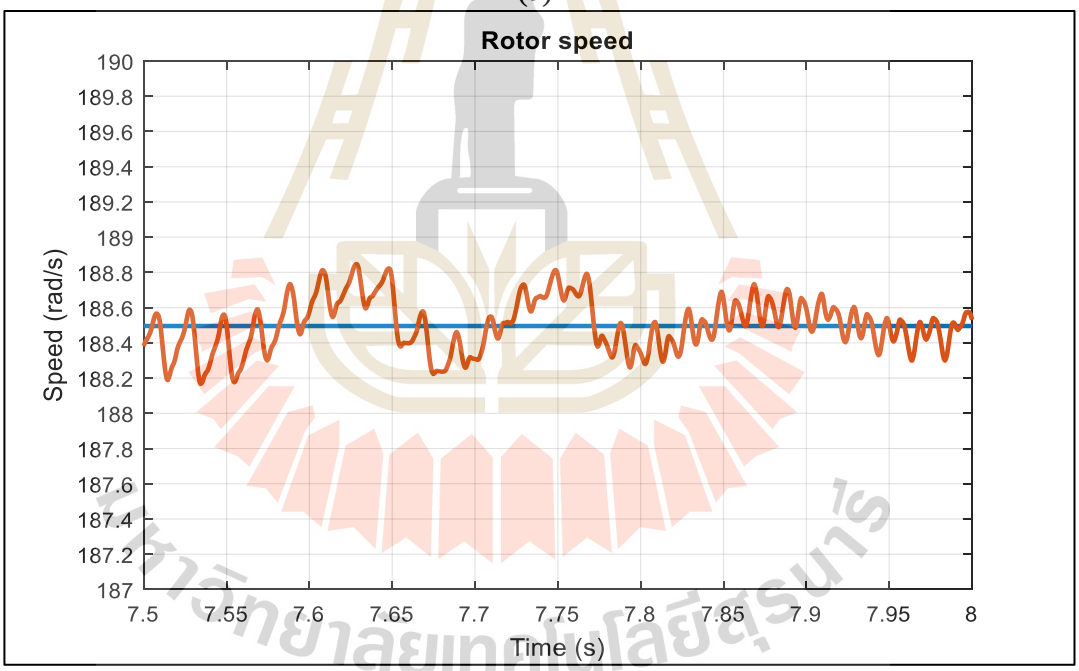

(b)

Figure 4.8 Rotor speed in fault state (a) Vector control (b) Fuzzy dual control.

Figure 4.9 (a) and (b) show torque behavior in terms of its performance for the DFIG. Due to the effect of the unbalanced system, the electromagnetic torque is highly distorted and its waveforms have very high oscillations in Figure 4.9 (a)

where vector control was used. Fuzzy-PI dual control output almost tracks the reference although there are constant oscillations.

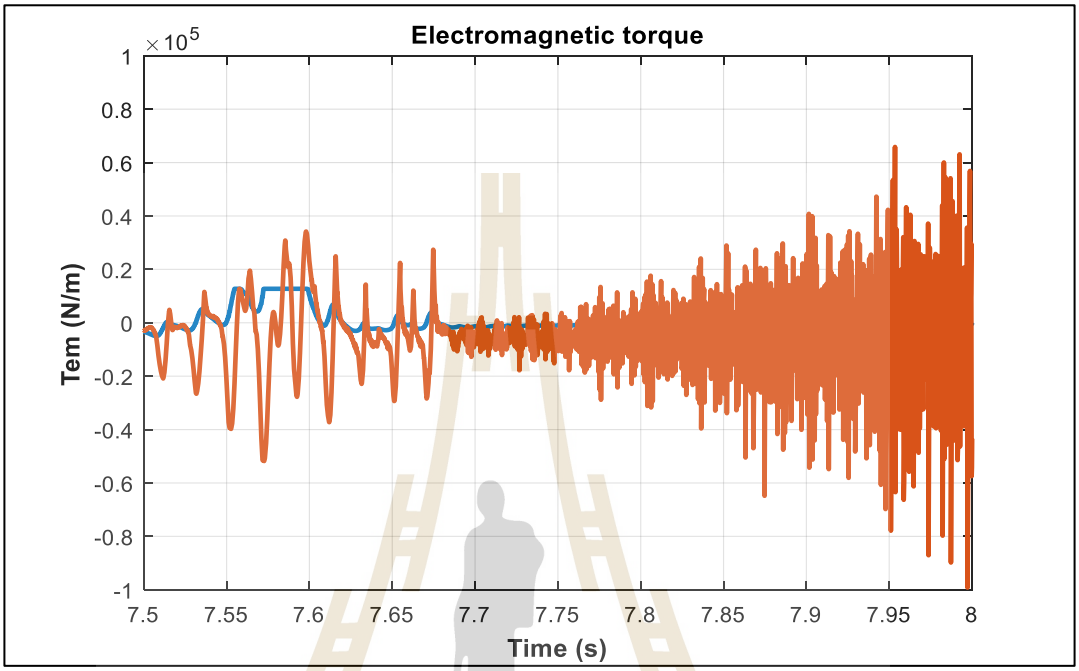

(a)

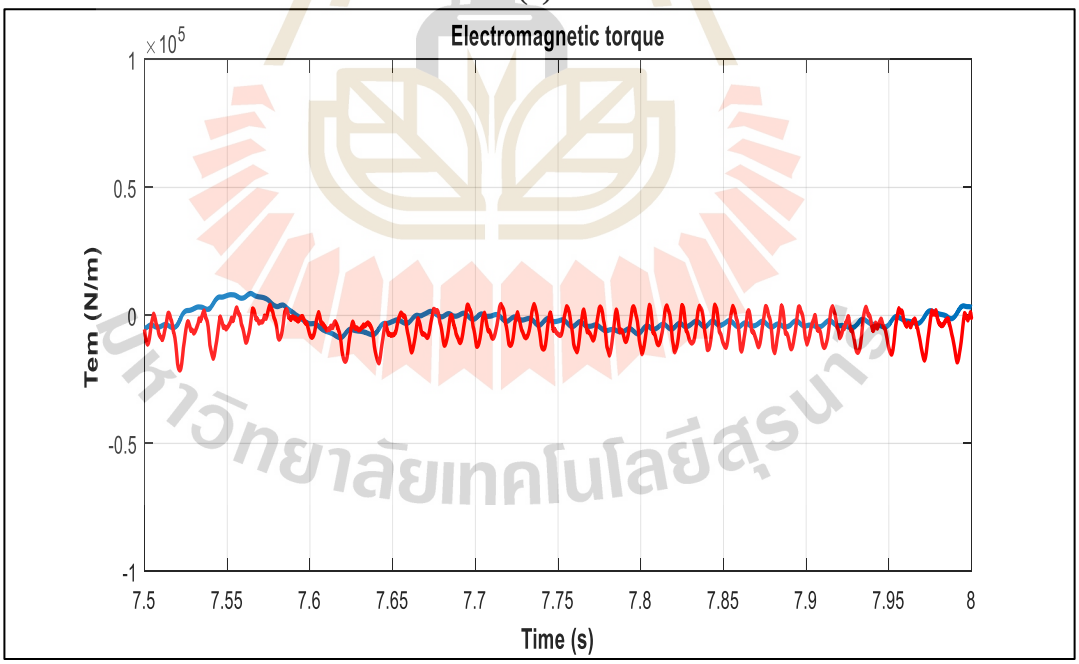

(b)

Figure 4.9 Torque in fault state (a) Vector control (b) Fuzzy dual control.

Figure 4.10 (a) and (b) show simulations results of the stator voltage performance of the DFIG for the two methods. Because of the unbalanced system, a distortion of the stator voltage is observed and the waveforms have very high oscillations as shown in Figure 4.10 (a) where Vector control was used. Fuzzy-PI dual control output shows a voltage dip but with very small oscillations. The difference in the amount of voltage between the phases is very small. Furthermore, oscillations are constant. They don't increase in magnitude.

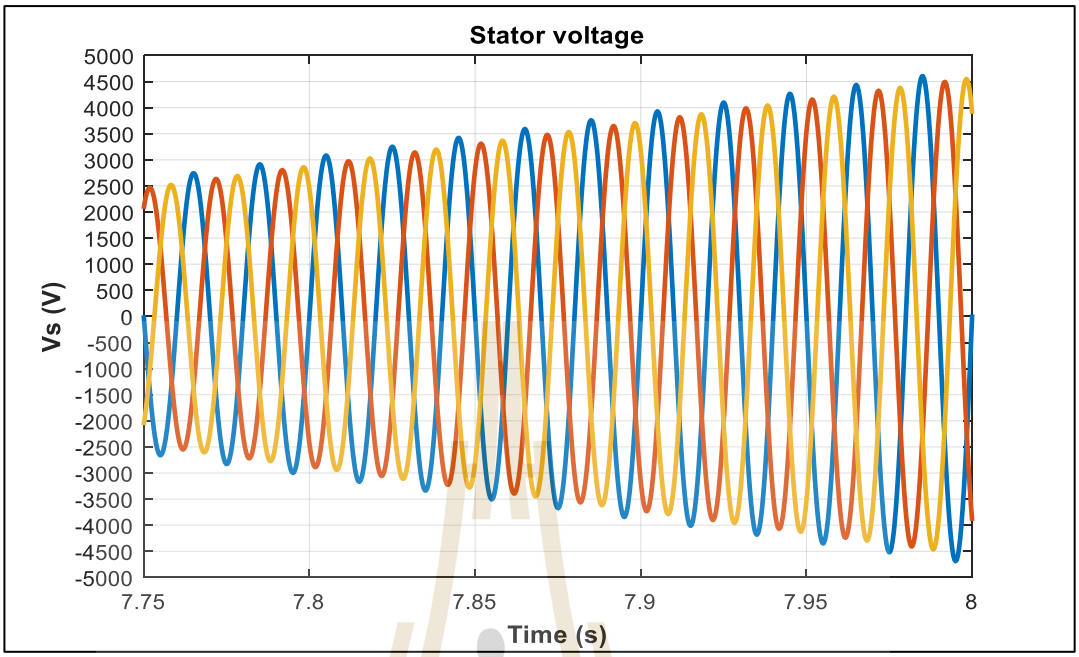

(a)

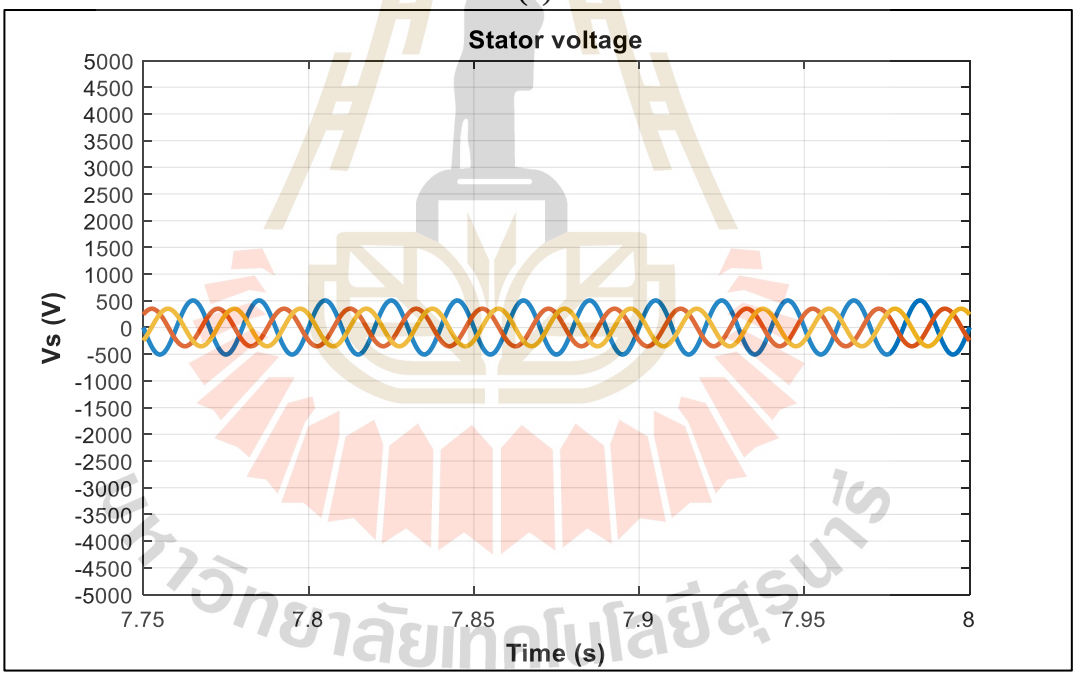

(b)

Figure 4.10 Stator voltage fault state(a) Vector control (b) Fuzzy dual control.

Vector and proposed control methods are tested with asymmetric voltage dip. Figure 4.11 (a) and (b) show simulations results of stator current of the DFIG. Because of the unbalanced system, there is a distortion of the stator current and

the waveforms increase to a very high value in Figure 4.11 (a) where Vector control was used. Fuzzy-PI dual control output also has oscillations but they are not as big as those in Figure 4.11 (a).

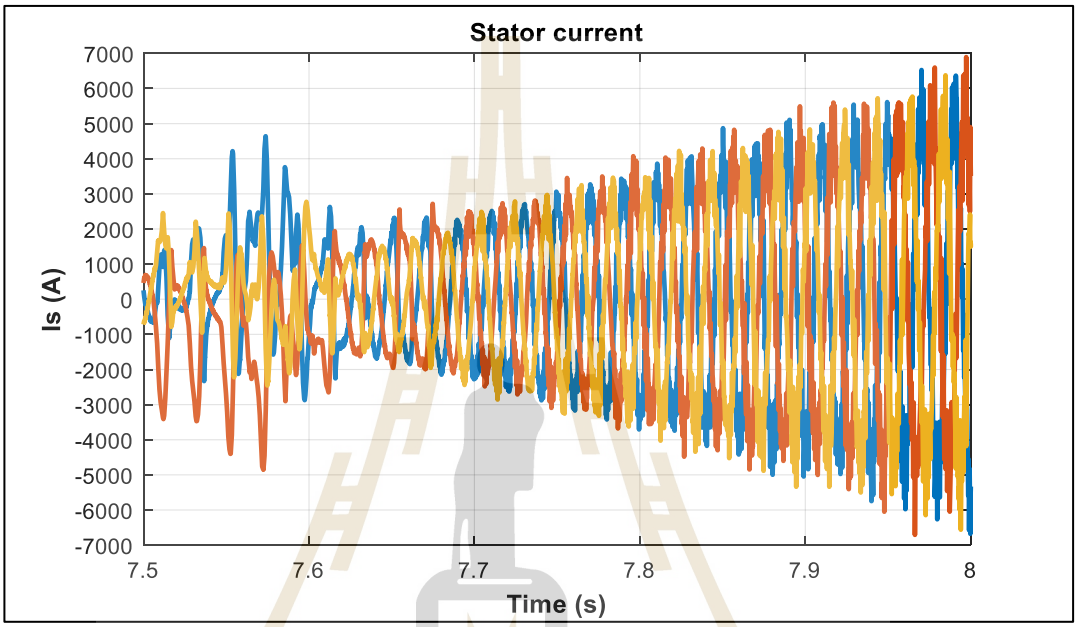

(a)

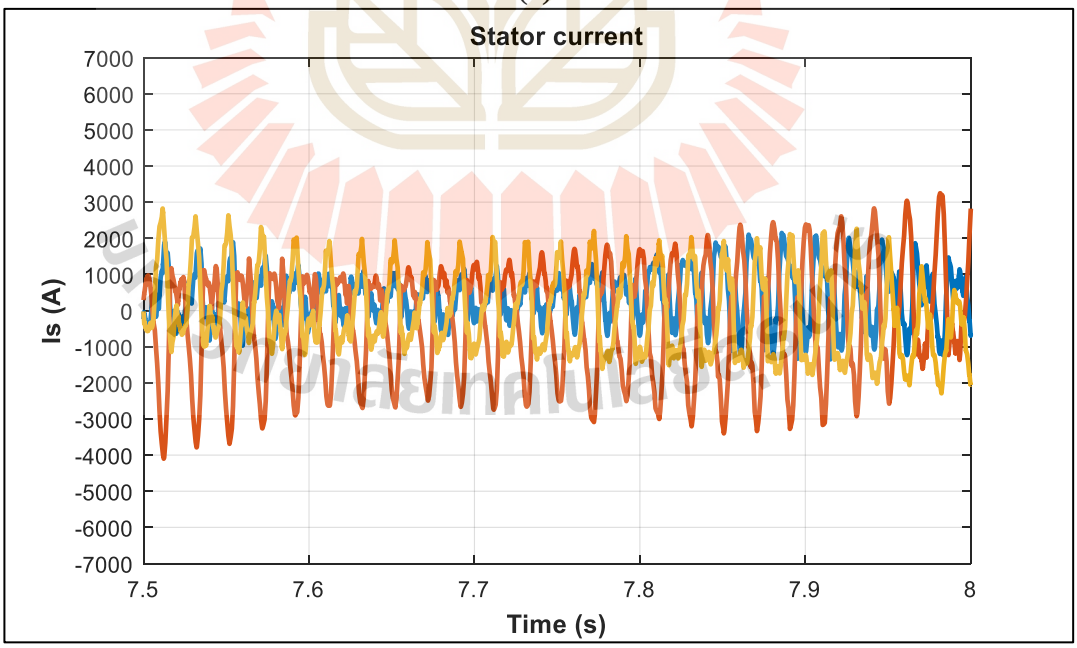

(b)

Figure 4.11 Stator current fault state (a) Vector control (b) Fuzzy dual control.

Figure 4.12 (a) and (b) show simulations results of the rotor current of the DFIG. Due to the effect of the unbalanced system, the rotor current is highly distorted and its waveforms have very high oscillations in both cases.

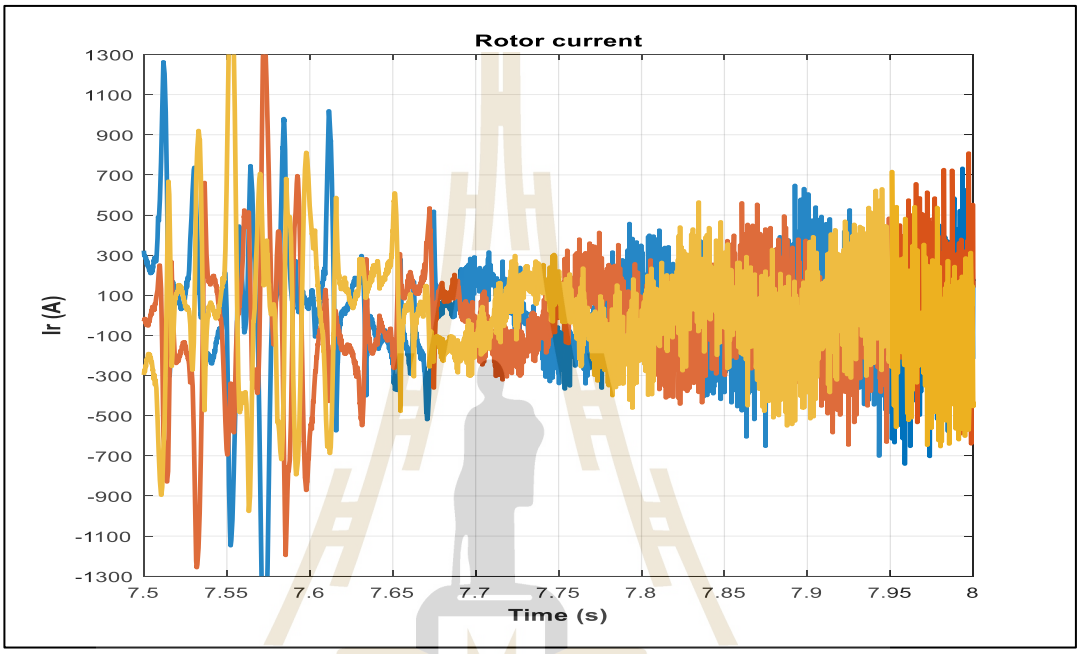

(a)

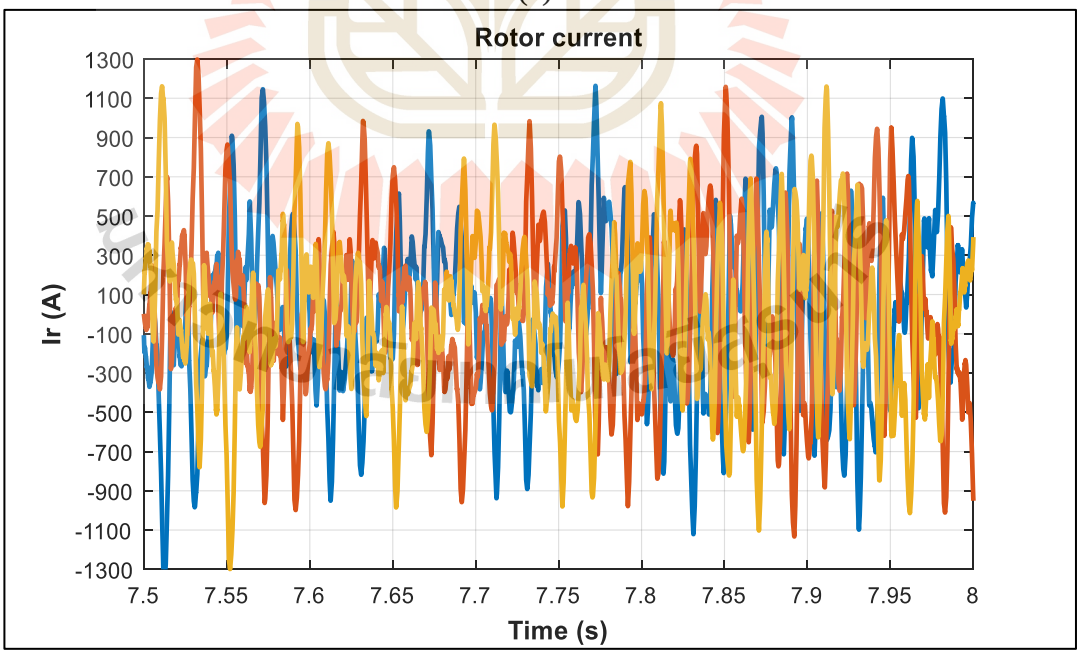

(b)

Figure 4.12 Rotor current fault state (a) Vector control (b) Fuzzy dual control.

Figure 4.13 (a) and (b) show simulations results of DC-link voltage performance of the DFIG. Due to the effect of an unbalanced system, DC link voltage increases and to a very high value in Figure 4.13 (a) where Vector control was used. Fuzzy-PI dual control output almost tracks the reference. There is a very small increase in voltage beyond reference value 7.8 s to 8.1 s.

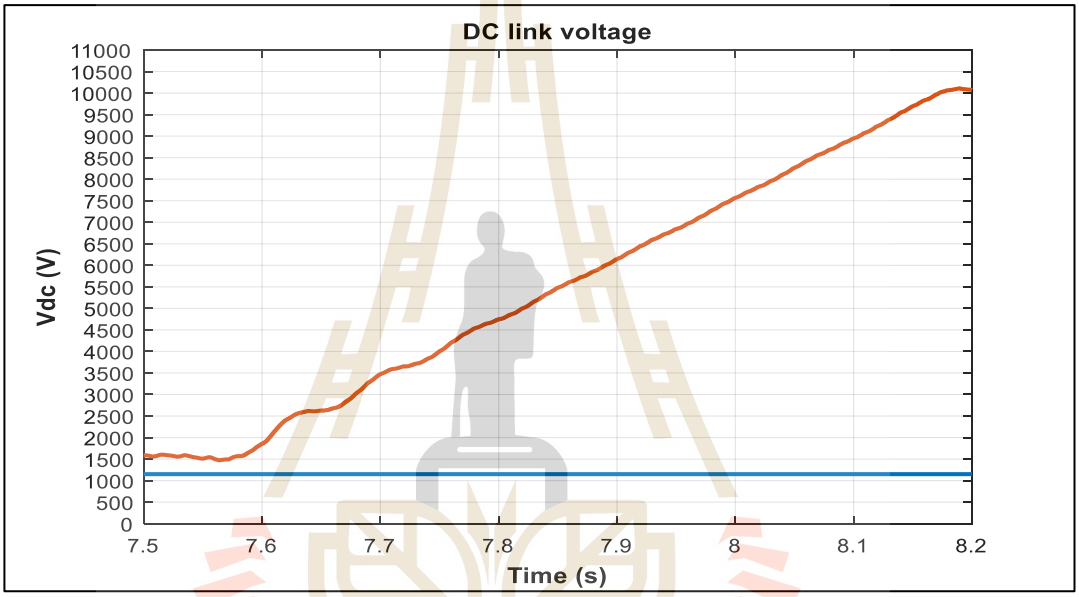

(a)

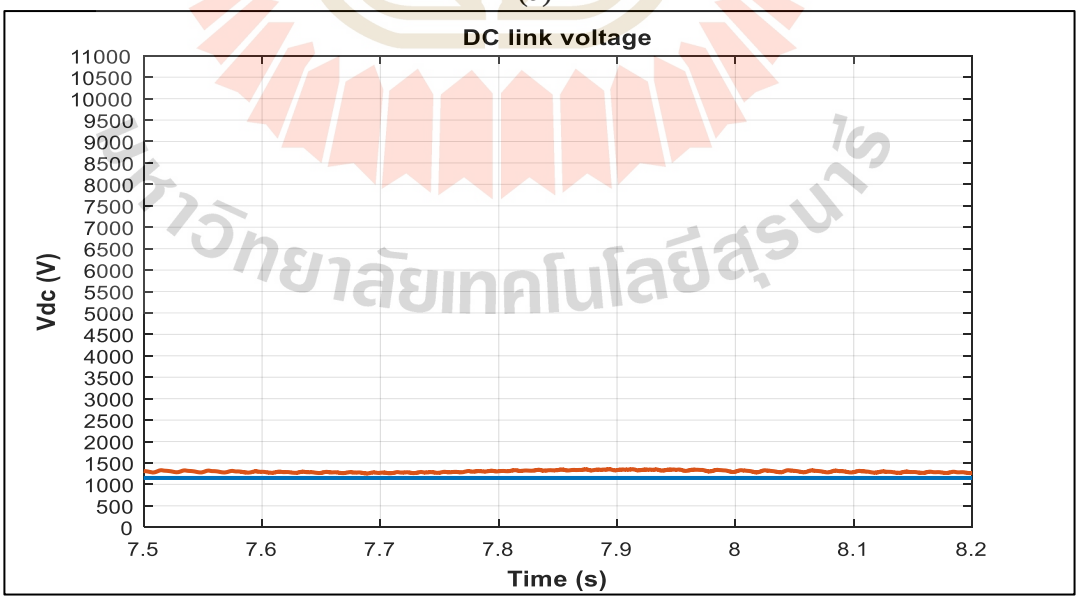

(b)

Figure 4.13 DC link voltage fault state (a) Vector control (b) Fuzzy dual control.

Figure 4.14 (a) and (b) show simulations results of the grid current of the DFIG. Due to the effect of the unbalanced system, the grid current is highly distorted and its waveforms have very high and random oscillations as shown in Figure 4.14 (a) where their vector control was used. Fuzzy-PI dual control output also has high oscillations but they follow a particular order.

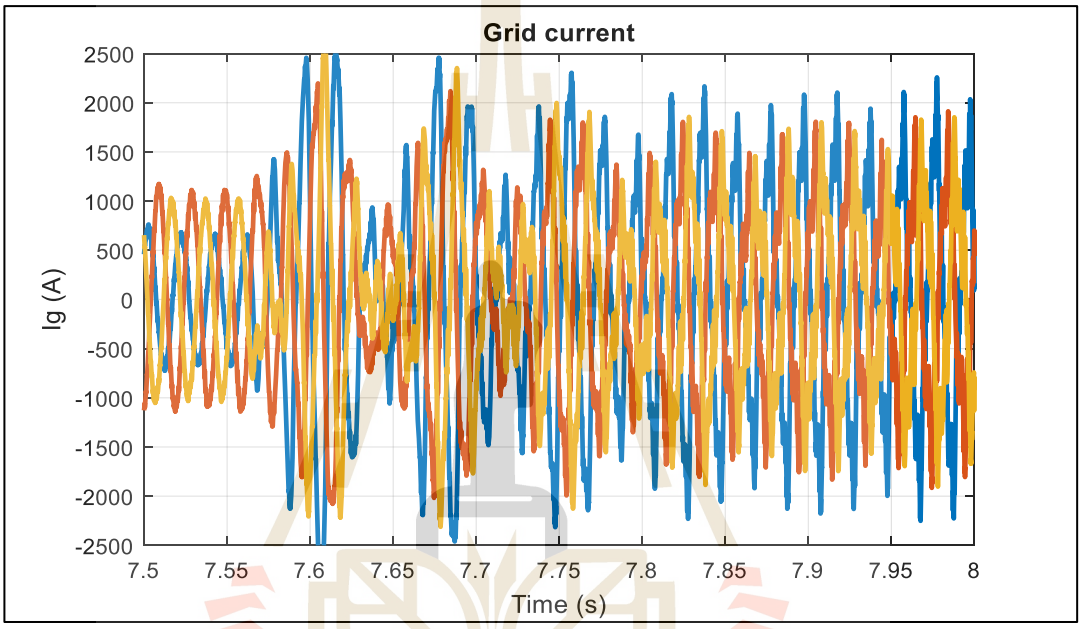

(a)

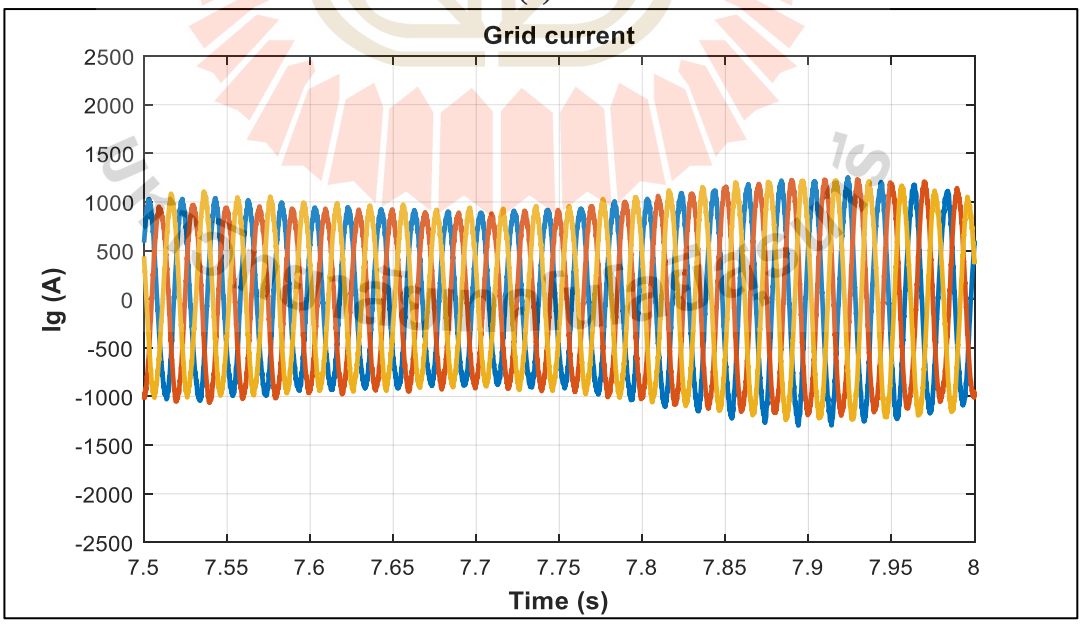

(b)

Figure 4.14 Grid current fault state (a) Vector control (b) Fuzzy dual control.

4.1.3 Post-fault state

After compensating with the proposed control scheme the steady-state value of rotor speed is reached which is 188.5 rad/s. Things are different from the output of Vector control. Rotor speed fails to track the reference value. The speed keeps on oscillating up to the end of the simulation as depicted in Figure 4.15 (a).

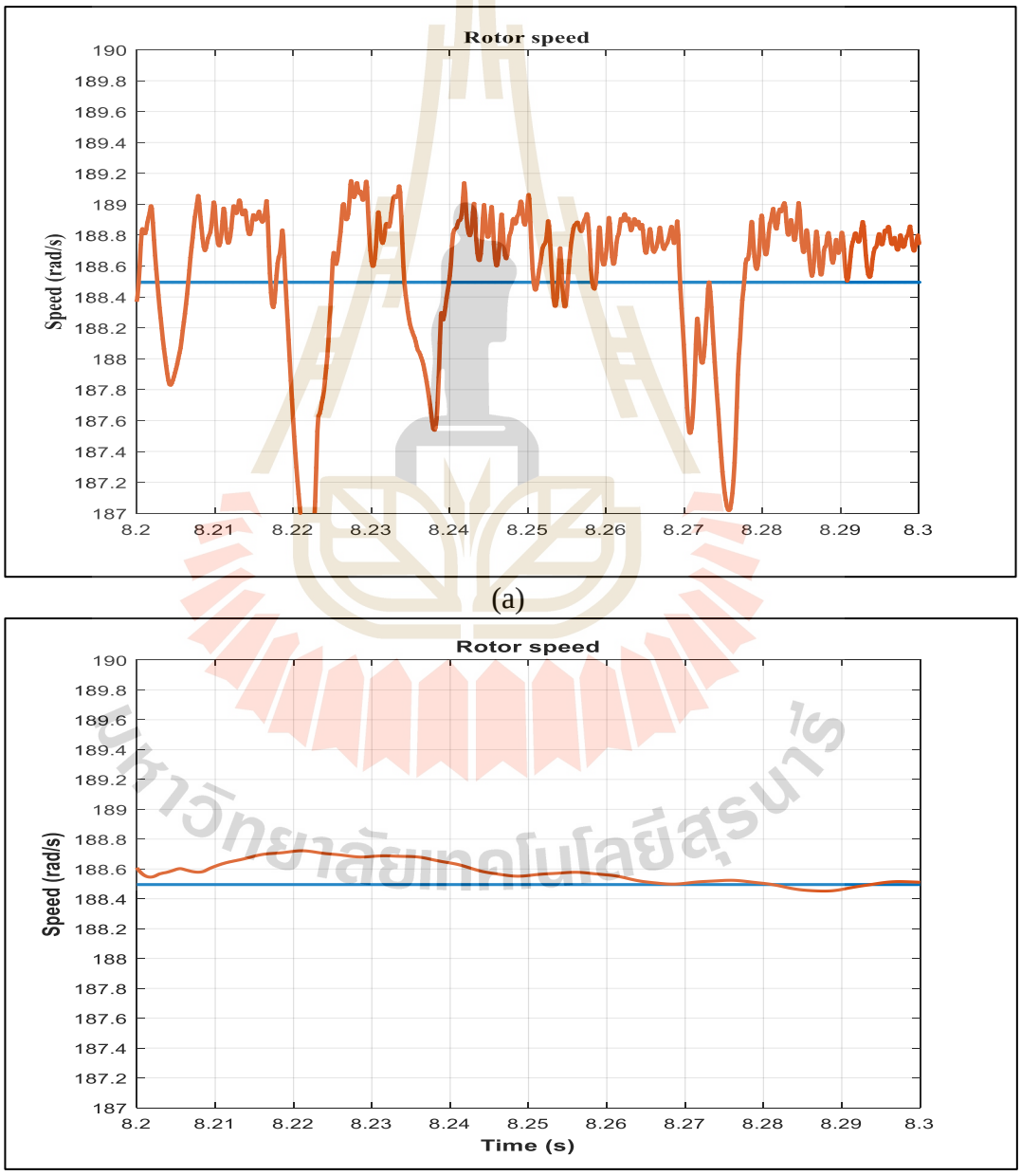

Figure 4.15 Rotor speed after fault (a) Vector control (b) Fuzzy dual control.

Optimum torque control is accomplished. After a transient, the torque reaches its steady-state value. This is surprising as compared to the vector control method, where the electromagnetic torque has serious instabilities which will end up harming the mechanical components of the turbine system. The distinction is seen in Figure 4.16 (a) and Figure 4.16 (b). This advantage is critical not only in serious sags but also in small disturbances, where the proposed method gives steady torque guaranteeing the safety of the gearbox and other mechanical components of the turbine.

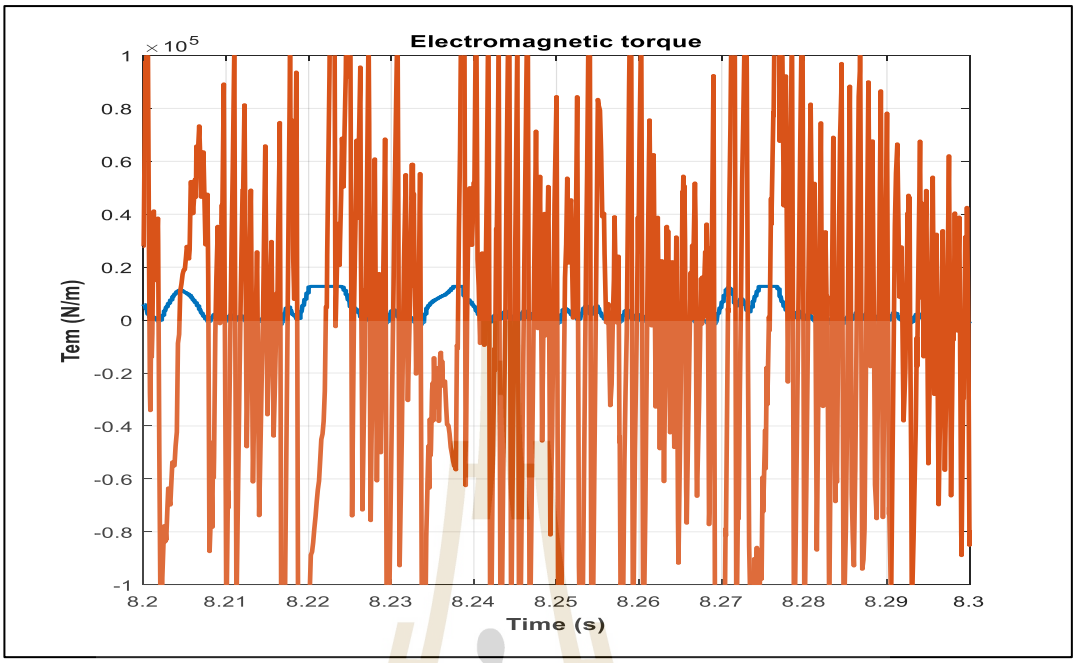

(a)

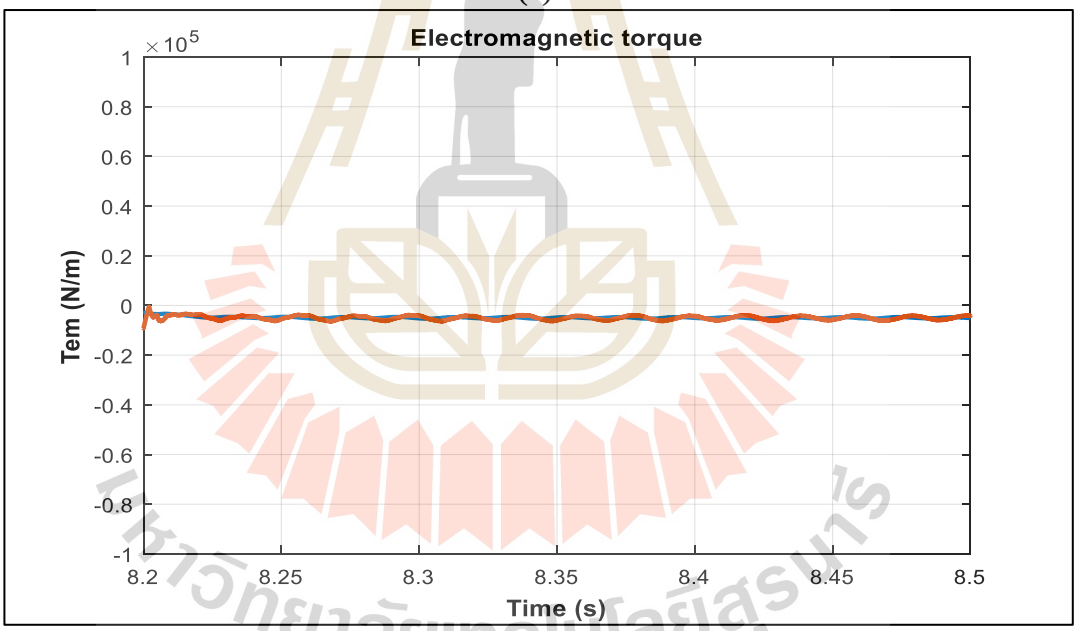

(b)

Figure 4.16 Electromagnetic torque after fault (a) Vector control (b) Fuzzy dual control.

This is one of the parameters which prove the robustness of the proposed control strategy as compared to conventional Vector control. The stator

voltage with the proposed controller after fault clearance is at its optimal reference value while with Vector control the system reaches more than 6000 V as shown in Figure 4.17 (b).

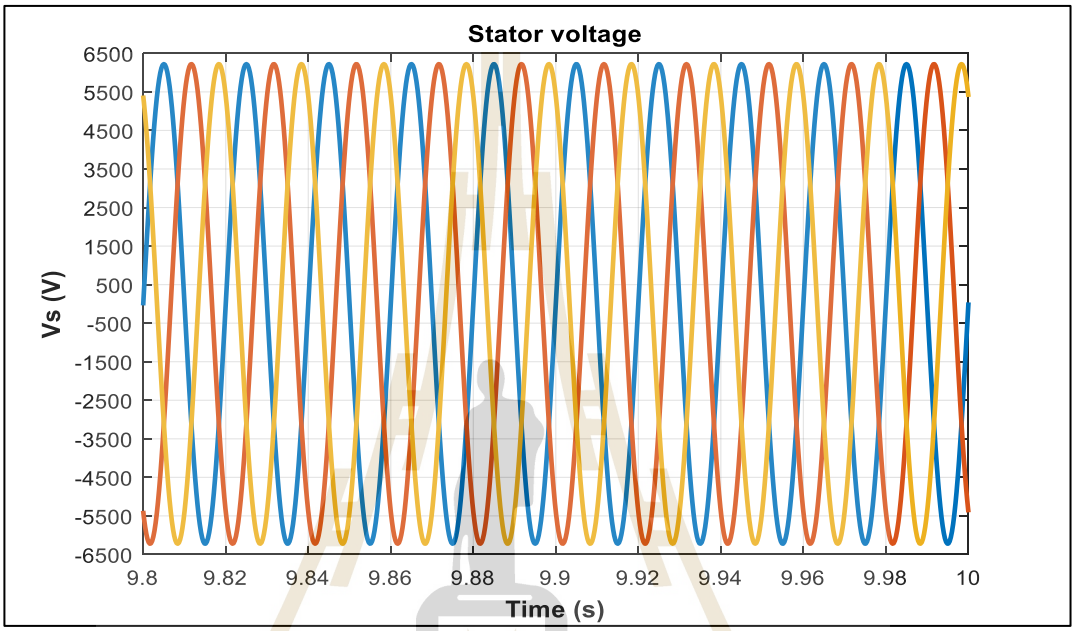

(a)

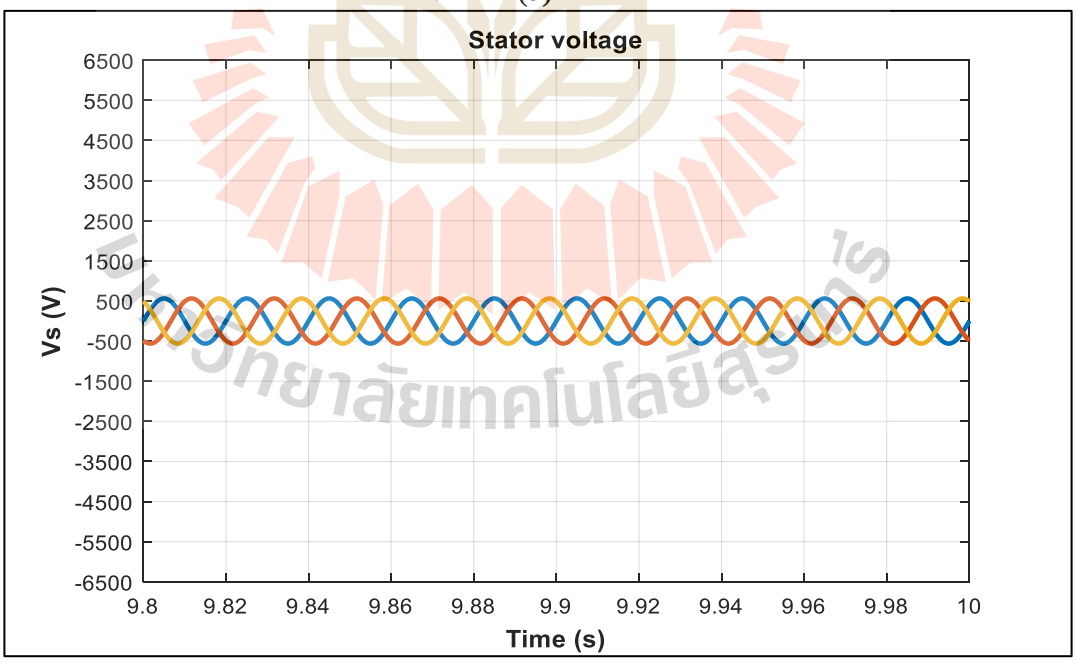

(b)

Figure 4.17 Stator voltage after fault state (a) Vector control (b) Fuzzy dual control.

The proposed controller manages to reject oscillations completely, and improve the stator current quality as shown in Figure 4.18 (b). With Vector control no improvement in stator current waveform. The current is very high and unstable.

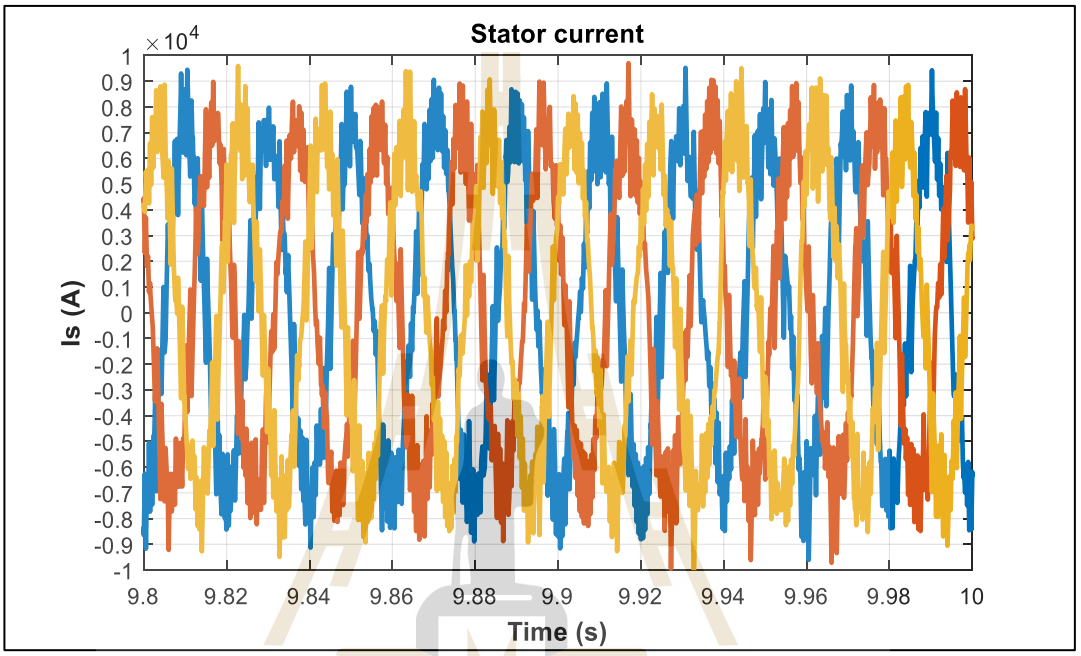

(a)

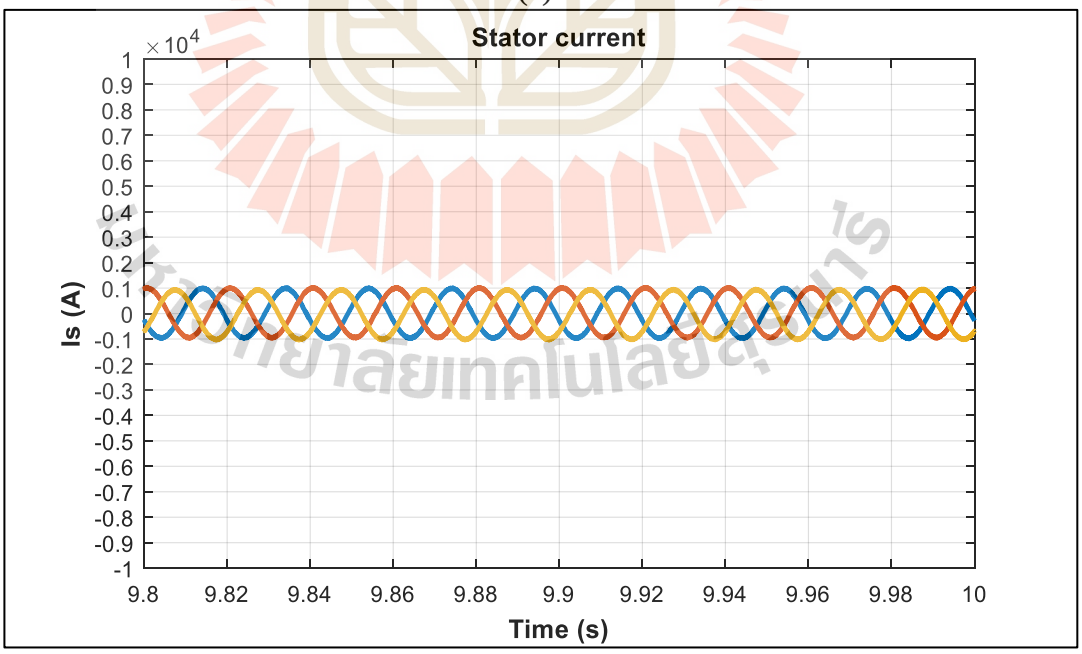

(b)

Figure 4.18 Stator current after fault state (a) Vector control (b) Fuzzy dual control.

Rotor current is shown in Figure 4.19 with Vector control and with the Fuzzy-PI dual control method. Due to the effect of asymmetric voltage dip rotor current is still distorted even after fault clearance when Vector control is applied. With the proposed control strategy rotor current waveforms are in good shape after fault clearance. Oscillations are completely dumped, and there is an improvement in the rotor current quality.

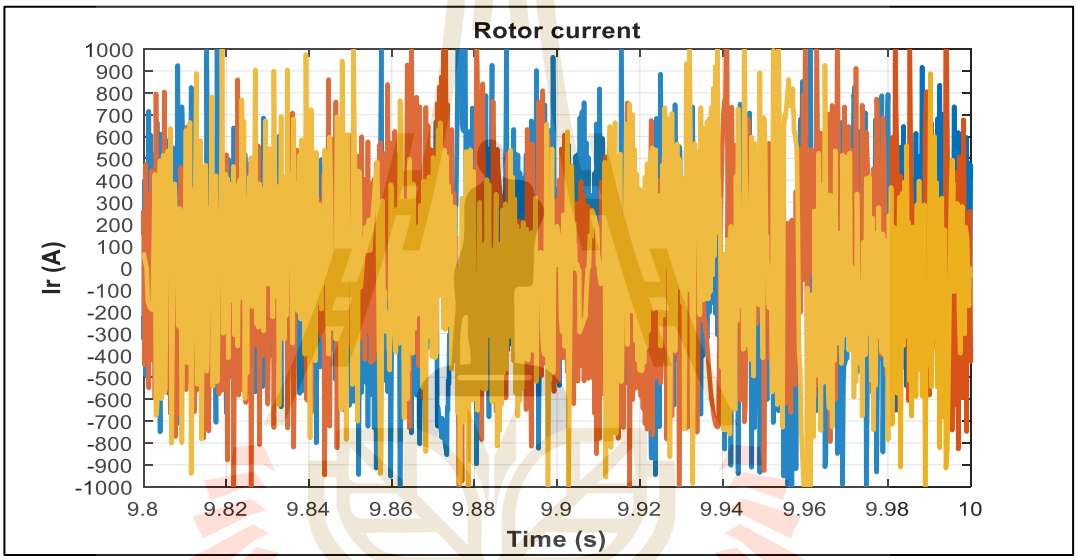

(a)

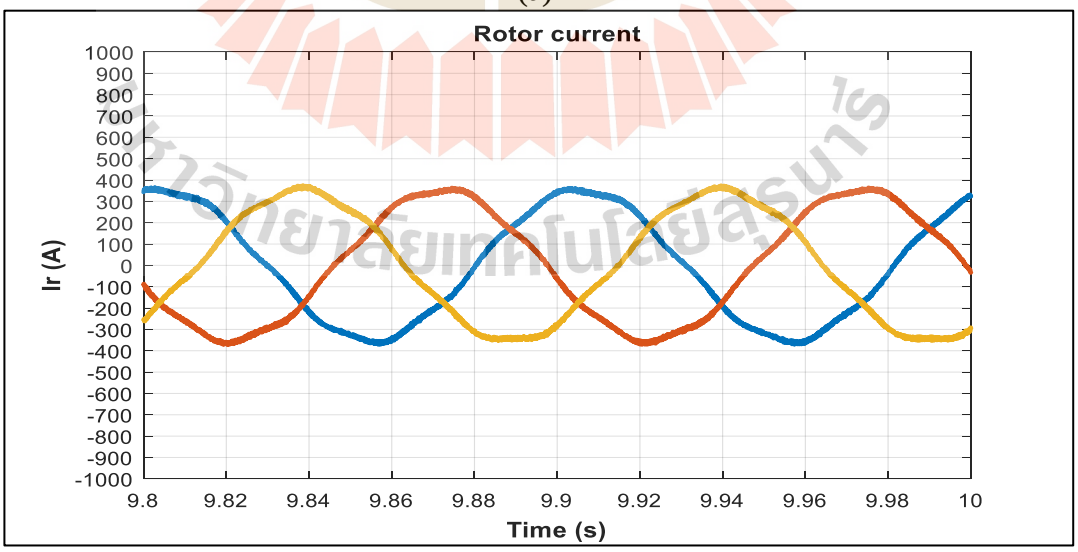

(b)

Figure 4.19 Rotor current after fault state (a) Vector control (b) Fuzzy dual control.

Figure 4.20 shows the voltage at the DC-link of the DFIG with Vector control and with the Fuzzy-PI dual control method. Due to the effect of an asymmetric voltage dip, there is still high overvoltage at the DC bus. Vector control fails to restore the DC voltage to its steady-state value. With the proposed control scheme, the DC-link voltage measured is the same as the reference value after fault clearance. Oscillations are completely dumped, and the DC voltage profile is improved.

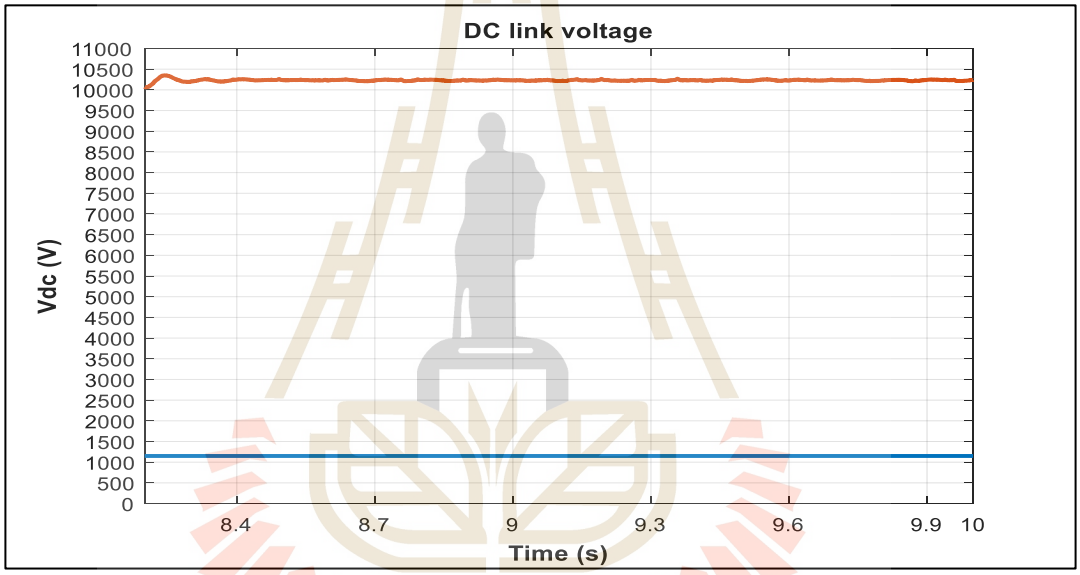

(a)

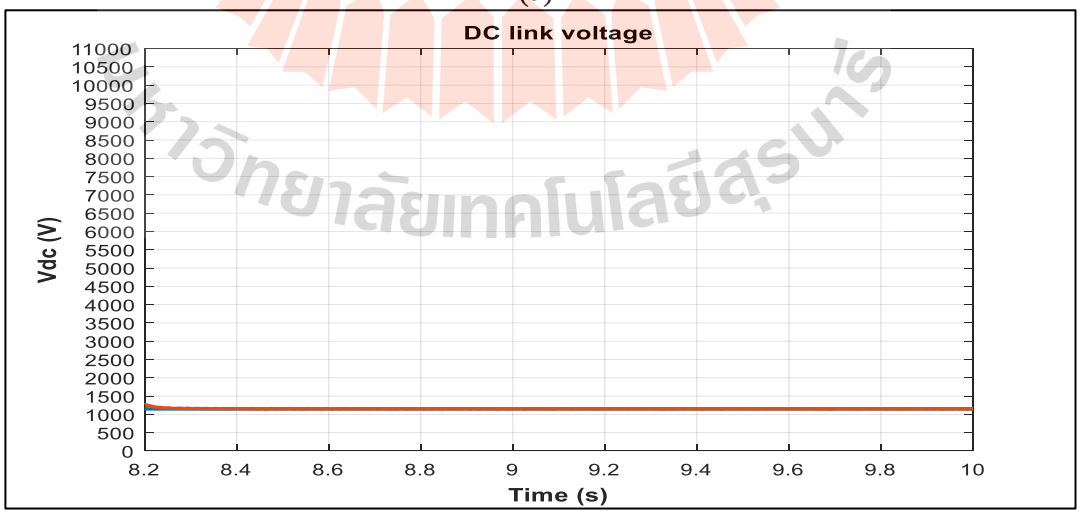

(b)

Figure 4.20 DC link voltage after fault state (a) Vector control (b) Fuzzy dual control.

The rotor current performance of the DFIG with Vector control and with the Fuzzy-PI dual control method is in Figure 4.21. Due to the effect of asymmetric voltage dip grid current is still distorted even after fault clearance when Vector control is applied. With the proposed control strategy rotor current waveforms are in good shape after fault clearance. Oscillations are completely dumped, and there experienced a significant improvement in the rotor current quality.

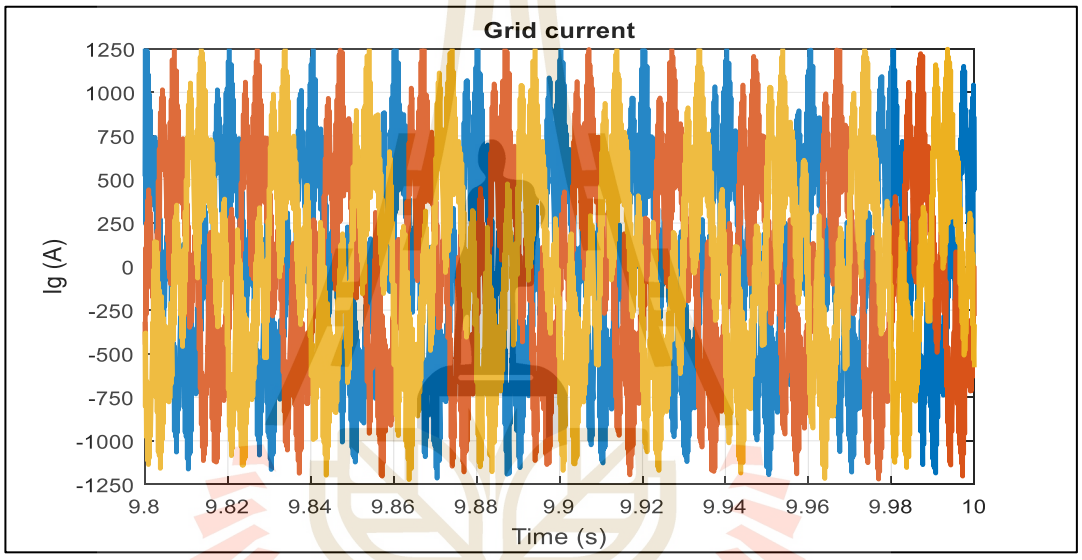

(a)

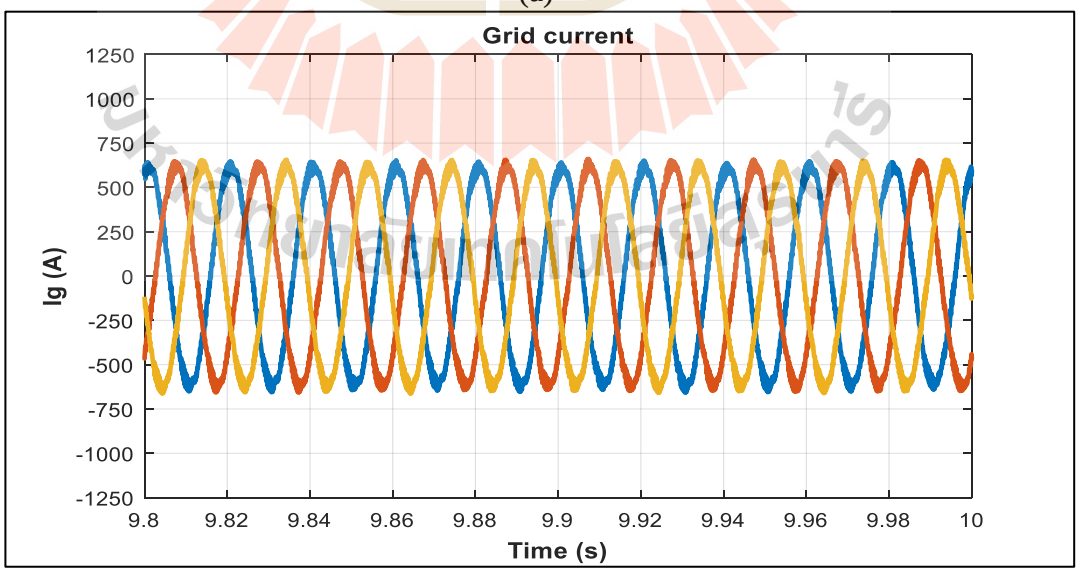

(b)

Figure 4.21 Grid current after fault state (a) Vector control (b) Fuzzy dual control.

4.1.4 Discussion

Proposed Fuzzy – PI dual control has illustrated to offer excellent results. These results are achieved after applying eight loops for controlling the current of the DFIG. The extended complexity of this method is based on having more degrees of adaptability in the control structure of RSC and the GSC. In all fault states, Fuzzy-PI dual control has shown its superiority over vector control. The proposed method has managed to stabilize all the parameters even during faults. Fuzzy logic control has fully restored the system soon after the fault.

4.2 Testing of the optimal controllers

Simulations were done using a state-space model of the systems shown in Figure 3.27 and Figure 3.28. The methods applied were pole placement and linear quadratic regulator. Noise in the input signal was added to monitor the robustness of the controller during disturbances. The step response is shown in Figure 4.22.

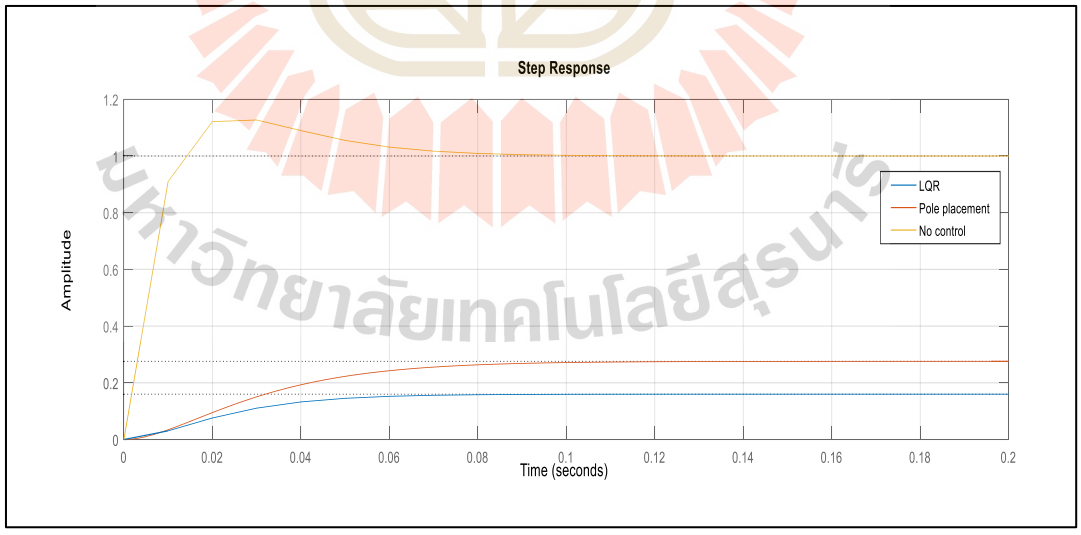

Figure 4.22 Step response of the DFIG without a controller, with Pole placement controller and with the LQR controller.

Table 4.2 shows the linear analysis results shown in the step response plot of Figure 4.22. The results show that LQR has the best results.

Table 4.2 Results of the step response of the DFIG with optimal controllers.

Performance	No control	Pole placement	LQR
Overshoot	12.7	0	0
Rise time	0.00879	0.0551	0.0549
Settling time	0.0679	0.0958	0.143
Steady state error	1	0.276	0.276

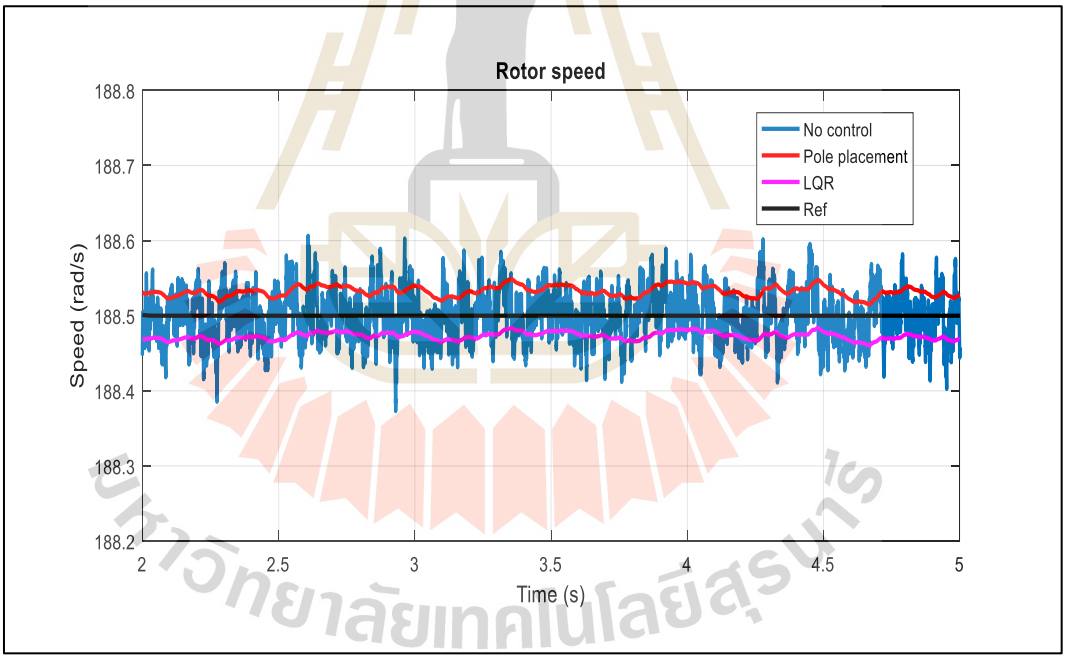

Figure 4.23 Rotor speed of the DFIG

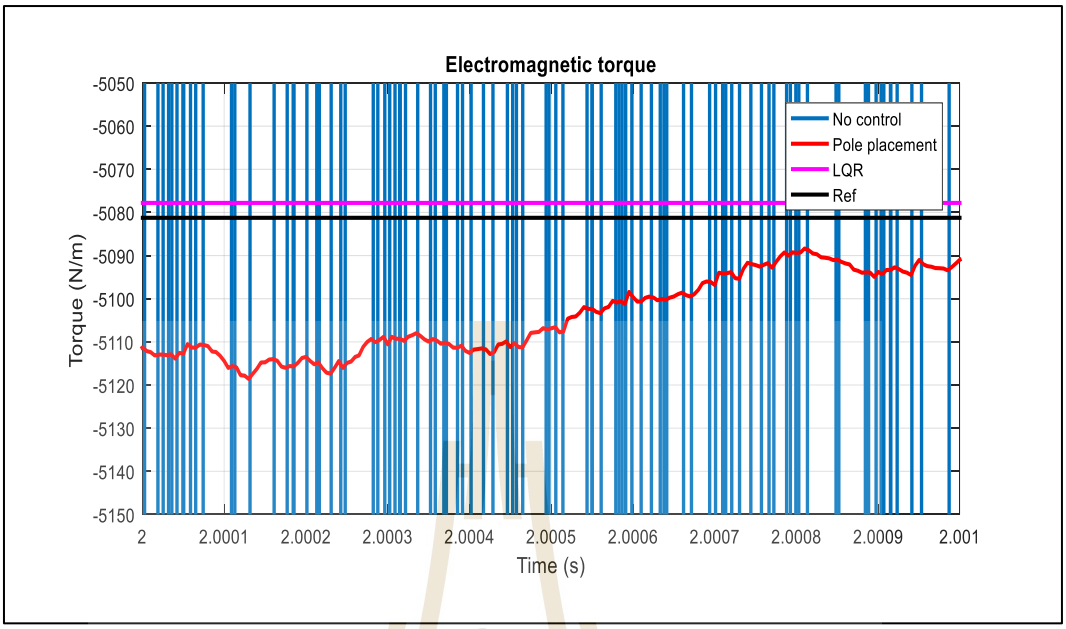

Figure 4.24 Electromagnetic torque of the DFIG.

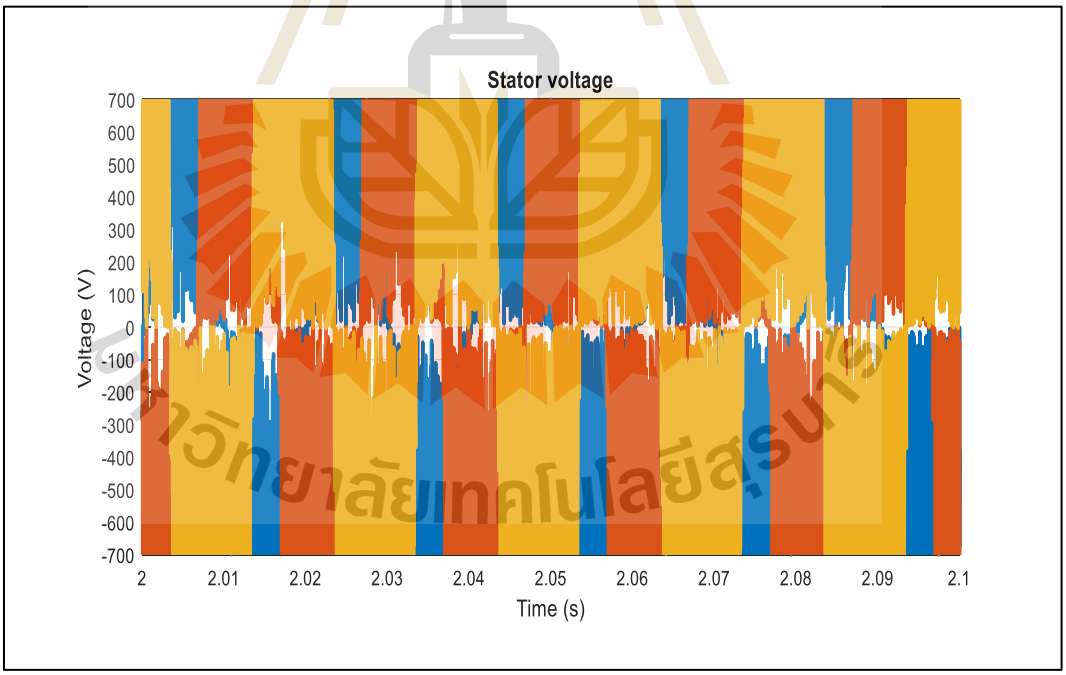

Figure 4.25 Stator voltage of the DFIG without an optimal controller.

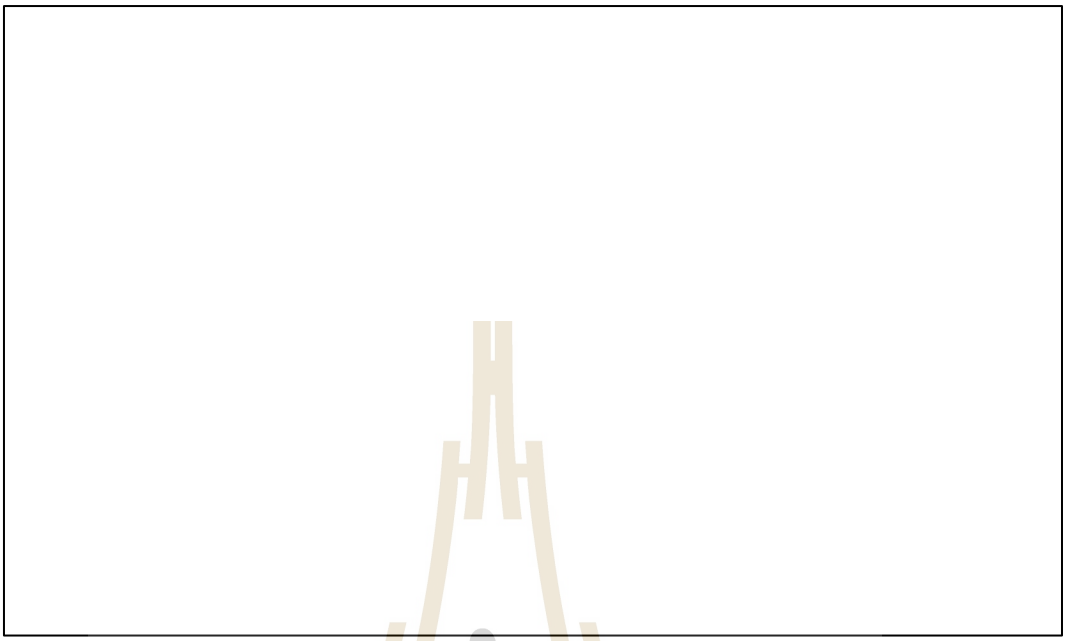

Figure 4.26 Stator voltage of the DFIG with the Pole placement controller.

Figure 4.27 Stator voltage of the DFIG with LQR.

4.3 Robust controllers testing

The methods h infinity optimal control and robust loop shaping control developed were tested with some faults common in the power system such as a line to line fault, three-phase fault, single line to ground fault, double line to ground fault, and three-line to ground fault.

4.3.1 Line-to-line fault

A line-to-line (LL) fault occurs when two phases are connected accidentally. In the case phase "b" is connected to phase"c", faulty currents are $I_{af}=0$, $I_{cf}=I_{bf}$. The analysis of the LL fault is done by denoting the fault currents in phases "a,b" and "c" as 0, I_{bf} and $-I_{bf}$. Then the sequence currents are computed as.

$$\underline{I}_S=\begin{bmatrix} I_s^0 \\ I_s^+ \\ I_s^- \end{bmatrix}=\underline{A}^{-1}\underline{I}_{abc}=\frac{1}{3}\begin{bmatrix} 1 & 1 & 1 \\ 1 & \alpha & \alpha^2 \\ 1 & \alpha^2 & \alpha \end{bmatrix}\begin{bmatrix} I_a \\ I_b \\ I_c \end{bmatrix}$$
$$=\frac{1}{3}\begin{bmatrix} 1 & 1 & 1 \\ 1 & \alpha & \alpha^2 \\ 1 & \alpha^2 & \alpha \end{bmatrix}\begin{bmatrix} 0 \\ I_{bf} \\ -I_{bf} \end{bmatrix}=\frac{1}{3}\begin{bmatrix} 0 \\ \sqrt{3}I_{bf}\angle 90^\circ \\ \sqrt{3}I_{bf}\angle -90^\circ \end{bmatrix} \quad (4.1)$$

It can be seen that the zero-sequence circuit is dead. The positive and negative sequence currents are equal and opposite. The two currents share the same circuit connection in which the positive sequence terminals are directly connected to the negative sequence terminals.

There is a similarity in the voltage phase angles of the two faulted phases. The two faulted phases face an equal drop in voltage. The voltage measured at the healthy phase remains unchanged. The two faulted phases also experience an

increase in the magnitude of the current, 180-degree phase shift between those currents, and almost zero ground or neutral current.

Simulations show that asymmetric voltage dip caused by line to line short circuit led to serious distortion to the DFIG. The harmonic distortion plot of Figure 4.36 is used to show the level of instability when the DFIG was without robust controllers. Total harmonic distortion (THD) recorded is 11.34% as shown in Figure 4.28. The stator voltage of the DFIG was highly affected by the dip as shown in Figure 4.29 without robust controllers.

With robust controllers, the spectrums show that THD is reduced to 4.05% with h-infinity optimal control and 1.36% with loop shaping control as shown in Figure 4.30 and 4.31 respectively. This can be validated by the behavior of the quadrature axis rotor current and electromagnetic torque of the induction machine as shown in Figure 4.32 and Figure 4.33 respectively, with robust h-infinity loop shaping control showing slight deviation from reference value but stable as compared to robust h-infinity optimal controller which experiences more oscillations of the torque and current.

With the h-infinity loop shaping control system distortion is highly reduced. This can be validated by the direct axis rotor current plots in Figure 4.34 and voltage plots in Figure 4.35 and Figure 4.36. The voltage plots show that stator voltage is optimally stabilized by the loop shaping controller as compared to the optimal controller which fails to stabilize the stator voltage affected by the fault.

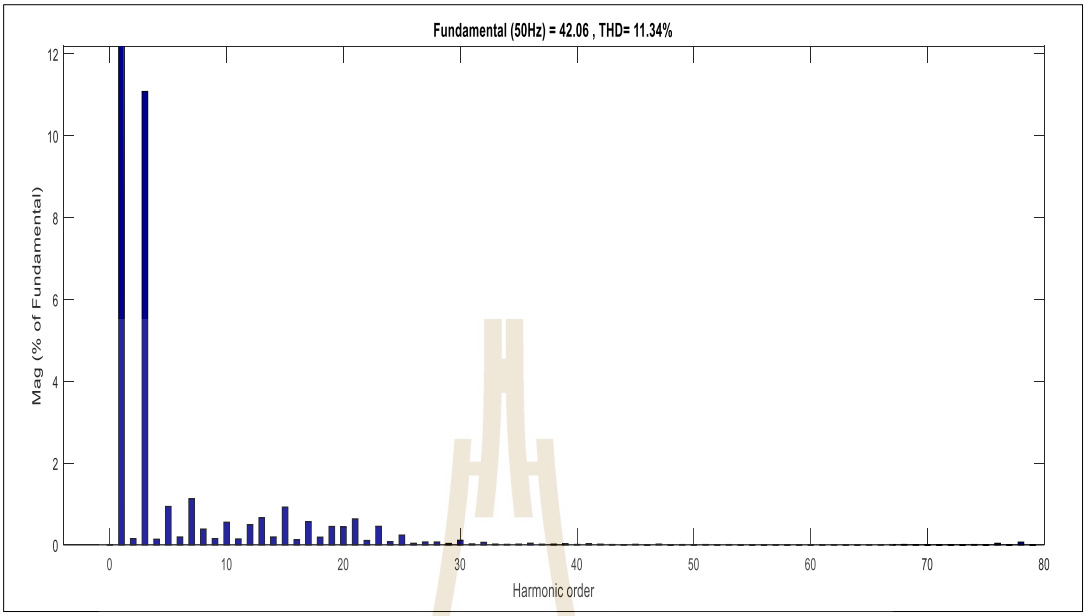

Figure 4.28 THD of the stator voltage due to a LL fault without robust controllers.

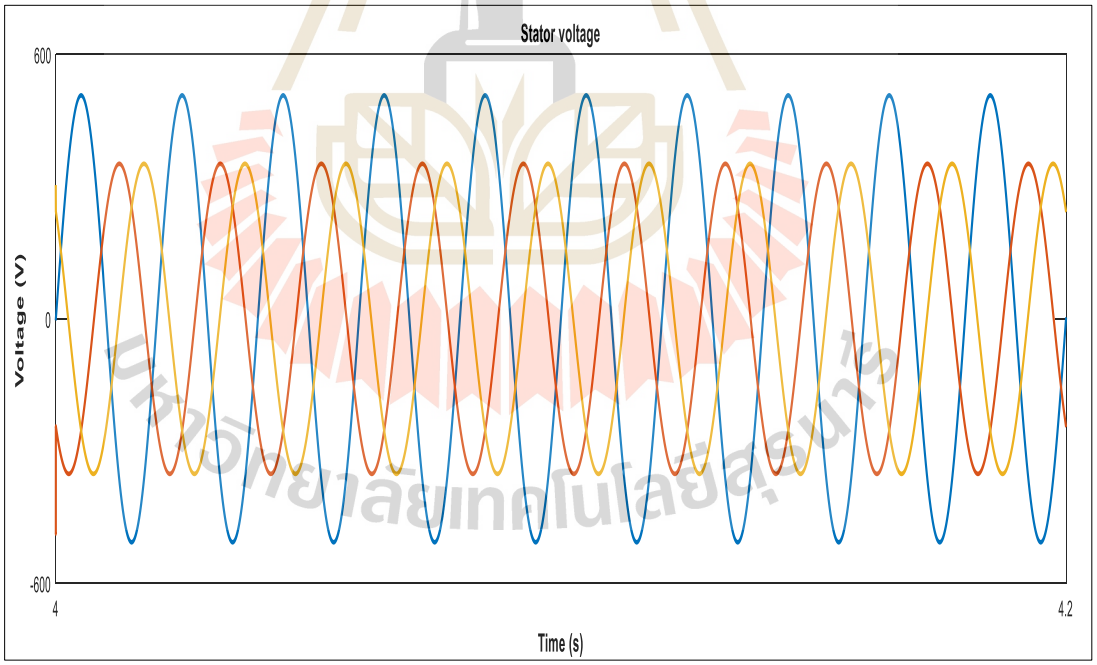

Figure 4.29 Stator voltage LL fault without robust controllers.

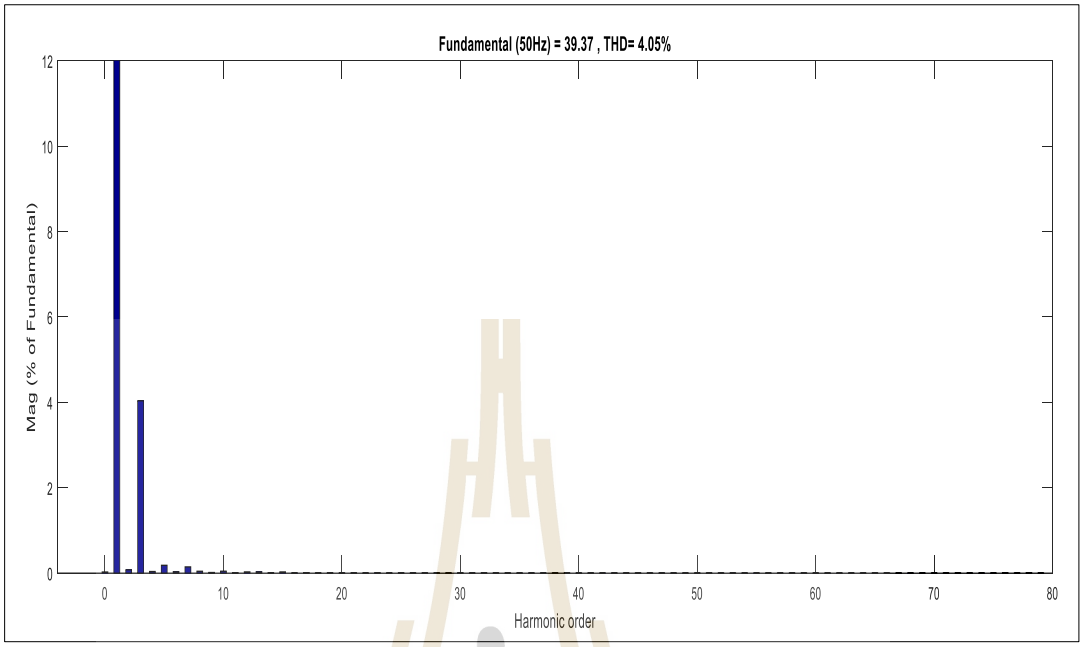

Figure 4.30 THD of the stator voltage due to a LL fault with robust h infinity optimal controller.

Figure 4.31 THD of the stator voltage due to a LL fault with a robust loop shaping controller.

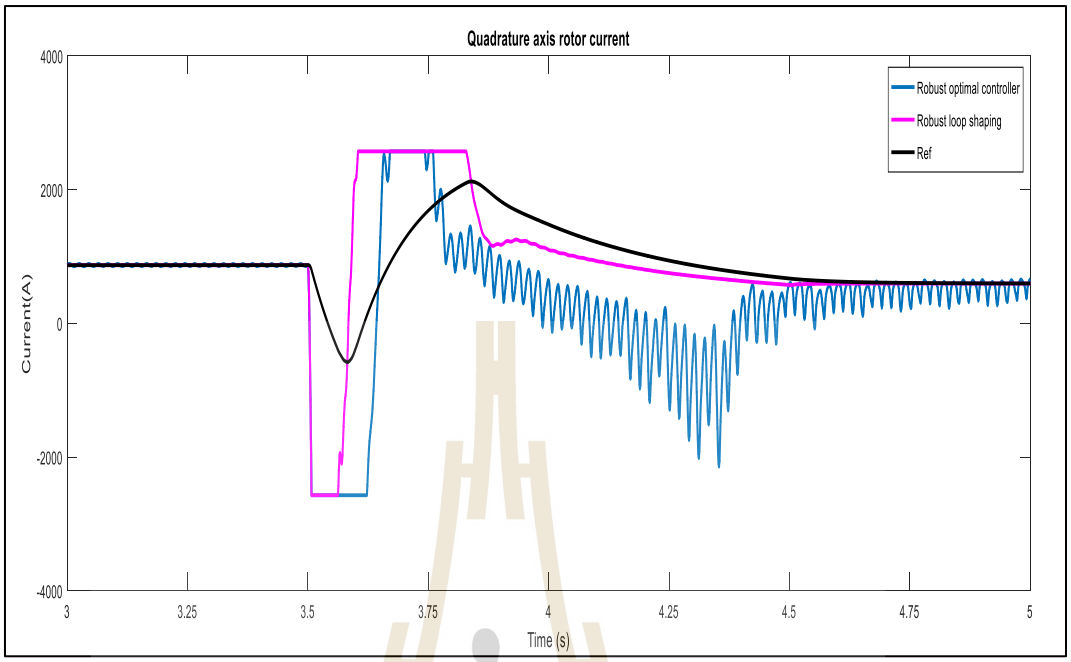

Figure 4.32 Quadrature axis rotor current before, during, and after a *LL* fault.

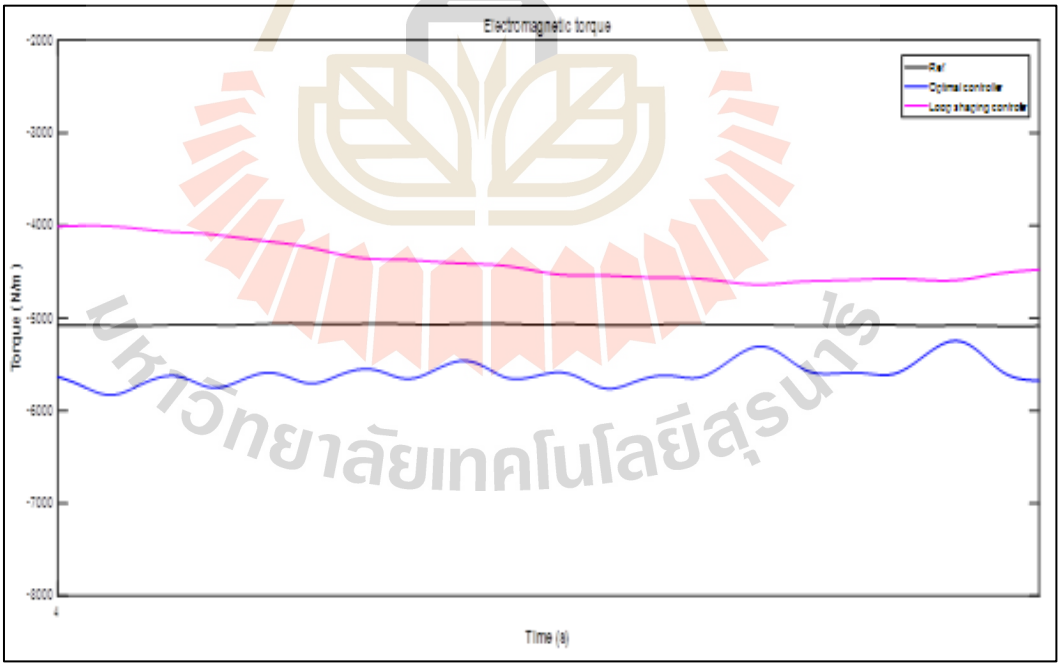

Figure 4.33 Electromagnetic torque during *LL* the fault.

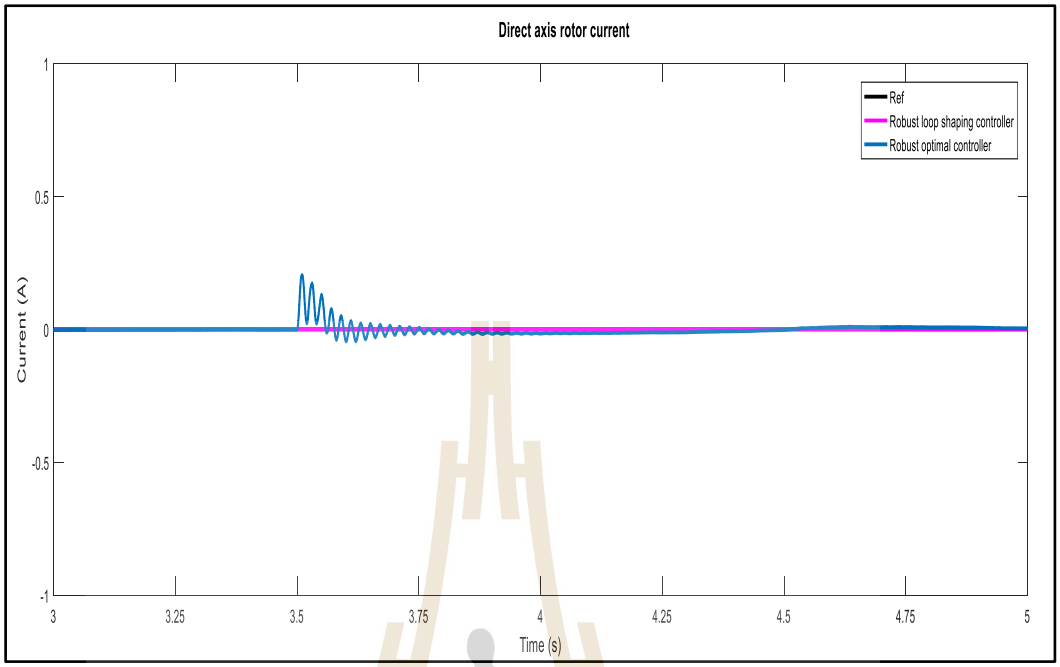

Figure 4.34 Direct axis rotor current before, during, and after LL the fault.

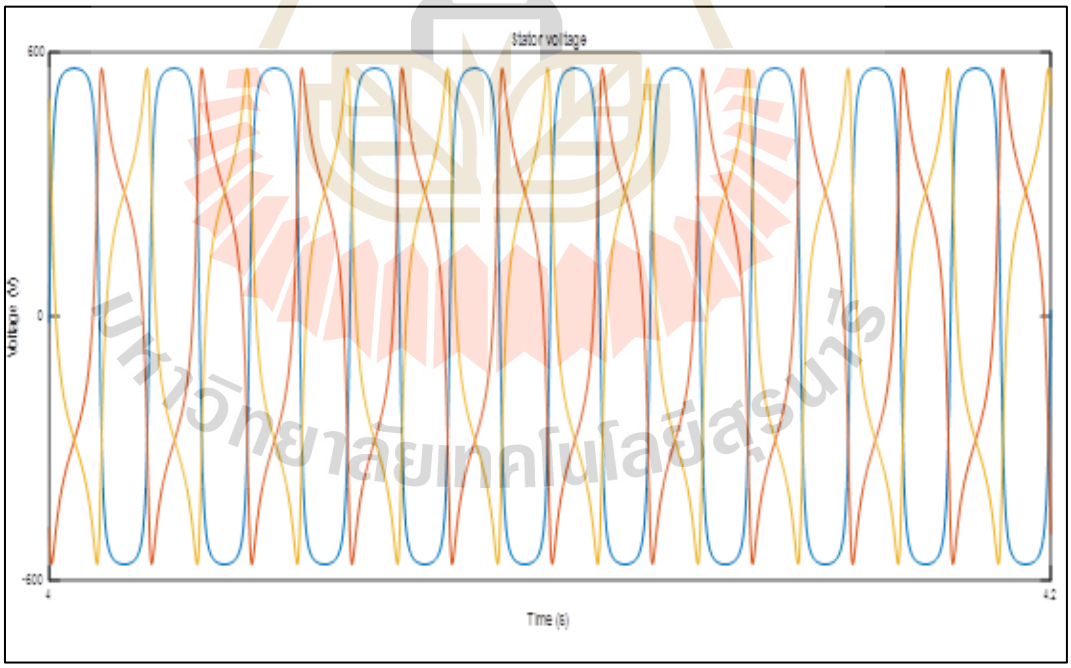

Figure 4.35 Stator voltage LL fault with the robust h infinity optimal controller.

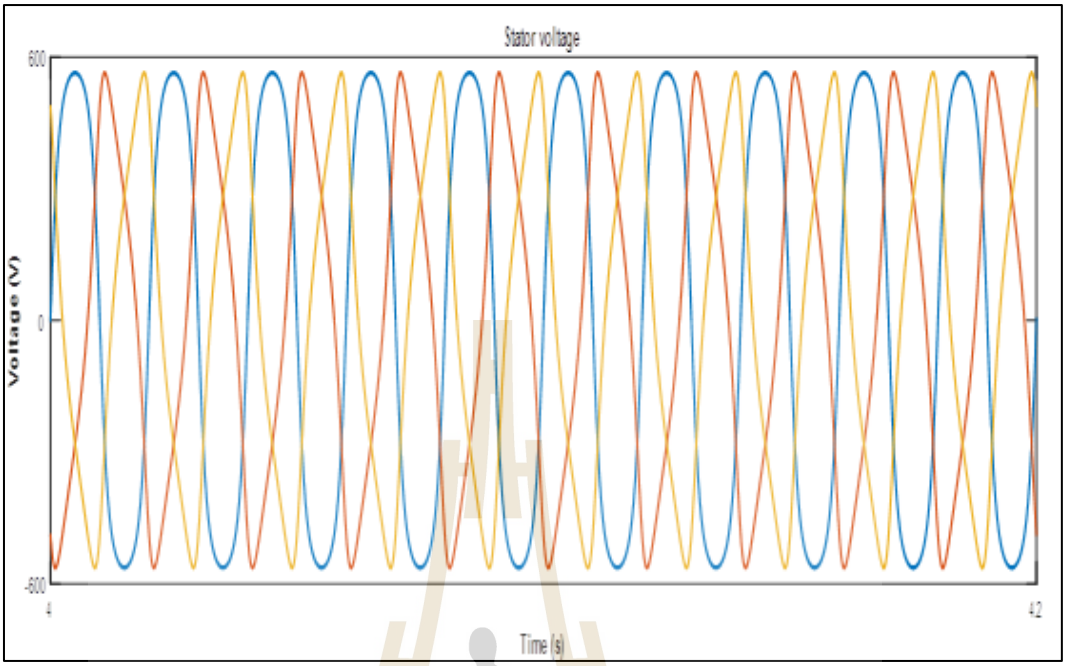

Figure 4.36 Stator voltage LL fault with robust loop shaping controller.

4.3.2 DFIG under short circuit fault (three-phase)

It is one of the most uncommon fault occurring only for about 5% of all 3 phase faults. The good thing for this is its symmetric behavior of making all the 3 phases share the same “load” even during the fault. This is of good help because the system remains balanced. Therefore, system analysis becomes easier even during faulty conditions although being a three-phase fault it is not at all “good” for the power system operation and control as the 3 phase fault is usually the most severe.

The method developed was also tested for this fault and a significant drop in stator voltage was experienced at the start of the fault. As time passes on this voltage keeps on increasing as shown in Figure 4.37. Echoing the results obtained from the line to line fault, in this fault robust h-infinity loop shaping control continues to prove its robustness by showing slight deviation of the quadrature axis rotor current and electromagnetic torque from reference value but stable as compared to the

optimal controller which experiences severe oscillations of the torque more than in the asymmetric voltage dip as shown in Figure 4.38 and Figure 4.39.

With robust h-infinity loop shaping control, there is no failure of the direct axis rotor current (Figure 4.40) and stator voltage (Figure 4.42) as compared to the optimal controller which experiences the variation of the rotor current and significant drop in stator voltage at the start of the fault as shown in Figure 4.41.

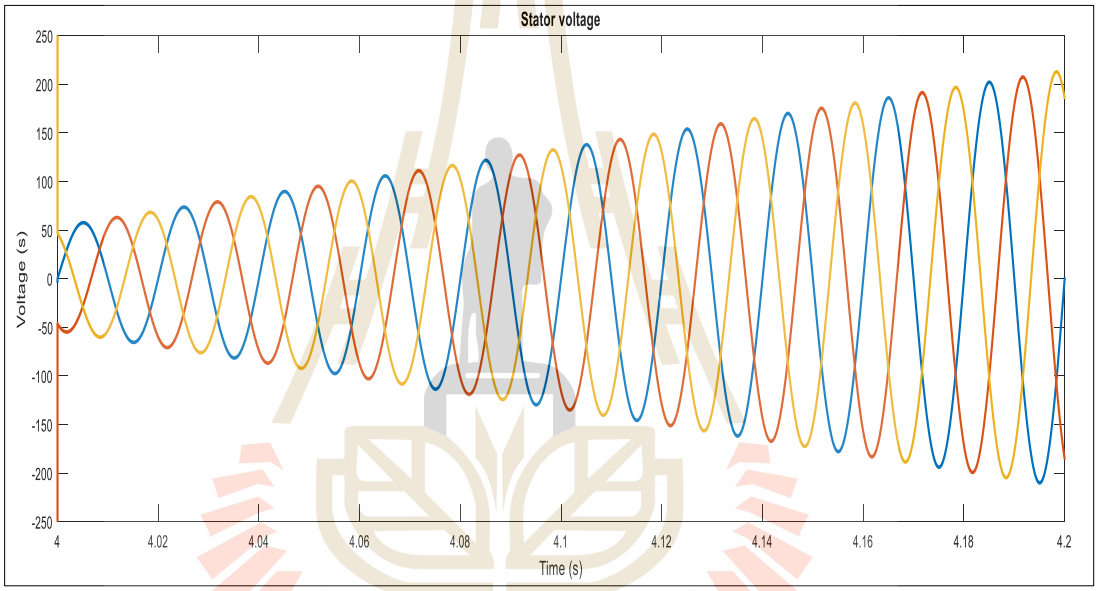

Figure 4.37 Stator voltage during LLL fault without robust controllers.

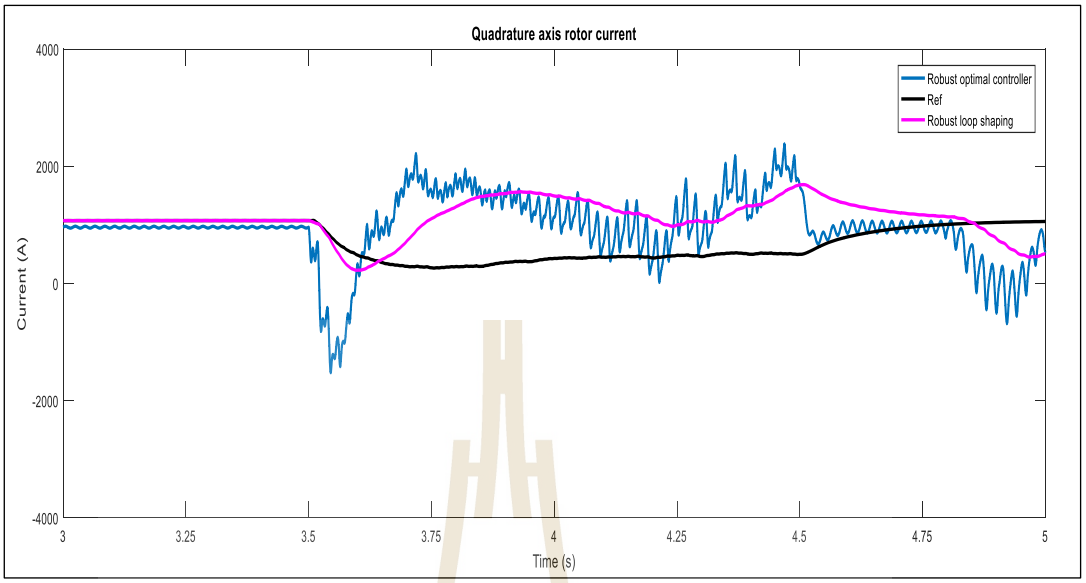

Figure 4.38 Quadrature axis rotor current before, during, and after LLL fault with robust controllers.

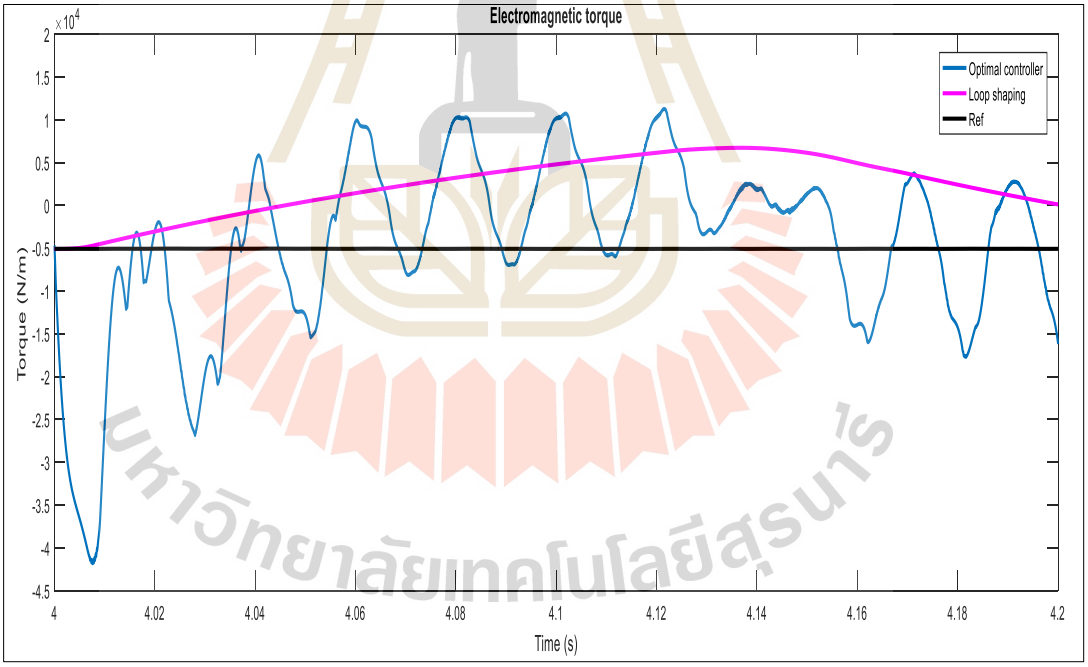

Figure 4.39 Electromagnetic torque during LLL fault with robust controllers.

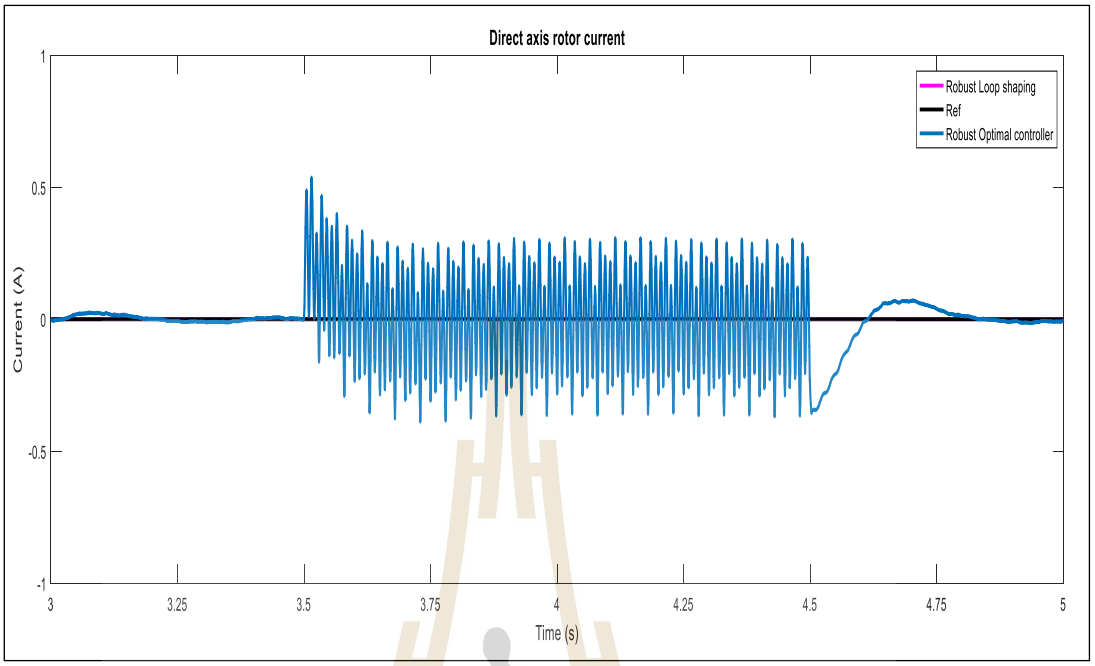

Figure 4.40 Direct axis rotor current before, during, and after LLL fault with robust controllers.

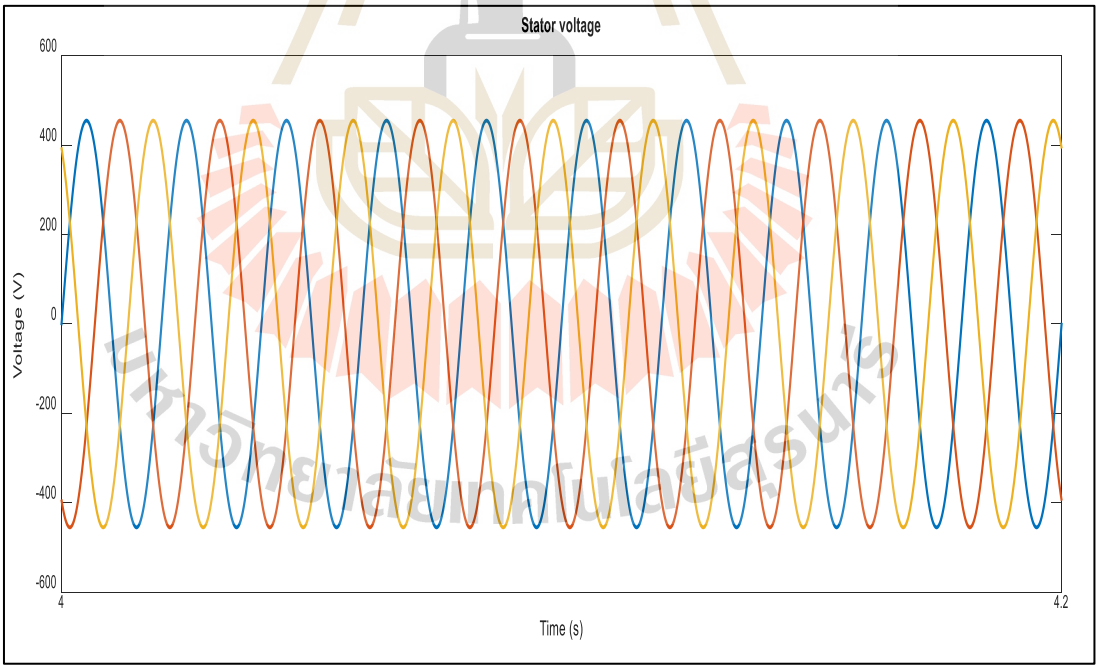

Figure 4.41 Stator voltage during LLL fault with the robust h infinity optimal controller.

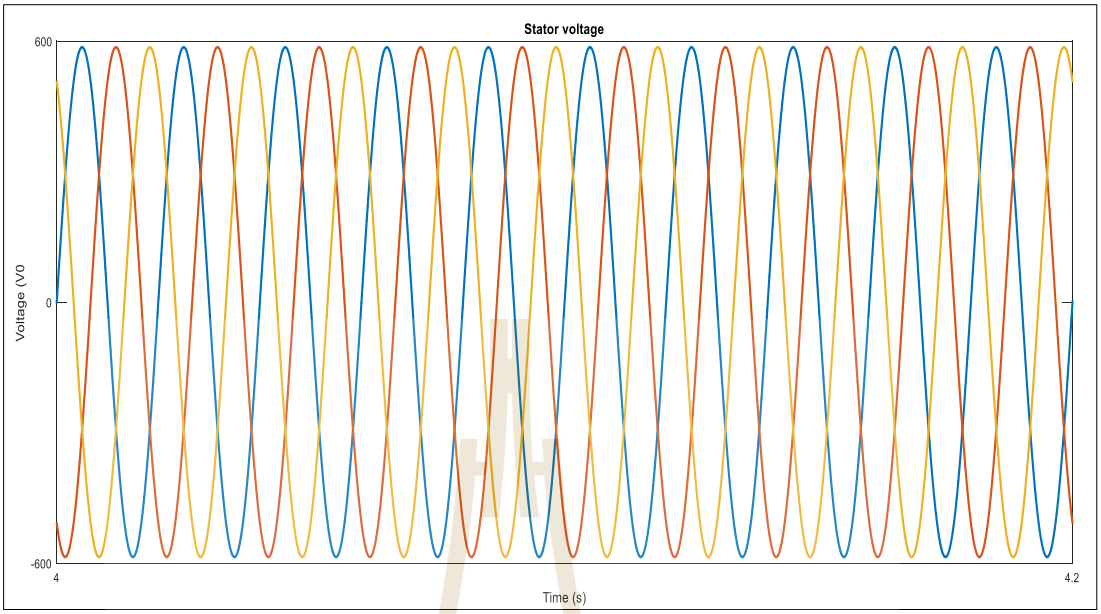

Figure 4.42 Stator voltage during LLL fault with a robust loop shaping controller.

4.3.3 DFIG under the single line to ground fault

This fault is well known as a single-line-to-ground (L-G) fault. In this fault, one phase is connected to the ground. The analysis is done by denoting the fault currents in phases a, b, and c as I_{af} , 0, and 0 (it can be seen that no impedance matrix is changed but instead a current source is added, to the substitution theorem). During this fault, the same current is flowing in all three sequence networks. The circuit connection involved is a series connection of the positive, negative, and zero-sequence circuits.

The method developed was tested with a single line to ground fault (L-G). The fault occurred at T=4s. The behavior of the quadrature axis rotor current in Figure 4.43 with its counterpart electromagnetic torque Figure 4.44 shows the significance of the fault. The effect of the fault is also realized by the direct axis rotor current Figure 4.45 and the stator voltage without robust controllers in Figure 4.46. Robust h-infinity loop shaping control continues to dominate the robust optimal

controller as it happened in the previous faults for all parameters as shown in the plots for rotor currents, electromagnetic torque except the stator voltages where the waveforms are very similar as shown in Figure 4.47 and Figure 4.48.

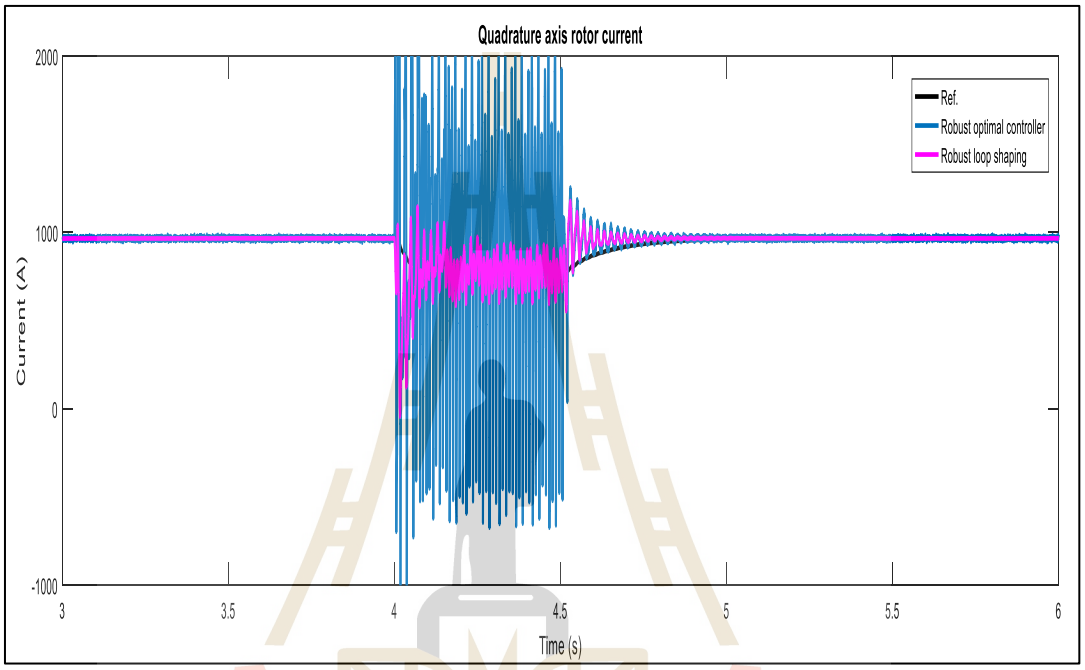

Figure 4.43 Quadrature axis rotor current before, during, and after L-G fault with robust controllers.

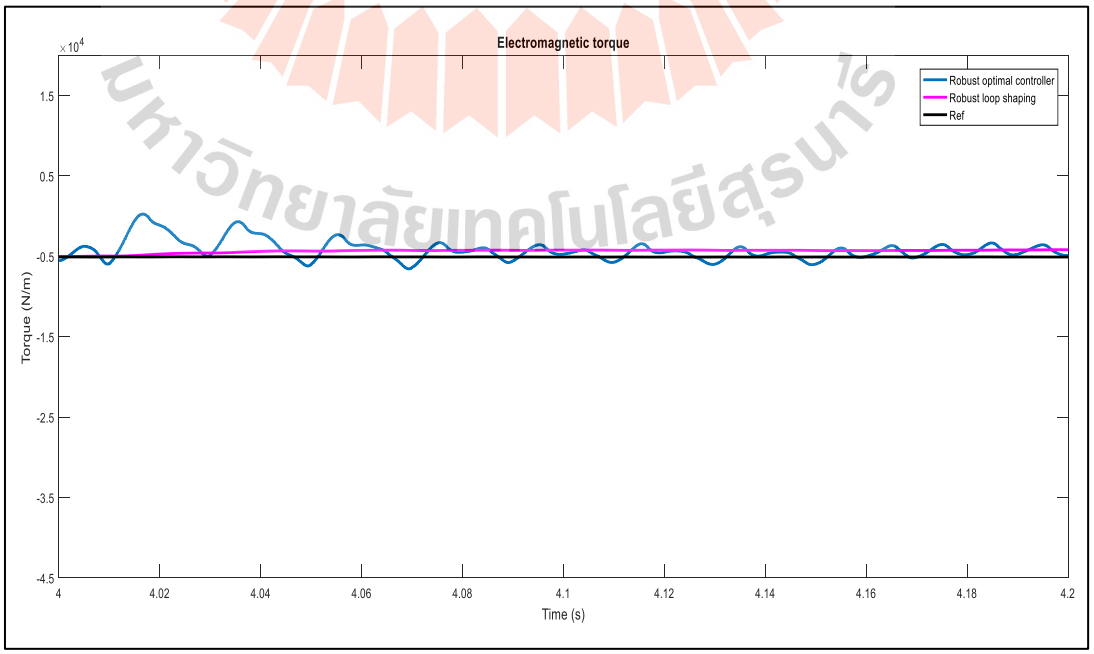

Figure 4.44 Electromagnetic torque during L-G fault with robust controllers.

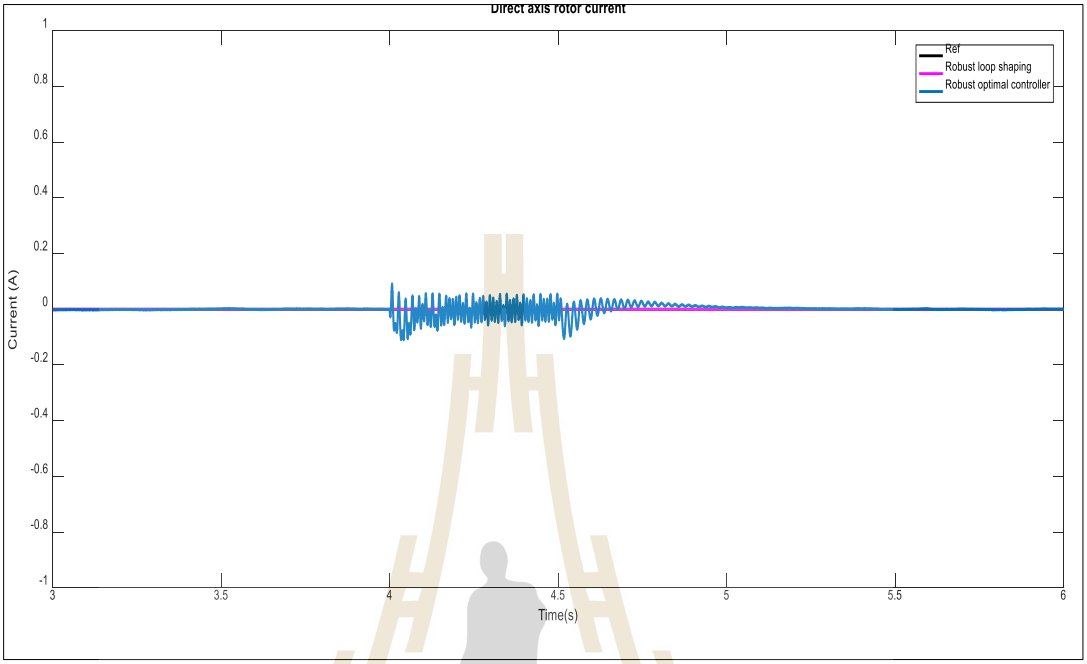

Figure 4.45 Direct axis rotor current before, during, and after L-G fault with robust controllers.

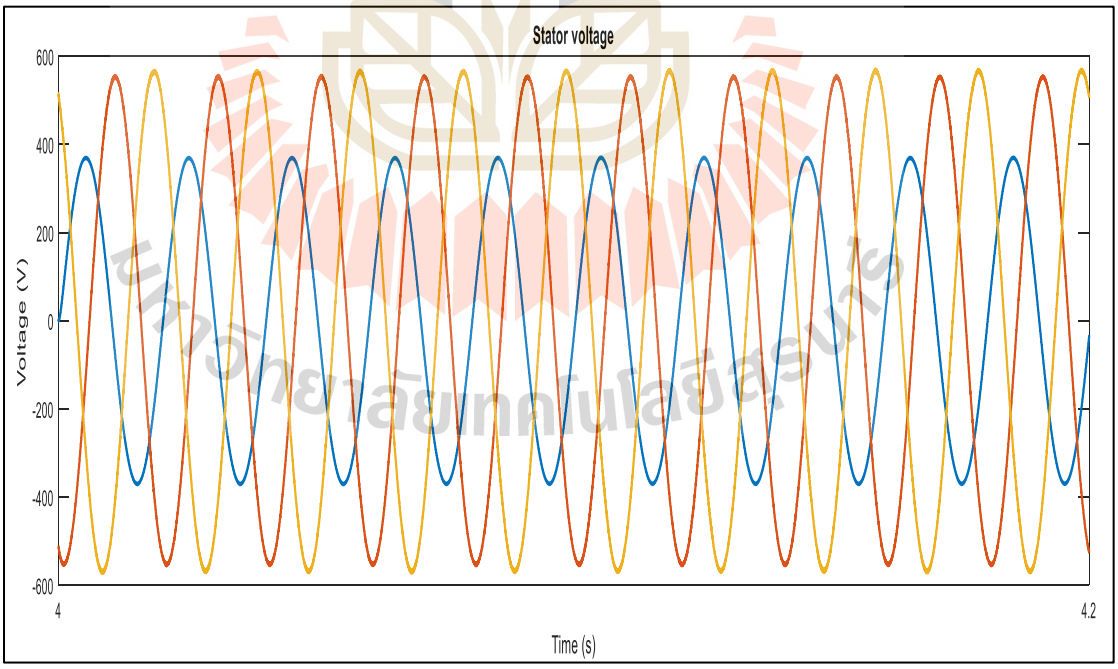

Figure 4.46 Stator voltage under L-G fault without robust controllers.

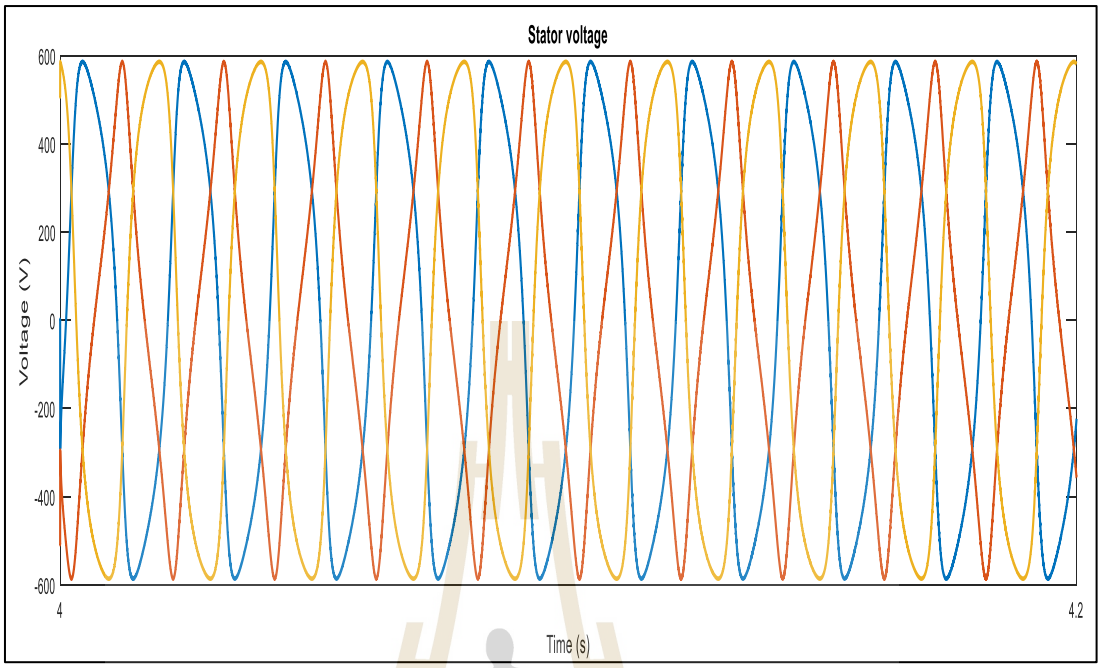

Figure 4.47 Stator voltage during L-G fault with robust h infinity optimal controller.

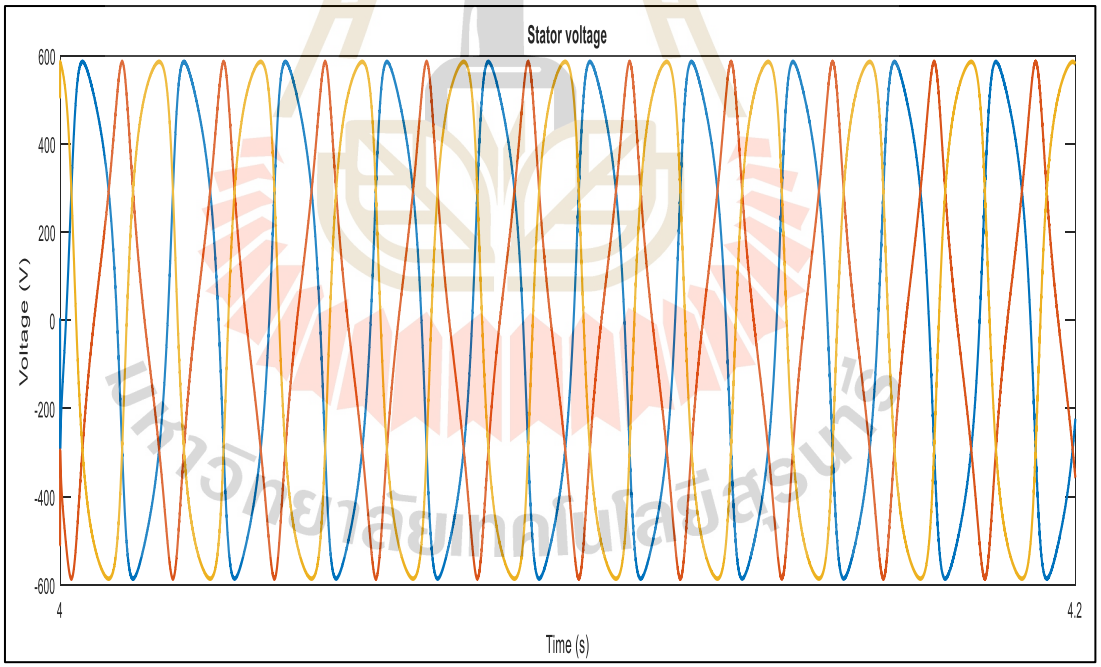

Figure 4.48 Stator voltage during L-G fault with a robust loop shaping controller.

4.3.4 DFIG under the double line to ground fault

This fault occurs when there is a short circuit between any two phases and the shorted part is circuited to the ground or neutral. There occurs a total collapse of the voltage on the two faulted phases. The voltage of the un-faulted phase remains intact. The positive sequence voltage becomes equal to the negative one. The current measured at the two faulted phases increase. No change in phase angles of the faulted currents but there is a significant amount of current flowing to the ground. All three sequence currents are present during this fault. The magnitude of the positive sequence current equals the sum of the negative and zero sequence currents. In the whole faulty period, the voltage of positive and negative sequence, are approximately the same.

The method was tested with this fault. The fault occurred at T=4s. The behavior of the quadrature axis rotor current in Figure 4.49 with its counterpart electromagnetic torque Figure 4.50 shows the significance of the fault. The effect of the fault is also realized by the direct axis rotor current in Figure 4.51 and the stator voltage without robust controllers in Figure 4.52. Robust h-infinity loop shaping control continues to dominate the robust optimal controller as it happened in the previous faults for all parameters as shown in the plots for rotor currents, electromagnetic torque, and stator voltage.

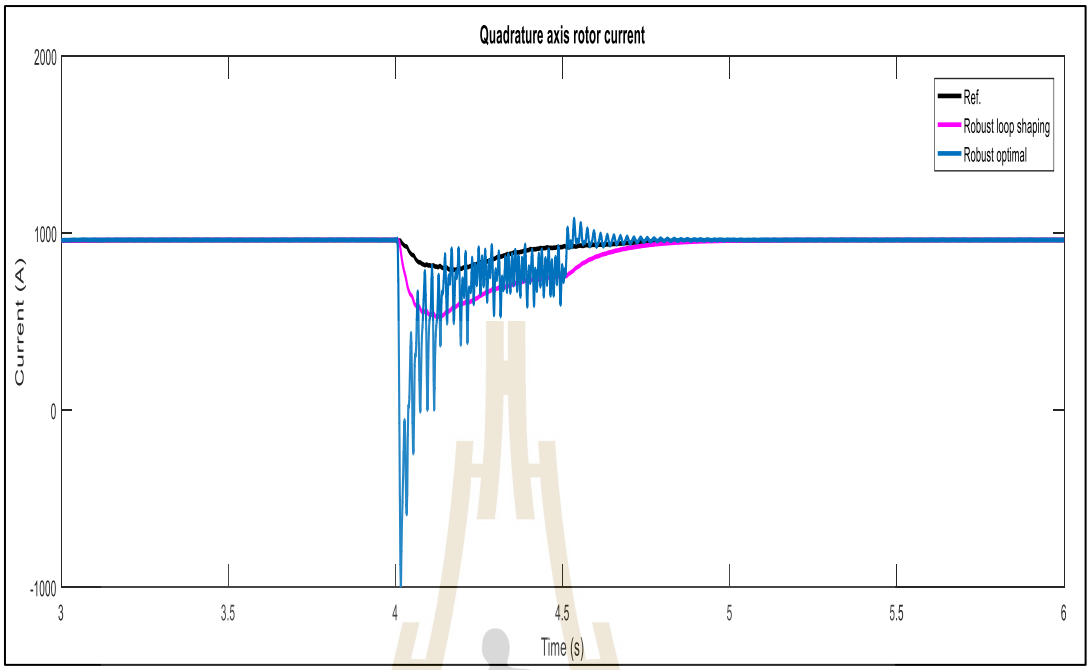

Figure 4.49 Quadrature axis rotor current before, during, and after LL-G fault with robust controllers.

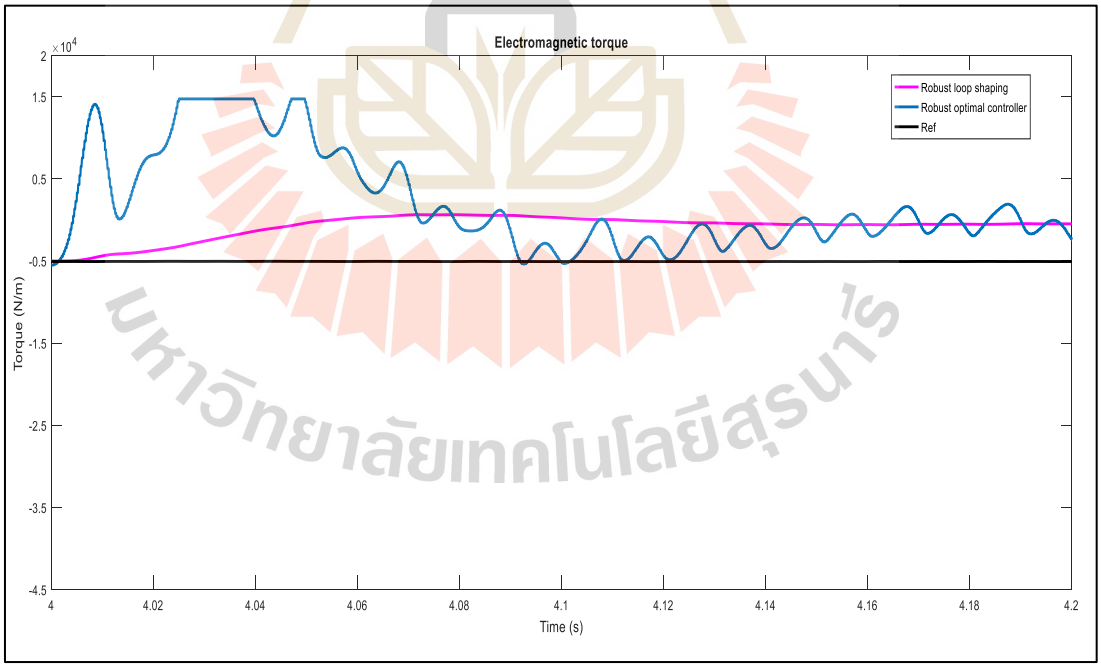

Figure 4.50 Electromagnetic torque during LL-G fault with robust controllers.

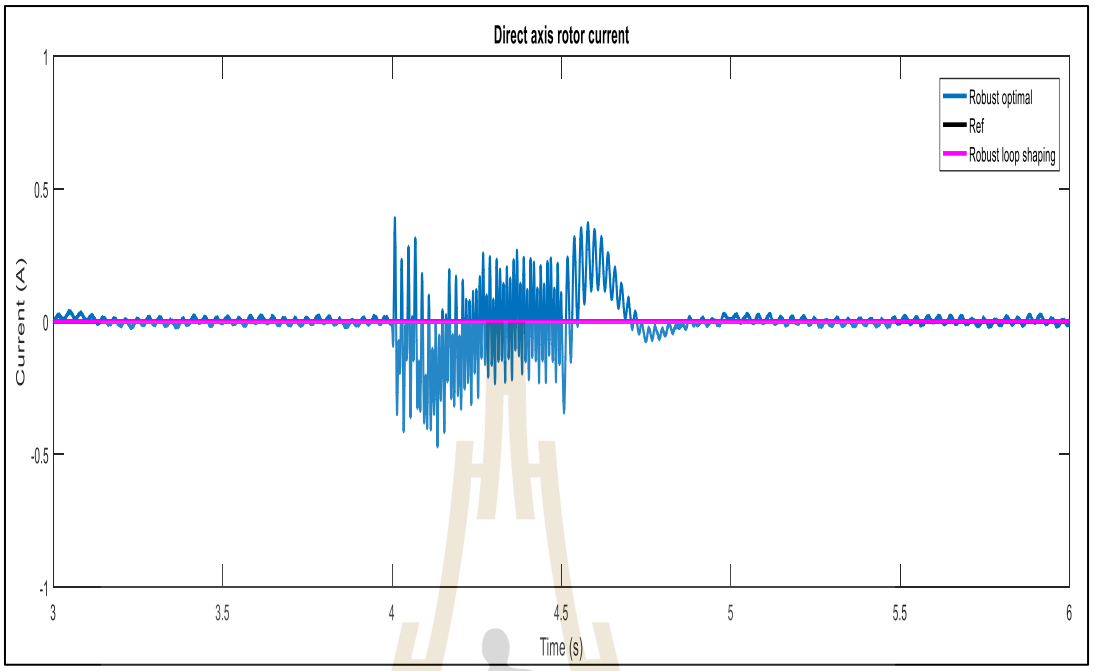

Figure 4.51 Direct axis rotor current before, during, and after LL-G fault with robust controllers.

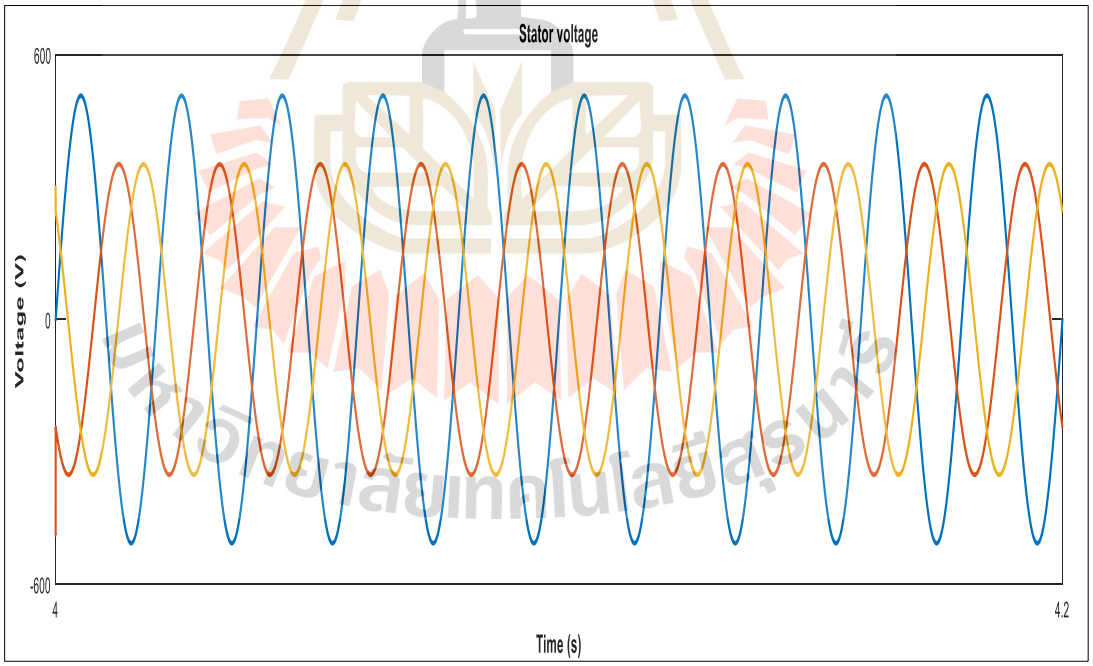

Figure 4.52 Stator voltage during LL-G fault without robust controllers.

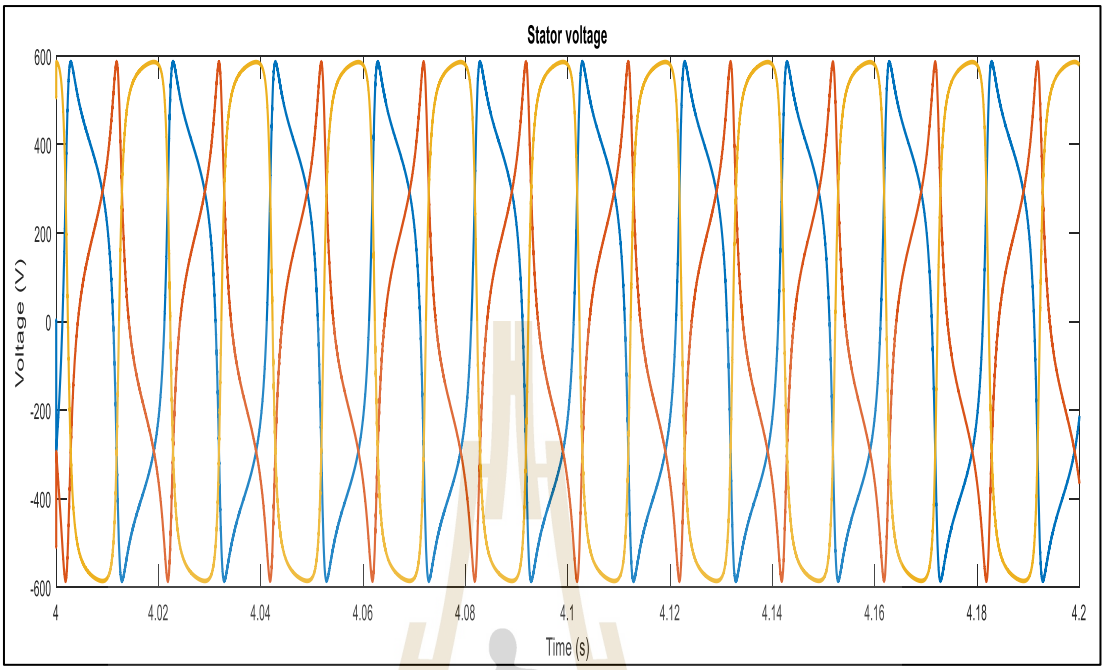

Figure 4.53 Stator voltage during LL-G fault with robust h infinity optimal controller.

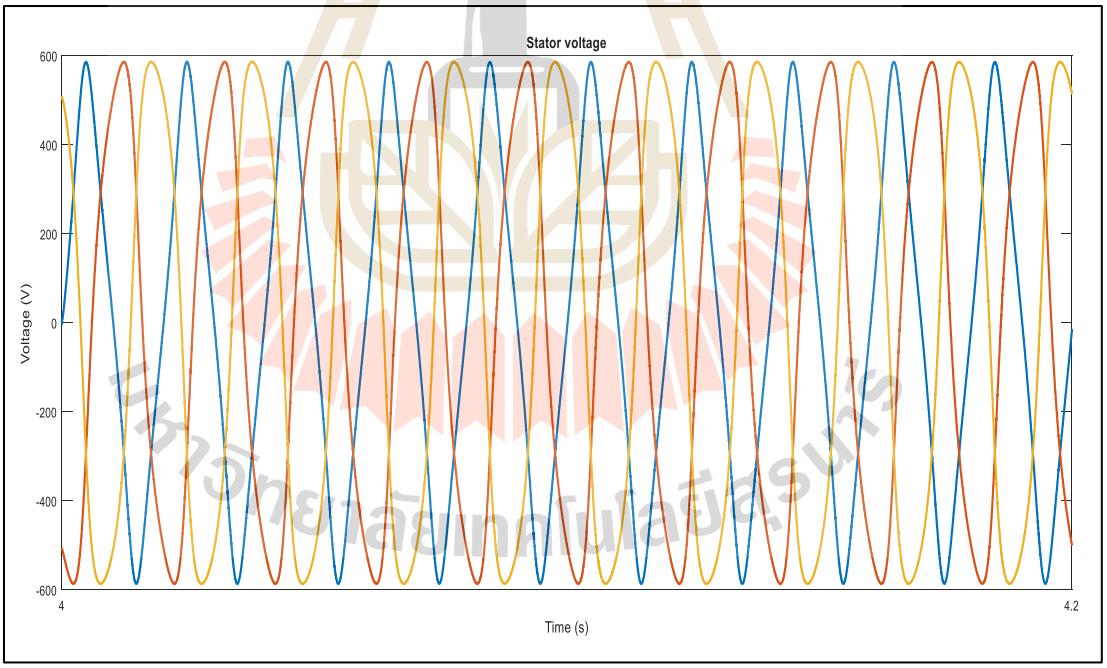

Figure 4.54 Stator voltage during LL-G fault with a robust loop shaping controller.

4.3.5 DFIG under three-phase to ground fault

In a three-phase fault, all three phases are connected and a ground connection is established for all. The fault leaves the system symmetrical. Its analysis also conducted by denoting fault currents in phases "a,b" and "c" as $I_{af}\angle 0^{o}$, $I_{bf}\angle -120^{o}$, $I_{cf}\angle 120^{o}$

The method developed was tested with this fault. The fault occurred at T=4s. The behavior of the quadrature axis rotor current in Figure 4.55 with its counterpart electromagnetic torque Figure 4.56 shows the significance of the fault. The effect of the fault is also realized by the direct axis rotor current in Figure 4.57 and the stator voltage without robust controllers in Figure 4.58. Robust h-infinity loop shaping control continues to dominate the robust optimal controller as it happened in the previous faults for all parameters as shown in the plots for rotor currents, electromagnetic torque, and stator voltage.

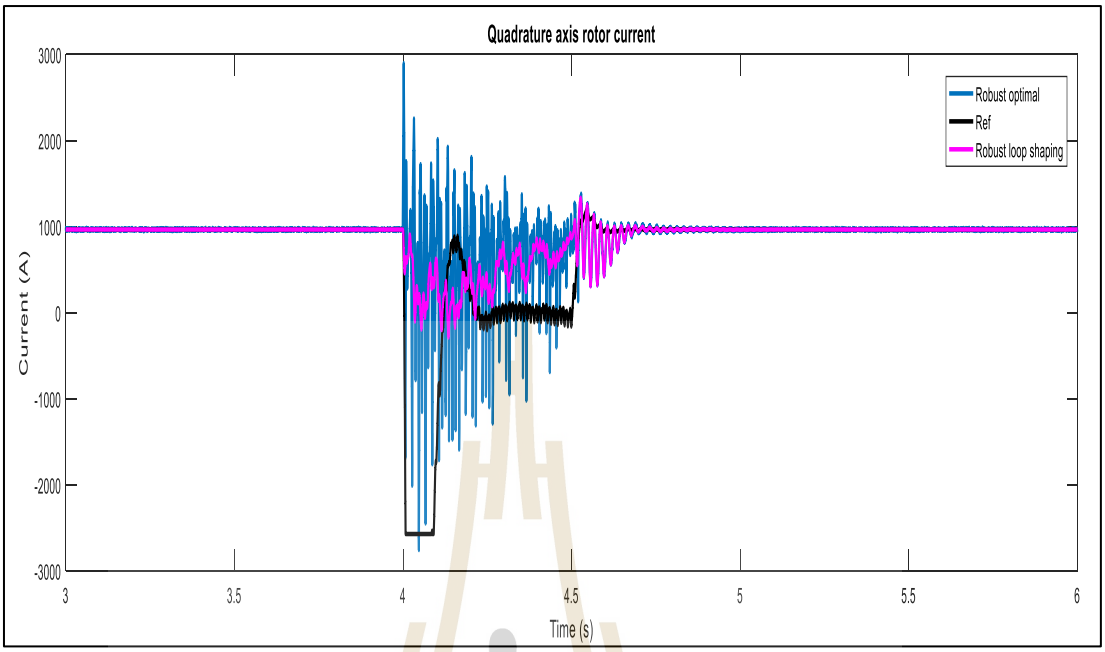

Figure 4.55 Quadrature axis rotor current LLL-G with robust controllers.

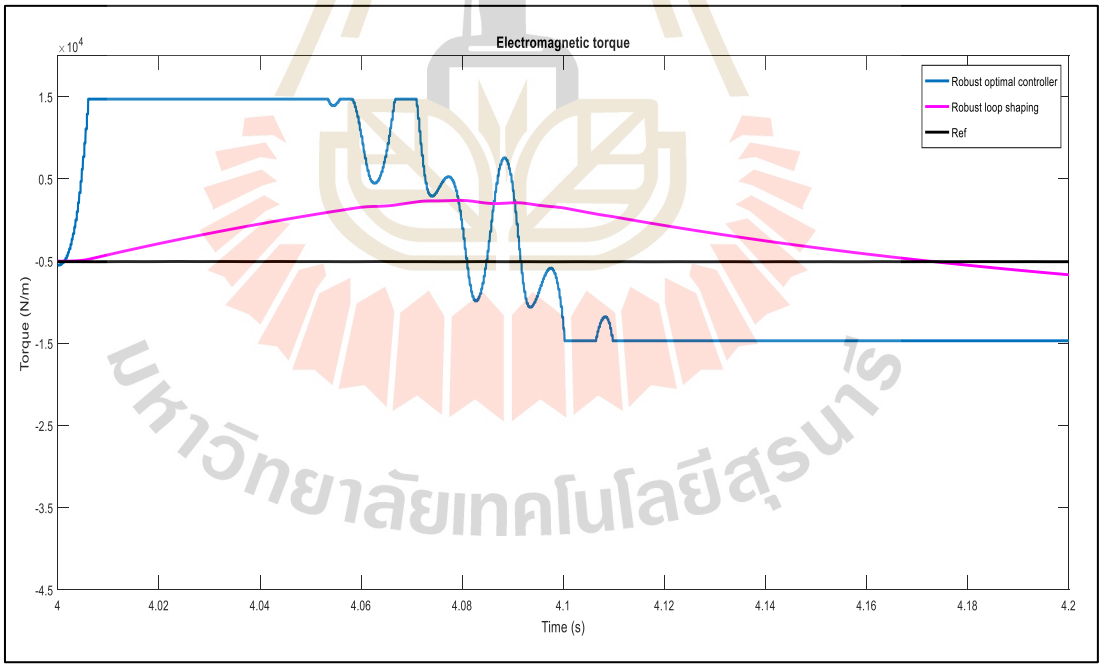

Figure 4.56 Electromagnetic torque during LLL-G fault with robust controllers.

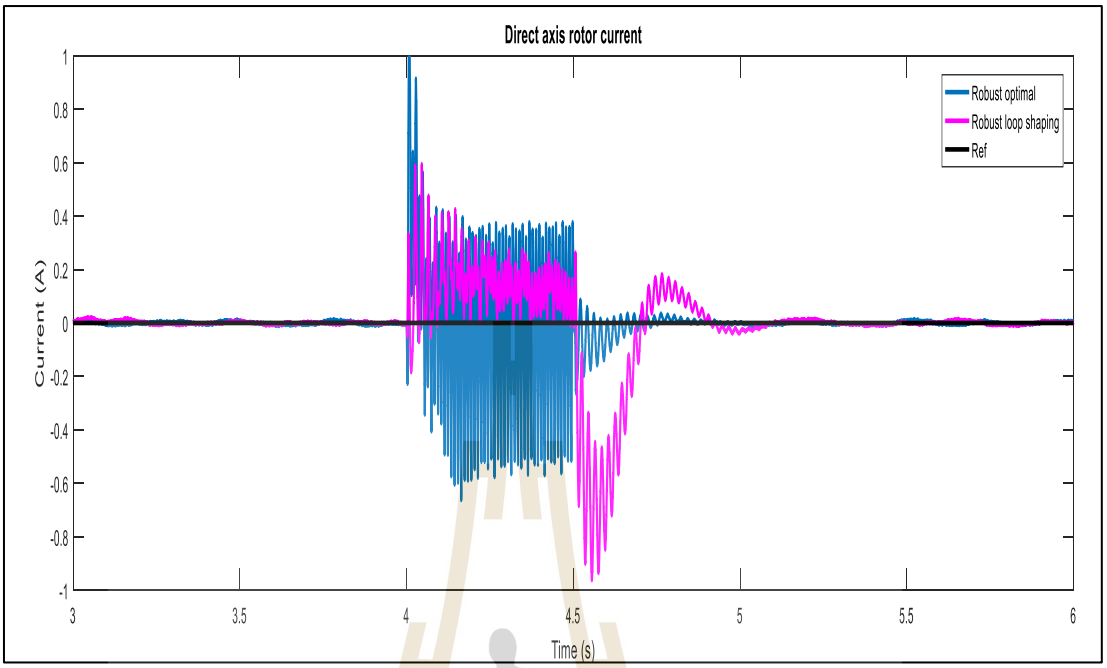

Figure 4.57 Quadrature axis rotor current during LLL-G fault with robust controllers.

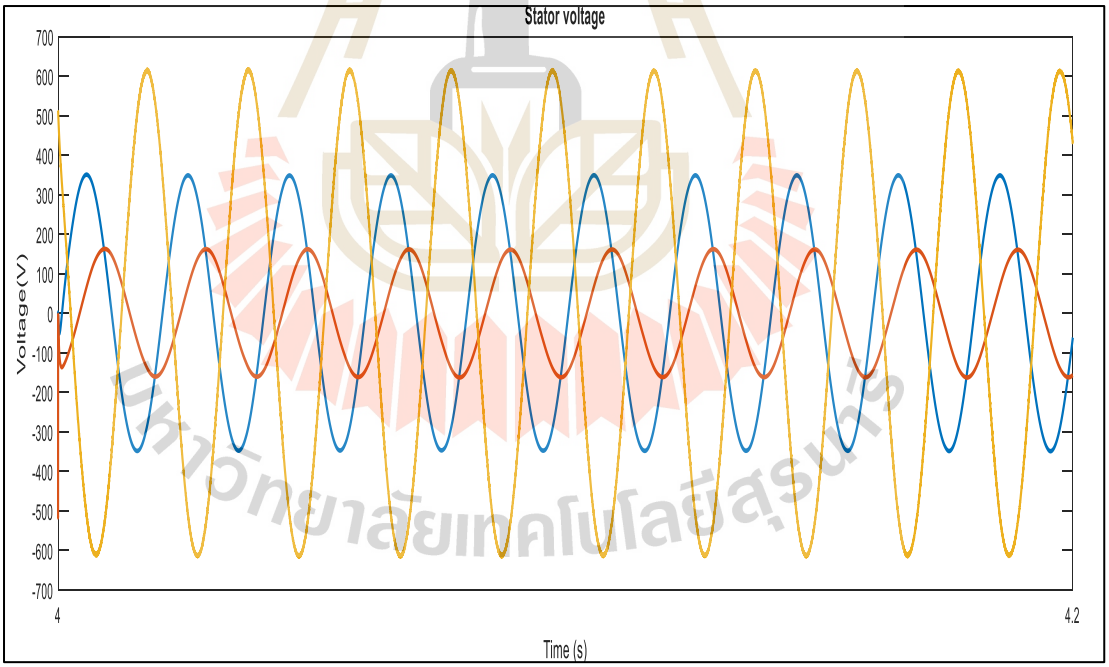

Figure 4.58 Stator voltage during LLL-G fault without robust controllers.

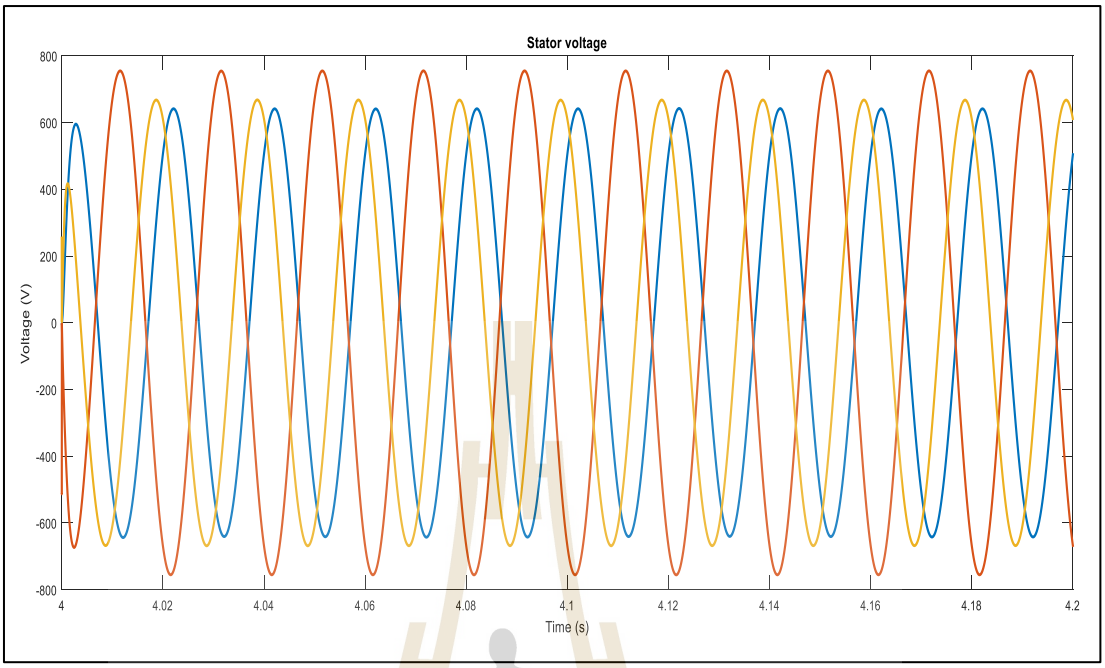

Figure 4.59 Stator voltage during LLL-G fault with the robust optimal controller.

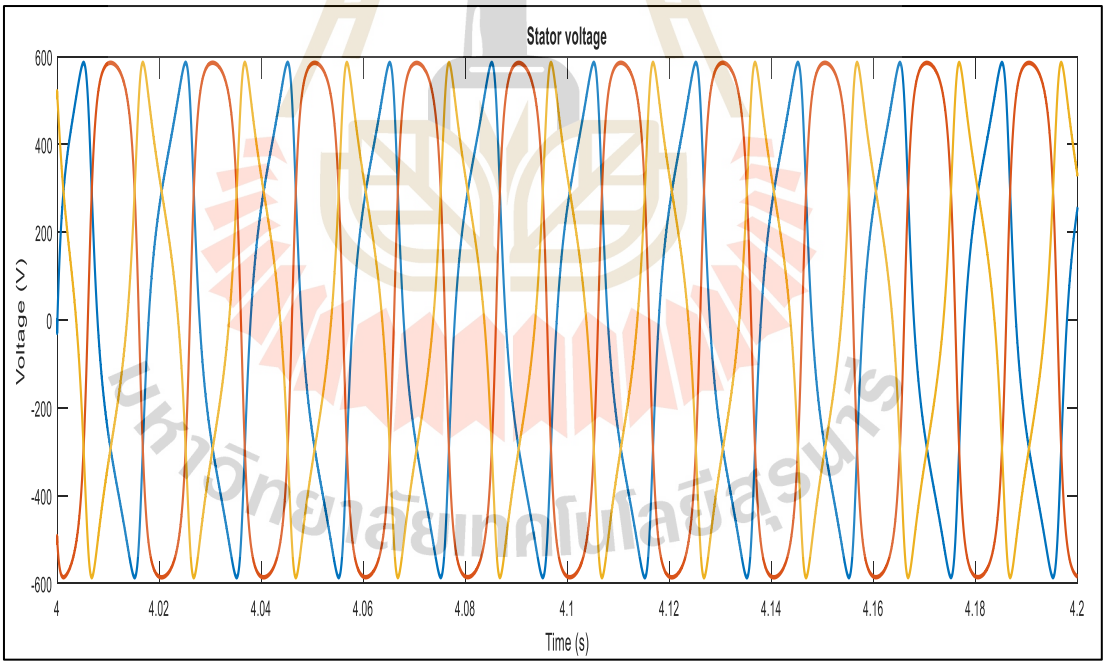

Figure 4.60 Stator voltage during LLL-G fault with a robust loop shaping controller.

4.4 Chapter summary

The fuzzy dual controller is tested and its results are compared with those of the vector control. Both controllers seem to have similar results in rotor speed, electromagnetic torque, and stator voltage during transient state. The robustness of the fuzzy dual controller is seen in the stator current, rotor current, DC link voltage, and grid current. Stator current for vector control has serious oscillations compared to the output of the fuzzy controller. The current output of the fuzzy controller is stable with few variations for all three phases. The same situation occurs with the rotor current. The DC link voltage takes so long to settle to its steady-state value when applying vector control compared when the DFIG is under fuzzy control. Additionally, the DC link voltage plot of the fuzzy controller is smooth and stable ensuring optimum performance of the rotor converter. The grid current is another parameter showing the effectiveness of the fuzzy controller over vector control. The current has fewer variations under fuzzy control compared to vector control.

The rotor speed and torque results obtained during fault state show that the fuzzy control manages to keep the parameters near their steady-state values even under severe conditions and reduces variations experienced when the machine is controlled by the vector control. During a fault, the variation of stator voltage keeps on increasing to more than 4500V when the DFIG is controlled by vector control. In this case, fuzzy control manages to control the voltage although there are some problems with the waveforms of all three phases. For stator current, both controls have poor performance although the variation with fuzzy control is small. Rotor current highly fluctuates during fault with vector control. A fuzzy controller rotor current is better to a certain extent. The DC link voltage deviates from the reference

value with vector control in operation while the voltage is stable and near the reference value when the DFIG is controlled by the fuzzy logic dual controller. Grid current with vector control has serious fluctuations as compared to the fuzzy controller which shows some stability.

A big difference is experienced in the behavior of rotor speed after fault between vector control and fuzzy dual control. The speed with the vector control is far away from the reference value and has fluctuations while fuzzy dual control gives a varying but stable signal. Damaging oscillations are seen in electromagnetic torque with vector control. On the other hand, fuzzy control offers near reference and stable torque. The behavior of the stator voltage, stator current, and rotor current verifies the robustness of the fuzzy controller over vector control. Although smooth and stable, stator voltage with vector control is still very high (6300V) for the distribution system compared to the stator voltage of about 600V from the fuzzy dual controller. Moreover, stator, rotor, and grid currents still fluctuate with vector control while fuzzy control manages to output smooth and stable currents' waveforms. The DC link voltage after fault also deviates from its rated value when the DFIG is controlled by vector control but a different and better behavior is seen when fuzzy dual control is applied.

In optimal control, the results obtained show that LQR is robust compared to the pole placement and vector control. During the fault, the speed of the DFIG with vector control has damaging oscillations when the input signal has noise. With the addition of optimal controllers, the speed plot has very small oscillations during the fault, with LQR showing the best performance. The same situation is also shown by electromagnetic torque during the fault. This shows that the stability of the studied

system is improved with optimal controllers. The step response of the system with the three methods verifies the results obtained. Step response shows that LQR has the best performance with the lowest overshoot, settling time, rise time, and steady-state error. The results obtained show that LQR has the best performance in tracking the reference speed and stabilizing the torque during and after the fault. One of the significant achievements of this study is that all three controllers have a fast response after fault, that rotor speed, and torque tracks the reference values very fast after the occurrence of the measurement noises compared to the results obtained in tracking the generator currents, electromagnetic torque, and stator voltage during faults.

The results obtained from h-infinity optimal control and robust loop shaping control show that the loop shaping controller offers effective system regulation. The big reduction of THD when the DFIG is controlled by the loop shaping control is a significant achievement. The electromagnetic torque and quadrature axis current with the loop shaping controller deviates from reference value during all faults except the three-phase to ground fault, but they show some stability better than the plots of the optimal controller. The direct axis current is nearly tracking the reference value all the way when the DFIG is controlled by the loop shaping controller during line to line fault, three-phase fault, single line to ground fault, double line to a ground fault but with the optimal controller, this current deviates from the reference value and has some fluctuations. Only during three-phase to ground fault that the plot of direct axis rotor current deviates from the reference value.

Without the application of h infinity control and robust loop shaping controller, the stator voltage faces serious voltage dips during line to line fault and is slightly restored by the robust optimal controller. This voltage is close to reaching

optimum stability with the loop shaping controller. In the three-phase fault initially, the voltage is seriously reduced and then starts to increase as time passes on. This voltage is partially restored by the optimal controller. The loop shaping controller steps it up to its steady-state value with almost no distortion. During line to ground fault, one phase voltage significantly drops, the optimal controller increases it but fails to stabilize, something which is managed by the loop shaping controller. Double line to ground fault causes two-phase voltages to drop to a very low value. Similar behavior as in the previous fault occurs when a robust loop shaping controller is applied. In the three-phase to ground fault, only one phase remains stable. The other two are affected. H infinity optimal controller fails to restore all the phases but robust loop shaping control manages to increase the magnitude of the voltage for all phases to the steady-state values but instability is seen on the voltage waveforms.

CHAPTER V

CONCLUSIONS AND RECOMMENDATIONS

5.1 Conclusions

The results obtained show that step response, singular value plot, and harmonic spectrum of the DFIG are highly improved when the induction generator is controlled by a robust h-infinity loop shaping controller than when using a robust h-infinity optimal controller. When the DFIG was without robust control, THD was 11.34%. With a robust h-infinity, optimal controller THD dropped to 4.05% while with the robust loop shaping control the distortion dropped to 1.36%. The step response, singular value plots, and the harmonic spectrum obtained were validated by SIMULINK simulations. The results obtained from the simulations prove the robustness of the loop shaping controller over h infinity controller. The big reduction in THD when the DFIG is controlled by the loop shaping control is validated by the restoration and stability of the stator voltage when the DFIG is controlled by the loop shaping controller as compared to h infinity control during line to line fault, double line to ground fault, three-phase fault, and line to ground fault. Additionally, the behavior of the electromagnetic torque and quadrature axis current which show some deviations from their reference values during all faults except the three-phase to ground fault, but stable, better than those of the h infinity optimal controller. Moreover, the effectiveness of the robust loop shaping control over h infinity optimal control can be seen with the results of the direct axis current which nearly tracks its

reference value before, during, and after line to line fault, three-phase fault, single line to ground fault, and double line to ground fault.

5.2 Recommendations

The thesis has discussed conventional control methods of Vector control, two optimal control methods of Pole placement and Linear quadratic regulator, and two robust control methods of robust h-infinity optimal control and robust h-infinity loop shaping control.

The methods have been tested with a single line to ground fault, double line fault, three-phase fault, double line to ground fault, and three-line to ground fault. The methods developed can be tested for other disturbances that might occur in the power system and compare the results obtained with the ones obtained in this work.

Moreover, further testing can be performed with the variation of the parameters of the DFIG. Additionally, the developed methods can be modified to improve their performance. The issue of the addition of flexible AC transmission systems (FACTS) and energy storage devices can also be considered as these devices are known to improve the voltage profile of the system.

5.3 Research publications

Part of this study was published, submitted, or presented in the following conferences and journals;

Oonsivilai, A., Zongo, O.A., and Oonsivilai, R. (June 2019, Published). Stability Enhancement of Doubly Fed Induction Generator Using a Linear Quadratic Regulator. GMSARN International Journal.

Zongo, O.A., Oonsivilai, A. (2019). Review on distributed generation technology in power systems. Walailak Procedia 2019; 2019(1): IC4IR.14.

Zongo, O.A., Oonsivilai, A. (May 2017, Published). Optimal placement of distributed generator for power loss minimization and voltage stability improvement. International Conference on Alternative Energy in Developing Countries and Emerging Economies (AEDCEE), Bangkok, Thailand.

Zongo, O.A., Oonsivilai, A. (April 2018, Submitted). Fuzzy-PI dual control of DFIG under asymmetrical voltage dips. ELEKTRONIKA JR ELEKTROTECHNIKA.

Zongo, O.A., Oonsivilai, A., Oonsivilai, R. (2018, July, Submitted). Loop shaping controller and extended Kalman filter for DFIG robust control. Nonlinear Dynamics Journal.

REFERENCES

Abdelsalam, H. A., Suriyamongkol, D., and Makram, E.B. (2017). A TSA-based consideration to design LQR auxiliary voltage control of DFIG. **In the North American Power Symposium (NAPS)**.

Abdelzaher, T., Diao, Y., Hellerstein, J. L., Lu, C., Zhu X. (2017). Introduction to control theory and its application to computing systems.

Abu-Rub, H., Malinowski, M., and Al-Haddad, K. (2014). Power electronics for renewable energy systems, transportation, and industrial applications. **IEEE Press and John Wiley & Sons Ltd.**

Abdallah, M.E., Arafa, O.M., Shaltot, A., Abdel-Aziz, G.A. (2016). MRAC-based vector-oriented control of a wind turbine-driven DFIG. **Eighteenth International Middle East Power Systems Conference (MEPCON)**.

Abdelrahem, M., Hackl, C., Kennel, R. (2015). Sensorless control of doubly-fed induction generators in variable-speed wind turbine systems. **International Conference on Clean Electrical Power (ICCEP)**.

Al-Quteimat, A., Roccaforte, A., and Schäfer, U. (2016). Performance improvement of direct torque control for doubly fed induction generator with 12 sector methodology. **IEEE International Conference on Renewable Energy Research and Applications (ICRERA)**.

REFERENCES (Continued)

Aliskan, I., Gulez, K., Tuna, G., Mumcu, T.V., and Altun, Y.. (2013). Nonlinear speed controller supported by direct torque control algorithm and space vector modulation for induction motors in electrical vehicles. **ELEKTRONIKA IR ELEKTROTECHNIKA**, ISSN 1392-1215, Vol. 19, No.6.

Altın, M., Göksu, Ö., Teodorescu, R., Rodriguez, P., Jensen, B-B., Helle L. (2010). Overview of recent grid codes for wind power integration. **12th International Conference on Optimization of Electrical and Electronic Equipment, OPTIM**.

Ackermann, T., Andersson G., Soder L. (2001). Distributed generation: a definition. **Electrical Power System Research**; 57(3):195-204.

Acharya N., Mahat, P., Mithulananthan, N. (2006). An analytical approach for DG allocation in the primary distribution network. **International Journal of Electrical Power & Energy Systems**, Vol. 28, No. 10, pp 669-678.

Adefarati, T., Bansal, R.C. (2005). Integration of renewable distributed generators into the distribution system: a review. **IET Renewable Power Generation**.

A. D. B. (2014). Guidelines for wind resource assessment: best practices for countries initiating wind development.

Aydn, E., Polat, A., Ergene, L.T. (2016). Vector control of DFIG in wind power applications and analysis for voltage drop condition. **IEEE International Conference on Renewable Energy Research and Applications (ICRERA)**.

REFERENCES (Continued)

Ashouri-Zadeh, A., Toulabi, M., Bahrami, S., and Ranjbar, A.M. (2017). Modification of DFIG's active power control loop for speed control enhancement and inertial frequency response. **IEEE Transactions on Sustainable Energy**, Vol. 8, No. 4.

Astr¨om, K.J., Murray, R.M. (2006). Feedback Systems: An Introduction for scientists and engineers. **Department of Automatic Control, Lund Institute of Technology. Control and Dynamical Systems, California Institute of Technology**, USA.

Badran, O., Abdulhadi, E. (2009). Evaluation of factors affecting wind power generation in Jordan. **The Seventh Asia-Pacific Conference on Wind Engineering,** November 8-12, Taipei, Taiwan.

Bakouri, A., Abbou, A., Mahmoudi, H., Elyaalaoui, K. (2014). Direct torque control of a doubly-fed induction generator of the wind turbine for maximum power extraction. **International Renewable and Sustainable Energy Conference (IRSEC)**.

Barker, P. P., de Mello R. W. (2000). Determining the impact of distributed generation on power systems: part 1 - radial distribution systems. **Power Technologies, Inc.**

Barker, P. (2000). Determining the Impact of Distributed Generation on Power Systems: part 1- Radial Distribution Systems. **IEEE, 2000**, pp.1645 1656.

REFERENCES (Continued)

Bounadja, M., Belmadani, B., Belarbi, A.W. (2009). A combined stator vector control–SVM-direct torque control for high-performance induction machine drives. ISSN 1392–1215, **ELECTRONICS AND ELECTRICAL ENGINEERING**, 2009. No. 8 (96).

Borges, C.L.T., Falcao, D.M. (2006). Optimal distributed generation allocation for reliability, losses, and voltage improvement. **Electric Power and Energy System**, 28: 413-420.

Brown R. E., Pan J., Feng X., Koutlev K. (1997). Siting distributed generation to defer T&D expansion. **Proc. IEEE. Generation, Transmission and Distribution**, Vol. 12, pp. 1151-1159.

Cao, W., Xie Y., Tan Z. (2012). Wind turbine generator technologies. advances in wind power. DOI: 10.5772/51780.

Camm, E. H., Behnke, M. R., Bolado, O., Bollen, M., Bradt, M., Brooks, C., Dilling, W., Edds, M., Hejdak, W. J., Houseman, D., Klein, S., Li, F., Li, J., Maibach, P., Nicolai, T., Patiño, J., Pasupulati. S. V., Samaan, N., Saylors, S., Siebert, T., Smith, T., Starke, M., Walling, R. (2009). Characteristics of wind turbine generators for wind power plants. **IEEE Power & Energy Society General Meeting**.

Calderón, G., Mina, J., Rosas, J., Madrigal, M., Claudio, A., and López, A. (2017). Simulation and comparative analysis of DFIG based WECS using stator voltage and stator flux reference frames. **IEEE Latin America Transactions**, Vol. 15, No. 6.

REFERENCES (Continued)

Chatterjee, K., Bhushan, R. (2016). Designing an optimized pitch controller of the DFIG system using a frequency response curve. **IEEE 6th International Conference on Power Systems (ICPS)**.

Chandrasekaran, S. (2014). "Grid-connected doubly-fed induction generator based wind turbine under LVRT," Ph.D. thesis, **Dept. Elect. Eng. Bologna Univ**., Bologna, Italy.

Chandrashekhar R. S., Prasad, P. V. N., Laxmi, A. J. (2012). Power quality improvement of the distribution system by optimal placement and power generation of DGs using GA and NN**. European Journal of Scientific Research**, Vol.69, No.3, pp. 326-336.

Chen, Q-z., Defourny, M., Brüls, O. (2011). Control and simulation of doubly fed induction generator for variable speed wind turbine systems based on an integrated finite element approach. **Proceedings of the European Wind Energy Conference and Exhibition** 2011 (EWEA 2011).

Cheng, P., Nian, H., Wu, C., and Zhu, Z.Q. (2017). Direct stator current vector control strategy of DFIG without phase-locked loop during network unbalance. **IEEE Transactions on Power Electronics**, Vol. 32, No. 1.

Chiradeja, P. (2005). The benefit of Distributed Generation: A line loss reduction analysis. **IEEE/PES Transmission and Distribution Conference & Exhibition: Asia and Pacific Dalian**, China.

REFERENCES (Continued)

Conley, M. (2000). Electricity market framework for renewable and distributed generation.

da Costa, J.P., Zacharias, P., Gafaro, F. (2011). Reduction of voltage violations at a remote location by intelligent active and reactive power control of a DFIG based wind turbine. **Proceedings of the 14th European Conference on Power Electronics and Applications**.

Dyanamina, G., and Kumar, A. (2016). Performance Improvement of grid-connected DFIG fed by three-level diode clamped MLI using vector control. **IEEE Region 10 Conference (TENCON)**.

Ding, R., Meng, C., Qiao, Y. (2015). The coordinating control of voltage and reactive power between SVC and DFIG after LVRT. **IEEE Eindhoven PowerTech.**

Dias, S.V., Silva, W.A., Neto, T.R.F., dos Reis, L.L.N., Torrico, B.C., Campos, J.C.T. (2016). Robust generalized predictive control applied to the mitigation of electromagnetic torque oscillations in a wind energy conversion system based on DFIG. **IEEE Biennial Congress of Argentina (ARGENCON)**.

Din, W.U., Zeb, K., Khan, B. Ali, S. M., Mehmood, C.A., Haider, A. (2016). Control of DC link voltage for grid interfaced DFIG using adaptive sliding mode & fuzzy based on Levenberg-Marquardt algorithm during a symmetrical fault. **International Conference on Computing, Electronics, and Electrical Engineering (ICE Cube)**.

Dosoglu, M.K. (2017). Nonlinear dynamic modeling for fault ride-through capability of DFIG-based wind farm. **Nonlinear Dyn**, 89:2683–2694.

REFERENCES (Continued)

Driesen, J., Belmans, R. (2006). Distributed generation: challenges and possible solutions. **IEEE Power Engineering Society General Meeting**.

Duong, M. Q., Grimaccia, F., Leva, S., Mussetta, M., and Le, K.H. (2016). A hybrid fuzzy-pi cascade controller for transient stability improvement in DFIG wind generators. **IEEE International Conference on Fuzzy Systems (FUZZ-IEEE).**

Dugan, R. C., Price, S. K. (2002). Issues for distributed generation in the US, **IEEE Power Engineering Society Winter Meeting**, vol.1, 2002, pp. 121- 126.

Eisa, S.A., Stone, W., and Wedeward, K. (2017). Mathematical modeling, stability, bifurcation analysis, and simulations of a type-3 DFIG wind turbine's dynamics with pitch control. **Ninth Annual IEEE Green Technologies Conference**.

El-Ela A.A.A., Allam, S.M., Shatla, M.M. (2010). Maximal optimal benefits of distributed generation using a genetic algorithm. **Electric Power Systems Research**, 80: 869-877.

El Chaar, L., Lamont, L. A., Elzein, N. (2011). Wind energy technology-industrial update. **IEEE Power and Energy Society General Meeting**.

El-Ahmar, M. H., El-Sayed, A-H. M., Hemeida, A. M. (2017). Evaluation of factors affecting wind turbine output. **Nineteenth International Middle East Power Systems Conference (MEPCON), Menoufia University, Egypt**, 19-21 December.

REFERENCES (Continued)

Errouissi, R., Al-Durra, A., Muyeen, S.M., Leng, S., and Blaabjerg, F. (2017) Offset-free direct power control of DFIG under continuous-time model predictive control. **IEEE Transactions on Power Electronics**, Vol. 32, No. 3.

Esmaeeli, M.R., Kianinejad, R., Razzaz, M. (2012). Field oriented control of DFIG based on modified MRAS observer. **Proceedings of 17th Conference on Electrical Power Distribution**.

Feyel, P. (2013). Loop-shaping Robust Control. **ISTE Ltd and John Wiley & Sons, Inc.,** Great Britain and the United States.

Francis, K. (2014). Optimization of Distributed Generation using the Simplex Algorithm. **Murdoch University ENG460: Engineering Thesis Project**.

Friedman, N. R. (2002). Distributed Energy Resources Interconnection Systems: Technology Review and Research Needs. **National Renewable Energy Laboratory, report**.

Gahinet, P., Apkarian, P. (2011). Structured H1 Synthesis in MATLAB. **In Proceedings IFAC, Milan**.

Gerwent, R. van. (2006). Distribution Generation and Renewables Introduction, **KEMA Nederland B.V., November 2006, Leonardo ENERGY**.

Gilev, B. (2017). Wind turbine model and loop shaping controller design. **AIP Conference Proceedings** 1910, 020018.

Ghafouri, M. (2018). “Subsynchronous resonance in DFIG-based wind farms.” Ph.D. dissertation. **Electrical Engineering Department, Polytechnic School of Montreal**, Canada.

REFERENCES (Continued)

Ghafouri, M., Karaagac, U., Karimi, H., Jensen, S., Mahseredjian, J., and Faried, S. O. (2017). An LQR controller for damping of subsynchronous interaction in DFIG-based wind farms. **IEEE Transactions on Power Systems**, Vol.32, no. 6.

Gogineni, J. "Implementation of wind energy systems to the existing power grid," M.S. thesis, **Dept. Elect. & Comp. Eng., Houston Univ., Houston, TX**, 2012.

Gomis-Bellmunt, O., Junyent-Ferr´e, A., Sumper, A., Bergas-Jan´, J. (2008). Ride-through control of a doubly-fed induction generator under unbalanced voltage sags. **IEEE Transactions on Energy Conversion**, Vol. 23, No. 4.

Goudarzi, N. Zhu, W. D. (2013). A review of the development of wind turbine generators across the world. **International Journal of Dynamic Control** 1:192–202.

Grogg, K. (2010). Harvesting the Wind: The Physics of Wind Turbines. **Digital Commons @ Carleton College**.

Gundavarapu, A., Misra, H., Jain, A. K. (2017). The direct torque control scheme for dc voltage regulation of the standalone DFIG-DC system. **IEEE Transactions on Industrial Electronics**.

Haidar, A.M.A., Muttaqi, K.M., Hagh, M.T. (2017). A coordinated control approach for dc-link and rotor crowbars to improve fault ride-through of DFIG based wind turbine. **IEEE Transactions on Industry Applications.**

REFERENCES (Continued)

Hasager, C. B., Astrup, P., Nielsen, P. (2007). QuikSCAT and SSM/I ocean surface winds for wind energy. **IEEE International Geoscience and Remote Sensing Symposium (IGARSS)**.

Hashemnia, M.N., Hosseini, S.M. (2016). A novel direct power control method for doubly fed induction generators. **IEEE Uttar Pradesh Section International Conference on Electrical, Computer, and Electronics Engineering (UPCON)** Indian Institute of Technology (Banaras Hindu University) Varanasi, India.

Hu, S., Zhu, G. (2016). A vector control strategy of grid-connected brushless doubly-fed induction generator based on the vector control of doubly fed induction generator. **IEEE Applied Power Electronics Conference and Exposition (APEC).**

Huchel, Ł., El Moursi, M.S., and Zeineldin, H.H. (2015). A parallel capacitor control strategy for enhanced FRT capability of DFIG. **IEEE Transactions on Sustainable Energy**, Vol. 6, No. 2.

Ilse, D., Vaziri, M., Zarghami, M., Vadhva, S. (2014). Review of Concepts to increase Distributed Generation into the Distribution Network. **Sixth Annual IEEE Green Technologies Conference**.

Islam, K.S., Shen, W., Mahmud, A., Chowdury, A., Zhang, J. (2016). Stability enhancement of DFIG wind turbine using LQR pitch control overrated wind speed. **IEEE 11th Conference on Industrial Electronics and Applications (ICIEA).**

REFERENCES (Continued)

Jang J-l., Kim Y-S., Lee D-C. (2006). Active and reactive power control of DFIG for wind energy conversion under unbalanced grid voltage. **CES/IEEE 5th International Power Electronics and Motion Control Conference**.

Jantzen, J. (1999). Design of fuzzy controllers. The **Technical University of Denmark, Department of Automation**, Bldg 326, DK-2800Lynghy, Denmark

Johnson, A., and Tleis, N. (2005). The development of grid code requirements for new and renewable forms of generation in great Britain. **Wind Engineering** 29(3):201-216.

Junyent-Ferr´e, A., Sumper, A., and Bergas-Jan´, J. (2008). Ride-through control of a doubly-fed induction generator under unbalanced voltage sags. **IEEE Transactions on Energy Conversion**, Vol. 23, No. 4.

Junli, X., Yangwu, S., Bin, Z., Shangfeng, X., Xun, M., Xuchang, Z., Zhemin, L., Yong, Z., Xiaotao, P. (2016). Research on transient reconfiguration and low voltage ride-through control for a doubly-fed induction generator wind turbine with the energy storage device. IEEE 8th **International Power Electronics and Motion Control Conference (IPEMC-ECCE Asia)**.

Kansal, S., Sai, B.B.R., Tyagi, B., Kumar, V. (2011). Optimal placement of distributed generation in distribution networks. **International Journal of Engineering, Science and Technology**, Vol. 3, No. 3, 2011, pp. 47-55.

REFERENCES (Continued)

Kane, A. (2009). Shifting Paradigm of Non-Grid-Connected Wind Power. **World Non-Grid-Connected Wind Power and Energy Conference**. Nanjing (123), China.

Kashkooli, M.R.A., Madani, S.M., Sadeghi, R. (2016). Improved direct torque control of DFIG with reduced torque and flux ripples at the constant switching frequency. **7th Power Electronics, Drive Systems & Technologies Conference (PEDSTC)**, Iran University of Science and Technology.

Kelley, J. (2016). Wind Energy: Application, Limits, and Potential. http://webpage.pace.edu/dnabirahni/DOCS/ENVIRONMENTAL%20LAW/Wind%20Energy.doc

Kersting, W. H. (2001). Radial distribution test feeders. **Power Engineering Society Winter Meeting, 2001. IEEE**, pp. 908-912 vol. 2.

Khoete, S., Manabe, Y., Kurimoto, M., Funabashi T., and Kato, T. (2016). Robust H – infinity Control for DFIG to Enhance Transient Stability during Grid Faults. **Proceedings of the World Congress on Engineering and Computer Science** Vol II WCECS, October 19-21, 2016, San Francisco, USA.

Khargonekar, P. P., Petersen, I. R., Rotea M. A. (1988). H infinity Optimal Control with State-Feedback. **IEEE Transactions on Automatic Control**, Vol 33, No. 8.

Kim, J., Seok, J-K., Muljadi, E., and Kang, Y. C. (2016). Adaptive q–v scheme for the voltage control of a DFIG-based wind power plant. **IEEE Transactions on Power Electronics**, Vol. 31, no. 5.

REFERENCES (Continued)

Kim, J., Muljadi, E., Park, J-W., and Kang, Y.C. (2016). Adaptive hierarchical voltage control of a DFIG-based wind power plant for a grid fault. **IEEE Transactions on Smart Grid**, vol. 7, no. 6.

Kojovic, L.A., Willoughby, R. (2001). Integration of Distributed Generation in a Typical USA Distribution System", **IEE- CIRED 2001 Conf. Rec., conference publication** No. 482, 2001, pp. 18-21.

Kuhn, B., Marquis, J., RotatorI, H. (2010). Wind turbine design and implementation. **Worcester Polytechnic Institute.** Project Number: LDA-1004.

Kumpulainen, L. K., Kauhaniemi, K. T. (2004). Analysis of the impact of distributed generation on automatic reclosing. **IEEE PES Power Systems Conference and Exposition**.

Lee, C. C. (2015). Fuzzy logic in control systems: Fuzzy logic controller – Part I. **IEEE Transactions on Systems, Man, and Cybernetics**, Vol. 20, No. 2.

Lebsir, A., Bentounsi, A., Benbouzid, M., Mangel, H. (2015). Electric Generators Fitted to Wind Turbine Systems: An Up-to-Date Comparative Study. **Journal of Electrical Systems, ESR Groups**, 2015, 11(3), pp.281-295.

Li, J., Corzine, K. (2015). A sensorless flux oriented control scheme for a DFIG connected to a dc link. **Clemson University Power Systems Conference (PSC)**.

Li, L., Nian, H., Ding, L., Zhou, B. (2017). Direct power control of the DFIG system without PLL under unbalanced and harmonically distorted voltage. **IEEE Transactions on Energy Conversion**.

REFERENCES (Continued)

Liu, S.Y. e Selênio, V.F.M., and R. Silva. (2011). Analysis of direct power control strategies applied to doubly fed induction generator. **Power Electronics Conference (COBEP)**, 2011, Brazil.

Li, S., Yu, Z., Wang, X., Su, X. (2016). The simulation of the wind power system vector control is based on Fuzzy PI. **Chinese Control and Decision Conference (CCDC)**.

Lima, F.K.A., Dantas, J.L., and Branco, C.G.C. (2012). Reactive power control of DFIG-based wind turbines during voltage sag. **IECON 2012 - 38th Annual Conference on IEEE Industrial Electronics Society**.

Li, Y., Hang, L., Li, G., Guo, Y., Zou, Y., Chen, J., Li, J., Zhuang, J., Li, S. (2016). An improved DTC controller for the DFIG-based wind generation system. **IEEE 8th International Power Electronics and Motion Control Conference (IPEMC-ECCE Asia)**.

Long, Y., Miyagj, H., Yamashita, K. (2000). Windmill power systems controller design using h-infinity theory. **IEEE international conference on systems, man and cybernetics**.

Lopes J. A. P., Hatziargyriou, N., Mutale, R., Djapic, P., Jenkins, P. (2006). Integrating distributed generation into electric power systems: A review of drivers, challenges, and opportunities. **Electric Power Systems Research**, vol. 77, pp. 1189-1203.

REFERENCES (Continued)

Lyons J. P., Robinson, M. C., Veers, P., Thresher, R. W. (2008). Wind Turbine Technology–The Path to 20% US Electrical Energy. **Power& Energy Society, IEEE General Meeting-Conversion and Delivery of Electrical Energy in the 21st Century.**

Mannah, M.A., Hammoud, A., Haddad, A., Elias, R., Bazzi, H. (2016). Modeling and real-time simulation of a DFIG-based wind energy conversion system. **3rd International Conference on Renewable Energies for Developing**.

Mahmoodzadeh, Z., Yazdanian, M., Ghaffarzadeh, H., Mehrizi-Sani, A. (2014). Overshoot control of the electromagnetic torque during fault recovery for a SCIG with a STATCOM. **International Conference on Electrical Sciences and Technologies in the Maghreb (CISTEM)**.

Mahalakshmi, R., Viknesh, J., Ramesh M.G, Vignesh, M.R., Thampatty, K.C.S. (2016). Fuzzy logic-based rotor side converter for constant power control of grid-connected DFIG. **IEEE Transactions on Sustainable Energy**.

Maegaard, P. (2009). Wind Energy Development and Application Prospects of Non-Grid-Connected Wind Power. **World Non-Grid-Connected Wind Power and Energy Conference** (WNWEC).

Marimuthu C., Kirubakaran, V. (2014). A critical review of factors affecting wind turbine and solar cell system power production. **International Journal of Advanced Engineering Research and Studies**. Int. J. Adv. Eng. Res. Studies/III/II/ Jan.-March, 2014/143-147.

REFERENCES (Continued)

Masaud T. “Modeling, analysis, control and design application guidelines of doubly fed induction generator (DFIG) for wind power applications,” Ph.D. dissertation, **Dept. Elect. Eng. & Comp. Sci**., Colorado School of Mines, Colorado, CO, 2013.

Marques, G.D., and Iacchetti, M.F. (2016). Field-weakening control for efficiency optimization in a DFIG connected to a dc-link. **IEEE Transactions on Industrial Electronics**, Vol. 63, No. 6.

Marques, G.D. (2011). Stator Flux Damping Methods of the Field Oriented Doubly-fed Induction Generator. 11th International Conference on Electrical Power Quality and Utilization. **IEEE Transactions on Energy Conversion**.

Marques, G.D. (2012). Stator Flux Active Damping Methods for Field-Oriented Doubly Fed Induction Generator. **IEEE Transactions on Energy Conversion**, Vol. 27, No. 3.

Marques, G.D., Iacchetti, M.F. (2014). Stator Frequency Regulation in a Field-Oriented Controlled DFIG Connected to a DC Link. **IEEE Transactions on Industrial Electronics**, Vol. 61, NO. 11.

Marques, G.D., Iacchetti, M.F. (2014). Stator Frequency Regulation in a Field-Oriented Controlled DFIG Connected to a DC Link. **IEEE Transactions on Industrial Electronics**, Vol. 61, NO. 11.

REFERENCES (Continued)

Mengxi, Y., Chen, J., Yanhui, D., Xiuwei, M., Liu, Y., Sun, C., Li, B. (2016). Reactive power coordinated control strategy based on PSO for wind farms cluster. **IEEE PES Asia-Pacific Power and Energy Conference**, Xi'an, China.

Mehdi, A., Reama, A., and Benalla, H. (2016). MRAS Observer for Sensorless Direct Active and Reactive Power Control of DFIG Based WECS with Constant Switching Frequency. **Eleventh International Conference on Ecological Vehicles and Renewable Energies (EVER)**.

Mechter, A., Kemih, K., and Ghanes, M. (2016). Backstepping control of a wind turbine for low wind speeds. **Nonlinear Dyn** (2016) 84:2435-2445.

Misra, H., Gundavarapu, A., and Jain, A.K. (2017). The control scheme for dc voltage regulation of stand-alone DFIG-DC system. **IEEE Transactions on Industrial Electronics**, Vol. 64, No. 4.

Misra, H., and Jain, A.K. (2017). Analysis of stand-alone DFIG-dc system and dc voltage regulation with reduced sensors. **IEEE Transactions on Industrial Electronics**, Vol. 64, No. 6.

Mohammad H., Kamarzarrin, M. (2016). Adel Ameshghi. Control of wind turbine's pitch angle based on DFIG by using MRAC and PIP controller. **The 4th Iranian Conference on Renewable Energy and Distributed Generation, Iran, Mashhad.**

REFERENCES (Continued)

Moghadasi, A., Moghaddami, M., Anzalchi, A., Sarwat, A., and Osama A.M. (2016). Prioritized coordinated reactive power control of wind turbine involving STATCOM using multi-objective optimization. **IEEE/IAS 52nd Industrial and Commercial Power Systems Technical Conference (I&CPS).**

Mohseni, M. (2011). "Enhanced Control of DFIG-Based Wind Power Plants to Comply with the International Grid Codes." Thesis, Ph.D. dissertation, Department of Electrical and Computer Engineering, Curtin University.

Mukhopadhyay, S. (2009). Distributed Generation - Basic Policy, Perspective Planning, and Achievement so far in India. **IEEE Power & Energy Society General Meeting**.

Murari, A.L.L.F., Rodrigues, L.L., Altuna, J.A.T., Potts, A.S., Almeida, L.A.L., and Sguarezi F.A.J. (2019). LQRI power control for DFIG tuned by a weighted-PSO. **Control Engineering Practice** 85: 41–49.

Naamane, A., M'sirdi, N.K. (2011). Indirect field-oriented control: a control strategy for electric wind power conversion. **International Conference on Communications, Computing, and Control Applications (CCCA)**.

Nebrir, M. H., Wang, C., Shaw, S.R. (2006). Fuel Cells: Promising Devices for Distributed Generation. **IEEE Power and Energy Magazine**, Vol. 4(1), pp. 47- 53, 2006.

REFERENCES (Continued)

Nguyen T.H., Scherer, C. W., Scherpen, Jacquelien M.A. (2007). The robust performance of self-scheduled LPV control of doubly-fed induction generator in wind energy conversion systems. **European Conference on Power Electronics and Applications**, EPE.

Nian, H., Cheng, P., and Zhu, Z.Q. (2016). Coordinated direct power control of the DFIG system without a phase-locked loop under unbalanced grid voltage conditions. **IEEE Transactions on Power Electronics**, Vol. 31, No. 4.

Nigim, K. A., Hegazy, Y. (2003). Intention Islanding of Distributed Generation for Reliability Enhancement. **IEEE- PES Annual Meeting**, p. 2451.

Nian, H., Wu, C., Cheng, P. (2017). Direct resonant control strategy for torque ripple mitigation of DFIG connected to dc-link through diode rectifier on the stator. **IEEE Transactions on Power Electronics**, Vol. 32, No. 9.

Oonsivilai, A., Zongo, O.A., and Oonsivilai, R. (2019). Stability enhancement of doubly fed induction generator using a linear quadratic regulator. **GMSARN International Journal**, Vol. 13.

Okedu, K. E., and Uhunwangho, R. (2019). Low voltage ride-through methods based on grid codes for doubly fed induction generator driven wind turbine. **Journal of Emerging Trends in Engineering and Applied Sciences (JETEAS)** 5(8): 221-226, Research Institute Journals, 2014 (ISSN: 2141-7016).

Ose-Zala, B., Pugachov, V. (2017). Methods to reduce cogging torque of permanent magnet synchronous generator used in wind power plants. **ELEKTRONIKA IR ELEKTROTECHNIKA**, ISSN 1392-1215, Vol. 23, No. 1.

REFERENCES (Continued)

Peresada, S., Blagodir, V., Zhelinskyi, M. (2016). Output feedback control of stand-alone doubly-fed induction generator. 2nd international conference on intelligent energy and power systems (IEPS). **2nd International Conference on Intelligent Energy and Power Systems (IEPS)**.

Pengfei Li, Weihao Hu, Rui Hu, and Zhe Chen. (2016). The integrated control strategy for primary frequency control of DFIGs is based on virtual inertia and pitch control. **IEEE Innovative Smart Grid Technologies - Asia (ISGT-Asia)** Melbourne, Australia.

Passino, K. M., Yurkovich, S. (2016). Fuzzy Control. **Department of Electrical Engineering**. The Ohio State University, USA.

Phan, V., and Lee, H. (2012). Performance enhancement of stand-alone DFIG systems with control of rotor and load side converters using resonant controllers. **IEEE Transactions on Industry Applications**, Vol. 48, No. 1.

Poli, R., Kennedy, J., and Blackwell, T. (2007). Particle Swarm Optimization: An Overview, **Swarm Intell**, vol. 1, pp. 33-57, 2007.

Prajapat, G.P., Senroy, N., Kar, I.N. (2018). Stability enhancement of the DFIG-based wind turbine system through a linear quadratic regulator. **IET Generation, Transmission & Distribution**.

Pujhari T. (2017). Islanding detection in distributed generation. **TENCON 2017 - 2017 IEEE Region 10 Conference**.

REFERENCES (Continued)

Pura, P., Iwanski, G. (2016). Direct power control-based torque oscillations cancellation in doubly-fed induction generator operating with an unbalanced grid. **10th International Conference on Compatibility, Power Electronics and Power Engineering (CPE-POWERING)**, Tehran, Iran.

Quezada, V. H. M., Abbad, J. R., Roman, T. G. S. (2006). Assessment of energy distribution losses for increasing penetration of distributed generation. **Power Systems, IEEE Transactions**, vol.21, no.2, pp. 533- 540.

Reyala, A.S.A. (2014). Load reduction in wind energy converters using individual pitch control," Ph.D. dissertation, **Dept., Islamic Univ. of Gaza, Gaza city, Gaza**.

Richardson, P., Keane, A. (2009). Impact of high penetrations of micro-generation on low voltage distribution networks. Electricity Distribution - Part 1, 2009. CIRED. **20th International Conference and Exhibition**, vol., no., pp.1-5, 8-11 June 2009.

Rigatos, G.G. (2014). A differential flatness theory approach to observer-Based adaptive fuzzy control of MIMO nonlinear dynamical systems. **Nonlinear Dyn** 76:1335–1354 DOI 10.1007/s11071-013-1213-0.

Ribeiro, M.I. (2004). Kalman and extended kalman filters: concept, derivation and Properties. Institute for Systems and Robotics Instituto Superior T´ecnico Av. Rovisco Pais, 11049-001 Lisboa PORTUGAL.

Rodríguez, F., and Marcela, D. (2012). Sliding mode control in grid-connected wind farms for stability enhancement. **Universidad Carlos** III de Madrid.

REFERENCES (Continued)

Rodriguez-Ayerbe, P., Quang. B, Ngo, V., Olaru, S. (2016). Model predictive direct power control for doubly fed induction generator-based wind turbines with a three-level neutral point clamped inverter. **IECON 2016 - 42nd Annual Conference of the IEEE Industrial Electronics Society**.

Dugan, R. (2009). Reference Guide: The Open Distribution System Simulator (OpenDSS). **Electric Power Research Institute**.

Saadat, H. (2011). Power system analysis. **PSA Publishing LLC**; 3rd edition.

Sahoo, S.K., Sinha, A.K., Kishore, N.K. (2016). Low voltage ride-through of a grid-connected doubly-fed induction generator with speed sensorless vector control. **National Power Systems Conference (NPSC)**.

Saeidi, S., de Marchi R.A. and Bim, E. (2016). Nonlinear predictive control for a DFIG under-voltage dip. **IECON 2016 - 42nd Annual Conference of the IEEE Industrial Electronics Society**.

Senapati, R., Sahoo, R.K., Rajendra, S.P., Senapati, N. (2017). Sinusoidal current control strategy for 3-phase shunt active filter in a grid-tied PV system. **International Conference on Energy, Communication, Data Analytics, and Soft Computing** (ICECDS-2017).

Saravanan, K.K., Stalin, N., Raja, T.S.R., Pandiyan, B.S. (2016). Modeling and simulation of a direct power control strategy for DFIG using the Vienna rectifier. **International Conference on Emerging Trends in Engineering, Technology, and Science (ICETETS)**.

REFERENCES (Continued)

Saroja Kanti Sahoo, A. K. Sinha, N. K. Kishore. (2016). Low voltage ride-through of a grid-connected doubly-fed induction generator with speed sensorless vector control. **National Power Systems Conference (NPSC)**.

Senanayaka, J. S. L. (2014). Power Dispatching of Active Generators using Droop Control in Grid-connected **Micro-grid. The University of Agder, Faculty of Engineering and Science Department of Engineering Sciences**.

Shen C. (2012). Various Wind Turbine Technologies. **Research Associate, Global Energy Network Institute (GENI)**.

Shi, K.L., Chan, T.F., Wong, Y.K., and Ho. S.L. (2002). Speed estimation of an induction motor drive using an optimized extended Kalman filter. **IEEE Transactions on Industrial Electronics**, Vol. 49, No. 1.

Shivalingappa, V. (2013). Robust h∞ control and analysis: application to electrical drives. Department of electronics and communication engineering, educational and research institute university, Chennai, India.

Shah P., and Singh, B. (2019). Kalman filtering technique for the rooftop-PV system under abnormal grid conditions. **IEEE Transactions on Sustainable Energy**.

Shen, Y., Zhang, B., Cui, T., Zuo, J., Shen, F., Ke, D. (2017). Novel control of DFIG with ESD to improve LVRT capability and to perform voltage support during grid faults. **First IEEE International Conference on Energy Internet (ICEI)**.

REFERENCES (Continued)

Shivarudraswamy, R., Gaonkar, D. N. (2012). Coordinated Voltage Regulation of Distribution Network with Distributed Generators and Multiple Voltage-control Devices. **Electric Power Components and Systems**, vol. 40, no. 9, pp. 1072-1088.

Singh B., Singh, D., Payasi, R. P., Sharma, J., Yadav, M. K., Charitra P. (2016). A Taxonomical Review on Distributed Generation Planning. **European Journal of Advances in Engineering and Technology**, 2016, 3(4): 23-38.

Singh B., Mishra, K. (2015). Fuzzy Logic Control System and its Applications. **International Research Journal of Engineering and Technology (IRJET).** Vol. 2, No. 08.

Simrock, S. (2008). Control theory. **DESY**, Hamburg, Germany.

Sharma, A., Saxena, B. K., Rao, K. V. S. (2017). Comparison of wind speed, wind directions, and Weibull parameters for sites having the same wind power density. **International Conference on Technological Advancements in Power and Energy (TAP Energy)**.

Sourkounis, C., Tourou, P. (2013). Grid code requirements for wind power integration in Europe. **Hindawi Publishing Corporation**, **Conference Papers in Energy, Volume 2013**.

REFERENCES (Continued)

Srirattanawichaikul, W., Premrudeepreechacharn, S., Kumsuwan. Y. (2016). A comparative study of vector control strategies for the rotor-side converter of DFIG wind energy systems. **13th International Conference on Electrical Engineering/Electronics, Computer, Telecommunications, and Information Technology (ECTI-CON)**.

Subudhi, B., and Ogeti, P.S. (2018). Optimal preview stator voltage-oriented control of DFIG WECS. **IET Generation, Transmission & Distribution**.

Szypulski, M., and Iwanski, G. (2016). Sensorless state control of stand-alone doubly-fed induction generator supplying nonlinear and unbalanced loads. **IEEE Transactions on Energy Conversion**, Vol. 31, No. 4.

Sunny, S.H., Mandal, M., Hossain, E., Rafiq, A. (2017). High-performance parameter observation of induction motor with sensorless vector control. **3rd International Conference on Electrical Information and Communication Technology (EICT)**.

Tamalouzt, S., Rekioua, T., Abdessemed, R. (2014). Direct torque and reactive power control of grid-connected doubly fed induction generator for the wind energy conversion. **International Conference on Electrical Sciences and Technologies in the Maghreb (CISTEM)**.

Tang, C. Y., Guo, Y., and Jiang, J. N. (2011). Nonlinear dual-mode control of variable-speed wind turbines with doubly fed induction generators. **IEEE Transactions on Control Systems Technology**, Vol. 19, No. 4.

REFERENCES (Continued)

Tang, H., He, W., Chi, Y., Tian, X., Li Y., and Wang, Y. (2016). Impact of grid side converter of DFIG on subsynchronous oscillation and its damping control. **IEEE PES Asia-Pacific Power and Energy Conference** - Xi'an – China.

Tao, H., Hongwei, M., Yadong, W., Yongdong, L., and Lie, X. (2016). A Novel Grid Connection Method for DFIG based on Direct Power Control. **IEEE Vehicle Power and Propulsion Conference (VPPC)**.

Tautiva, C., Cadena, A. (2008). Optimal Placement of Distributed Generation on Distribution Network. **Proceeding of Transmission and Distribution Conference and Exposition-IEEE/PES-Bogota**,

Taveiros, F.E.V., Barros, L.S., Costa, F.B. (2019). Heightened state-feedback predictive control for DFIG-based wind turbines to enhance its LVRT performance. **Electrical Power and Energy Systems** 104: 943–956.

Tian, J., Zhou, D., Su, C., Chen, Z., and Blaabjerg, F. (2017). Reactive power dispatch method in wind farms to improve the lifetime of power converter considering wake effect. **IEEE Transactions on Sustainable Energy**, Vol. 8, No. 2.

Tiwari, V., Das, S., and Pal, A. (2017). sensorless speed control of induction motor drive using extended Kalman filter observer. **IEEE PES Asia-Pacific Power and Energy Engineering Conference (APPEEC)**.

Tong, W. Fundamentals of wind energy. **Transactions on State of the Art in Science and Engineering**, Vol. 44.

REFERENCES (Continued)

Verma, S.M.R., Sharma, B. (2016). Calculation of THD in vector controlled IGBT fed doubly-fed induction generator. **International Conference on Electrical Power and Energy Systems (ICEPES)** Maulana Azad National Institute of Technology, Bhopal, India.

Wang, D., Hou, Y., Hu, J. (2016). Stability of dc-link voltage control for paralleled DFIG-based wind turbines connected to weak AC grids. **IEEE Power and Energy Society General Meeting (PESGM)**.

Wagner, H. J. (2017). Introduction to wind energy systems. **EPJ Web of Conferences**.

Wang, Y., Gong, W., Wu, Q. (2013). Robust current control of doubly-fed wind turbine generator under unbalanced grid voltage conditions. **IEEE PES Asia-Pacific Power and Energy Engineering Conference (APPEEC)**.

Wu, B., Lang, Y., Zargari, N., and Kouro, S. (2011). Power conversion and control of wind energy systems.

W. Qiao. (2009). Dynamic modeling and control of doubly-fed induction generators driven by wind turbines. **IEEE/PES Power Systems Conference and Exposition**, 2009.

World Energy Council. (2013). World energy perspective: cost of energy technologies. (Bloomberg New Energy Finance, 2013), pp. 1–20.

Xiao, H., Liu, Y., Liu, H. (2013). Harmonic analysis by modeling and simulation of the wind farm based on DFIG. **ELEKTRONIKA IR ELEKTROTECHNIKA**, ISSN 1392-1215, VOL. 19, NO. 7.

REFERENCES (Continued)

Xiong P., and Sun, D. (2016). Backstepping-based DPC Strategy of a wind turbine-driven DFIG under normal and harmonic grid voltage. **IEEE Transactions on Power Electronics**, Vol. 31, No. 6.

Yang, H., Xie, Z., Zhang, X., Yang, S. (2016). The control strategy for the grid-side converter of DFIG under asymmetrical voltage swell. **IEEE 8th International Power Electronics and Motion Control Conference (IPEMC ECCE Asia)**.

Yun, W., Qiuwei, W., Wenming, G., and Sidoroff, G.M.P. (2016). H robust current control for DFIG based wind turbine subject to grid voltage distortions. **IEEE Transactions on Sustainable Energy.**

Zarei, M.E., Nicolás, C.V., and Arribas, J.R. (2017). Improved predictive direct power control of doubly fed induction generator during unbalanced grid voltage based on four vectors. **IEEE Journal of Emerging and Selected Topics in Power Electronics**, Vol. 5, No. 2.

Zhai, J., Liu, H. (2014). Reactive power control strategy of DFIG wind farms for regulating the voltage of the power grid. **IEEE PES General Meeting/Conference & Exposition**.

Zhu, R., Chen, Z., Tang, Y., Deng, F., and Wu, X. (2016.). Dual-loop control strategy for DFIG-based wind turbines under grid voltage disturbances. **IEEE Transactions on Power Electronics**, Vol. 31, No. 3.

REFERENCES (Continued)

Zongo, O.A., Oonsivilai, A. (2017). Optimal placement of distributed generator for power loss minimization and voltage stability improvement. **International Conference on Alternative Energy in Developing Countries and Emerging Economies (AEDCEE)**, VoL. 138, Pages 1-1202, Bangkok, Thailand.

Zongo, O.A., Oonsivilai, A. (2019). Review on distributed generation technology in power systems. **Walailak Procedia** 2019; 2019(1): IC4IR.14.

Zobaa, A. F., Cecati, C. (2006). A Comprehensive Review on Distributed Power Generation. **International Symposium on Power Electronics, Electrical Drives, Automation, and Motion. SPEEDAM**.

BIOGRAPHY

Mr. Oscar Andrew Zongo was born on May 18, 1975, in Pwani Region, Tanzania. He received his Bachelor's Degree in Electrical Engineering from Dar-es-salaam Institute of Technology in 2008 and a Master's Degree in Electrical Engineering from the Suranaree University of Technology in 2015. He is currently a Ph.D. candidate at the Suranaree University of Technology, Nakhon Ratchasima, Thailand.